

Microwave Electronics

Development and Investigations of Mobile Antennas for less Radiation Hazards

A thesis submitted by

LAILA D

in partial fulfillment of the requirements for the degree of

DOCTOR OF PHILOSOPHY

Under the guidance of

Prof. P MOHANAN



**DEPARTMENT OF ELECTRONICS
FACULTY OF TECHNOLOGY
COCHIN UNIVERSITY OF SCIENCE AND TECHNOLOGY
KOCHI-22, INDIA**

October 2012

Development and Investigations of Mobile Antennas for less Radiation Hazards

Ph.D. Thesis under the Faculty of Technology

Author

Laila D.
Research Scholar
Department of Electronics
Cochin University of Science and Technology
Kochi - 682022
Email: lailacusat@gmail.com

Supervising Guide

Dr. P. Mohanan
Professor
Department of Electronics
Cochin University of Science and Technology
Kochi - 682022
Email: drmohan@gmail.com

Centre for Research in Electromagnetics and Antennas (CREMA)
Department of Electronics
Cochin University of Science and Technology
Kochi - 682022

October, 2012

Dedicated to the Almighty.

My parents, Teachers and Dear ones...



DEPARTMENT OF ELECTRONICS
COCHIN UNIVERSITY OF SCIENCE AND TECHNOLOGY
KOCHI – 682 022

Dr. P. Mohanan
Professor

Ph: 0484 2576418
E-mail: drmohan@cusat.ac.in

Certificate

This is to certify that this thesis entitled “**Development and Investigations of Mobile Antennas for less Radiation Hazards**” is a bonafide record of the research work carried out by Smt. LAILA D under my supervision in the Department of Electronics, Cochin University of Science and Technology. The results embodied in this thesis or parts of it have not been presented for any other degree.

Kochi -22
18th October 2012

Prof. P. Mohanan
(Supervising Teacher)

Declaration

I hereby declare that the work presented in this thesis entitled **“Development and Investigations of Mobile Antennas for less Radiation Hazards”** is a bonafide record of the research work done by me under the supervision of Dr. P. Mohanan, Professor, Department of Electronics, Cochin University of Science and Technology, India and that no part thereof has been presented for the award of any other degree.

Kochi - 22
18th October 2012

Laila D

Words of Gratitude...

I would like to express my sincere gratitude to my supervising guide, Dr. Mohanan Pezholil, Professor, Department of Electronics, Cochin University of Science and Technology, for his guidance, encouragement and the timely care that he rendered to me during my research period. His imminent way of thinking has helped me to explore my research abilities and encouraged in implementing the ideas with absolute satisfaction. I was able to successfully complete this research work and deliver this thesis because of his able guidance and immense patience.

My sincere acknowledgement goes to Dr. C. K. Aanandan, Professor, Head, Department of Electronics, for extending the enormous facilities at Department of Electronics for my research work. I am also grateful for his valuable suggestions and encouragements during my work.

I am grateful to Dr. K. Vasudevan, Professor of the Department of Electronics for his constant encouragement and concern for my research. I also wish to thank him for his valuable suggestions and exposure that he offered during the course of my research.

Dr. K.G. Nair, Director, Centre for Science in Society, Cochin University of Science and Technology and the founder of Centre for Research in Electromagnetics and Antennas, for his vision and commitment for the research that has led to this great establishment with wonderful teachers, resources and facilities.

Let me thank Prof. P.R.S. Pillai, and Dr. Tessamma Thomas, Dr. James Kurian and Dr. Supriya M.H and other faculties of Department of Electronics, Cochin University of Science and Technology for their support.

My sincere thanks to all non teaching staff of Department of Electronics and Administrative office for their sincere cooperation and valuable helps.

I remember with appreciation Dr. Sujith R, Dr. Nishamol , Mr.Sarin V P, Shameena V.A about the supreme support we shared together during the entire research period . Very special thanks to their immense care, technical and scientific talks shared together during my research period.

Special thanks to Mr.Nijas C.M Mr.Dinesh.R, and Mr. Deepak U. for being at the beck and call to sort out all my hardware and software problems. My words are illimitable to thank Mr. Tony D, Mr. Lindo A.O, Mr.Abdul Rasheed, Mr .Vinesh P V, Mr. Sreejith M. Nair , Ms.Roshna ,Ms.sajitha ,Mr.Vipin Ms. Anju P Mathews, Mr. Sreenath S, Mrs. Sarah Jacob, Ms. Sreekala, for their whole hearted support and encouragement. My senior research scholars Dr. Suma M.N and Dr. Deepu V, Dr. Gijo Augustine, Dr. Jitha B, Dr. Bybi P.C, and Dr.Deepti Das Krishna and Dr. Gopikrishna for their encouragement and help rendered to me.

Special thanks to Dr. Mridula S, Dr. Binu Paul and Mrs. Anju Pradeep, School of Engineering, CUSAT for their whole hearted support.

My words are boundless to thank all my research and project colleagues in Centre for Ocean Electronics (CUCENTOL), Microwave Tomography and Material Research Laboratory (MTMR) and Audio and Image Research Lab (AIRL), Department of Electronics, Cochin University of Science and Technology.

I wish to acknowledge The Director, Institute of Human resources and Development (IHRD), Thiruvantapuram for providing financial assistance, support and helps rendered to me. I also wish to place on record my gratitude to the Principal, Model Engineering College, Ernakulam, and Principal, College of Engineering, Adoor for their support.

My deepest gratitude to my Achan and my late amma for their deep love, care, patience and the courage they have given to move on with my research work,

I am really proud about the deep love, care, support and patience showered from my husband K. Radhakrishnan. Special thanks to my kids Gokul and Gautham for being patient during my research period. My mother in law, without her prayers and blessings I would never been able to achieve my aim.

Above all there is the god almighty whose blessings and kindness helped a lot to tide over.

Laila D

Abstract

Antennas, the key element in wireless communication devices had undergone amazing developments especially in the direction of compactness and safety aspects. In the last two decades, the use of the cellular phones has become the most popular mode of communication across the globe. At the same time, the concerns about the radiation effects have increased in the general public. The main concern of this thesis is to develop a mobile antenna which gives reduced RF interference to the user. The reduction of the power absorbed by the user can tremendously avoid any possible health hazards.

The radiation characteristic of a monopole antenna is modified with good radiation characteristics suitable for a mobile handset. The modification is implemented by using different resonating structures which provides reduced radiation along one direction. The direction of less radiation can be changed by modifying the planar antenna structure to a ground folded antenna. This modified structure with excellent radiation characteristic is suitable for modern wireless handheld devices with less user RF interference. Specific Absorption Rate (SAR) is an important parameter for mobile handset. The SAR is estimated for the newly developed antenna for different conditions and discussed in this thesis.

Contents

Chapter 1

INTRODUCTION	01 - 35
1.1 Introduction	02
1.2 Electromagnetic radiations	02
1.2.1 Frequency range of spectrum	03
1.2.2 Ionizing and Non ionizing radiations	05
1.2.3 Exposure to RF radiation	06
1.3 Glimpse through history of microwave communication	07
1.4 Wireless communication bands	10
1.5 Mobile phone antennas	11
1.5.1 Monopole	12
1.5.2 Normal Mode Helical Antenna	13
1.5.3 Microstrip antenna	14
1.5.4 Planar Inverted-L Antenna	16
1.5.5 Planar Inverted-F Antenna (PIFA)	17
1.5.6 Metamaterial based antenna	19
1.5.7 Electronic Band gap structure antennas	20
1.6 Analysis of antennas	20
1.6.1 Transmission Line Matrix method (TLM)	22
1.6.2 Method of Moments (MoM)	23
1.6.3 Finite Element Method (FEM)	24
1.6.4 Finite Difference Time Domain (FDTD) method	25
1.7 Motivation of present research	26
1.8 Thesis organization	28
References	30

Chapter 2

METHODOLOGY AND ANTENNA REVIEW	37 - 94
2.1 Fabrication of the proposed antenna	38
2.2 Antenna measurement facilities	40
2.2.1 HP 8510C Vector Network analyzer (VNA)	40
2.2.2 Agilent E8362B PNA	41
2.2.3 Anechoic chamber	42
2.2.4 Automated turntable assembly for far field measurement	43
2.2.5 Crema Soft: Automated antenna measurement	43
2.3 Measurement procedure	43
2.3.1 Reflection coefficient, Resonant frequency and Bandwidth	44
2.3.2 Far field radiation Pattern	45
2.3.3 Antenna Gain	47
2.4 Planar Near field measurement set up	48

2.4.1	Block diagram-----	48
2.4.2	Block diagram details -----	49
2.4.2.1	Phantom Head model and Head simulating liquid -----	49
2.4.2.2	The Electric probe (E field probe)-----	50
2.4.2.3	X-Y Scanning system and X-Y Controller -----	51
2.4.2.4	Interfacing with Network Analyser and Software for automation -----	51
2.5	Cavity perturbation method for dielectric constant measurement of phantom equivalent liquid -----	53
2.6	Electromagnetic simulation tools -----	55
2.6.1	3D Electromagnetic simulator HFSS-----	55
2.6.2	Computer simulation Technology (CST microwave studio®) --	56
2.7	Planar antennas-Review -----	56
2.7.1	Planar transmission line -----	57
2.7.2	Printed antenna design -----	59
2.7.3	Planar Printed monopole antenna -----	61
2.7.4	Coplanar Waveguide Fed monopole Antennas -----	64
2.8	Mobile antenna with reduced user interference –review -----	68
2.9	Chapter conclusion -----	80
	References-----	81

Chapter 3

DEVELOPMENT AND ANALYSIS OF MODIFIED MONOPOLE

ANTENNA SUITABLE FOR MOBILE HANDSET 95 - 152

3.1	Introduction -----	96
3.2	Requirements for Antennas used in mobile handsets-----	96
3.3	Coplanar Wave Guide feeds: an over view-----	99
3.3.1	Field distribution in CPW -----	100
3.3.2	Transmission and reflection characteristics of the conventional CPW transmission line -----	100
3.4	CPW fed printed monopole antenna -----	102
3.4.1	Reflection Characteristics -----	103
3.4.2	Resonance phenomenon -----	105
3.4.3	Parametric analysis -----	106
3.4.3.1	Effect of signal strip length (L_1) on reflection coefficient -----	106
3.4.3.2	Effect of ground plane width (W_2) on the reflection coefficient -----	107
3.4.3.3	Effect of ground plane length (L_2) on reflection coefficient -----	107
3.4.4	Gain -----	108
3.4.5	Radiation characteristics-----	109
3.4.6	Inferences -----	110

3.5	Modified CPW fed antenna with radiation characteristic suitable for mobile handset	111
3.5.1	Development of Mobile antenna with Split Ring Resonator (SRR)	111
3.5.1.1	Antenna geometry	114
3.5.1.2	Reflection and Impedance Characteristics	115
3.5.1.3	Simulated 3D radiation characteristics	115
3.5.1.4	Modified monopole with SRR printed on the same substrate.	116
3.5.1.5	Reflection characteristics	118
3.5.1.6	Radiation pattern	118
3.5.1.7	3D radiation pattern	120
3.5.1.8	Effect of SRR parameters on antenna performance	121
3.5.1.8.1	SRR location	121
3.5.1.9	Inferences	123
3.5.2	Development of Mobile antenna with single metal strip	124
3.5.2.1	Antenna Geometry	124
3.5.2.2	Reflection characteristics	125
3.5.2.3	Radiation pattern	126
3.5.2.4	Parametric Analysis	128
3.5.2.4.1	Effect of strip width (W3) on reflection characteristics of the antenna	128
3.5.2.4.2	Effect of strip length (L3) on reflection characteristics	129
3.5.2.5	Gain	130
3.5.2.6	Resonance phenomenon	130
3.5.2.7	Validation at different substrates	132
3.5.2.8	Inferences	135
3.5.3	Development of Mobile antenna with vertical metal stripes	135
3.5.3.1	Antenna Geometry	135
3.5.3.2	Reflection characteristics	136
3.5.3.3	Input impedance characteristics	137
3.5.3.4	Far field radiation characteristics	138
3.5.3.5	Parametric Analysis	141
3.5.3.5.1	The effect of printed metal stripes parameters (W ₃ & d) on reflection characteristics	141
3.5.3.5.2	Effects of substrate parameters on reflection characteristics	142
3.5.3.5.3	Effect on radiation pattern with number of stripes (n)	145
3.5.3.6	Gain	146
3.5.4	Inferences	146
3.5.5	Surface Impedance Plot for Proposed Antennas	147
3.6	Chapter conclusion	148
	References	151

Chapter 4

DEVELOPMENT AND ANALYSIS OF A GROUND FOLDED

PLANAR ANTENNA (GFPA) 153 - 185

4.1	Introduction	154
4.2	Folded antenna-review	154
4.3	Characteristics of the conventional CPW transmission line	156
4.4	Introduction to Ground Folded transmission line	157
4.4.1	Geometry of the Ground Folded Transmission line	157
4.4.2	Transmission and reflection characteristics of the folded transmission line	158
4.4.3	Parametric analysis	161
4.5	Compact ground folded monopole antenna	163
4.5.1	Antenna Geometry	163
4.5.2	Reflection Characteristics	164
4.5.3	Effect of strip length L_1 on the resonant frequency	164
4.5.4	Radiation patterns	166
4.5.5	Antenna Gain	167
4.5.6	Electric field distribution at resonance frequency	168
4.5.7	Inferences	169
4.6	Modified ground folded antenna for mobile handset	169
4.6.1	Antenna Geometry	170
4.6.2	Reflection characteristics	171
4.6.3	Radiation pattern	172
4.6.4	Parametric Analysis	173
4.6.4.1	Effect of strip position (P)	174
4.6.4.2	Effect of ground width (W_2)	175
4.6.4.3	Effect of strip width (W_3)	176
4.6.4.4	Effect of strip length (L_3)	177
4.6.4.5	Effect of dielectric constant (ϵ_r) of Substrate Material	178
4.6.5	Polarization	180
4.6.6	Gain	181
4.7	Chapter conclusion	183
	References	184

Chapter 5

SIMULATION AND EXPERIMENTAL ANALYSIS OF NEAR-FIELD

PERFORMANCE OF THE ANTENNAS 187 - 220

5.1	Introduction	188
5.2	SAR Definition	188
5.3	RF Exposure Limits	190
5.4	Tissue equivalent liquid parameters	193
5.5	Near field characteristic study of antennas	195

5.5.1	Near Field Simulation pattern of the proposed antenna -----	195
5.5.1.1	Simulated 3D near field radiation pattern of planar monopole antenna-----	195
5.5.1.2	Simulated 3D near field radiation pattern of the SRR embedded antenna-----	196
5.5.1.3	Simulated 3D near field radiation pattern of the Single strip embedded antenna-----	198
5.5.1.4	Simulated 3D near field radiation pattern of the antenna with printed vertical stripes-----	199
5.5.1.5	Simulated 3D near field radiation pattern of the Ground Folded Monopole antenna -----	200
5.5.1.6	Simulated 3D near field radiation pattern of the Ground Folded monopole with printed strip -----	201
5.5.2	Simulated SAR value of proposed antennas with head model --	202
5.5.2.1	SAR simulation of planar monopole antenna, (Antenna1)-----	203
5.5.2.2	Simulated SAR of antenna with SRR (Antenna 2) -----	205
5.5.2.3	Simulated SAR of antenna with Single strip (Antenna3) -----	206
5.5.2.4	Simulated SAR of antenna with vertical stripes (Antenna 4)---	208
5.5.2.5	Simulated SAR of Ground Folded Monopole antenna (Antenna5)-----	209
5.5.2.6	Simulated SAR of Ground Folded Monopole antenna with vertical strip (Antenna 6)-----	210
5.6	Experimental result in the Near Field Phantom -----	213
5.7	Chapter conclusion -----	218
	References-----	219

Chapter 6

CONCLUSION AND FUTURE PERSPECTIVE..... 221 - 227

6.1	Thesis Highlights -----	222
6.2	Inferences from the analysis of planar CPW fed monopole antenna and CPW fed monopole antenna with a parasitic element for reduced RF interference towards user-----	223
6.3	Inferences from the Ground Folded monopole antenna -----	224
6.4	Inferences from the near field study of antenna with modified radiation pattern-----	225
6.5	Comparison of Different antennas presented in this thesis-----	225
6.6	Suggestions for future work -----	227

APPENDICES ----- 229 - 243

Appendix -1	Compact Asymmetric Coplanar Strip Fed Antenna for Wide Band Applications-----	229
Appendix -2	CSRR Based Microstrip Antenna for Compact Wireless Applications -----	236

PUBLICATIONS -----245 - 247

RESUME -----249 - 251

INDEX -----253 - 254

List of Tables

Table 1.1.	Parts of Radio spectrum -----	03
Table 1.2.	ITU radio bands of the Electromagnetic spectrum -----	04
Table 1.3.	Milestones in Communication-----	09
Table 1.4.	Wireless Communication-----	10
Table 1.5.	Downsizing technique for microstrip antenna-----	16
Table 1.6.	The effect of PIFA parameters on its characteristics -----	18
Table 2.1.	Specifications of PNA -----	42
Table 3.1.	Characteristics of the CPW fed monopole antenna -----	110
Table 3.2.	Parameters of the antenna for different dielectric substrates at 1.8GHz -----	133
Table 3.3.	Parameters of the antenna for different frequencies-----	134
Table 3.4.	The simulated parameters for different dielectric substrate. -----	143
Table 3.5.	Parameters of the antenna with vertical stripes for different frequencies-----	144
Table 3.6.	Summarised result-----	149
Table 4.1.	Radiation pattern of the Ground Folded antenna with metallic strip on different substrates -----	180
Table 4.2.	Characteristics of the ground folded antenna -----	182
Table 5.1.	Recommended SAR limits for a non-occupational /uncontrolled environment set in different countries and regions. -----	192
Table 5.2.	Ingredients (% by weight) Head/Brain Body/Muscle-----	193
Table 5.3.	Dielectric values for tissue equivalent liquids at specific frequencies-----	194
Table 5.4.	Simulated SAR value of the antenna with various distances from the head model. -----	212

List of Figures

Fig.1.1.	Radio waves in Electromagnetic Spectrum -----	04
Fig 1.2.	Types of radiations in Electromagnetic spectrum [3] -----	06
Fig 1.3.	(a) Normal wire monopole with ground plane (b) Planar monopole antenna -----	13
Fig 1.4.	(a) Geometrical configuration (b) Photograph of a helix antenna -----	14
Fig 1.5.	Geometry of a conventional microstrip antenna excited with a microstrip line -----	14
Fig. 1.6.	Structure of (a) Inverted-L antenna (b) Inverted F antenna -----	17
Fig.1.7.	Structure of Planar Inverted-F Antenna -----	18
Fig.1.8.	Family of EM analysis techniques -----	21
Fig.1.9.	Analysis of a microwave circuit -----	22
Fig. 2.1.	Various steps involved in the fabrication process -----	39
Fig. 2.2.	Measurement setup and PNA Specifications -----	41
Fig. 2.3.	Photograph of the anechoic chamber used for the antenna measurements -----	42
Fig. 2.4.	Radiation Pattern Measurement Setup -----	46
Fig. 2.5.	Close view of the antenna gain measurement set up -----	48
Fig. 2.6.	The block diagram of the measurement system -----	49
Fig. 2.7.	Photograph of the Experimental set up -----	51
Fig. 2.8.	Measurement window for SAR estimation -----	52
Fig. 2.9.	Cavity perturbation method setup -----	53
Fig. 3.1.	CPW fed transmission line -----	99
Fig. 3.2.	E field and H field distribution in a CPW fed transmission line -----	100
Fig.3.3.	(a) Transmission and reflection characteristics (b) Radiation characteristic of a CPW transmission line (width=3mm, $\epsilon_r=4.4, h=1.6\text{mm}$) -----	101
Fig.3.4.	Geometry of the Coplanar Waveguide Fed Monopole Antenna.(a) top view (b) side view ($L_1 = 25\text{mm}, W_1 =$ $3\text{mm}, g = 0.35\text{mm}, L_2 = 17\text{mm}, W_2 = 14\text{mm}, h=1.6\text{mm}$ and $\epsilon_r=4.4$). -----	102
Fig.3.5.	(a) Reflection characteristics (b) input impedance characteristics of the CPW fed monopole antenna at 2.3 GHz ($L_1 = 25\text{mm}, W_1 = 3\text{mm}, g = 0.35\text{mm}, L_2 = 17\text{mm},$ $W_2 = 14\text{mm}, h=1.6\text{mm}$ and $\epsilon_r=4.4$). -----	104
Fig.3.6.	Computed surface current density ($L_1 = 25\text{mm}, W_1 = 3\text{mm},$ $g = 0.35\text{mm}, L_2 = 17\text{mm}, W_2 = 14\text{mm}, h=1.6\text{mm}$ and $\epsilon_r=4.4$). -----	105

Fig 3.7.	Effect of signal strip length L_1 on the input reflection of the monopole antenna ($W_1 = 3\text{mm}$, $g = 0.35\text{mm}$, $L_2 = 17\text{mm}$, $W_2 = 14\text{mm}$, $h=1.6\text{mm}$ and $\epsilon_r=4.4$).	106
Fig 3.8.	Effect of ground plane width (W_2) of the monopole antenna on the reflection coefficient ($L_1 = 25\text{mm}$, $W_1 = 3\text{mm}$, $g = 0.35\text{mm}$, $L_2 = 17\text{mm}$, $h=1.6\text{mm}$ and $\epsilon_r=4.4$).	107
Fig 3.9.	Variation of reflection coefficient of the antenna with Ground plane length of the monopole antenna ($L_1 = 25\text{mm}$, $W_1 = 3\text{mm}$, $g = 0.35\text{mm}$, $W_2 = 14\text{mm}$, $h=1.6\text{mm}$ and $\epsilon_r=4.4$).	108
Fig.3.10.	Measured gain of the Coplanar Waveguide Fed printed Monopole Antenna ($L_1 = 25\text{mm}$, $W_1 = 3\text{mm}$, $g = 0.35\text{mm}$, $L_2 = 17\text{mm}$, $W_2 = 14\text{mm}$, $h=1.6\text{mm}$ and $\epsilon_r=4.4$).	108
Fig.3.11.	Simulated 3D radiation pattern ($L_1 = 25\text{mm}$, $W_1 = 3\text{mm}$, $g = 0.35\text{mm}$, $L_2 = 17\text{mm}$, $W_2 = 14\text{mm}$, $h=1.6\text{mm}$ and $\epsilon_r=4.4$).	109
Fig 3.12.	2D radiation pattern of the antenna (a) E plane (b) H plane ($L_1 = 25\text{mm}$, $W_1 = 3\text{mm}$, $g = 0.35\text{mm}$, $L_2 = 17\text{mm}$, $W_2 = 14\text{mm}$, $h=1.6\text{mm}$ and $\epsilon_r=4.4$).	110
Fig.3.13.	Schematic drawing of an SRR unit cell	112
Fig 3.14.	(a) SRR unit cell above the microstrip line (b) S_{21} plot of SRR superstrate	113
Fig 3.15.	Geometry of the CPW fed monopole antenna with SRR as substrate (a) Top view (b) side view ($L_1 = 25\text{mm}$, $W_1 = 3\text{mm}$, $g = 0.35\text{mm}$, $L_2 = 17\text{mm}$, $W_2 = 14\text{mm}$, $h=1.6\text{mm}$ and $\epsilon_r=4.4$, $r_1 = 6.3\text{mm}$, $W = 0.9\text{mm}$, $d = 0.6\text{mm}$, $t = 0.5\text{mm}$).	114
Fig 3.16	(a) Reflection characteristics (b) Impedance plot of CPW fed monopole antenna loaded with SRR ($L_1 = 25\text{mm}$, $W_1 = 3\text{mm}$, $g = 0.35\text{mm}$, $L_2 = 17\text{mm}$, $W_2 = 14\text{mm}$, $h=1.6\text{mm}$ and $\epsilon_r=4.4$, $r_1 = 6.3\text{mm}$, $W = 0.9\text{mm}$, $d = 0.6\text{mm}$, $t = 0.5\text{mm}$).	115
Fig 3.17.	Simulated 3D radiation pattern of CPW fed monopole antenna with SRR as substrate ($L_1 = 25\text{mm}$, $W_1 = 3\text{mm}$, $g = 0.35\text{mm}$, $L_2 = 17\text{mm}$, $W_2 = 14\text{mm}$, $h=1.6\text{mm}$ and $\epsilon_r=4.4$, $r_1 = 6.3\text{mm}$, $W = 0.9\text{mm}$, $d = 0.6\text{mm}$, $t = 0.5\text{mm}$).	116
Fig 3.18.	Geometry of the CPW fed monopole antenna with printed SRR ($L_1 = 25\text{mm}$, $W_1 = 3\text{mm}$, $g = 0.35\text{mm}$, $L_2 = 17\text{mm}$, $W_2 = 14\text{mm}$, $h=1.6\text{mm}$ and $\epsilon_r=4.4$, $r_1 = 6.3\text{mm}$, $W = 0.9\text{mm}$, $d = 0.6\text{mm}$, $t = 0.5\text{mm}$, $a=1.7\text{mm}$, $b=1.3\text{mm}$).	117
Fig 3.19.	Reflection coefficient of the CPW fed monopole antenna with printed SRR ($L_1 = 25\text{mm}$, $W_1 = 3\text{mm}$, $g = 0.35\text{mm}$, $L_2 = 17\text{mm}$, $W_2 = 14\text{mm}$, $h=1.6\text{mm}$ and $\epsilon_r=4.4$, $r_1 = 6.3\text{mm}$, $W = 0.9\text{mm}$, $d = 0.6\text{mm}$, $t = 0.5\text{mm}$).	118

Fig 3.20	Simulated 2D radiation pattern in XZ and YZ plane of the monopole antenna with printed SRR ($L_1 = 25\text{mm}$, $W_1 = 3\text{mm}$, $g = 0.35\text{mm}$, $L_2 = 17\text{mm}$, $W_2 = 14\text{mm}$, $h=1.6\text{mm}$ and $\epsilon_r=4.4$, $r_1 = 6.3\text{mm}$, $W = 0.9\text{mm}$, $d = 0.6\text{mm}$, $t = 0.5\text{mm}$)-----	119
Fig 3.22.	Simulated 3D radiation pattern of the monopole antenna with printed SRR ($L_1 = 25\text{mm}$, $W_1 = 3\text{mm}$, $g = 0.35\text{mm}$, $L_2 = 17\text{mm}$, $W_2 = 14\text{mm}$, $h=1.6\text{mm}$ and $\epsilon_r=4.4$, $r_1 = 6.3\text{mm}$, $W = 0.9\text{mm}$, $d = 0.6\text{mm}$, $t = 0.5\text{mm}$)-----	120
Fig 3.21	Measured 2D radiation pattern of the monopole antenna with printed SRR (a)XY plane (b)YZ plane ($L_1 = 25\text{mm}$, $W_1 = 3\text{mm}$, $g = 0.35\text{mm}$, $L_2 = 17\text{mm}$, $W_2 = 14\text{mm}$, $h=1.6\text{mm}$ and $\epsilon_r=4.4$, $r_1 = 6.3\text{mm}$, $W = 0.9\text{mm}$, $d = 0.6\text{mm}$, $t = 0.5\text{mm}$)-----	120
Fig 3.23.	The variation of reflection characteristic with the effect of position 'a' of the printed SRR ($L_1 = 25\text{mm}$, $W_1 = 3\text{mm}$, $g = 0.35\text{mm}$, $L_2 = 17\text{mm}$, $W_2 = 14\text{mm}$, $h=1.6\text{mm}$ and $\epsilon_r=4.4$, $r_1 = 6.3\text{mm}$, $W = 0.9\text{mm}$, $d = 0.6\text{mm}$, $t = 0.5\text{mm}$, $b=1.3\text{mm}$)-----	121
Fig 3.24.	The variation of reflection characteristic with the effect of position 'b' of the printed SRR ($L_1 = 25\text{mm}$, $W_1 = 3\text{mm}$, $g = 0.35\text{mm}$, $L_2 = 17\text{mm}$, $W_2 = 14\text{mm}$, $h=1.6\text{mm}$ and $\epsilon_r=4.4$, $r_1 = 6.3\text{mm}$, $W = 0.9\text{mm}$, $d = 0.6\text{mm}$, $t = 0.5\text{mm}$, $a=1.7\text{mm}$)-----	122
Fig. 3.25.	Simulated 3D radiation pattern at different position of SRR (a) $a=8\text{mm}, b=1.3\text{mm}$ (b) $a=10\text{mm}, b=1.3\text{mm}$ ($L_1 = 25\text{mm}$, $W_1 = 3\text{mm}$, $g = 0.35\text{mm}$, $L_2 = 17\text{mm}$, $W_2 = 14\text{mm}$, $h=1.6\text{mm}$ and $\epsilon_r=4.4$, $r_1 = 6.3\text{mm}$, $W = 0.9\text{mm}$, $d = 0.6\text{mm}$, $t = 0.5\text{mm}$)-----	123
Fig3.26.	Geometry of the monopole antenna with single strip (a)3D schematic diagram (b)bottom view (c) Side view ($L_1=25\text{mm}, W_1=3\text{mm}, L_2=17\text{mm}, W_2=14\text{mm}, g=0.35\text{mm}, L_3=26\text{mm}, W_3=9.9\text{mm}, h=1.6\text{mm}, \epsilon_r=4.4, P=4.5\text{mm}$ and $S=2\text{mm}.$)-----	125
Fig.3.27.	The reflection characteristic of the antenna (a) Experiment and simulation (b) with and without metal strip ($L_1=25\text{mm}, W_1=3\text{mm}, L_2=17\text{mm}, W_2=14\text{mm}, g=0.35\text{mm}, L_3=26\text{mm}, W_3=9.9\text{mm}, h=1.6\text{mm}, \epsilon_r=4.4, P = 4.5\text{mm}$ and $S=2\text{mm}.$)-----	126
Fig 3.28.	Simulated 3D pattern of the monopole antenna with printed single strip ($L_1=25\text{mm}, W_1=3\text{mm}, L_2=17\text{mm}, W_2=14\text{mm}, g=0.35\text{mm}, L_3=26\text{mm}, W_3=9.9\text{mm}, h=1.6\text{mm}, \epsilon_r=4.4, P=4.5\text{mm}$ and $S=2\text{mm}$)-----	126
Fig. 3.29.	Measured radiation pattern (a) YZ plane (b) XY plane ($L_1=25\text{mm}, W_1=3\text{mm}, L_2=17\text{mm}, W_2=14\text{mm}, g=0.35\text{mm}, L_3=26\text{mm}, W_3=9.9\text{mm}, h=1.6\text{mm}, \epsilon_r=4.4, P = 4.5\text{mm}$ and $S=2\text{mm}$)-----	127

Fig. 3.30.	Radiation pattern of the antenna with and without printed strip ($L_1=25\text{mm}, W_1=3\text{mm}, L_2=17\text{mm}, W_2=14\text{mm}, g=0.35\text{mm},$ $L_3=26\text{mm}, W_3=9.9\text{mm}, h=1.6\text{mm}, \epsilon_r=4.4, P=4.5\text{mm}$ and $S=2\text{mm}$) -----	128
Fig.3.31.	Effect of W_3 on reflection characteristics ($L_1=25\text{mm},$ $W_1=3\text{mm}, L_2=17\text{mm}, W_2=14\text{mm}, g=0.35\text{mm}, L_3=26\text{mm},$ $h=1.6\text{mm}, \epsilon_r=4.4, P=4.5\text{mm}$ and $S=2\text{mm}$) -----	129
Fig. 3.32.	Effect of L_3 on reflection characteristics ($L_1=25\text{mm}, W_1=3\text{mm}, L_2=17\text{mm}, W_2=14\text{mm}, g=0.35\text{mm}, W_3=9$ $.9\text{mm}, h=1.6\text{mm}, \epsilon_r=4.4, P=4.5\text{mm}$ and $S=2\text{mm}$) -----	129
Fig 3.33.	Measured gain of the antenna with printed strip ($L_1=25\text{mm}, W_1=3\text{mm}, L_2=17\text{mm}, W_2=14\text{mm}, g=0.35\text{mm}, L_3=$ $26\text{mm}, W_3=9.9\text{mm}, h=1.6\text{mm}, \epsilon_r=4.4, P=4.5\text{mm}$ and $S=2\text{mm}$) -----	130
Fig. 3.34.	3D radiation characteristic and current density plots at (a) 1.62GHz (b)1.82GHz(c)2.34GHz ($L_1=25\text{mm}, W_1=3\text{mm},$ $L_2=17\text{mm}, W_2=14\text{mm}, g=0.35\text{mm}, L_3=26\text{mm}, W_3=9.9\text{mm},$ $h=1.6\text{mm}, \epsilon_r=4.4, P=4.5\text{mm}$ and $S=2\text{mm}$) -----	131
Fig 3.35.	Reflection characteristics of the antenna with different substrate materials ($L_1=25\text{mm}, W_1=3\text{mm}, L_2=17\text{mm},$ $W_2=14\text{mm}, g=0.35\text{mm}, L_3=26\text{mm}, W_3=9.9\text{mm}, h=1.6\text{mm},$ $\epsilon_r=4.4, P=4.5\text{mm}$ and $S=2\text{mm}$)-----	133
Fig.3.36.	Reflection characteristics of the monopole antenna with strip at different frequencies ($L_1=0.247\lambda_g, L_2=0.168\lambda_g,$ $W_2=0.139\lambda_g, L_3=0.26\lambda_g, W_3=0.098\lambda_g, h=1.6\text{mm}, \epsilon_r=4.4,$ $S=0.019\lambda_g, P=0.045\lambda_g$) -----	134
Fig.3.37.	3-Dimensional radiation pattern of the antenna with printed strip at (a) 900MHz (b) 1.8GHz (c) 2.4GHz ($L_1=25\text{mm}, W_1=3\text{mm}, L_2=17\text{mm}, W_2=14\text{mm}, g=0.35\text{mm}, L_3=$ $26\text{mm}, W_3=9.9\text{mm}, h=1.6\text{mm}, \epsilon_r=4.4, P=4.5\text{mm}$ and $S=2\text{mm}$) -----	135
Fig. 3.38.	Geometry of the antenna (a) 3D schematic diagram (b) bottom view (c) side view ($L_1=25\text{mm}, W_1=3\text{mm}, L_2=17\text{mm},$ $W_2=14\text{mm}, g=0.35\text{mm}, L_3=30\text{mm}, W_3=0.3\text{mm}, d=0.5\text{mm},$ $h=1.6\text{mm}, \epsilon_r=4.4$.)-----	136
Fig. 3.39.	Reflection characteristics of the monopole antenna with vertical stripes ($L_1=25\text{mm}, W_1=3\text{mm}, L_2=17\text{mm}, W_2=14\text{mm}, g=0.35\text{mm},$ $L_3=30\text{mm}, zW_3=0.3\text{mm}, d=0.5\text{mm}, h=1.6\text{mm}, \epsilon_r=4.4$.)-----	137
Fig. 3.40.	Variation of (a) real part (b) imaginary part of the input impedance (c) Smith chart with different number of stripes ($L_1=25\text{mm}, W_1=3\text{mm}, L_2=17\text{mm}, W_2=14\text{mm}, g=0.35\text{m}$ $m, L_3=30\text{mm}, W_3=0.3\text{mm}, d=0.5\text{mm}, h=1.6\text{mm}, \epsilon_r=4.4$.) -----	138
Fig. 3.41.	Measured radiation pattern of the proposed antenna in (a) YZ (b) XY plane. ($L_1=25\text{mm}, W_1=3\text{mm}, L_2=17\text{mm}, W_2=14\text{mm},$ $g=0.35\text{mm}, L_3=30\text{mm}, W_3=0.3\text{mm}, d=0.5\text{mm}, h=1.6\text{mm},$ $\epsilon_r=4.4$.) -----	139

Fig.3.42.	The 2D radiation patterns of the antenna with and without stripes in YZ plane ($L_1=25\text{mm}, W_1=3\text{mm}, L_2=17\text{mm}, W_2=14\text{mm}, g=0.35\text{mm}, L_3=30\text{mm}, W_3=0.3\text{mm}, d=0.5\text{mm}, h=1.6\text{mm}, \epsilon_r=4.4$.)-----	140
Fig. 3.43.	3D radiation pattern ($L_1=25\text{mm}, W_1=3\text{mm}, L_2=17\text{mm}, W_2=14\text{mm}, g=0.35\text{mm}, L_3=30\text{mm}, W_3=0.3\text{mm}, d=0.5\text{mm}, h=1.6\text{mm}, \epsilon_r=4.4$.) -----	140
Fig. 3.44.	Effect of W_3 (a) & d (b) of metal stripes on reflection characteristics of monopole antenna with vertical stripes ($L_1=25\text{mm}, W_1=3\text{mm}, L_2=17\text{mm}, W_2=14\text{mm}, g=0.35\text{mm}, L_3=30\text{mm}, h=1.6\text{mm}, \epsilon_r=4.4$.) -----	141
Fig. 3.45.	Variation of Reflection characteristics with different substrate materials (ϵ_r) ($L_1=25\text{mm}, W_1=3\text{mm}, L_2=17\text{mm}, W_2=14\text{mm}, g=0.35\text{mm}, L_3=30\text{mm}, W_3=0.3\text{mm}, d=0.5\text{mm}, h=1.6\text{mm}, \epsilon_r=4.4$.) -----	143
Fig 3.46	Reflection characteristics of the antenna at different frequencies ($L_1=0.25\lambda_g, L_2=0.17\lambda_g, W_2=0.14\lambda_g, L_3=0.31\lambda_g, W_3=0.0031\lambda_g, P=0.044\lambda_g, Q=0.084\lambda_g$) -----	144
Fig 3.47.	3D radiation pattern of the antenna at different frequencies (a)900MHz (b) 1.8GHz (c) 2.4GHz ($L_1=0.25\lambda_g, L_2=0.17\lambda_g, W_2=0.14\lambda_g, L_3=0.31\lambda_g, W_3=0.0031\lambda_g, P=0.044\lambda_g, Q=0.084\lambda_g$) -----	145
Fig. 3.48.	2D radiation pattern with different number of stripes. ($L_1=25\text{mm}, W_1=3\text{mm}, L_2=17\text{mm}, W_2=14\text{mm}, g=0.35\text{mm}, L_3=30\text{mm}, W_3=0.3\text{mm}, d=0.5\text{mm}, h=1.6\text{mm}, \epsilon_r=4.4$.) -----	145
Fig. 3.49.	Measured gain of the monopole antenna with vertical stripes antenna. ($L_1=25\text{mm}, W_1=3\text{mm}, L_2=17\text{mm}, W_2=14\text{mm}, g=0.35\text{mm}, L_3=30\text{mm}, W_3=0.3\text{mm}, d=0.5\text{mm}, h=1.6\text{mm}, \epsilon_r=4.4$.) -----	146
Fig. 3.50.	Simulated surface impedance at different frequencies of monopole antenna with printed SRR (a)1.6GHz (b)1.81GHz (c)2.2GHz ($L_1=25\text{mm}, W_1=3\text{mm}, g=0.35\text{mm}, L_2=17\text{mm}, W_2=14\text{mm}, h=1.6\text{mm}$ and $\epsilon_r=4.4, r_1=6.3\text{mm}, W=0.9\text{mm}, d=0.6\text{mm}, t=0.5\text{mm}$) -----	147
Fig. 3.51.	Simulated surface impedance at different frequencies of the monopole antenna with single (a)1.6GHz (b)1.81GHz (c)2.2GHz strip ($L_1=25\text{mm}, W_1=3\text{mm}, L_2=17\text{mm}, W_2=14\text{mm}, g=0.35\text{mm}, L_3=26\text{mm}, W_3=9.9\text{mm}, h=1.6\text{mm}, \epsilon_r=4.4, S=4.5\text{mm}$ and $S=2\text{mm}$) -----	148
Fig.3.52.	Simulated surface impedance at different frequencies of the monopole antenna with vertical stripes (a)1.6GHz (b)1.81GHz (c)2.2GHz ($L_1=25\text{mm}, W_1=3\text{mm}, L_2=17\text{mm}, W_2=14\text{mm}, g=0.35\text{mm}, L_3=26\text{mm}, W_3=9.9\text{mm}, h=1.6\text{mm}, \epsilon_r=4.4, S=4.5\text{mm}$ and $S=2\text{mm}$) -----	148

Fig.4.1.	Transmission and reflection characteristics of a CPW transmission line (width=3mm, $\epsilon_r=4.4$,h =1.6mm) -----	157
Fig.4.2.	(a) Ground folded transmission line (b) photograph of the folded transmission line (w=3mm,g=1.7mm, $\epsilon_r =4.4$ and h =1.6mm)-----	158
Fig. 4.3.	Transmission and reflection characteristics of ground folded transmission line (w=3mm,g=1.7mm, $\epsilon_r =4.4$, h =1.6mm) -----	159
Fig.4.4.	Impedance diagram of open ended ground folded transmission line (w=3mm,g=1.7mm, $\epsilon_r =4.4$, h =1.6mm) -----	159
Fig. 4.5.	3D radiation pattern of open ended structure-----	160
Fig.4.6.	Variation of transmission coefficient for different w+2g of ground folded transmission line (w=3mm, $\epsilon_r =4.4$, h =1.6mm)-----	161
Fig.4.7.	Variation of reflection coefficient for different w+2g of ground folded transmission line (w=3mm,g=1.7mm, $\epsilon_r =4.4$, h =1.6mm)-----	162
Fig.4.8.	Geometry of(a) planar (b) folded antenna (c) photograph of the antenna ($L_1=25$ mm, $W_1=3$ mm, $L_2=17$ mm, $W_2=14$ mm, g=1.7mm,h=1.6mm, $\epsilon_r=4.4$.)-----	163
Fig. 4.9.	Reflection coefficient of the ground folded antenna ($L_1=25$ mm, $W_1=3$ mm, $L_2=17$ mm, $W_2=14$ mm,g=1.7mm,h=1.6mm, $\epsilon_r=4.4$.)-----	164
Fig. 4.10.	Effect of L_1 on reflection coefficient of the ground folded antenna ($W_1=3$ mm, $L_2=17$ mm, $W_2=14$ mm,g=1.7mm, h=1.6mm, $\epsilon_r=4.4$.)-----	165
Fig. 4.11.	Surface Current distribution of the ground folded antenna ($L_1=25$ mm, $W_1=3$ mm, $L_2=17$ mm, $W_2=14$ mm,g=1.7mm,h=1.6mm, $\epsilon_r=4.4$.)-----	166
Fig.4.12.	Measured radiation pattern of the ground folded antenna at resonant frequency (a) XZ plane (b) YZ plane ($L_1=25$ mm, $W_1=3$ mm, $L_2=17$ mm, $W_2=14$ mm,g=1.7mm,h=1.6mm, $\epsilon_r=4.4$.)-----	166
Fig.4.13.	3D radiation pattern of the ground folded antenna at resonant frequency ($L_1=25$ mm, $W_1=3$ mm, $L_2=17$ mm, $W_2=14$ mm, g=1.7mm,g=1.7mm, h=1.6mm, $\epsilon_r=4.4$.) -----	167
Fig.4.14.	Measured gain of the ground folded antenna ($L_1=25$ mm, $W_1=3$ mm, $L_2=17$ mm, $W_2=14$ mm,g=1.7mm,h=1.6mm, $\epsilon_r=4.4$.)-----	168
Fig.4.15.	Simulated Electric field distribution at resonant frequency of (a) monopole (b) folded monopole ($L_1=25$ mm, $W_1=3$ mm, $L_2=17$ mm, $W_2=14$ mm, g=1.7mm,h=1.6mm, $\epsilon_r=4.4$.) -----	168

Fig.4.16. Geometry of the ground folded monopole antenna with printed metal strip (a)side view (b) front side(c)top view(d) photograph of the antenna ($L_1=25\text{mm}$, $W_1=3\text{mm}$, $L_2=17\text{mm}$, $W_2=9.5\text{mm}$, $L_3=27\text{mm}$, $W_3=2\text{mm}$, $P=2\text{mm}$, $g=1.7\text{mm}$, $h=1.6\text{mm}$, $\epsilon_r=4.4$.) -----	170
Fig.4.17. Reflection characteristics of the GFPA with printed metal strip($L_1=25\text{mm}$, $W_1=3\text{mm}$, $L_2=17\text{mm}$, $W_2=9.5\text{mm}$, $L_3=27\text{mm}$, $W_3=2\text{mm}$, $g=1.7\text{mm}$, $h=1.6\text{mm}$, $\epsilon_r=4.4$.) -----	171
Fig.4.18. 3D Radiation pattern of the GFPA with printed metal strip for different viewing angle (a) $\phi=-180^\circ$ (b) $\phi=0^\circ$ (c) $\phi=180^\circ$ ($L_1=25\text{mm}$, $W_1=3\text{mm}$, $L_2=17\text{mm}$, $W_2=14\text{mm}$, $L_3=27\text{mm}$, $W_3=2\text{mm}$, $g=1.7\text{mm}$, $h=1.6\text{mm}$, $\epsilon_r=4.4$.)-----	172
Fig.4.19. Measured Radiation characteristics of the GFPA with printed metal strip (a)xz plane(b)yz plane ($L_1=25\text{mm}$, $W_1=3\text{mm}$, $L_2=17\text{mm}$, $W_2=9.5\text{mm}$, $L_3=27\text{mm}$, $W_3=2\text{mm}$, $g=1.7\text{mm}$, $p=2\text{mm}$, $h=1.6\text{mm}$, $\epsilon_r=4.4$.) -----	173
Fig.4.20. Effect of strip position on reflection characteristics of the GFPA with printed metal strip ($L_1=25\text{mm}$, $W_1=3\text{mm}$, $L_2=17\text{mm}$, $W_2=9.5\text{mm}$, $L_3=27\text{mm}$, $W_3=2\text{mm}$, $g=1.7\text{mm}$, $h=1.6\text{mm}$, $\epsilon_r=4.4$.) -----	174
Fig.4.21. 3 D radiation pattern of the GFPA with printed metal strip at (a) $P=0\text{mm}$, (b) $P=(-4)\text{mm}$, ($L_1=25\text{mm}$, $W_1=3\text{mm}$, $L_2=17\text{mm}$, $W_2=9.5\text{mm}$, $L_3=27\text{mm}$, $W_3=2\text{mm}$, $g=1.7\text{mm}$, $h=1.6\text{mm}$, $\epsilon_r=4.4$.) -----	175
Fig.4.22. Effect of ground width (W_2) on reflection characteristics of the GFPA with printed metal strip ($L_1=25\text{mm}$, $W_1=3\text{mm}$, $L_2=17\text{mm}$, $L_3=27\text{mm}$, $W_3=2\text{mm}$, $g=1.7\text{mm}$, $P=2\text{mm}$, $h=1.6\text{mm}$, $\epsilon_r=4.4$.) -----	176
Fig.4.23. Effect of strip width (W_3) on reflection characteristics of the GFPA with printed metal strip ($L_1=25\text{mm}$, $W_1=3\text{mm}$, $L_2=17\text{mm}$, $W_2=9.5\text{mm}$, $L_3=27\text{mm}$, $W_3=2\text{mm}$, $g=1.7\text{mm}$, $P=2\text{mm}$, $h=1.6\text{mm}$, $\epsilon_r=4.4$.)-----	177
Fig.4.24. Effect of strip length (L_3)on reflection characteristics of the GFPA antenna with printed metal strip ($L_1=25\text{mm}$, $W_1=3\text{mm}$, $L_2=17\text{mm}$, $W_2=9.5\text{mm}$, $W_3=2\text{mm}$, $g=1.7\text{mm}$, $h=1.6\text{mm}$, $\epsilon_r=4.4$.) -----	178
Fig.4.25. Effect of dielectric constant on reflection characteristic of the GFPA with printed metal strip ($L_1=25\text{mm}$, $W_1=3\text{mm}$, $L_2=17\text{mm}$, $W_2=9.5\text{mm}$, $L_3=27\text{mm}$, $W_3=2\text{mm}$, $g=1.7\text{mm}$, $h=1.6\text{mm}$.)-----	179

Fig.4.26.	Co and Cross polarization along H plane of the GFPA with printed metal strip ($L_1=25\text{mm}, W_1=3\text{mm}, L_2=17\text{mm}, W_2=9.5\text{mm}, L_3=27\text{mm}, W_3=2\text{mm}, g=1.7\text{mm}, h=1.6\text{mm}, \epsilon_r=4.4.$)-----	181
Fig.4.27.	Measured gain of the GFPA with printed metal strip ($L_1=25\text{mm}, W_1=3\text{mm}, L_2=17\text{mm}, W_2=9.5\text{mm}, L_3=27\text{mm}, W_3=2\text{mm}, g=1.7\text{mm}, P=2\text{mm}, h=1.6\text{mm}, \epsilon_r=4.4.$)-----	182
Fig 5.1.	Simulated 3D radiation patterns of Monopole antenna (a) in far field region(b)50mm (c)40mm(d)30mm(e)20mm from center of the antenna-----	196
Fig 5.2.	3D radiation patterns of Monopole antenna with SRR (a) in far field (b)50mm (c) 40mm (d)30mm (e)20mm from center of the antenna-----	197
Fig. 5.3.	3D radiation patterns Monopole antenna with singlestrip (a)farfield (b)50mm (c)40mm (d) 30mm(e) 20mm from center of the antenna-----	198
Fig. 5.4.	3D simulated radiation patterns of Monopole antenna with vertical stripes (a) in far field(b)50mm(c)40mm(d)30mm (e)20mm from center of the antenna-----	199
Fig. 5.5.	Simulated 3D radiation patterns of Ground folded monopole antenna (a) farfield (b) 50mm (c) 40mm (d) 30mm (e) 20mm from center of the antenna-----	200
Fig. 5.6.	3D simulation of Ground folded Monopole antenna with single strip (a)farfield(b)50mm(c)40mm(d)30mm(e)20mm from center of the antenna-----	201
Fig. 5.7.	SAM head model provided by CST microwave studio -----	202
Fig 5.8	Simulated electric field distribution of the antenna with head model -----	203
Fig.5.9.	Simulated SAR with planar monopole structure for different distances (a)10mm(b)20mm(c)30mm(d)40mm-----	204
Fig. 5.10.	Simulated electric field distribution of the SRR printed antenna with head model-----	205
Fig 5.11.	Simulated SAR with SRR structure for different distances (a) 10mm (b) 20mm(c)30mm(d)40mm -----	206
Fig. 5.12.	Simulated electric field distribution of the antenna with single strip and head model-----	206
Fig. 5.13.	Simulated SAR with single strip structure for different distances (b)10mm(c)20mm(d)30mm(e)40mm -----	207
Fig. 5.14.	simulated electric field distribution of the vertical stripes printed antenna with head model -----	208
Fig.5.15.	Simulated SAR with vertical stripes structure for different distances (a)10mm (b)20mm (c)30mm(d)40mm -----	209

Fig 5.16	Simulated SAR with Ground Folded monopole structure for different distances (a)10mm (b) 20mm(c)30mm(d)40mm -----	210
Fig. 5.17.	simulated electric field distribution of ground folded monopole antenna with single strip and head model -----	211
Fig. 5.18.	simulated SAR with Ground Folded monopole structure with vertical strip for different distances(a)10mm (b) 20mm(c)30mm(d)40mm-----	211
Fig. 5.19.	(a) Radial variation in E field distribution of planar monopole antenna for different distances from phantom head model edge (i)10mm (ii)20mm (iii)30mm(iv)40mm(v)50mm -----	214
Fig. 5.19.	(b) Radial variation in E field distribution of planar monopole antenna with vertical stripes for different distances from phantom head model edge (i)10mm(ii)20mm(iii)30mm(iv)40mm(v)50mm -----	215
Fig. 5.20.	(a) Radial variation in E field distribution of Ground folded monopole antenna for different distances from phantom head model edge (i)10mm (ii)20mm(iii) 30mm(iv)40mm(v)50mm-----	216
Fig.5.20.	(b) Radial variation in E field distribution of Ground folded monopole antenna with strip for different distances from phantom head model edge (i)10mm(ii)20mm (iii)30mm(iv)40mm(v)50mm -----	217
Fig 5.21.	(a)Radial variation in normalized SAR value of planar monopole antenna with and without vertical stripes (b)) Radial variation in normalized SAR value of Ground folded monopole antenna with and without strip-----	218

Abbreviations

RF	–	Radio Frequency
EMR	–	Electromagnetic radiation
EM	–	Electromagnetics
TLF	–	Tremendously Low Frequency
ELF	–	Extremely Low Frequency
SLF	–	Super Low Frequency
ULF	–	Ultra Low Frequency
LF	–	Low frequency
MF	–	Medium frequency
HF	–	High Frequency
VHF	–	Very High frequency
UHF	–	Ultra High frequency
SHF	–	Super High Frequency
EHF	–	Extremely High Frequency
THz or THF	–	Tremendously High Frequency
ITU	–	International Telecommunication Union
DNA	–	Deoxyribonucleic Acid
FM	–	Frequency Modulation
TV	–	Television
PDA	–	Personal digital assistant
PC	–	Personal Computer
GSM	–	Global System Mobile
TDMA	–	Time Division Multiple Access
PDC	–	Personal Digital Cellular
CDMA	–	Code Division Multiple Access
IEEE	–	Institute of Electrical and Electronics Engineers
1G	–	1 Generation
CPW	–	Coplanar Waveguide
FCC	–	Federal Communications Commission

GPS	– Global Positioning System
PCB	– Printed Circuit Board
PIFA	– Planar Inverted-F Antenna
PILA	– Planar Inverted-L Antenna
Q	– Quality-factor
UWB	– Ultra Wide-Band
VSWR	– Voltage Standing Wave Ratio
WiMAX	– Worldwide Interoperability for Microwave Access
WLAN	– Wireless Local Area Network
SCMSA	– short circuited rectangular microstrip antenna
BW	– backward wave
NIM	– Negative Index Material
SRR	– Split Ring Resonators
EBG	– Electromagnetic Band Gap
PBG	– Photonic Band Gap
CEM	– Computational ElectroMagnetics
FDTD	– Finite Difference Time Domain method
FEM	– Finite Element method
TLM	– Transmission Line Matrix method
MoM	– Method of Moments
EFIE	– Electric Field Integral Equation
MFIE	– Magnetic Field Integral Equation
IE	– Integral Equation
SAR	– Specific Absorption Rate
SMA	– SubMiniature version A
VNA	– Vector Network Analyzer
AUT	– Antenna Under Test
CREMA	– Center for Research in Electromagnetics and Antennas
HFSS	– High Frequency Structure Simulation
CST	– Computer simulation Technology
SAM	– Specific Anthropomorphic Mannequin
GFPA	– Ground Folded Planar Antenna

- ISM – The industrial, scientific and medical
- CP – Circularly Polarized
- LP – Linearly Polarized
- ICNIRP – International Commission on Non-Ionizing Radiation Protection
- ANSI – American National Standards Institute
- MPE – Maximum Permissible Exposure
- CENELEC – European Committee for Electrotechnical Standardization

.....❧.....

C o n t e n t s	1.1	<i>Introduction</i>
	1.2	<i>Electromagnetic radiations</i>
	1.3	<i>Glimpse through history of microwave communication</i>
	1.4	<i>Wireless communication bands</i>
	1.5	<i>Mobile phone antennas</i>
	1.6	<i>Analysis of antennas</i>
	1.7	<i>Motivation of present research</i>
	1.8	<i>Thesis organization</i>

This chapter starts with a brief overview of electromagnetic spectrum and its classification based on types of radiation. The progress in microwave communication system and various wireless communication bands used are discussed in this chapter. The different antennas, which are the most essential components of any wireless communication system, are also discussed. Various analytical techniques used for the analysis of the antenna are also addressed in this chapter. Finally the motivation behind the development of mobile antenna with reduced RF interference is presented. The chapter concludes with the description of the organization of the subsequent chapters.

1.1 Introduction

Wireless and mobile communication industry made a revolutionary remark in the 21st century with the development of modern communication equipments having ultra compact size with multi features. The driving force behind wireless communication is the promises of portability, mobility and accessibility. It has an enormous impact on daily life. ‘Antennas’ the key element in wireless communication devices had undergone amazing developments especially in the direction of compactness and safety aspects. In general, an antenna is used to either transmit or receive electromagnetic waves. It is a transition device or a transducer between a guided wave and a free space wave or vice versa. Antennas have found several important applications in the entire radio frequency range. Modern antennas or antenna systems require careful design through thorough understanding of the radiation mechanism of electromagnetic waves.

1.2 Electromagnetic radiations

Electromagnetic radiation (abbreviated as EM radiation or EMR) is a form of energy which exhibits wave like behavior and travels through space with a velocity of light. These EM waves consist of electric and magnetic components, which oscillate perpendicular to each other and moves through space at the speed of light. Different forms of electromagnetic energy are categorized by their wavelengths or frequencies. The different parts of the radio spectrum are used for different radio transmission technologies and applications as shown in Table 1.1 Radio waves and microwaves are part of this electromagnetic spectrum.

Table 1.1. Parts of Radio spectrum [1]

Band name	Abbreviation	ITU band	Frequency and wavelength in air	Example uses
Tremendously low frequency	TLF		< 3Hz, > 100,000 km	Natural man-made electromagnetic noise
Extremely low frequency	ELF		3-30Hz, 100,000 km – 10,000 km	Communication with submarines
Super low frequency	SLF		30-300Hz, 100,000 km – 1000 km	Communication with submarines
Ultra low frequency	ULF		300-3000Hz, 1000 km – 100 km	Submarine communication, Communication within mines
Very low frequency	VLF	4	3-30 kHz, 100 km – 10 km	Navigation, time signals, submarine communication, wireless heart rate monitors, geophysics
Low frequency	LF	5	30-300 kHz, 10km – 1 km	Navigation, time signals, AM longwave broadcasting (Europe and parts of Asia), RFID, amateur radio
Medium frequency	MF	6	300-3000 kHz, 1km – 100m	AM (medium-wave) broadcasts, amateur radio, avalanche beacons
High frequency	HF	7	3-30 MHz, 100m – 10m	Shortwave broadcasts, citizen's band radio, amateur radio and over –the-horizon aviation communications, RFID, Over-the horizon radar, Automatic link establishment (ALE)/Near Vertical incidence Skywave (NVIS)radio communications, Marine and mobile radio telephony
Very high frequency	VHF	8	30-300MHz, 10m-1m	FM television broadcasts and line-of-sight ground-to-aircraft and aircraft-to-aircraft communications, Land Mobile and Maritime Mobile communications, amateur radio, weather radio
Ultra high frequency	UHF	9	300-3000MHz, 1m-100mm	Television broadcasts, microwave ovens, microwave devices/communications, radio astronomy, mobile phones, wireless LAN, Bluetooth, ZigBee, GPS and two way radios such as Land Mobile, FRS
Super high frequency	SHF	10	3-30GHz, 100mm -10mm	Radio astronomy, microwave devices/ communications, wireless LAN, most modern radars, communications satellites, satellite television broadcasting, DBS, amateur radio
Extremely high frequency	EHF	11	30-300GHz, 10mm-100mm	Radio astronomy, high-frequency microwave radio relay microwave remote sensing, amateur radio directed-energy weapon, millimeter wave scanner
Terahertz or Tremendously high frequency	THz or THF	12	300-3,000GHz, 1mm-1000m	Terahertz imaging – a potential replacement for X-rays in some medical applications, ultrafast molecular dynamics, condensed-matter physics, terahertz time-domain spectroscopy, terahertz computing/communications, sub-mm remote sensing, amateur radio

1.2.1 Frequency range of spectrum

Generally, electromagnetic radiation is classified by their wavelength into radio wave, microwave, terahertz (or sub-millimeter) radiation, infrared, visible light, ultraviolet, X-rays and gamma rays. The radio frequency (RF) part of the electromagnetic spectrum is generally defined as that part of the spectrum where electromagnetic waves have frequencies in the range of about 3 kilohertz (3 kHz) to 300 gigahertz (300 GHz). In the order of increasing frequency or decreasing wavelength, different electromagnetic radiations in an electromagnetic spectrum are shown in figure 1.1

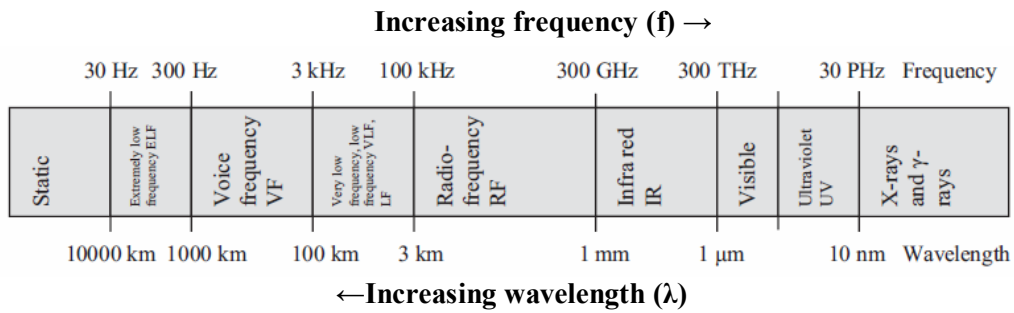


Fig.1.1. Radio waves in Electromagnetic Spectrum

According to the International Telecommunication Union (ITU) radio bands defined in the ITU Radio Regulations, states that "the radio spectrum shall be subdivided into nine frequency bands, which are designated by progressive whole numbers" [1]. The frequency bands as per ITU are shown in table 1.2. Each band is given a number, in which the number is the logarithm of the approximate geometric mean of the upper and lower band limits in Hz.

Table 1.2. ITU radio bands of the Electromagnetic spectrum

Band Number	Symbols	Frequency Range	Wavelength Range
4	VLF	3 to 30 kHz	10 to 100km
5	LF	30 to 300kHz	1 to 10km
6	MF	300 to 3000kHz	100 to 1000m
7	HF	3 to 30 MHz	10 to 100m
8	VHF	30 to 300 MHz	1 to 10m
9	UHF	300 to 3000 MHz	10 to 100cm
10	SHF	3 to 30 GHz	1 to 10cm
11	EHF	30 to 300 GHz	1 to 10mm
12	THF	300 to 3000 GHz	0.1 to 1mm

The most important use of RF energy is for telecommunications services. Radio & television broadcasting, cellular telephones, radio communications, amateur radio, microwave point-to-point links, and satellite communications are some telecommunication applications. Microwave oven, radar, industrial heating and sealing are some of the noncommunication uses of RF energy.

1.2.2 Ionizing and Non ionizing radiations

The electromagnetic radiations are divided into two types. Ionizing radiations and Non ionizing radiations. Electromagnetic radiation is designated as non-ionising when the frequency is below 10^{15} Hz (wavelength $\lambda=10^{(-8)}$ to 10^4 m) and as ionising at higher frequencies. Radiation that has energy to move atoms in a molecule around or cause them to vibrate, but not carry enough energy to remove electrons, is referred to as "non-ionizing radiation". Instead of producing charged ions when passing through matter, non-ionizing radiation induces electric fields and currents and can generate heat. Thus, this radiation is

not directly interfering with DNA but it can increase tissue temperature at high exposure [2]. Sound waves, RF signals, microwave signals, infrared light, and visible light are the examples of non ionizing radiations. Whereas ionizing radiation has enough energy to remove tightly bound electrons from atoms, thus creating ions. Ultra violet, X-ray, Nuclear and Gamma rays come under ionizing radiation and which are more harmful than non-ionizing radiation. Figure 1.2 shows different types of radiations in the electromagnetic spectrum.

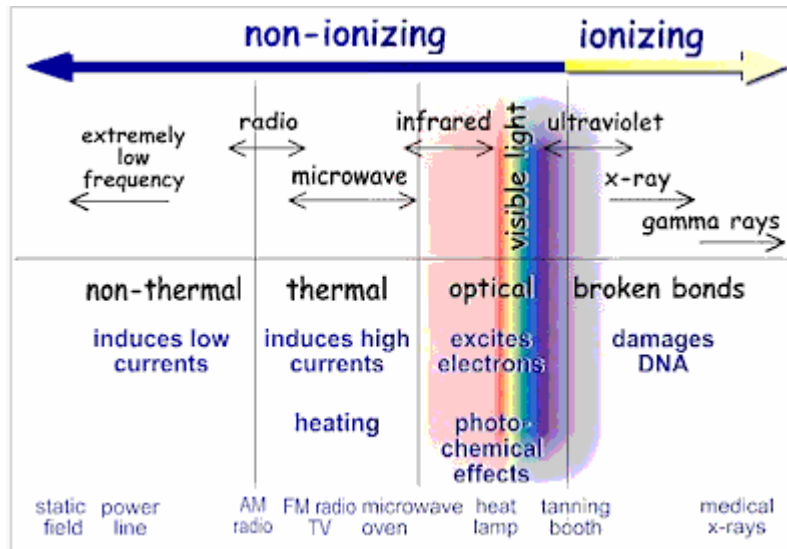


Fig 1.2. Types of radiations in Electromagnetic spectrum [3]

The electromagnetic fields have a great influence on the behavior of all living systems. Biological effects that result from heating of tissue by RF energy are often referred to as "thermal" effects. This heating effect from RF devices mainly focused on RF absorption by the head, particularly from mobile handsets. Thus the possible physiological damage in human beings from EM wave exposures is due to temperature increase. The temperature increase of 4.5 °C in the brain has been remarked to be an allowable limit,

which does not lead to any physiological damage (for exposures of more than 30 minutes) [2]. The heating effects in biological tissue escalate with the increase in frequency, even though the heat's penetration depth in the tissue decreases.

1.2.3 Exposure to RF radiation

Wireless and mobile communication is one of the fastest growing areas of modern world. It has an enormous impact on our daily life.

The biological effects and health implications of RF & microwave radiation associated with cellular mobile telephones or wireless systems have become a focus of international scientific interest. Even though our knowledge regarding the biological effects of RF and microwave radiation has increased considerably, the scientific evidence on health effects of RF and microwave radiation associated with these wireless devices is still tentative. The overall evidence from case control and cohort studies of phone usage suggests that there are large increased risks of intracranial tumors, or other cancers, in relation to cellular phone use for a long period [4]. Rising from these aspects, antenna designers have been forced to pay a growing amount of interest in reducing the radiation towards the user. The reduction of power absorbed by the user reduces potential health hazards.

1.3 Glimpse through history of microwave communication

Wireless communication history starts with Hertz when he proved Maxwell's theoretical prediction of electromagnetic waves by his classical experiments in 1880s [5]. In 1896 Guglielmo Marconi demonstrated wireless telegraph to English telegraph office [6]. In the preceding years, 1894-1900 the generation and use of millimeter wave for communication has performed by

Jagadish Chandra Bose with the first Horn antenna [7]. Over the past century research in wireless communication has witnessed remarkable revolution. The modern wireless technology allows simultaneous transmission of multiple channels of television, radio, video and audio to a range of multi-media devices including mobile phones, PDA, PCs and other handheld devices. The need to develop an efficient public mobile communication system has been driving a lot of researchers. Guglielmo Marconi gained a patent for his wireless telegraph in 1909[8]. The competitive rush to design and implement digital systems led again to a variety of standards such as GSM (Global System Mobile), TDMA (Time Division Multiple Access) PDC (Personal Digital Cellular) and CDMA (Code Division Multiple Access). In 1982 GSM group is formed which laid the foundation of the modern wireless mobile networks. The demonstration of L band digital radio and the release of first GSM specification were the key events in wireless communication history in the beginning of the 19th century. The first GSM call was made in the year 1991 in Finland and six years later the IEEE 802.11 standard also known as Wi-Fi was created [9]. The 1G analog systems of 1980's evolved into 2G digital technology in the 90's and to third generation mobile communication which includes wireless multimedia services. The 3G mobile system evolved in 2002's eliminating previous incompatibilities and became a truly global system. The forthcoming 4G mobile communication systems are projected to solve the still remaining problems of 3G systems and to provide a wide diversity of new services, from high quality voice to high definition video to high data rate wireless channels.

Milestones in the development of wireless communication are summarized in Table 1.3.

Table 1.3. Milestones in Communication [10-14]

1837	Morse demonstration of telegraph
1865	Prediction of electromagnetic wave propagation by Maxwell
1876	Alexander Graham Bell invented the Telephone
1887	The existence of Electromagnetic waves is verified by Heinrich Rudolph Hertz.
1894	Wireless telegraphy by Marconi
1895	Jagadish Chandra Bose gave his first public demonstration of electromagnetic waves.
1901	First wireless transmission by Guglielmo Marconi with his transatlantic transmission.
1906	Radio broadcasting by Fessenden
1915	Direct telephone communications opened for service.
1921	Radio dispatch service initiated for police cars in Detroit, Michigan
1924	Directive Yagi-Uda antenna developed by Prof. Hidetsugu Yagi
1927	First television transmission.
1929	Microwave communication established by Andre G. Clavier
1933	Frequency Modulation techniques by Armstrong
1934	AM (Amplitude Modulation) mobile communications systems used by state and municipal forces in the U.S
1935	RADAR by Watson Watt, Radio astronomy by Jansky
1943	The first telephone line from Calcutta, India to Kunming, China.
1944	Telephone cable laid across the English channel
1946	Radiotelephone connections made to PSTN (Public-switched telephone network), 3.7-4.2 LOS link by AT&T
1947	First Mobile phone demonstration
1953	Deep space communication proposed by John Pierce.
1957	Soviet Union launches Sputnik, humanity's first artificial satellite.
1958	Invention of Integrated Circuit
1968	Development of the cellular telephony concept at Bell Laboratories.
1979	A 62,000 mile telecommunications system is implemented in Saudi Arabia
1980	1G first generation - only mobile voice service
1981	Beginning of first commercial cellular mobile communication
1982	Two way video teleconferencing service started
1986	Integrated Service Digital Network deployed
1990	2G-Second generation digital cellular deployed throughout the world.
1995	CDMA is introduced
2000	3G Standard is proposed.
2008	ITU-R organization specified the IMT-Advanced (International Mobile Telecommunications Advanced) requirements for 4G standards.
2010	Optical communication satellite

1.4 Wireless communication bands

Different frequency bands are allotted in communication systems for different applications. This avoids the congestion during the communication process. The different frequency bands allocated by the governing council for smooth running of communication process are given in the Table1.4 with corresponding category of antenna.

Table 1.4. Wireless Communication [10-14]

Name of the Wireless Communication Service	Allocated frequency band	Commonly used Antenna
Digital Video Broadcasting (DVB-H)	470MHz-702MHz	Compact printed Antennas
Radio Frequency Identification (RFID)	865-868MHz, 2.446-2.454GHz	Loops, Folded-F, Patch and Monopole
Global System for Mobile (GSM 900)	890MHz-960MHz	Dipole, patch arrays and Monopoles.
Global Positioning System (GPS1400, GPS1575)	1227MHz -1575MHz, 1565MHz-1585MHz	Microstrip patch or bifilar helix
Digital Communication System (DCS 1800)	1710MHz-1880MHz	Dipole or patch arrays in base stations. Monopoles, sleeve dipoles and patch in mobile handset
Personal Communication System (PCS 1900)	1850MHz-1990MHz	
International Mobile Telecommunication-2000 (3G IMT-2000)	1885MHz-2200MHz	
Universal Mobile Telecommunication Systems (UMTS 2000)	1920MHz-2170MHz	
Industrial ,Scientific, Medical(ISM 2.4, ISM 5.2, ISM 5.8)	2400MHz-2484MHz, 5150MHz-5350MHz, 5725MHz-5825MHz	
Ultra Wide Band (UWB) communication	3.1GHz-10.6GHz	Planar printed antennas, Horn Antennas

1.5 Mobile phone antennas

Antenna serves as one of the critical component in any wireless communication system. They act as electronic eyes and ears to the world. Antennas are the essential communication link to space, aircraft and ships. *IEEE Standard Definitions of Terms for Antennas* (IEEE std 145-1973)[15] defines the antenna or aerial as “a means for radiating or receiving radio waves”. In the last few years, the trend of the mobile phone technology was to decrease its size and weight. Due to this trend, the antenna used for mobile handheld devices became small and light weight. These low profile antennas have non-directional radiation pattern in the horizontal plane to provide maximum coverage. But there are challenges in the antenna’s performance during the interaction with head. Therefore, antennas used in mobile hand held devices for personal communications has been recognized as a crucial element.

Monopole antennas were the best choice for the automobiles and mobile devices because of its simplicity in design with excellent radiation characteristic for mobile equipment. The antenna used for the first phone was a half wavelength monopole antenna. Nowadays this viral part of wireless gadgets has endured renovation from a metallic rod to ceramic chip, reconfigurable, active and complicated smart antenna. It can also be seen that the built-in antennas are more preferable than the half-wavelength monopole antenna.

Since antenna is the fundamental part of any wireless systems, major advancement in antenna design is required for this explosive growth of wireless devices. These antennas are used in close proximity of biological tissues of the user, it should radiate enormous power towards the user. Modern communication system requires reliable communication with less radiation towards the user.

The antenna designer must consider the following electrical characteristics while designing a mobile handset antenna.

- a) Operating frequency
- b) Return loss
- c) Bandwidth
- d) Gain
- e) Radiation pattern
- f) Antenna tuning

In addition to size of the antenna, the RF interference towards the user has to be considered.

Some of the commonly used mobile antennas are discussed in this section.

1.5.1 Monopole

The radiator frequently used in communication is some form of thin wire arranged in a linear configuration. The fundamental mobile antenna is the quarter-wavelength monopole antenna. It has a simple structure as shown in Figure 1.3. Generally, a monopole antenna consists of a thin vertical wire mounted over the ground plane, whose bandwidth increases with increase in its diameter. For a half-wavelength monopole (length $l=\lambda/2$), the maximum current amplitude occurs around the center of the monopole therefore current amplitude around the feed point is small. However, for a quarter-wavelength monopole ($l=\lambda/4$) the maximum current amplitude occurs around the feed point [16]. When a monopole of length $l= \lambda/4$ mounted above a ground plane, an image of length $\lambda/4$ is formed and it behaves as $\lambda/2$ dipole. Moreover, the $3/8$ or $5/8$ wavelengths monopole antennas have been employed for mobile terminals as they have the appropriate input impedance for matching the feed line. This antenna is also named as the “whip” antenna.

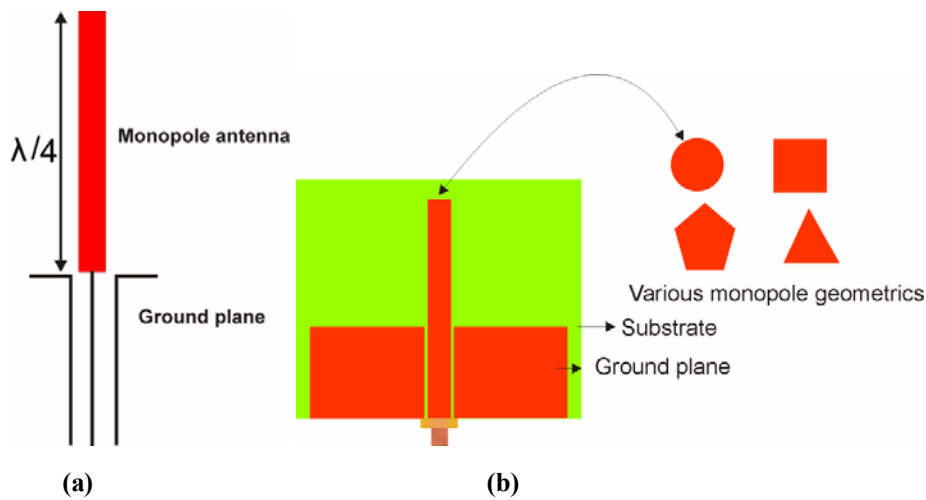


Fig 1.3. (a) Normal wire monopole with ground plane (b) Planar monopole antenna

Planar monopole antennas are popular for their large bandwidth, moderate gain with nearly omni-directional radiation characteristics. They are very attractive for wireless communication applications due to its compact nature [17,18]. The major limitations of these antennas are the ground plane size and orientation of the radiator. The geometry of a wire monopole antenna with ground plane and planar monopole antenna are shown in fig1.3(a) and fig1.3(b) respectively.

1.5.2 Normal Mode Helical Antenna

Another type of antenna with omni-directional radiation pattern used in wireless devices is helical antenna. A helical antenna consists of a single conductor or multiple conductors wound into a helical shape. In the normal mode or broadside mode, the antenna acts similarly to an electrically short dipole or monopole with maximum radiation at right angles to the helix axis. In this mode, the dimensions of the helix are small compared with the wavelength and the radiation is maximum and parallel to the helix axis. [19]. A normal helix has been used as an effective means for reducing the length of thin wire

type (whip) antennas for personal and mobile communication systems. Figure 1.4 (a) and (b) shows the structure and photograph of a helical antenna.

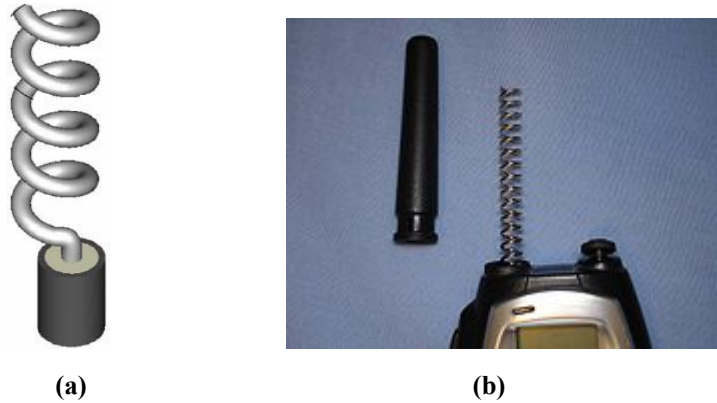


Fig 1.4. (a) Geometrical configuration (b) Photograph of a helix antenna

1.5.3 Microstrip antenna

The microstrip antennas have wide range of applications in wireless communication systems due to their great advantages. Microstrip structure consists of a thin sheet of low loss dielectric substrate. The radiating structure or antenna is printed on one side of the substrate and the other side is completely covered with a metal called ground. A typical microstrip element is illustrated in Fig. 1.5

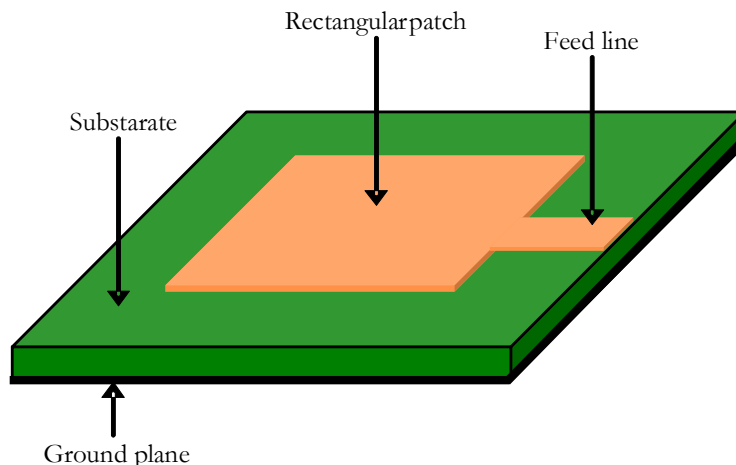


Fig 1.5. Geometry of a conventional microstrip antenna excited with a microstrip line

The advantages of microstrip antenna are

- a) Low volume and light weight
- b) Low profile planar configuration
- c) Easy fabrication
- d) Easy integration with Microwave Integrated circuits.
- e) Supports both linear as well as circular polarization
- f) Capable of multiple frequency operations
- g) Mechanically robust when mounted on rigid surfaces

On the other hand they offer some disadvantages as

- a) Narrow bandwidth
- b) Low gain
- c) Low polarization purity
- d) Excitation of surface waves

Microstrip antennas have very high antenna quality factor (Q). This large Q leads to narrow bandwidth and low efficiency. So the conventional microstrip patch is not a good candidate for the mobile wireless applications due to its inherent disadvantage of narrow bandwidth.

Different techniques are employed for reducing microstrip antenna size. Dielectric loading, top hat loading, and use of shorting pins are some of the techniques used to reduce the size and are summarised in Table 1.5 [20].

Table 1.5. Downsizing technique for microstrip antenna

Downsizing technique	Geometrical (size reduction with respect to conventional resonant size)	Impedance bandwidth enhancement ratio	Radiation pattern (symmetry vs low cross polarization)
Material: high dielectric, slow wave etc	70%	2%	High
Shorting planes: Walls, pins etc	50%	5%	Low
Patch etching: slits, slots, notches, etc	50%	7%	Medium
Multilayered:fold, bend, stack, etc	60%	10%	high

1.5.4 Planar Inverted-L Antenna

The origin of the planar inverted-F Antenna can be traced all the way back to the Inverted-L Antenna (ILA). ILA consists of a short monopole as a vertical element and a horizontal wire element attached at the end of the monopole.

The ILA is basically a low profile antenna as the height of the vertical element is usually much less than a wavelength as shown in figure 1.6(a). The horizontal element is not necessarily very short, and usually has a length of about a quarter wave length. The design is simple and can be easily manufactured on microwave substrates. Additionally, many of the electrical characteristics of the inverted-L are similar to those of the well understood short monopole. The ILA has low input impedance and its input impedance is equal to sum of the impedance of a short monopole and the impedance of the horizontal element closely placed to the ground plane [21]. Hence to increase the radiation impedance, another inverted- L element is attached to the end of the vertical element and this is how the inverted-F Antenna (IFA), as depicted in Fig. 1.6(b), is formed from the ILA.

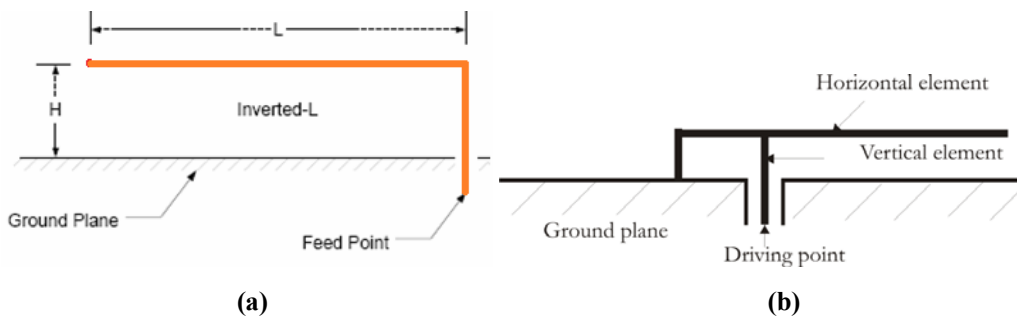


Fig. 1.6. Structure of (a) Inverted-L antenna (b) Inverted F antenna

This adjustment can be vital because the input impedance of an IFA can be set to have an appropriate value to match the circuit, without using any additional circuit between the antenna and the input. For this reason, the IFA, rather than the ILA, has been used practically and applied often to moving bodies such as rockets and aircraft due to its low profile structure. In addition to the above-mentioned features, its performance with two polarizations would be useful for urban environments. This is especially true for application on mobile equipment like the hand-held transceiver.

1.5.5 Planar Inverted-F Antenna (PIFA)

The Planar Inverted F Antenna (PIFA) is well known as terminal antenna. The small size and low profile nature of the PIFA, make it an excellent choice on portable equipment. These antennas offer reduced size over traditional microstrip antennas because it resonates at quarter wave length. PIFA consists of a top patch, ground plane, a feed wire and a shorting mechanism which shorts top patch to the ground. Typical geometry of a PIFA is shown in figure.1.7. The PILA/PIFA can be considered as a combination of the inverted-L/F (ILA/IFA) antenna and the short circuited rectangular microstrip antenna (SCMSA). The shorting mechanism makes it a quarter wave resonator and reduces the electrical length. Bandwidth of the antenna can be enhanced by increasing the

height, the width of the shorting plate and width of the radiating patch. [22]. Stacking and insertion of slits are included in PIFA's to create multiband operation [23-24]. Table 1.6 summarizes the effect of different PIFA design parameters (height, width, length, location of feed and shorting pin / wall and size of the ground plane) and its radiation characteristics.

Table 1.6. The effect of PIFA parameters on its characteristics

Parameters	Effect
Height	Control bandwidth
Width	Impedance matching
Length	Increase inductance of the antenna and determine resonance frequency
Width of short strip	Affect on the antiresonance and increase bandwidth
Feed position from short strip	Affect on resonance frequency and bandwidth

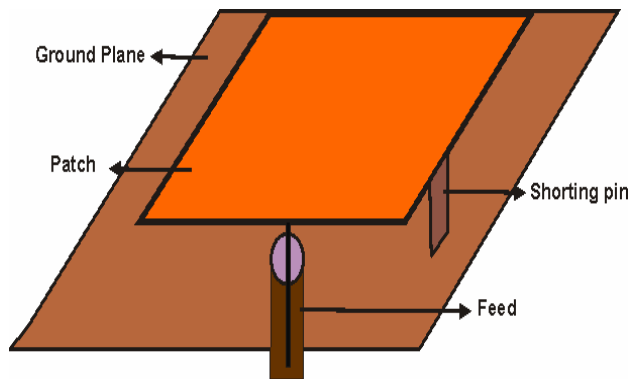


Fig.1.7. Structure of Planar Inverted-F Antenna

The mechanical stability, the requirement of precise position between feed pin connection and short circuited plate to obtain input impedance of 50 ohm, is another problem in the practical application of PIFAs.

1.5.6 Metamaterial based antenna

Recently there has been a growing interest in metamaterials with negative permittivity and permeability as candidates for design of novel microwave devices. An electromagnetic wave propagating through such material has a Poynting vector anti-parallel with its phase-velocity vector as demonstrated theoretically by Veselago [25]. Such materials have been termed by several names including “left handed” [26]–[29], “negative refractive index” [30], “negative phase velocity” [31] and “backward wave (BW) media” [32], [33]. Such materials have been realized in the microwave range by Smith *et al.* [25], [26]. An application of Negative Index Material (NIM) to increase the power radiated from electrically small antennas has been suggested by Ziolkowski and Kipple [34]. Moreover, Engheta recently proposed [35] the use of NIMs to design thin sub-wavelength cavity resonators.

This interest has come from the demonstration that specific sub-wavelength structures, that is, structures having electrically small dimensions compared to the wavelength, can exhibit effective permeability which can be tuned to negative values over a finite frequency range. A negative permittivity medium can be obtained by arranging thin metallic wires periodically [36], [37]. The continuous wire structure behaves like a high-pass filter which means that the effective permittivity will take negative values below the plasma frequency [36]. However, for discontinuous wire structures, the negative permittivity region does not extend to zero frequency, and there appears a stopband around the resonance frequency. In 1999, Pendry *et al.* have suggested that an array of Split Ring Resonators (SRRs) might exhibit a negative effective magnetic permeability for frequencies close to the resonance frequency of these structures [27]. By combining these SRRs and thin wires, Smith *et al.* reported the first experimental demonstration of left-handed metamaterials. [29].

1.5.7 Electronic Band gap structure antennas

The Electromagnetic Band Gap (EBG) structure, also referred to as a Photonic Band Gap (PBG) structure or a high-impedance surface, has attracted the scientists recently. Extensive studies in applying its band gap phenomena for practical uses both in the optical domain and microwave & millimeter wave areas has been reported. An EBG structure is a periodic, normally dielectric structure with certain geometry and dimensions, exhibiting in its spectral behavior so called band gap, a range of frequencies, at which electromagnetic waves are not allowed to propagate in the structure. The EBGs have already been widely exploited for antenna related applications. They were used as substrates, superstrates and coatings for shaping and improving the radiation characteristics of antennas of different types [38]-[40]. In particular, their ability of confining and guiding electromagnetic energy has opened up new applications and solutions in microwave and optical devices design. These novel concepts can be realized in EBGs with cavities or defects [41] which can function as resonators, waveguides. Point defects in EBGs were applied to antennas in order to achieve larger directivities and higher efficiencies [42].

1.6 Analysis of antennas

The art of computation of electromagnetic problems has grown exponentially during the last three decades due to the availability of powerful computer resources. Computational ElectroMagnetics (CEM) an important field in the design and modeling of communication systems, medical imaging, radar, antenna and cellular handset antenna. CEM typically solves the electromagnetic problem of computing the E (Electric) and H (Magnetic) fields across its domain. System modeling involving electromagnetic wave interactions based on frequency domain techniques [43-44] and integral equation method [45-46]

or time domain techniques such as Finite Difference Time Domain method (FDTD). Frequency domain numerical solutions are achieved by approximating the relevant differential or integral equations and solving large matrix equations. But differential equation solutions such as Finite Difference Method (FDM) and Finite Element method (FEM) are the easiest techniques to implement. The family of EM analysis techniques for the solution of Maxwell's equations is shown in the figure 1.8.

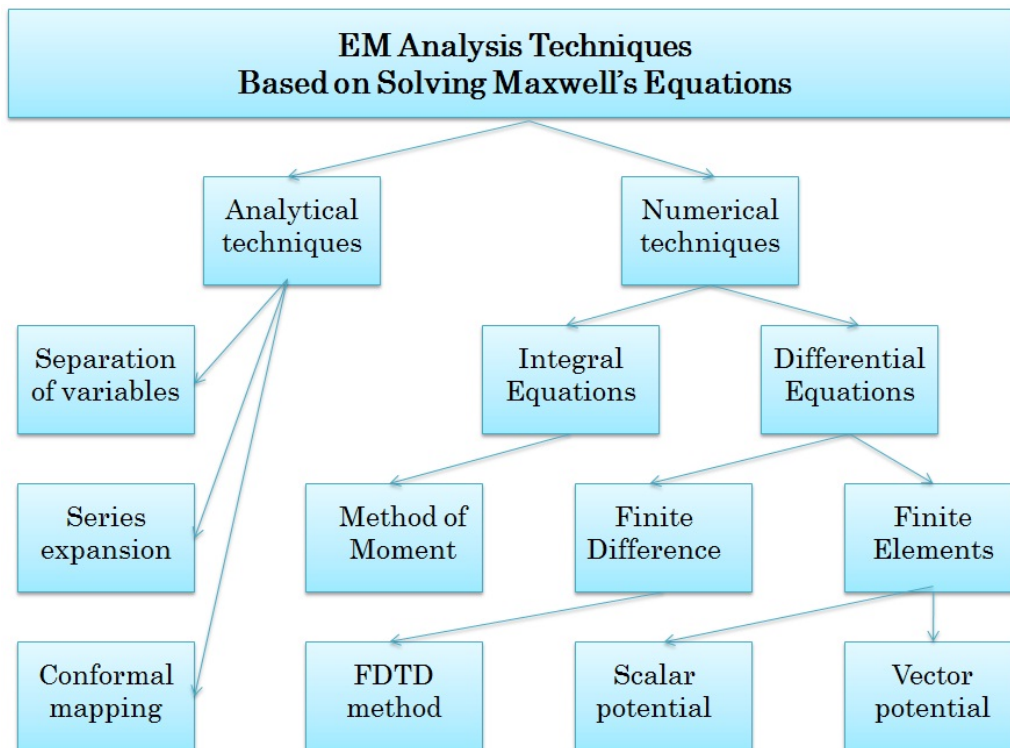


Fig.1.8. Family of EM analysis techniques

Operating principle and design characteristics of an antenna can be studied using antenna analysis. Target geometry, electrical parameter and excitation used in the structure should be defined prior to the antenna analysis. The analysis of a microwave circuit can be considered as shown in figure.1.9.

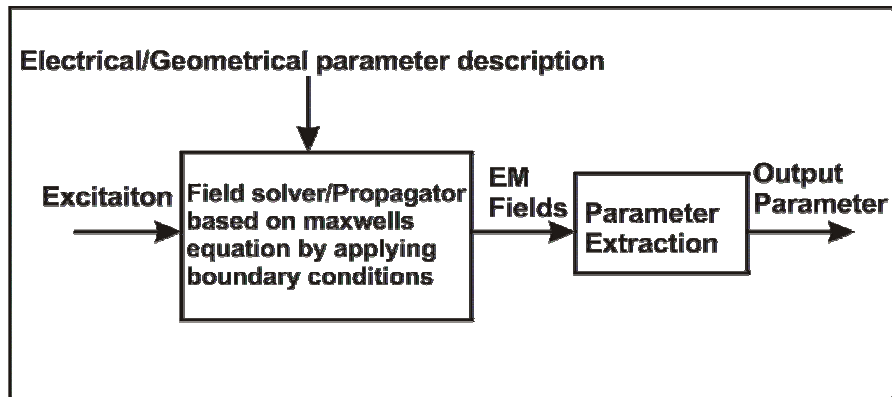


Fig.1.9. Analysis of a microwave circuit

Transmission line model, cavity model and multi port network model are used for the analysis. Full wave method for the analysis of an antenna, solves Maxwell's equation subject to boundary conditions at the interface. Different methods for the analysis of antennas are described in the following sections

1.6.1 Transmission Line Matrix method (TLM)

The transmission line matrix method was originally developed by Johns and Beurle [47]. It replaces the structure by a mesh, either 2D or 3D. The nodes of the grid are interconnected by virtual transmission lines. Excitation at the source nodes propagate to adjacent nodes through the transmission lines at each time step. Generally, dielectric loading is accomplished by loading nodes with reactive stubs, whose characteristics impedance is appropriate for the amount of loading desired. Lossy media can be modeled by introducing loss into the transmission line equations or by loading the nodes with lossy stubs. Absorbing boundaries are constructed in TLM meshes by terminating each boundary node transmission line with its characteristics impedance. Analysis is performed in the time domain. Complex, nonlinear materials are readily modeled, impulse responses and time-domain behavior of the systems are determined explicitly. The technique is suitable for implementation on massively parallel machines.

But, voluminous problems using fine grids require excessive amounts of computation. TLM method shares the advantages and disadvantages of the FDTD method, and discussed later.

1.6.2 Method of Moments (MoM)

The use of MoM for solving electromagnetic structures became popular by the work of Richmond in 1965 and Harrington in 1967[48-49]. MoM is a method of solving a differential equation or an integral equation numerically by transforming the equation into simultaneous equations. Regarding antenna analysis integral equation for electric field on the surface of the conductor is usually used to obtain the surface current on the antenna. The substrate and ground plane are assumed to be infinite in lateral dimensions and formulation of the problem is based on rigorously enforcing the boundary condition. In Electric Field Integral Equation (EFIE) the boundary condition is applied to the total tangential electric field where as in Magnetic Field Integral Equation (MFIE) boundary condition is expressed in terms of magnetic field. Mixed Potential Integral Equations (MPIE) has both scalar and vector potentials in its formulation [50]. The integral equation is then solved either in spectral domain or spatial domain by taking appropriate transformations. The procedure for applying MoM to solve an electromagnetic problem involves four steps:

- Derivation of the appropriate integral equation (IE)
- Conversion (discretization) of the IE into a matrix equation using basis (or expansions) functions and weighting (or testing) functions.
- Evaluation of the matrix elements
- Solving the matrix equation and obtaining the parameters of interest.

To solve Integral Equation it is discretised into set of linear equations by means of moment method. By solving the matrix equation the surface current on the patch conductor can be obtained which is then used for extracting the radiation pattern, polarization, directivity etc. MoM depends upon expanding the unknown quantity in the equation in terms of known entire domain or sub domain basis functions with unknown coefficients. The selection of basis function is very important step in the numerical solution since they have the ability to accurately represent and resemble the anticipated unknown function while minimizing computational effort [51-53]. The popularly used basis functions are piece wise sinusoidal, pulse basis and roof top basis functions. A set of equations is generated by enforcing the boundary conditions with a suitable set of testing functions. This results in a matrix whose order is proportional to the number of segments on which the current distribution is represented. The solution to the problem is found by inverting this matrix.

1.6.3 Finite Element Method (FEM)

The mathematical concept of FEM was provided by Courant in 1943[54]. This concept was not in use to EM problems until 1968. The FEM is used for finding the approximate solution of Partial Differential Equations (PDEs) and Integral Equations (IEs). FEM uses a volumetric approach which requires the entire volume of the configuration to be meshed as opposed to surface integral techniques, which require only the surfaces to be meshed. The properties of the neighboring mesh elements are entirely different. In general, the FEM is a good choice for solving PDEs over complex domains or when the desired precision varies over the entire domain. . However, unbounded radiation problems are not handled as effectively as MoM. It uses both tetrahedral and prismatic elements to mesh the structure.

The FE analysis of any problem involves basically four steps [55]:

- a) Discretizing the solution region into a finite number of sub-regions or elements;
- b) Deriving governing equations for a typical element;
- c) Assembling of all elements in the solution region; and
- d) Solving the system of equations obtained.

The major weakness of FEM is that it is relatively difficult to model open configurations. However, in finite element methods, the electrical and geometric properties of each element can be defined independently. This permits the problem to be set up with a large number of small elements in regions of complex geometry and fewer but large elements in relatively open regions. Thus it is possible to model configurations that have complicated geometries and many arbitrarily shaped dielectric regions in a relatively efficient manner

1.6.4 Finite Difference Time Domain (FDTD) method

The Finite Difference Time Domain (FDTD) technique is arguably the most popular numerical method for the the solution of problem in electromagnetic. First proposed K.S.Yee in 1966 [56] and refined and reinvented by Taflove [57] in the 1970's. The FDTD method belongs in the general class of differential time -domain numerical modeling methods. Maxwell's (differential form) equations are simply modified to central-difference equations, discretised, and implemented in software. The electric field is solved at a given instant in time. Then the magnetic field is solved at the next instant in time, and the process is repeated over and over again. This method permits the modelling of electromagnetic wave interactions with a level of detail as high as that of the Method of Moments. Each field component is

updated with the knowledge of the immediately adjacent field components calculated one-half time step earlier. Therefore, overall computer storage and running time requirements for FDTD are linearly proportional to the number of field unknowns in the finite volume of space being modelled. FDTD method is well known in the field of Computational Electromagnetics. FDTD is a time domain technique, and when a time domain pulse (Gaussian pulse) is used as the source pulse, then a wide frequency range is solved with only one simulation. The displacement between electric and magnetic field components in Yee's FDTD, is modified by Chen et al. [36]. This new formulation is exactly equivalent to the symmetric condensed node model used in the TLM method. Thus the TLM algorithm can be formulated in FDTD form and vice versa. However, both algorithms have their unique advantages. FDTD is a very versatile modeling technique and parameters are directly introduced, while the modeling of boundaries and the partitioning of the solution region can be done easily in TLM. The selection of algorithm for numerical investigation is completely user dependent.

1.7 Motivation of present research

The thesis is the outcome of the experimental and simulation investigations on mobile antennas with less radiation hazards. In the last two decades, the use of the cellular phones has become the most popular mode of communication across the globe and it is the most common media used for making connections with different people. Due to the rapid growth in the use of mobile phones and other wireless communication systems, there is a great concern about the harmful radiation from these devices. Rising from these aspects, antenna designers have been forced to pay a growing amount of interest in reducing the radiation absorbed by the user. The reduction of power absorbed by the user reduces potential health hazards. Protect users against radiations

from cellular phones can be achieved in two ways either by reducing the emitted power of electromagnetic radiations towards the user to a minimum value or by limiting the time of exposure to such fields. The latter condition depends largely on the user. The former condition of cutting down the amount of radiation power absorbed by the user's head can be met by modifying the omnidirectional radiation pattern of the antennas used in cellular phones. The near field characteristics of these antennas are also studied to determine the interaction between the human head with antennas.

The main objectives of the thesis are

- The experimental and simulation investigations on the possibility of resonance of a coplanar wave guide fed monopole antenna by varying the signal strip and ground plane dimension.
- Create mobile antenna by modifying the radiation characteristics of a CPW fed monopole antenna with less radiation towards a single quadrant (users head) using a parasitic element.
- Study the radiation characteristics of antenna with different parasitic elements using both simulation and experiment.
- Modify an Open Ended planar Transmission line into a ground folded transmission line.
- Design a more compact antenna to steer the null using folding technique.
- Create a ground folded antenna with modified radiation characteristic by the introduction of a single strip as a parasitic element without affecting the compactness.

- Study the experimental and simulation investigations on near field radiation characteristics.

1.8 Thesis organization

The thesis comprises of six chapters.

Chapter 1 describes an overview of antenna research, state of the art of technologies in antennas, radiation effects due to such antennas and finally the motivation of present research.

Chapter 2 Illustrate the antenna fabrication method and the experimental facilities utilized. The measurement methods employed to study the characteristics of the antenna in the near and far field are presented in this chapter. It also provides a thorough review of planar antennas and mobile antenna with reduced Specific Absorption Rate.

Chapter 3 deals with the development of a mobile antenna with less radiation towards human head. Figure of eight radiation characteristics of the coplanar wave guide fed monopole antenna is modified to produce a pattern with a single null. This modification in radiation characteristics is studied for different parasitic structures. The design criteria and parametric analysis are also presented.

The development of an antenna by modifying the ground plane to change the direction of null is discussed in chapter 4. The modification of an Open Ended Coplanar Waveguide Transmission line into an effective open ended ground plane folded transmission line is elaborately described in this chapter. A ground folded mobile antenna operating in the GSM 1800 band with radiation characteristics suitable for mobile handset is also elaborately presented and discussed.

The near field radiation characteristics of the proposed antennas are studied in detail in Chapter 5. In this chapter both the simulation and measured results in the near field region of the antenna are discussed. Antenna characteristic and Specific Absorption Rate (SAR) with head model are also presented in this chapter.

Chapter 6 describes conclusions of the thesis. The scope for future works is also described.

Other major works carried out during the research period is given in appendix.

Appendix 1 gives the design of a compact asymmetric coplanar strip fed antenna for wide band applications.

Appendix 2 gives the development of a compact CSRR based patch antenna for wireless applications.

References

- [1] http://en.wikipedia.org/wiki/Radio_spectrum
- [2] A. Hirata and T Shiozawa, "Correlation of maximum temperature increase and peak SAR in the human head due to handset antennas" IEEE Transactions on Microwave theory and techniques, Vol. 51, No. 7, pp1834-1841. , July 2003
- [3] http://en.wikipedia.org/wiki/Non-ionizing_radiation
- [4] James C Lin "Advances in electromagnetic fields in living systems " volume 5 publication Springer
- [5] Jack Ramsay "Highlights of antenna history", IEEE Antennas and Propagation Society Newsletter, pp. 8-20, December 1981.
- [6] W.J.G Beynon, "Marconi, radio waves and the ionosphere", radio science, vol.10, no.7, pp 657-664, July 1975.
- [7] John D. Kraus, "Antennas since Hertz and Marconi", IEEE Trans. Antennas and Propagat. vol.33, no.2, pp 131-136, February 1985.
- [8] Andy D. Kucar, "Mobile radio: An overview", IEEE communications magazine, pp 72-85, November 1991.
- [9] Blake, G. G. "History of Radio Telegraphy and Telephony" London: Chapman & Hall, 1928 (reprinted by Arno Press, 1974).
- [10] John D Kraus and Ronald J Marhefka, "Antennas and Wave propagation", Tata McGraw hill, 2010
- [11] Tapan K Sarkar, "History of Wireless" , John Wiley and Sons
- [12] M.Salazar Palma, T K Sarkar and D Sengupta "A chronological of development of wireless communication and electronics from 1921-1940"IEEE Antennas propagation Soc Int. Symp, Boston, vol.1 pp2-5 July 2001.

- [13] Bernard Sklar, "Digital Communication-Fundamentals and Applications" Pearson Education Asia 2nd edition 2003
- [14] Dr.Kamilo feher "Wireless Digital Communications-Modulation and spread spectrum applications" Prentice Hall of India edition 2005
- [15] Constantine A Balanis "Antenna theory analysis and design" John wiley & sons Inc 2005
- [16] John D. Kraus, Antennas Mc. Graw Hill International, second edition, 1988
- [17] Antenna system guide,NIJ Guide 202-00,pp 17-26
- [18] Kuo, J.-S.; Huang, C.-Y "Triple-frequency planar monopole antenna for side feed communication device on GSM/DCS/PCS operation" IEE Electronics Letters, Vol.42, pp. 268-270, 2006.
- [19] Liang, X.-L.; Zhong, S.-S.; Wang, W. "Elliptical planar monopole antenna with extremely wide bandwidth", IEE Electronics Letters, Vol.42, No.8, pp.441-442, 2006
- [20] X.Zhang,J.Fang,y.Liu and K.K Mei, "Calculation of dispersive characteristics of Microstrips by time domain finite difference method", IEEE Trans. Mirowave theory and tech. vol 36,pp.263-267,1988.
- [21] Richard C Johnson, Henry Jasik "Antenna Engineering Handbook" Second edition Mc Graw Hill book company
- [22] Yi-Fang Lin, Hua-Ming Chen, Che-Yen Lin, and Shan-Cheng Pan "Planar Inverted-L Antenna With a Dielectric Resonator Feed in a Mobile Device" IEEE Transactions on Antennas and propagation" Vol. 57, No. 10,pp3342-3346, , October 2009
- [23] "Design of Conformal Antennas for Telephone Handsets" Thesis by Andrew James Causley, University of Queensland.

- [24] Benito sanz Izquierdo, John C.Batchelor, Richard J.Ingley and Mohammed I.Sobhy, “Single and Double layer planar multi band PIFAs”, IEEE Transactions on Antennas and Propagat,vol.54, no.5, pp 416-422, May 2006.
- [25] V. G. Veselago,“The electrodynamics of substances with simultaneously negative values of permittivity and permeability,” Sov. Phys. Uspekhi, vol. 10, pp. 509–514, 1968.
- [26] R. A. Shelby, D. R. Smith, S. C. Nemat-Nasser, and S. Schultz, “Microwave transmission though a two-dimensional, isotropic, left-handed metamaterial,” Appl. Phys. Lett., vol. 78, pp. 489–491, 2001.
- [27] R. A. Shelby, D. R. Smith, and S. Schultz, “Experimental verification of a negative index of refraction,” Sci., vol. 292, no. 5514, pp. 77–79, 2001.
- [28] D. R. Smith, W. J. Padilla, D. C. Vier, S. C. Nemat-Nasser, and S. Schultz, “Composite medium with simultaneously negative permeability and permittivity,” Phys. Rev. Lett., vol. 84, no. 18, pp. 4184–4187, May 2000.
- [29] D. R. Smith and N. Kroll, “Negative refractive index in left-handed materials,” Phys. Rev. Lett., vol. 85, no. 14, pp. 2933–2936, Oct. 2000.
- [30] J. B. Pendry, “Negative refraction makes a perfect lens,” Phys. Rev. Lett.,vol. 85, pp. 3966–3969, 2000.
- [31] Lakhtakia, M. W. McCall, and W. S. Weiglhofer, “Brief overview of recent developments on negative phase-velocity mediums (alias left-handed materials),” Int. J. Electron Commun. (AEU), vol. 56, pp. 407–410, 2002.
- [32] V. Lindell, S. A. Tretyakov, K. I. Nikoskinen, and S. Ilevonen, “BW media-media with negative parameters, capable of supporting backward waves,” Microwave Opt. Tech. Lett., vol. 31, no. 2, pp. 129–133, Oct. 2001.

- [33] V. Lindel and S. Ilvonen, "Waves in a slab of uniaxial BW medium," *J. Electromagn. Waves Appl. (JEMWA)*, vol. 16, no. 3, pp. 303–318, 2002.
- [34] R. W. Ziolkowski and A. D. Kipple, "Application of Double Negative Materials to Increase the Power Radiated by Electrically Small Antennas," *IEEE Transactions on Antennas and Propagation*, Vol. 51, No. 10, pp. 2626–2640, October 2003.
- [35] N. Engheta, "An Idea for Thin Subwavelength Cavity Resonators Using Metamaterials With Negative Permittivity and Permeability," *IEEE Antennas and Wireless Propagation Letters*, Vol. 1, No. 1, pp. 10–13, 2002.
- [36] J. B. Pendry, A. J. Holden, W. J. Stewart, and I. Youngs, "Extremely low frequency plasmons in metallic mesostructures," *Phys. Rev. Lett.*, vol. 76, no. 25, pp. 4773–4776, June 1996.
- [37] J. B. Pendry, A. J. Holden, D. J. Robbins, and W. J. Stewart, "Magnetism from conductors and enhanced nonlinear phenomena," *IEEE Trans. Microwave Theory Tech.*, vol. 47, pp. 2075–2084, Nov. 1999
- [38] M. M. Sigalas, C. T., K. M. Ho, and C. M. Soukoulis, "Metallic photonic band gap materials," *Phys. Rev. B*, vol. 52, no. 11 744, Oct. 1995.
- [39] Gonzalo, R., I. Ederra, C. M. Mann, and P. de Maagt, "Radiation properties of terahertz dipole antenna mounted on photonic crystal," *Electronics Letters*, Vol. 37, No. 10, 613–614, May 2001.
- [40] Kesler, M. P., J. O. Maloney, and B. L. Shirley, "Antenna design with the use of photonic band-gap materials as all-dielectric planar reflectors," *Microwave and Opt. Technology Lett.*, Vol. 11, No. 4, 169–174, 1996.
- [41] Khromova, I., R. Gonzalo, I. Ederra, and P. de Maagt, "Resonance frequencies of cavities in three-dimensional electromagnetic band gap structures," *Journal of Appl. Phys.*, Vol. 106, No. 1, 1–7, 2009.

- [42] Cheype, C., C. Serier, M. Thevenot, T. Monediere, A. Reinex, and B. Jecko, "An electromagnetic bandgap resonator antenna," *IEEE Trans. Antennas Propag.*, Vol. 50, No. 9, 1285-1290, 2002.
- [43] Keller J.B., "Geometrical Theory of Diffraction" *J. Optical Society of America* vol.52, pp. 116-130, 1962.
- [44] Kouyoumjian R.G and P.H Pathak "A uniform geometrical theory of diffraction for an edge in a perfectly conducting surface", *Proc. IEEE* vol.62, 1974, pp 1448-1461.
- [45] Constantine A Balanis., "Advanced Engineering Electromagnetics," John Wiley and Sons, USA, 1989.
- [46] Umashankar K.R., "Numerical analysis of electromagnetic wave scattering and interaction based on frequency domain integral equation and method of moments techniques" *Wave motion*, Vol.10, pp.493-525, 1988.
- [47] P. B. Johns and R. L. Beurle, "Numerical solutions of 2-dimensional scattering problems using a transmission-line matrix," *Proc. Inst. Elec.Eng.*, vol. 118, pp. 1203–1208, Sept. 1971.
- [48] J.H. Richmond, "Digital computer solutions of the rigorous equations for scattering problems," *Proc. IEEE*, Vol. 53, pp. 796–804, Aug. 1965
- [49] Constantine A Balanis., "Advanced Engineering Electromagnetics," John Wiley and Sons, USA, 1989.
- [50] Mosig, J.R., "Arbitrarily shaped microstrip structures and their analysis with a mixed potential integral equation", *IEEE Trans.*, MTT-36, pp. 314-323, 1988.
- [51] R.Mitra and C.A Klein, "Stability and Convergence of Moment Method solutions", in *Numerical and Asymptotic Techniques in Electromagnetics*, R.Mitra (Ed.), Springer Verlag, New York, Chapter 5, pp 129-163, 1975.

- [52] T.K Sarkar, "A Note on the choice of weighing functions in the Method of Moments", IEEE Trans. Antennas and Propogat., Vol. AP-33,no.4,pp 436-441, April 1985.
- [53] T.K Sarkar, A.R Djordjevic and E.Arvas, "On the choice of expansion and weighing function in the solution of operator equations", IEEE Trans. Antennas and Propogat. Vol AP-33,no.9,pp 988-996, September 1985.
- [54] "The finite element method part 1 R L Courant Historical corner" Antenna propagation magazine Vol.49.issue 2 pp180-182, April 2007.
- [55] "Design and performance enhancement of cellular handset antennas and assessment of their EM interaction with a human" Thesis by Salah Ismaeel Yahya Al-Mously, August 2009.
- [56] K.S.Yee, "Numerical solution of initial boundary value problems involving Maxwell's equations in isotropic media," IEEE Trans. Antennas Propagat., Vol.14, no.4, pp.302-307, May 1966
- [57] Allen.Taflove, "Numerical issues regarding finite-difference time-domain modelling of Microwave structures," Time-Domain Methods for Microwave structures – Analysis and Design, Ed.Tatsuo Itoh and Bijan Houshmand, IEEE Press.

.....❧.....

METHODOLOGY AND ANTENNA REVIEW

C o n t e n t s	2.1	<i>Fabrication of the proposed antenna</i>
	2.2	<i>Antenna measurement facilities</i>
	2.3	<i>Measurement procedure</i>
	2.4	<i>Planar Near field measurement set up</i>
	2.5	<i>Cavity perturbation method for dielectric constant measurement of phantom equivalent liquid</i>
	2.6	<i>Electromagnetic simulation tools</i>
	2.7	<i>Planar antennas-Review</i>
	2.8	<i>Mobile antenna with reduced user interference –review</i>
	2.9	<i>Chapter conclusion</i>

This chapter describes the experimental and simulation facilities utilized to characterise the behavior of a mobile antenna in the near and far field were presented. The proposed antennas were fabricated using the photolithographic facility. The antenna characteristics such as return loss, radiation pattern and gain measurements were carried out at our test facility consisting of vector network analyzer and anechoic chamber. The Finite Element Method (FEM) based Ansoft High Frequency Structure Simulator (HFSS) and SAM head model provided by CST microwave studio were employed, for simulation studies and SAR estimation. A PIC based probe mounted scanner is used for near field study. A concise description of the measurement techniques employed to analyze the experimental results are also included. The chapter concludes with the literature survey of Coplanar Waveguide fed antennas and mobile antennas with reduced user interference.

2.1 Fabrication of the proposed antenna

Proper selection of substrate material is the essential part for the design of planar antennas. As frequency of operation increases, the loss tangent of the material used for substrates slightly increases, which in turn adversely affect the efficiency of the antenna. The power handling capability of the antenna also depends on the substrate materials also. A variety of substrate materials are available in the market. Polytetrafluoroethylene (PTFE), polystyrene, polyolefin, polyphenylene, alumina, sapphire, quartz, ferromagnetic, rutile and semiconductor substrates permit considerable flexibility in the choice of substrates. For the antenna design at the microwave frequencies substrates such as PTFE and quartz can be preferred for good radiation efficiency. These offer excellent electrical performance, but the substrate costs are often too high. Flexible substrate materials are also available, so that the antenna can be mounted on curved surfaces. The selection of dielectric constant of the substrate depends on the application of the antenna and the radiation characteristics specifications. It is worth noting that high dielectric constant substrates cause surface wave excitation and low bandwidth performance. This will generate spurious radiations in unwanted directions from the antenna. The low cost and easily available substrate material like FR4 epoxy substrate can also be used for initial studies.

After the proper selection of the substrate material, a computer aided design of the geometry is made and a negative mask of the geometry to be generated is printed on a butter paper. The double side copper cladded substrate of suitable dimension is properly cleaned using acetone and dried in order to avoid discontinuities caused by the impurities. Any disparity in the etched structure will shift the resonant frequency from the predicted values, especially when the operating frequency is very high. One side of the substrate is made liquid proof by covering it with plastic sealing tape. A thin layer of negative

photo resist material is applied on the opposite side using spinning technique and is allowed to dry.

The negative mask is placed just above it without any air layer and exposed to ultra violet radiation. The layer of photo-resist material in the exposed portions hardens. Now the board is immersed in developer solution for few minutes. The hardened portions will not be washed out by the developer solution. The board is then dipped in the dye solution in order to clearly view the hardened photo resist portions on the copper coating. After the developing phase the unwanted copper portions are etched off using Ferric Chloride (FeCl_3) solution to get the required antenna geometry on the substrate. The etched board is rinsed in running water to remove any remaining etchant. FeCl_3 dissolves the copper parts except underneath the hardened photo resist layer after few minutes. The laminate is then cleaned carefully to remove the hardened photo resist using acetone solution. The same procedure and steps were repeated on the other side of the substrate. The various steps involved in the fabrication process are illustrated in figure 2.1. The SMA connector is carefully soldered to the structure at the precise position.

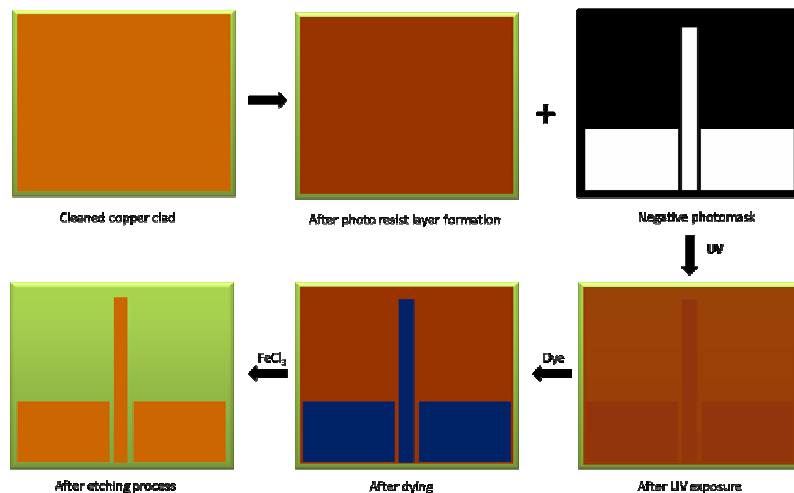


Fig. 2.1. Various steps involved in the fabrication process

2.2 Antenna measurement facilities

A brief description of equipments and facilities used for the measurements of antenna characteristics is presented in this section. Antenna radiation characteristics such as return loss, radiation pattern and gain are measured using HP8510C Vector Network Analyser and associated setup. The indigenously developed CREMA SOFT is used for the automatic measurement and data acquisition using HP 8510C Network analyzer. The important systems used for the antenna characterization are Vector network Analyzer, Anechoic Chamber, Automated turn table etc.

2.2.1 HP 8510C Vector Network analyzer (VNA)

This is a sophisticated Vector Network Analyzer (VNA) from Hewlett Packard with time domain operation capability [1]. The 32 bit microcontroller MC68000 based system can measure the magnitude and phase of the two port network parameters such as s_{11} , s_{12} , s_{21} and s_{22} very accurately. The inbuilt signal processing algorithms of the network analyzer processes the transmit and receive data and displays the results in many plot formats. The network analyzer consists of microwave source, S parameter test set, signal processor and display unit. The synthesized sweep generator HP 83651B uses an open loop YIG tuned element to generate the RF stimulus. It can synthesize frequencies from 10 MHz to 50 GHz. The frequencies can be set in step mode or ramp mode depending on the required measurement accuracy. The antenna under test (AUT) is connected to the two port S parameter test set unit, HP8514B. The forward and the reflected wave at the port are then down converted to an intermediate frequency of 20MHz and fed to the detector. These signals are suitably processed to display the magnitude and phase information in the required format. The constituent modules are interconnected

using GPIB system bus. An in-house developed MATLAB based data acquisition system coordinates the measurements and saves the data in the text format.

2.2.2 Agilent E8362B PNA

The Agilent E8362B is a member of the PNA series network analyzer platform and provides the combination of speed and precision for the demanding needs of today's high frequency, high performance component test requirements. The PNA Series meets these testing challenges by providing the right combination of fast sweep speeds, wide dynamic range, low trace noise and flexible connectivity. The operating frequency of the system is from 10 MHz to 20 GHz. It has 16,001 points per channel with $< 26 \mu\text{sec/point}$ measurement speed. This analyzer is used for the reflection coefficient studies. The measurement setup and the specifications of the PNA are depicted in figure 2.2 and table2.1 respectively.

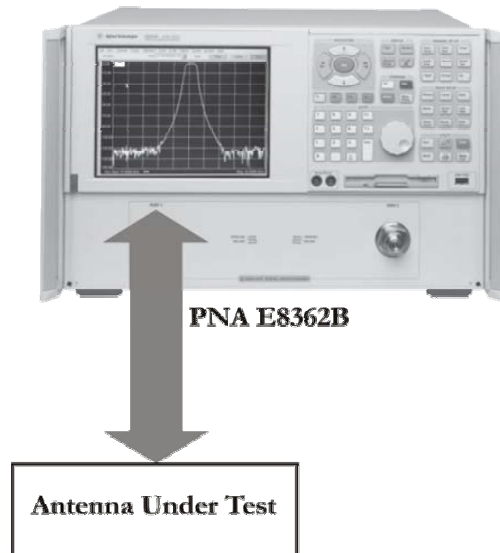


Fig. 2.2. Measurement setup and PNA Specifications

Table 2.1. Specifications of PNA

Operating Band	10MHz to 20 GHz
IF Bandwidth	1Hz to 40KHz
RF Connector	3.5mm, 50 Ω
CPU	Intel Pentium 1.1 GHz
I/O ports	USB, LAN, GPIB
O/S	Windows XP
Measurement Automation Software	CREMA Soft

2.2.3 Anechoic chamber

The anechoic chamber provides a ‘quite zone’, free from all types of EM distortions. All the antenna characterizations were done in an Anechoic chamber to avoid reflections from nearby objects. The room consists of microwave absorbers [2] fixed on the walls, roof and the floor to avoid the EM reflections. A photograph of the anechoic chamber used for the study is shown in Fig. 2.3 below.

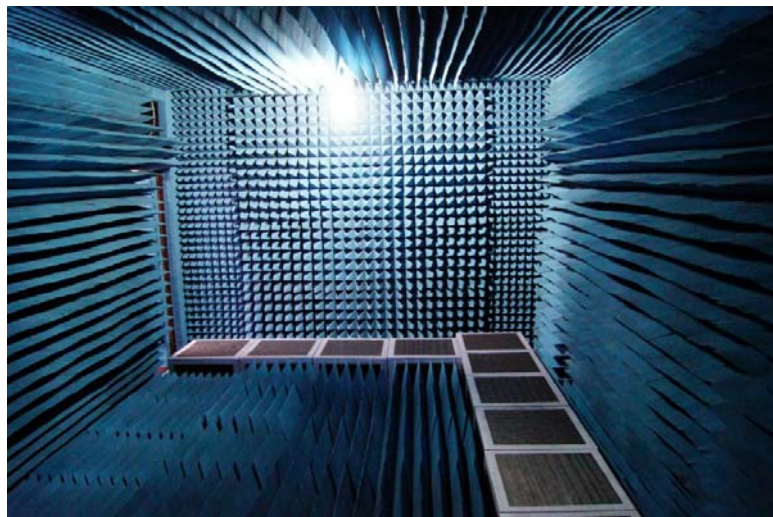


Fig. 2.3. Photograph of the anechoic chamber used for the antenna measurements

High quality low foam impregnated with dielectrically / magnetically lossy medium is used to make the microwave absorber. The tapered shapes of the absorber provide good impedance matching for the microwave power impinges upon it. Aluminium sheets are used to shield the chamber to avoid electromagnetic interference from surroundings.

2.2.4 Automated turntable assembly for far field measurement

The turn table assembly kept at distance greater than $2D^2/\lambda$ consists of a stepper motor driven rotating platform for mounting the Antenna Under Test (AUT). An indigenously developed microcontroller based antenna positioner STIC 310C is used for radiation pattern measurement. The AUT is used as the receiver and a standard wideband ridged horn (1-18GHz) is used as transmitting antenna for radiation pattern measurements. The main lobe tracking for gain measurement and radiation pattern measurement is done using this setup. Antenna positioner is interfaced to the computer and with the in-house developed software '*Crema Soft*' will co-ordinate the automatic measurements.

2.2.5 Crema Soft: Automated antenna measurement

The user friendly software CremaSoft is built in MATLABTM environment. The powerful instrument control toolbox of the package is used for communicating with the stepper motor control and Network Analyzer using RS232C and GPIB interfaces. This automated software can be used for calibration, antenna measurements and material characterization of the substrate used for the antenna.

2.3 Measurement procedure

The experimental procedures followed to determine the antenna characteristics are discussed in the following sections. Power is fed to the antenna from the

network analyzer through different cables and connectors. The connectors and cables will have its losses associated at higher microwave bands. Hence the instrument should be calibrated with known standards of open, short and matched loads to get accurate scattering parameters. There are many calibration procedures available in the network analyzer. Single port, full two port and TRL calibration methods are usually used. The two port passive or active device scattering parameters can be accurately measured using TRL calibration method. Return loss, VSWR and input impedance can be characterized using single port calibration method.

2.3.1 Reflection coefficient, Resonant frequency and Bandwidth

The reflection coefficient (Γ) at the antenna input is the ratio of the reflected voltage (current) to the incident voltage (current) and is same as the S_{11} when the antenna is connected at the port 1 of the network analyzer. It is a measure of the impedance mismatch between the antenna and the source line. The degree of mismatch is usually described in terms of input VSWR or the return loss. The return loss (RL) is the ratio of the reflected power to the incident power, expressed in dB as

$$RL = -20\log (|\Gamma|) = -20\log (|S_{11}|)$$

The return loss characteristic of the antenna is obtained by connecting the antenna to any one of the network analyzer port and operating the VNA in S_{11}/S_{22} mode. The calibration of the port is done for the frequency range of interest using the standard open, short and matched load. The calibrated instrument including the port cable is now connected to the device under test. The frequency vs reflection parameter (S_{11}/S_{22}) values is then stored on a computer using the 'Crema Soft' automation software.

The frequency for which the reflection coefficient value is minimum is taken as resonant frequency of the antenna. The range of frequencies for which the reflection coefficient value is within the -10dB points is usually treated as the bandwidth of the antenna. The antenna bandwidth is usually expressed as percentage of bandwidth, which is defined as

$$\%Bandwidth = \frac{bandwidth}{centre\ frequency} * 100$$

The voltage standing wave ratio (VSWR) is the ratio of the voltage maximum to minimum of the standing wave existing on the antenna input terminals. A well-matched condition will have return loss of 15dB or more. A VSWR equal to 2 gives a return loss of ≈ 10 dB and it is set as the reasonable limits for a matched antenna.

2.3.2 Far field radiation Pattern

The measurement set up for radiation pattern is illustrated in figure 2.4. The radiation pattern of an antenna is graphical representation of its radiation properties as a function of the space coordinates. This is usually a three dimensional (3-D) pattern. Because of the practical limitation of the 3D measurement setup, usually patterns are measured in the two principal coordinate planes (YZ and XZ) for antennas fabricated on the XY plane. The far field patterns are measured at a distance $d > 2D^2/\lambda$, where D is the largest dimension of the antenna and λ is the smallest operating wavelength, to ensure far field criteria.

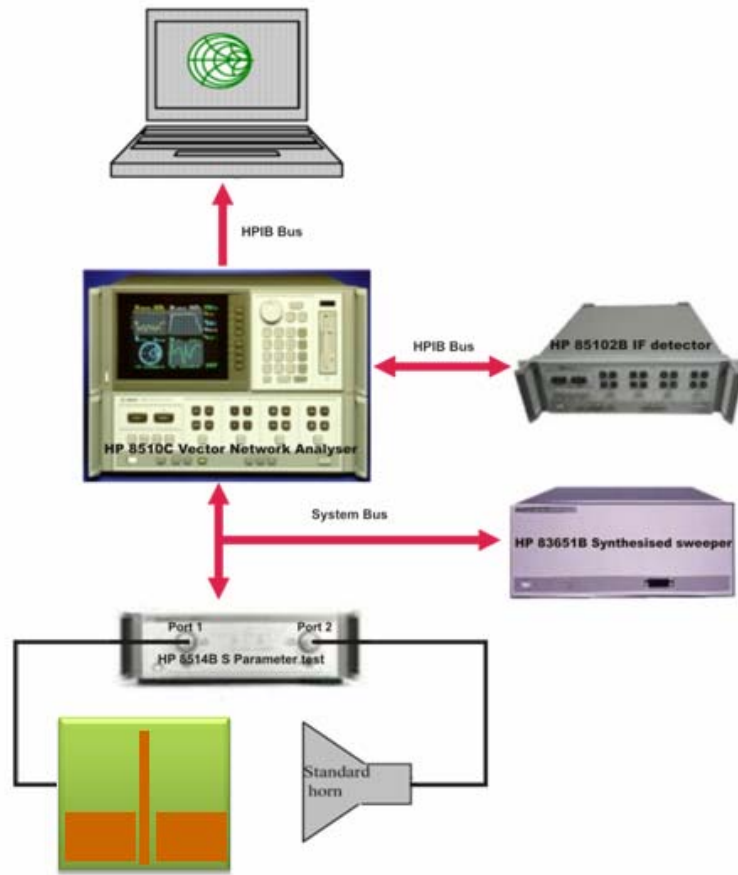


Fig. 2.4. Radiation Pattern Measurement Setup

The measurement of far field radiation pattern is conducted in an anechoic chamber with the time gating facility of Vector Network Analyser HP8510C to ensure a reflection free environment. The AUT is placed in the quiet zone of the chamber on a turn table and connected to one port of the network analyzer. A wideband horn is used as a transmitter and connected to the other port of the network analyzer. The turn table is controlled by STIC positional controller. The automated radiation pattern measurement process is coordinated by the ‘*Crema Soft*’ software in the computer, interfaced with the network analyzer and the positional controller.

In order to measure the radiation pattern, the network analyzer is kept in S_{21}/S_{12} mode with the frequency range within the -10dB return loss bandwidth of the antenna under test. The number of frequency points is set according to the convenience. The start angle, stop angle and step angle of the motor is also configured in the 'Crema Soft'. The antenna positioner is bore sighted and a THRU calibration is performed for the frequency band of interest. This is saved in the CAL set of the network analyzer. Suitable gate parameters are provided in the time domain to avoid spurious radiations if any. The *Crema Soft* will automatically perform the radiation pattern measurement and store it as a text file.

2.3.3 Antenna Gain

The gain of the antenna under test is measured in the bore sight direction. The gain transfer method using a standard gain antenna is employed to determine the absolute gain of the AUT [3-4]. This method uses a standard wide band ridged horn antenna and the AUT. The standard horn antenna whose gain chart is available is chosen as the reference antenna (G_{ref} (dBi)). The reference antenna is placed in the antenna positioner and THRU calibration is done for the frequency range of interest. Standard antenna is then replaced by the AUT and the transmission coefficient S_{21} (dB) is recorded. Gain measurement set up is shown in figure 2.5. Note that the AUT should be aligned for maximum received power so that the gain in the main beam direction is measured. This is the relative gain of the antenna with respect to the reference antenna. The absolute gain of the antenna is obtained by adding this relative gain to the original gain of the standard antenna.

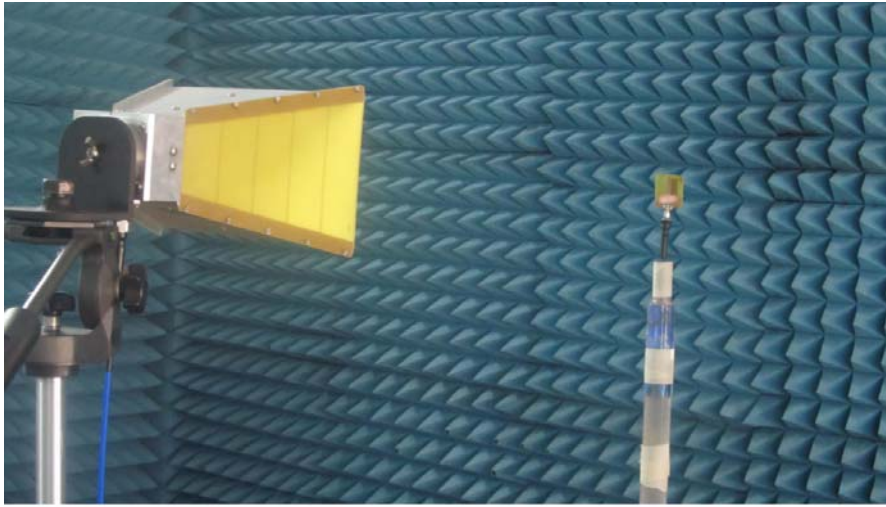


Fig. 2.5. Close view of the antenna gain measurement set up

2.4 Planar Near field measurement set up

The near field characteristic of the antenna in the presence of phantom fluid is measured using the indigenously developed measurement setup and the supporting software developed by CREMA. The aim is to measure the E-field distribution in a volume of biological phantoms, filled with a tissue equivalent fluid. The designed antenna is placed near the phantom and the field probes are inserted in to the phantom fluid. The transmitted power deposition was measured using a short E field probe antenna. The electric field at various locations within the phantom are sampled using the probe. The sum of the squared magnitudes of all the three components of electric field in each location will provide the power at that location in the phantom.

2.4.1 Block diagram

The block diagram of the system, developed is shown in figure 2.6 and the photograph of the experimental setup is shown in figure 2.7.

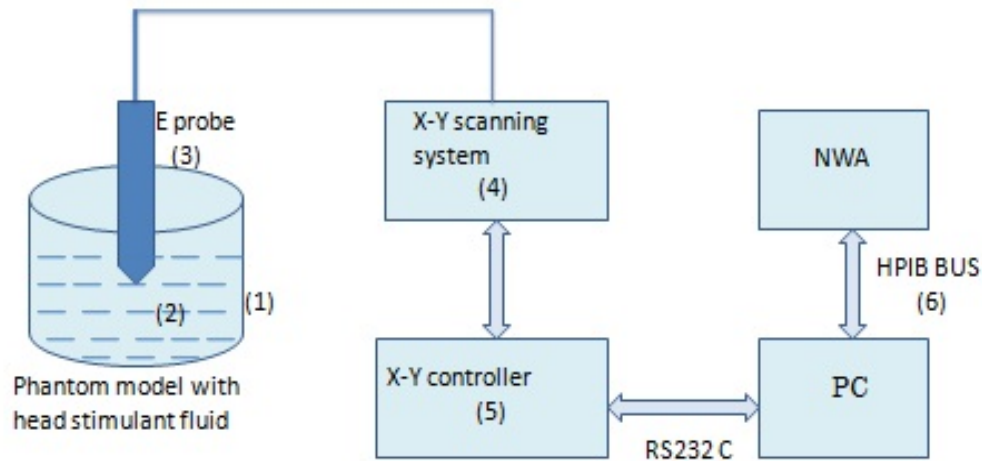


Fig 2.6. The block diagram of the measurement system

The system comprises of the following parts.

- 1) Phantom head model
- 2) Head simulating fluid
- 3) E field probe
- 4) X-Y Scanning system
- 5) X-Y Controller
- 6) HPiB Interface and Network Analyser
- 7) Software for automation

2.4.2 Block diagram details

24.2.1 Phantom Head model and Head simulating liquid

The semi cylindrical phantom head model is fabricated with low loss plaster of Paris material. The phantom is filled with a saline/sucrose solution, mixed in proportions based on standard recipe [5]. The prepared phantom equivalent liquid is measured for its dielectric constant and compared with the dielectric constant of the head. The dielectric constant of the material was

measured using cavity perturbation technique to ensure its suitability as a brain simulation liquid.

Since recipes for ingredients do not produce exactly correct values, partly because of inaccuracies in mixing and partly because of variations in the properties of ingredient, the measured value is slightly different from the standard specifications. However, this liquid will provide nearly brain like medium for EM waves and can be used to provide a qualitative idea of specific absorption rate in head tissue.

The microwave antenna under test is mounted very close to the phantom head model by using a RG/178BU flexible coaxial cable. To evaluate the performance of the antenna experimentally, the antenna is placed very close to the surface of a cylindrical phantom filled with a phantom equivalent material.

24.2.2 The Electric probe (E field probe)

The Electric probe (E field probe) to detect the electric field is fabricated by removing the outer conductor and Teflon dielectric of a long semi rigid coaxial cable. The length of the stripped section is 3mm. The E field probe tip is inserted into the phantom fluid. The position of the E probe and antenna is adjusted such that XY scanner can scan 5cm X 5cm area in XY plane with 0.25mm resolution. After each scan in XY plane, the probe is moved in the Z direction by 0.25mm and the process is repeated. Thus scanning in the Z plane is also carried out for 5cm, to have an effective measurement in a cube of dimension 5cm³.

The measured electric field in three orthogonal polarizations allows the reconstruction of the electric field in the phantom from which the relative SAR

can be deduced. The measurement is repeated for various fabricated antenna structures and their characteristics are analyzed.

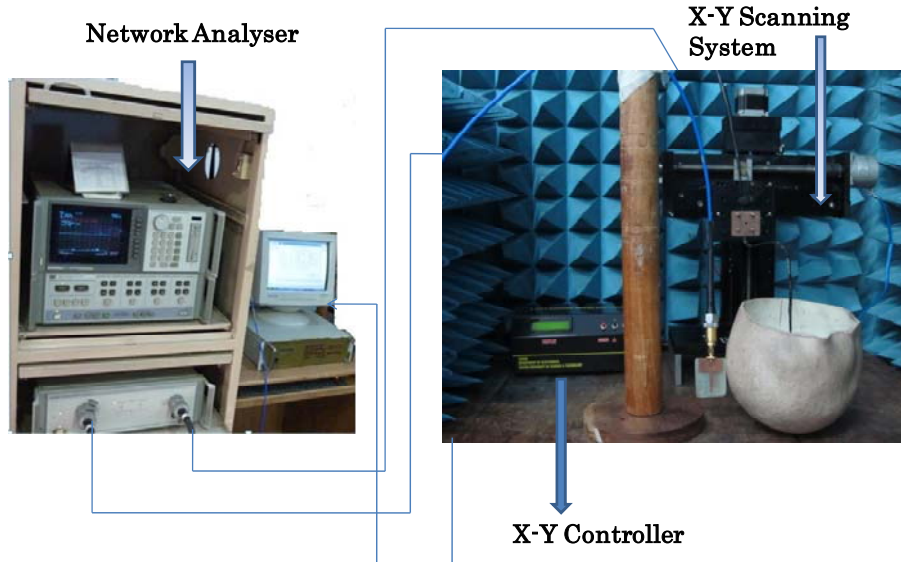


Fig. 2.7. Photograph of the Experimental set up

24.2.3 X-Y Scanning system and X-Y Controller

A Microcontroller (PIC16F73) based stepper motor controller is used to move E field probe inside the phantom fluid at different positions. This is interfaced with the X-Y Scanning system. The above system is interfaced with HP8510C Network Analyser using GPIB interface.

24.2.4 Interfacing with Network Analyser and Software for automation

A user friendly software, for automatic SAR measurement developed in MATLAB by CREMA, CUSAT is used for data acquisition and measurement.

The GUI developed (measurement window) for the measurement is shown in figure 2.8.

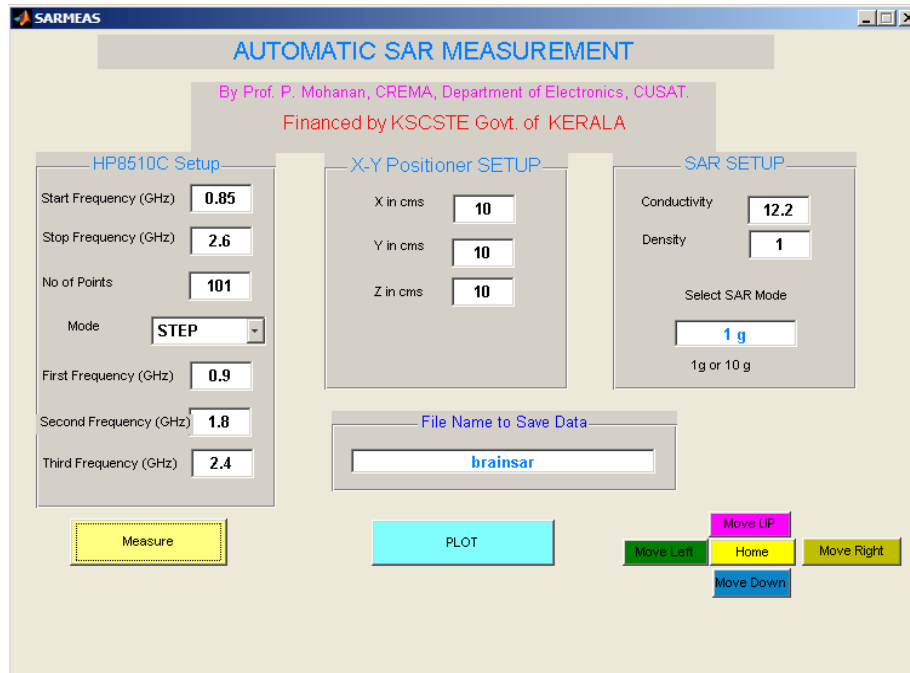


Fig 2.8. Measurement window for SAR estimation

The electric field at the required position can be directly computed by measuring the transmission coefficient parameter (S_{21}) of the antenna. The antenna under test and the E-field probe are properly positioned at the desired position from where the scanning is to be started. The scanning area can be either above or below the original position of the E-field probe. The required scanning volume of the measurement system can be suitably selected by choosing the X, Y and Z dimensions. Options are given to scan either top or bottom of the original position. The movement of the E field probe is controlled by a stepper motor controller. The stepper motor controlled by a controller (PIC 16F77A) is interfaced with the PC using a MATLAB program. The start frequency, the stop frequency and number of data points can be selected from the software. The conductivity and density of the phantom fluid can also be specified in the GUI. SAR can be estimated either over 1g or 10g of the tissue. The measure button starts the measurement over the required volume.

2.5 Cavity perturbation method for dielectric constant measurement of phantom equivalent liquid

Perturbation method otherwise known as cavity perturbation method [6] based on perturbation theory is simple and accurate method to solve many of the electromagnetic field problems. The cavity perturbation technique is widely used for the determination of the dielectric characteristics of samples having of low and medium dielectric loss. The material under test is taken in a capillary tube and inserted into the rectangular waveguide cavity resonator where the maximum perturbation occurs. The real and imaginary parts of the permittivity can then be calculated from the shift in the resonance frequency and Q measurements.

A rectangular X band waveguide cavity of nearly 100 mm length is used for the measurement. The cross-section dimensions are 22 mm in width and 10 mm in height. Two thin conducting sheets with optimum iris are used to form the cavity and to close the two ends of the waveguide. Figure 2.9 shows the waveguide resonator and measurement set up.

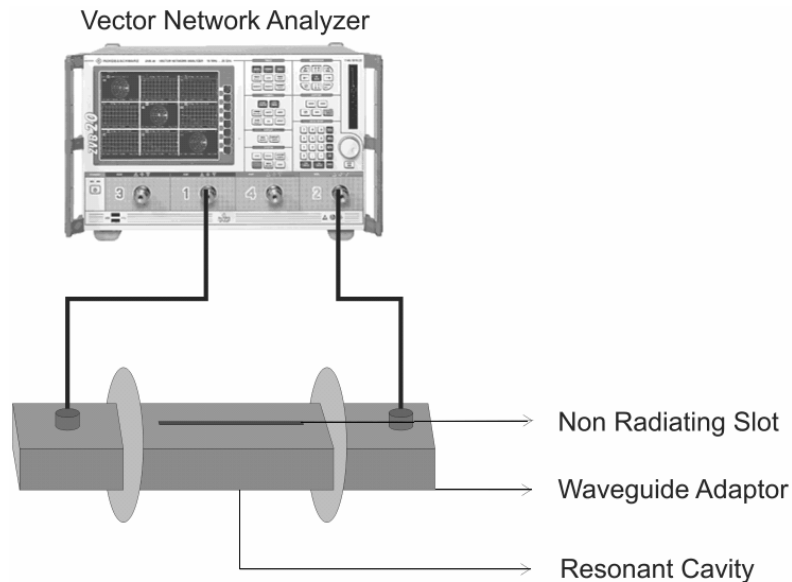


Fig 2.9. Cavity perturbation method setup

In order to insert the material into the waveguide resonator, a non-radiating slot is constructed at the top of the waveguide. The length and width of the slot are 50 and 3 mm, respectively. The waveguide resonator is excited by TE₁₀ mode. The dielectric material is inserted using the sample holder.

When the material under test (capillary tube with phantom equivalent fluid) is inserted in the resonator, the resonance peaks are shifted. The shifted resonance frequency is found using network analyzer at the maximum field position. In order to achieve this, sample is moved along the non-radiating slot with the help of a moving holder, till maximum shift to the lower frequency side. The real and imaginary parts of the dielectric constant are related to:

- the resonance frequency of the cavity with and without the sample,
- the volume ratio of the resonator and sample,
- the quality factors at resonance frequency with and without the sample.

Since the shift in resonance frequencies depends on the dielectric constant of the materials, the permittivity of each material is measured on that specific frequency. The complex relative permittivity of the material is given by

$$\epsilon_r' = 1 + (V_0 (f_0 - f_s) / (f_s V_s))$$

$$\epsilon_r'' = (V_0 / 4V_s) [1/Q_s - 1/Q_0]$$

where f_0 = resonant frequency in the unperturbed cavity (cavity alone)

f_s = resonant frequency in the perturbed cavity (cavity with sample)

V_0 = volume of the waveguide cavity

V_s = volume of the material sample

2.6 Electromagnetic simulation tools

Micro wave simulation (MWS) tools enable the fast and accurate analysis of high frequency devices such as antennas, filters, couplers, planar and multi-layer structures etc. The user friendly MWS quickly gives an insight into the EM behavior of high frequency designs.

2.6.1 3D Electromagnetic simulator HFSS

HFSS utilizes a 3D full-wave Finite Element Method (FEM) to compute the electrical behavior of high-frequency and high-speed components [7]. With HFSS, one can extract the parameters such as S, Y, Z, visualize 3D electromagnetic fields (near and far-field), and optimize design performance. An important and useful feature of this simulation engine is the availability of different kinds of port schemes. It provides lumped port, wave port, incident wave scheme etc. The simulation of coplanar waveguides and microstrip lines can be done using lumped port.

The optimization algorithm available with HFSS is very useful for antenna engineers to optimize the dimensions very accurately. There are many kinds of boundary schemes available in HFSS. Radiation boundary and PML boundary are widely used in this work. The vector as well as scalar representation of E, H, J values of the device under simulation gives a good insight into the problem under simulation.

The first step in simulating a system in HFSS is to define the geometry of the system by giving the material properties and boundaries for 3D or 2D elements available in HFSS window. The suitable port excitation scheme is then implemented. A radiation boundary filled with air is then defined surrounding the structure to be simulated. Now, the simulation engine can be invoked by giving the proper frequency of operations and the number of

frequency points. Finally the simulation results such as scattering parameters, current distributions and far field radiation pattern can be displayed.

2.6.2 Computer simulation Technology (CST microwave studio®)

CST MWS is based on Finite Integral Time-Domain technique (FITD) proposed by Weiland in 1976 [8]. It is the powerful and easy to use electromagnetic field simulation tool. Once the design of a mobile phone is finalized (assuming it in free space), the performance of the phone needs to be tested in more realistic surroundings such as near the human head. This is important since the field distribution and radiation pattern will be influenced by the human tissue. Finally the Specific Absorption Rate (SAR) also needs to be evaluated to fulfill the international mobile phone standard. The CST MWS transient solver provides an efficient Phantom head known as SAM Phantom head (SAM means "Specific Anthropomorphic Mannequin"). The head is modelled by a shell filled with a liquid which represents the average material properties of the head. So it can be easily used not only to design and optimize the antenna but also to check its performance in the presence of a human head and hand. The very high efficiency of the transient solver can be conveniently used with less simulation time. In just one simulation the broadband return-loss, the field distribution, the radiation pattern and the SAR-values for various frequencies can be determined.

2.7 Planar antennas-Review

This section presents different technologies so far proposed by the research groups across the world for the development of planar transmission line, planar antennas and coplanar wave guide fed (CPW) antennas for mobile applications. Due to the attractive features of direct integration with the final RF stage of the

communication system, various scientists and research groups are attracted by the printed antenna technology.

2.7.1 Planar transmission line

A conventional CPW (CoPlanar Wave guide) fed transmission line on a dielectric substrate consists of a centre strip conductor with semi-infinite ground planes printed on the same side of the conducting strip. CPW fed transmission lines are nothing but energy guiding devices that can be used to transfer electromagnetic signal from one part of the system to another. The relevant works in the field of coplanar wave guide fed transmission line and folded antennas are discussed in this section.

The CPW concept was proposed by Wen [9] in 1969. In the proposed structure two ground planes of width 'w' are parallel to the conducting strip. A zeroth-order quasi-static approximation has been employed to estimate the phase velocity and the characteristic impedance of the transmission line.

P. A. J. Dupuis.[10] reported the dependence of the characteristic impedance of a coplanar waveguide as a function of slot width and substrate thickness.

V. FouadHanna [11] presented analytic closed-form expressions for impedance and effective dielectric constant of Coplanar Strip Lines (CPS) with finite substrate thickness using conformal mapping techniques.

Design information for coplanar waveguide directional couplers using quasi-static zeroth order approximations was presented by Cheng P Wen [12]. The first analytic formulae for calculating quasi-static wave parameters of CPW's have been studied using conformal mapping by Wen, [13].

Veyres and Fouad Hanna have extended the application of conformal mapping to CPW's with finite dimensions and substrate thicknesses [14]. N. K. Das and D. M. Pozar [15] used the conformal mapping to derive the analytic formulae for CPW's and CPS's on multilayer substrates.

Analytic formula for the characteristics of coplanar transmission lines on multilayer substrates have been obtained using conformal mapping and the accuracy of this formula has been verified experimentally by Erli Chen and Stephen Y. Chou [16] on a variety of coplanar transmission lines using Differential Electro-Optic Sampling (DEOS).

Ching-Cheng Tien [17] reported the guiding characteristics of FW-CBCPW (Finite-Width Conductor-Backed Coplanar Waveguide) by the rigorous method of mode matching.

T.Kitazawa, Y. Hayashi and M. Suzuki proposed theoretical method for the analysis of a coplanar waveguide [18] with thick metal-coating which causes an increase in wavelength and a decrease in characteristic impedance

A new analytical expression for the impedance and the permittivity of coplanar waveguides with lower ground plane is presented [19].by G. Ghione and C. Naldi.

Equivalent capacitances of coplanar waveguide discontinuities on multilayered substrates were calculated using a three-dimensional finite difference method by Mohsen Naghed [20].

William H. Hayd [21] reported the resonances and associated power loss which occurs in conductor backed coplanar transmission lines at selected frequencies from 1 to 230 GHz by three dimensional (3-D) EM simulations.

Circular Polarisation [22] (CP) radiation achieved from an asymmetric inductively coupling slot in the ground plane of the CPW feed line is discussed by Chih-Yu Huang and Ching-Wei Lingin.

Wen-Hua Tu [23] presented a coplanar waveguide-fed inductively coupled stepped-impedance slot antenna with 32% size reduction compared to the conventional uniform slot antenna, with better harmonic suppression.

Reconfigurable Defected Ground Structure (DGS) resonator fabricated on coplanar waveguide (CPW) technology is presented [24] by Heba B. El-Shaarawy, exploits the transversal dimension of the coplanar wave transmission line (CPW-TL) with four different states of the diode configuration .

Paper [25] presents the design and analysis of Compact Coplanar Waveguide (CPW)-fed Zeroth-Order Resonant (ZOR) antenna. Taehee Jang, Jaehyurk Choi, and Sungjoon Lim reported ZOR phenomenon to reduce the antenna size and composite right/left-handed (CRLH) unit cell on a vialess single layer, which simplifies the fabrication process.

2.7.2 Printed antenna design

The printed antenna was originally started in 1953 [26] when Deschamps proposed the use of microstrip feed lines to feed an array of printed antenna elements. Shortly thereafter, radiation from strip line discontinuities was reported by Lewin [27].

After the introduction of microstrip antenna, different methods of analysis for these antennas, including the transmission line model [28], the cavity model [29] and the spectral- domain method [30] were appeared.

A novel coupled line fed single-layer rectangular patch antenna is described by M.D. Van Wyk et al.[31]. This coupled line matching technique increases the bandwidth of the patch antenna by a factor of more than 2.5 as compared to the normal edge-fed patch with the same geometrical dimension.

A planar monopole broadband antenna with a parasitic radiator is proposed by Xing Jiang et al. [32]. The bandwidth of the monopole antenna is considerably improved with a parasitic element earthed with a matching inductor.

H.K. Kan et al. [33] presented a compact dual concentric ring printed antenna. Each ring is loaded by a localized dielectric layer and can therefore be optimized to operate at a certain frequency, thus enhancing the overall bandwidth of the antenna.

A novel folded monopole antenna is investigated numerically and experimentally by G. Ruvio et al. [34]. The proposed antenna comprises a short folded monopole suitably shaped at the base with two vertical grounding probes. This small antenna occupies impedance bandwidth up to 125% (1.6GHz to 7.5GHz) for a 10dB return loss.

The spectral domain full wave approach using Green's function for the mixed dielectric nature of the microstrip antenna was proposed by Deshpande and Bailey[35]. The analysis of a rectangular patch and circular disc geometries were studied using this method by Chew, Aberle and Bailey[36-37].

A circularly polarized rectangular microstrip antenna with a single point feed is also designed by Haneishi and Yoshida [38]. The narrow bandwidth of microstrip patch antennas are mitigated by using stacked patch radiators.[39].

The Defected Ground Structures (DGS) are introduced on microstrip patch antennas to suppress the higher order harmonics are introduced by Y J Sung [40].

2.7.3 Planar Printed monopole antenna

There are a number of printed monopole antenna design can be found in the literature ranging from single band monopoles, multiband monopoles and ultra wideband antennas. The very basic design is in the form of a straight metallic conductor usually operated with one-quarter wavelength. But this design results large antenna height and it is impossible to integrate such an antenna in a compact communication gadget like mobile phone.

In order to reduce the height of the monopole a number of techniques such as bending, folding or wrapping two-dimensional planar monopoles to three-dimensional structures. These techniques reduce the total antenna height up to a large extent. Thus the development in the planar antenna design, resulted compact communication gadgets.

Printed monopoles are widely used in the case of compact applications due to the simplicity in design and optimum reflection and radiation performances. In this section some of the most relevant work on printed monopoles have been discussed.

S. Honda et al. [41] presented a circular disk monopole antenna with 1:18 impedance band width and omni-directional radiation characteristics. M.Hammoud et al. [42] proposed a circular disc monopole antenna having a large band width. The antenna provides a broad band width of 2.25-17.25 GHz for VSWR<2.

A.P Agrawall et al. [43] proposed a new configurations of wide band monopole antennas such as elliptical (with different ellipticity ratios), square, rectangular, and hexagonal disc. A simple formula is also proposed to predict the frequency corresponding to the lower edge of the band for each of these configurations.

Z. N. Chen presented [44] a new planar monopole antenna for broad band application. The antenna consists of a square parasitic planar radiator and a probe-fed strip, which are separated by a thin dielectric slab. The electromagnetic coupling of the planar radiator improves the impedance characteristics of a conventional monopole antenna.

A broadband triangular planar monopole is presented by Z. N. Chen et al.[45]. The equilateral triangular radiating sheet electromagnetically coupled with a probe-driven strip forms the EMC planar monopole. The antenna has the advantage of about 50% area reduction.

A type of annular planar monopole antenna is presented by Z. N. Chen et al.[46] and demonstrated that the proposed antennas are still capable of offering dramatically broad impedance bandwidths and acceptable radiation patterns even when more than half of the circular element of the structure has been removed.

Kin-Lu Wong et al. [47] developed a novel planar monopole antenna with a very low profile and capable of multiband operation. The proposed antenna is operated with the inner sub patch resonating as a quarter-wavelength structure and the outer one resonating as both a quarter-wavelength and a half-wavelength structure.

M. J. Ammann et al. [48] proposed a wide-band shorted planar monopole with beveling technique. A combination of beveling and shorting technique is used to increase the impedance bandwidth of the antenna.

A novel shorted, folded planar monopole antenna for application in GSM/DCS dual-band mobile phones is proposed by C.Y. Chiu in [49]. The antenna is shorted to the system ground plane, to improve impedance match.

A square planar monopole antenna including two feed points is developed by E. A. Daviu et al. [50]. Double feed is used in order to generate a pure and intense vertical current distribution in the whole structure and to avoid horizontal currents, which degrade the polarization properties and the impedance bandwidth performance of the antenna.

Jen-Yea Jan et al. [51] proposed a small planar monopole antenna with a shorted parasitic Inverted-L wire for wireless communications in the 2.4-5.2 and 5.8-GHz bands. The driven monopole element and shorted parasitic wire can separately control the operating frequencies of two excited resonant modes.

The application of genetic algorithm (GA) optimization to the design and analysis of planar monopole antenna is presented by Aaron J. Kerkhoff et al. [52]. Through analysis of the GA generated designs, it was shown that the wideness of the radiating element base and its close proximity to the ground plane cause the Reverse bow tie (RBT) to achieve a wider matching bandwidth with a reduced size compared with the conventional bow tie (BT).

Shun-Yun Lin [53] introduced a folded planar monopole antenna, which has a very low profile of about one twentieth of the wavelength of the lowest operating frequency. The effect is achieved by using a bended rectangular radiating patch and an inverted L-shape ground plane.

A square planar metal-plate monopole antenna fed by a novel trident shaped feeding strip is presented by Kin-Lu Wong et al. in [54]. With the use of the proposed feeding strip, the square planar monopole antenna studied shows a very wide impedance bandwidth of about 10 GHz which is larger than three times the bandwidth obtained using a simple feeding strip (about 1.5–3.3 GHz, bandwidth ratio about 1:2.3).

Wang-Sang Lee et al. [55] proposed a Multiple Band-Notched Planar Monopole Antenna for Multiband Wireless Systems. The proposed antenna consists of a wideband planar monopole antenna and the multiple U-shape slots, producing band-notched characteristics Wang-Sang Lee et al. [56] presented a wideband planar monopole antenna with dual band-notched characteristics. In order to generate dual band-notched characteristic, they proposed nine types of planar monopole antennas, which have two or three shaped slots (or inverted L) in the radiator. This technique is suitable for creating ultra-wideband antenna with narrow frequency notches or for creating multiband antennas.

Sheng-Bing Chen et al. [57] proposed a modified T-shaped planar monopole antenna for multiband operation. In the proposed antenna, two asymmetric horizontal strips were used as additional resonators to produce the lower and upper resonant modes. An ultra-wideband (UWB) planar monopole antenna with a tunable bandnotched response is proposed by E. Antonino-Daviu et al. in [58]. Tuning of the rejected frequency is realized by loading an embedded resonant slot with a varactor.

2.7.4 Coplanar Waveguide Fed monopole Antennas

Coplanar wave guide has become an attractive feeding technique and can be effectively utilized in the design of compact printed antenna designs. CPW antennas have many features, such as easy fabrication and integration with monolithic microwave integrated circuits. CPW employs a simplified configuration with a single metallic layer. The key features of Coplanar Wave Guide monopole are the availability of ground in the same plane and good transfer characteristics. This figured the scientists all over the world. As such, relevant papers in this area are summarized in the following section.

A CPW-fed dual frequency monopole antenna has been presented by Horng-Dean Chen et al. [59]. The proposed antenna utilizes the advantages of the CPW line to simplify the structure of the antenna into a single metallic level, thereby making easier for integration with the microwave integrated circuits. The antenna consists of a combination of two monopoles connected in parallel at the feed point, each operating at a specified frequency mode.

K. Chung et al. [60] presented a wideband CPW-fed monopole antenna with parasitic elements and slots. The wide bandwidth is achieved by adding two parasitic elements along the length of the monopole and three narrow slots.

W.C. Liu [61] presented a new design of a planar monopole antenna consisting of a rectangular microstrip patch with a rectangular notch. The antenna is fed by a coplanar waveguide (CPW) line such that only a single-layer substrate is required for this antenna. To produce dual frequency wide impedance band behavior a notch is introduced to the radiating patch. He has also presented a paper on broadband dual-frequency meandered CPW-fed monopole antenna [62]. The antennas were developed to widen the narrow bandwidth of the coplanar patch antenna. This was achieved by inserting a meandered line between the 50 ohm CPW lines and radiating patch.

A novel wideband dual-frequency design of a coplanar waveguide (CPW)-fed monopole antenna is proposed by W.C. Liu [63]. The antenna comprises a planar patch element with a sided L-shaped slit to become a double inverted-L monopole and is capable of generating two separate resonant modes with good impedance match.

J. Liang et al. [64] presented a study of coplanar waveguide (CPW) fed circular disc monopole antenna for ultra-wideband (UWB) applications. It has

been shown that the feed gap, the width of the ground plane, and the dimension of the CPW-fed circular disc monopole antenna are the most important parameters that determine the performance of the antenna.

A miniature dielectric loaded monopole antenna fed by coplanar waveguide is proposed by Yi-Fang Lin et al. in [65] for WLAN applications in the 2.4/5-GHz bands. The proposed antenna has small size, effective feeding structure and adequate operational bandwidth, such that it is suitable for use in WLAN applications.

The analysis of a new printed antenna is presented by V. Zachou et al. [66]. This antenna consists of a printed monopole, with one or two sleeves on each side, fed by a coplanar waveguide (CPW) line. Switches are used to control the length of the monopole and the sleeves and to tune the resonant frequencies of the antenna.

A simple and compact ultrawideband (UWB) aperture antenna with extended band-notched designs was presented by Yi-Cheng Lin et al. [67]. The antenna consists of a rectangular aperture on a printed circuit board ground plane and a T shaped exciting stub. The proposed planar coplanar waveguide fed antenna is easy to integrate with radio-frequency/microwave circuitry for low manufacturing cost.

M.-T. Zhang et al. [68] developed a dual-band CPW-fed folded-slot monopole antenna for RFID application. A coplanar waveguide fed monopole antenna for 5 GHz wireless communication is proposed by W. C. Liu [69]. The proposed antenna consists of a hook strip, CPW feeding structure with a rectangular ground and an inverted L-shaped ground. The antenna has compact size, good impedance bandwidth and good radiation characteristics suitable for

5.2 (5.15–5.35 GHz) or 5.8 GHz (5.725–5.825 GHz) WLAN and RFID operation.

Joon Il Kim developed [70] an ultra wideband coplanar waveguide fed LI-shape planar monopole antenna. The proposed antenna consists of an L-shaped monopole and an I-shaped open stub monopole connected at the end of a CPW feed line.

A novel dual-band design of a CPW fed monopole antenna with a cross slot was proposed by C.M. Wu [71]. The antenna, comprising a planar patch element embedded with a cross slot, is capable of generating two separate resonant modes with good impedance match. The CPW-feed technology is applied to the design.

T.A. Djaiz developed [72] a CPW-fed miniaturized antenna with bandwidth enhancement for biomedical localization applications. A meander arm is used as the radiating element and an additional layer as superstrate to reduce the antenna area to improve the performance in terms of bandwidth.

To achieve dual-band antenna performance with less interdependency of the two operation bands, a dual-band CPW-fed slot monopole hybrid antenna with orthogonal polarizations was proposed by Xian-Chang Lin [73]. Guorui Han presented [74] a novel compact dual-band CPW-fed antenna with a microstrip stub. The proposed dual-band antenna works at of 2.4 GHz and 5.8 GHz simultaneously.

The pulse preserving capabilities of the CPW-fed circular disk monopole antenna with improved correlation factor of 7% by selecting suitable substrate parameters are discussed by Q.Wu [75]. The ringing and pulse-width spreading of the radiated signals caused by the energy-storage effects of the dielectric substrate are also discussed.

Simple and compact CPW-fed planar monopole antenna for ultra-wideband applications with a gourd-like radiation element and a modified stair-style ground is reported by Y.B.Yang [76]. The antenna exhibits a nearly omnidirectional radiation pattern, stable antenna gain, and good time-domain characteristics across the operation band.

Novel coplanar waveguide-fed monopole UWB antenna and a miniaturized version of an asymmetric coplanar strip-fed half monopole antenna is reported by P Fei[77].

2.8 Mobile antenna with reduced user interference –review

The large amount of electromagnetic radiation everywhere in the environment has increased the concern about the possible health risks of wireless devices. Rising from these aspects, antenna designers have been forced to pay a growing amount of interest in reducing the radiation absorbed by the user. Different methods are used for reducing this type of radiations. Adding an external shield to mobile phones is the most common method adopted for reducing the unnecessary radiations. Here shielding structure has to be integrated with the antenna to provide better shielding effectiveness. Material selection and position of the external shield is also very important. A ferrite sheet attached to the front side, close to head can also reduce radiation. However, the parameters such as attaching location, size and material properties of ferrite sheet played an important role in the reduction effectiveness. Highly directive antennas can also reduce radiation towards human head significantly. However, the adoption of highly directive antennas certainly causes degradation in signal reception from other directions. Parasitic elements are also used to get end fire pattern. Complicated truncated ground plane is used to get end fire pattern throughout the operating band. Large reflectors are also used to reduce

radiations. Researchers have explored PIFA (Planar Inverted F Antenna) with EBG (Electromagnetic Band Gap) surface on the ground plane to reduce radiation towards human head. But this deteriorates the structure simplicity and compactness, and also there is no appreciable reduction in radiation towards human head.

This section presents different technologies so far proposed by the research groups across the world for the development of antennas for mobile applications with less effect on human body.

Andi Hakim Kusuma et.al[78] proposed a novel low SAR dual-band PIFA structure operating at 0.9 GHz and 1.8 GHz bands. They are considered, to reduce exposure of electromagnetic radiation towards the human head. The SAR reduction is accomplished by inserting a thin metallic layer between the patch and the ground plane and to reduce the current flowing in the ground plane. This layer is connected to the ground plane through few posts located at selected optimum positions. Additionally, three vertical sidewalls are used to reduce radiation from the patch to the human head. Results show that the proposed structure can reduce SAR up to 76%.

In the reported work by R. Augustine et.al[79], flexible polymeric ferrite sheets are characterised on the basis of their shielding efficiencies. SAR measurements were carried out with a planar wearable antenna and polymeric ferrite shielding to confirm its competence. A low profile, conformal antenna has been designed to resonate at 2.4 GHz. Specific absorption rate is reduced by polymeric ferrite sheets which are particularly attractive as they are low profile, flexible and conformal. So the antenna could be thought of to be printed on them to attain certain flexibility in its use. Polymeric ferrite sheets will be best suited for RFID (868 MHz) application where antennas are made of metallic

ink and deposited on a plastic sheet. The characteristics of ferrite will lead to the miniaturization of antennas.

The electromagnetic interaction between the antenna and the human head is reduced with materials and metamaterials. The reduction of Specific Absorption Rate (SAR) with materials and metamaterial is performed by the finite-difference time-domain method with Lossy-Drudemodel by CST Microwave Studio by Mohammad Tariqul Islam et.al[80]. The metamaterials can be obtained by arranging split ring resonators (SRRs) periodically. The SAR value has been observed by varying the distances between head model to phone model, different width, different thickness, different height of material and metamaterial design. Materials has achieved 47.18% reduction of the initial SAR value while metamaterial achieved a reduction of 42.12%. These results can provide helpful information in designing the mobile communications equipments for safety compliance.

K H Chan et.al[81] studied spherical phantom heads by the use of a reduced-size on the the (SAR) calculation, which is usually extremely complicated and time demanding. Antenna performance and the SAR value were studied by using the Finite- Difference Time-Domain (FDTD) method. Results have shown that both the return loss and the radiation pattern of the mobile phone antenna are only slightly affected by the fractional head model for almost all cases when the phantom head is truncated to not more than 25% in volume. Results have also indicated that the percentage difference in the SAR value for the full head model and the fractional head model is less than 5%.

In the paper by L.K.Ragha[82] et.al has introduced a radio frequency (RF) shield on dipole antenna to reduce SAR in the implanted spherical head model. RF shields made of ferrimagnetic material are used to suppress surface

current on antenna. Conducting cylindrical implant of resonant length is embedded eccentrically into a head model and it is irradiated by dipole antenna (0.4wavelength) at 900 MHz. Effect of wireless device on implanted head and SAR reduction techniques to minimize fears of patients are discussed. Simulations are performed to find the effect of RF fields on implanted medical device by varying its parameters like length and location using CST-Microwave studio. Paper includes numerical evaluation of the SAR reduction using RF shield and also analyzes the SAR data for shielding effectiveness. Drastic reduction in SAR was observed in case of Ferrite3 material of 1mm thickness when both implant location and length were varied. Simulation results will be useful for compliance testing of wireless communication devices.

The paper by K. H. Chan et.al[83] provides an experimental study on the effectiveness of SAR reduction by attaching conductive materials to mobile phones, and the corresponding effects of the antenna performance of the mobile phones. The results show a typical trade-off of a 20% reduction in the SAR value with a maximum 1.8dB reduction in the received power of the antenna. The results also conclude that the position of the shielding material is an important factor, whereby the hot spot of the SAR distribution of the mobile phone must be well covered in order to achieve good SAR reduction.

M.A. Mangoud et.al [84] presented a two-element phased antenna array for mobile handset using the FDTD hybrid method. The array is designed to provide a spatial null in the near field zone in the direction of the human head. Compared with an omnidirectional antenna, the overall efficiency and azimuth coverage are improved and the peak specific absorption rate in the head can be reduced by at least 10dB.

Denise L. Hamblin[85] et.al investigated the influence of EEG electrode caps on SAR in the head from a GSM900 mobile phone (217-Hz modulation, peak power output 2 W). SAR measurements were recorded in an anthropomorphic phantom using a precision robotic system. Peak 10 g average SAR in the whole head and in just the temporal region were compared for three phantom arrangements; no cap, 64-electrode “Electro-Cap,” and 64-electrode “Quick-Cap”. Relative to the “no cap” arrangement, the Electro-Cap and Quick-Cap caused a peak SAR (10 g) reduction of 14% and 18% respectively in both the whole head and in the temporal region. Additional computational modeling confirmed that SAR (10 g) is reduced by the presence of electrode leads and that the extent of the effect varies according to the orientation of the leads with respect to the radiofrequency (RF) source. The modeling also indicated that the nonconductive shell between the electrodes and simulated head material does not significantly alter the electrode lead shielding effect

Cheng Tse Lee and Kin-Lu Wong[86] presented an internal wireless wide-area network (WWAN) antenna suitable for GSM850/900/1800/1900/UMTS operation in the clamshell mobile phone with reduced ground plane effects. Small variations in the performances of the antenna for the clamshell mobile phone in the open state (talk condition) and closed state (idle condition) are obtained. This is owing to the reduced effects of the upper (cover) ground plane on the performances of the internal antenna obtained by embedding a slit at the edge of the upper ground plane close to the connecting strip between the two (upper and main) ground planes of the clamshell mobile phone. In this case, large surface currents excited around the slit are achieved, with other portions of the upper ground plane showing much weaker surface current distributions, which makes the embedded slit behaves like a current trap for the excited surface currents. This condition results in reduced effects of the upper ground plane. This also

makes the near-field radiation of the clamshell mobile phone with the proposed antenna easily meet the specific absorption rate (SAR) and hearing aid compatibility (HAC) specifications required for practical applications.

A new conformal antenna for hand held mobile telephones is proposed by H.O Ruoss and F.M. Landstorfer[87]. The slot antenna is investigated with a modified method of moments. It enables an accurate modelling of the slot and calculate input impedance as well as electric and magnetic near and far fields taking the influence of the user's head and hand into consideration. The interaction with the human body can be reduced significantly.

Jiunn-Nan Hwang and Fu-Chiarng Chen [88] performed the preliminary study of SAR reduction with metamaterials by the finite-difference time-domain method with lossy Drude model. It is found that the SAR in the head can be reduced by placing the metamaterials between the antenna and the head. The antenna performances and radiation pattern with metamaterials are analyzed. A comparative study with other SAR reduction techniques is also provided. The metamaterials can be obtained by arranging SRRs periodically. In this research, the SRRs are operated at 900 and 1800 MHz bands. The design procedure is described. Numerical results of the SAR values in a muscle cube with the presence of SRRs are shown to validate the effect of SAR reduction. These results can provide helpful information in designing the mobile communication equipments for safety compliance.

Andi Hakim Kusuma et.al[89] proposed a novel low SAR PIFA structure to reduce exposure of the human head to mobile-set antenna radiation. Dual-band PIFA structures operating at 0.9 GHz and 1.8 GHz bands are considered. SAR is decreased by reducing the back-radiation coming from the patch and the ground plane. This SAR reduction is accomplished by inserting a thin metallic

layer between the patch and the ground plane to reduce the current flowing in the ground plane. This layer is connected to the ground plane through few posts located at selected optimum positions. Additionally, three vertical sidewalls are used to reduce radiation from the patch to the human head. Results show that the proposed structure can reduce SAR up to 76%.

In the reported work by R. Augustine et.al [90] flexible polymeric ferrite sheets are characterised on the basis of their shielding efficiencies. SAR measurements are carried out with a planar wearable antenna and polymeric ferrite shielding to confirm its competence.

The paper by K. H. Chan et.al[91]provides an experimental study on the effectiveness of SAR reduction by attaching conductive materials to mobile phones. The corresponding effects of the antenna performance are discussed elaborately. The results show a typical trade-off of a 20% reduction in the SAR value with a maximum 1.8dB reduction in the received power of the antenna. They conclude that the attachment position of the shielding material is an important factor.

In the paper by L.K.Ragha and M.S.Bhatia [92] proposed radio frequency (RF) shields on mobile phone to reduce SAR in spherical head model. Shields made of ferrimagnetic materials are used to suppress surface currents. Many kinds of simulation are performed to investigate the effect of various parameters like location, size, shape and thickness of the shield on the SAR and also on the antenna performance. Paper includes numerical evaluation of the SAR reduction and also analyzes the SAR data for shielding effectiveness.

S.I. Kwak[93] performed experimental tests of SAR reduction on a mobile phone. To protect a human head from exposure to electromagnetic fields

and comply with exposure guide- lines, the electromagnetic bandgap (EBG) structures are inserted in a commercial personal communication services (PCS) mobile phone. The measured results demonstrate the movement of hot spot and the reduction of SAR in the human head.

In the paper by M. B. Manapati and R. S. Kshetrimayum [94], single negative metamaterial is used to reduce the electromagnetic interaction between the mobile phone and human head. The specific absorption rate in the head can be reduced by placing the metamaterials between the antenna and the head. Single negative metamaterials from periodic arrangement of split ring resonators (SRRs), spiral resonators (SRs) and open split ring resonators (OSRRs) are employed. By properly designing structural parameters of SRRs, the effective medium parameter can be made negative around 900MHz and 1800MHz bands. The design procedure and principle operation of resonators are explained. The performance and size comparison of resonators are described. Numerical results of the SAR values in the human head with the presence of resonators exhibit SAR reduction. These results can provide useful information in designing safety mobile communication equipments.

An attempt to solve the problem of electromagnetic wave hazard caused by the radiation from handset mobile antenna as well as the problem of the handset mobile operation with differently tuned frequencies was suggested by Marai M. Abousetta[95].

Weiping Dou investigated the chassis influence on the SAR characteristics of handset antenna with the finite-difference time domain method [96]. The chassis is conductive and equipped with a quarter-wavelength monopole. The optimal chassis sizes have been presented for 900 MHz and 2 GHz operation

S V Amos [97] raised important aspects concerning SAR modelling and reduction techniques necessary to comply with industry standards. From studies the following points have been concluded: The ear is an important parameter in the design model used in simulations. A standard model would be beneficial so that comparisons can be drawn. Parameters such as the amount of shielding can, feed position and electrical parameters of tissues may all have significant effects on the resulting SAR. Increased distance between the radiating element and head can significantly reduce SAR.

A new design using a dielectric reflector to reduce the back radiation of aperture coupled antennas is proposed and developed [98] by Qinjiang Rao et.al. To validate the proposed design, a concise theory analysis is first conducted and then the proposed design is analyzed in a modified aperture coupled microstrip antenna. In this design, a radiating patch and a microstrip feed line are etched on the same side of a top substrate and a coupled slot is etched on the opposite side of this substrate. To examine the effect of the dielectric reflector on the antenna performance, theoretical simulations and experimental investigations were carried out. A good agreement between the theoretical expectation and the measured results validates the proposed design. The measured radiation patterns show that the proposed structure can offer high radiation efficiency, a high front to back radiation ratio, and a high co-cross polarization ratio. With these features, the proposed design is significant in the electromagnetic interference and electromagnetic compatibility (EMI/EMC) designs for reduced undesirable radiation.

The paper by Sang il Kwak[99] proposed a optimized multilayer PIFA in PCS bands based on the EBG for SAR reduction. The EBG structure which has band gap capability and acts as PMC surfaces can reduce the surface waves and

prevent the undesired radiation from the antenna. Thus, the EBG structure can reduce the electromagnetic fields toward the human head direction. Optimization of multilayer PIFA structure using the EBG structure is conducted for S parameters, radiation patterns and on the SAR values. A parametric study of location and height of a PIFA with the EBG structure is performed. The results demonstrated the reduction of SAR value without sacrificing the antenna performance.

An efficient electrically small wide band planer antenna for Specific Absorption Rate is designed by Jung-han Kim [100]. The proposed antenna consists of two inductive loading arms and inverted L-type monopole antenna. Also, the proposed antenna is designed to have a CPW feed structure and a superstrate layer. Two inductive loading arms are electromagnetically coupled with main monopole for the dual resonance mode of the antenna operation. The dual resonance characteristics are shown at 2.184GHz and 2.44GHz, respectively. The measured impedance bandwidth ($VSWR \leq 2$) is 624 MHz (1.984~2.608 GHz). The maximum gain of 2.8 dBi and radiation efficiency of 80.3 % at 2.184 GHz is observed. With this arrangement the proposed antenna is mounted at the front of the mobile handset cover plane. The radiated power difference between the forward and backward directions is about 10dBi. Moreover, disadvantage of the conventional electrically small antenna, such as narrow impedance bandwidth and radiation efficiency, are improved by simple inductive loading structure.

Filippo Costa et.al used [101] High-Impedance Surfaces (HIS) comprising lossy Frequency Selective Surfaces (FSS) to design thin electromagnetic absorbers. The structure, despite its typical resonant behavior, is able to perform a very wideband absorption for reduced thickness. Losses in the frequency

selective surface are introduced by printing the periodic pattern through resistive inks and hence avoiding the typical soldering of a large number of lumped resistors. The effect of the surface resistance of the FSS and dielectric substrate characteristics on the input impedance of the absorber is discussed by means of a circuit model. It is shown that the optimum value of surface resistance is affected both by substrate parameters (thickness and permittivity) and FSS element shape. The equivalent circuit model is then used to introduce the working principle of the narrowband and the wideband absorbing structures.

Dan Sievenpiper et.al[102] introduced a new type of metallic electromagnetic structure that is characterized by having high surface impedance. Although it is made of continuous metal, and conducts dc currents, it does not conduct ac currents within a forbidden frequency band. Unlike normal conductors, this new surface does not support propagating surface waves, and its image currents are not phase reversed. The geometry is analogous to a corrugated metal surface in which the corrugations have been folded up into lumped-circuit elements, and distributed in a two-dimensional lattice.

Ming-Shing Lin et.al[103] used HIS to reduce interaction between a wireless antenna and its user. Mushroom and Jerusalem Cross HIS structures were designed for the PCS band (1.8 GHz). The performance of these HIS structures were investigated by surface-wave and reflection- phase methods. A new test method was also proposed to characterize the reflection phase of an HIS by using a GTEM cell. The effects of HIS sheets on antenna performance and the SAR were studied. Results revealed that these HIS structures can reduce SAR values.

Cavity resonance antennas with dielectric superstrate are considered with different ground plane types namely, Perfect Electric Conductor (PEC), Perfect Magnetic Conductor (PMC), and Artificial Magnetic Conductor (AMC) by

Alireza Foroozesh et.al[104]. It is shown that the effects of angular and polarization dependency of artificial ground planes can be beneficial or detrimental to the antenna performance especially for directivity.

In a communication by I. Gallego-Gallego[105], the combination of soft surfaces with traditional microstrip patch antennas for reducing the level of back radiation in wearable applications has been proposed. The studies have been extended to the case of cylindrical antenna shape to take into account the conformability required for the textile antenna.

A new type of metallic electromagnetic structure has been reported by D. Sevenpiper [106] that is characterized by having high surface impedance. Unlike normal conductors, this new surface does not support propagating surface currents, and it reflects electromagnetic waves with no phase reversal. They suggested that unique material can serve as the ground plane for new kinds of low-profile antennas.

The design of a meta-material realization of AMC surfaces for a high-gain reflector antenna application is presented by Jwo-Shiun Sun et.al[107]. Artificial materials of periodic dielectrics exhibiting an EBG performance have been proposed and applied to planar inverted-F antenna. The Artificial Dielectric Material (ADM) can enhance antenna radiation performance, spread antenna bandwidth and improve antenna radiation gain and efficiency. The artificial defected dielectric material has useful characteristics of harmonic rejection, band suppression and surface wave suppression.

An AMC surface, comprised of Hilbert and/or Peano space- filling curve inclusions is utilized as a thin electromagnetic absorber by John McVay et.al[108] . Numerical results are presented to show the effects of the incident

angle, conducting strip widths and substrate thicknesses on the absorbing properties of such surfaces. The performance of a fabricated thin absorber in reducing the RCS of a conducting plate is demonstrated through measurement.

The paper by Ricardo Gómez-Villanueva et.al reviews the different methods employed in the last years for the development of low SAR antennas inside portable terminals of mobile phone systems[109]. Specifically, auxiliary antenna elements, ferrite loading, EBG/AMC surfaces and metamaterials techniques are examined.. From the methods reviewed the EBG and metamaterial techniques appear as feasible low SAR options that need more study to improve the size and bandwidth parameters that limits their use.

An artificial magnetic conductor using the SRRs printed on conductor-backed dielectric substrate is presented by Chen, Z N et.al[110]. The simulation and measurement verify that the magnetic conductor is successfully accomplished around the resonant frequency. As an antenna application, the characteristics of a horizontal wire antenna placed above the SRR array, as well as a conducting ground plane and a grounded dielectric slab, are investigated and compared. A maximum gain of 4.34 dBi is obtained for the wire antenna above the SRR array. The results confirm that the split resonators can successfully be used to replace the antenna ground plane in order to improve their performance.

2.9 Chapter conclusion

This chapter has discussed the methodology to simulate, optimize and fabricate the various mobile antennas mentioned in the following chapters of the thesis. The simulation and measurement techniques used to study the performances of the antennas in the near field and far field are discussed. Finally a detailed literature review of CoPlanar waveguide fed antennas and mobile antennas with reduced user interference also conducted.

References

- [1] HP8510C Network Analyzer operating and programming manual, Hewlett Packard, 1988.
- [2] Design, Development and Performance Evaluation of an Anechoic Chamber for Microwave Antennas Studies, E. J. Zachariah, K. Vasudevan, P. A. Praveen Kumar, P. Mohanan and K. G. Nair, Indian Journal of Radio and Space Physics, Vo. 13, pp. 29-31, February 1984.
- [3] C. A. Balanis, Antenna Theory: Analysis and Design, Second Edition, John Wiley & Sons Inc. 1982
- [4] John D. Kraus, Antennas Mc. Graw Hill International, second edition, 1988
- [5] Hartsgrove "Simulated Biological Materials for Electromagnetic Radiation absorption Studies," Bioelectromagnetics 8:29-36 ,pp. 126-129, February 2004,.
- [6] M. Hajian,¹ K. T. Mathew,² and L. P. Lighthart¹ Measurement of complex permittivity with waveguide resonator using perturbation technique" Microwave and optical technology letters, Vol. 21, No. 4, pp 269 -272, May 1999
- [7] HFSS user manual, version 10, Ansoft Corporation, July 2005
- [8] Computer Simulation Technology (CST), "CST Design Studio", <http://www.cst.com/Content/Products/DS/Overview.aspx>
- [9] Cheng P Wen "Coplanar Waveguide: A Surface Strip Transmission Line Suitable for Nonreciprocal Gyromagnetic Device Applications"IEEE Trans on microwave theory and techniques.,vol-MTT 17,No 12, December 1969.pp1087-1090
- [10] P. A. J. Duuis and C. K. Campbell " Characteristic impedance of surface strip coplanar waveguides" Electronics Letters Vol.9, No. 1, August 1973 pp 354-355.

- [11] V.Fouad Hanna “Finite Boundary Corrections to coplanar stripline analysis Electronics Letters Vol. 16 No. 15, 17th July 1980 pp604-606
- [12] Cheng P.Wen “Coplanar-Waveguide Directional Couplers” IEEE Trans on microwave theory and techniques.,vol.MTT-18, no. 6, June 1970,pp318-322
- [13] C. P. Wen, “Coplanar waveguide: A surface strip transmission line suitable for nonreciprocal gyromagnetic device applications,” IEEE Trans. Microwave Theory Tech., vol. MTT-17, pp. 1087–1090, 1969.
- [14] C.Veyres and V. Fouad Hanna, “Extension of the application of conformal mapping techniques to coplanar lines with finite dimensions,” Int. J. Electron., vol. 48, pp. 47–56, 1980.
- [15] N. K. Das and D. M. Pozar, “A generalized spectral-domain Green’s function for multilayer dielectric substrates with application to multilayer transmission lines,” IEEE Trans. Microwave Theory Tech., vol. 35, pp. 326–335, 1997.
- [16] Erli Chen and Stephen Y. Chou,” Characteristics of Coplanar Transmission Lines on Multilayer Substrates: Modeling and Experiments” IEEE Trans. Microwave Theory Tech, Vol. 45, p.p 939-945 no. 6, June 1997
- [17] Ching-Cheng Tien, Ching-Kuang C. Tzuang, , S. T. Peng, , and ChungChi Chang“ Transmission Characteristics of Finite-Width Conductor-Backed Coplanar Waveguide” IEEE Trans. Microwave Theory Tech, Vol. 41, no. 9, September 1993
- [18] T. Kitazawa, Y. Hayashi and M. Suzuki “ A Coplanar Waveguide with Thick Metal-Coating IEEE Trans. Microwave Theory and Tech, Setember 1976 pp 604- 608
- [19] G. Ghione and C. Naldi “Parameters Of Coplanar Waveguides with lower Ground Plane” Electronics Letters September 1983 Vol. 19 No. 18 pp 734-735

- [20] Mohsen Naghed and Ingowolff “ Equivalent Capacitances of Coplanar Waveguide Discontinuities and Interdigitated Capacitors Using a Three-Dimensional Finite Difference Method” IEEE Trans. Microwave Theory and Tech VVL 38, No 12, December 1990 pp 1807-1815
- [21] William H. Haydl “Resonance Phenomena and Power Loss in Conductor-Backed Coplanar Structures” IEEE Microwave and Guided wave letters, vol. 20, no. 12, December 2000 pp 514-516
- [22] Chih-Yu Huang and Ching-Wei Ling “CPW feed circularly polarised microstrip antenna using asymmetric coupling slot” Electronics Letters Vol. 39 No. 23, 13th November 2003
- [23] Wen-Hua Tu “Compact Harmonic-Suppressed Coplanar Waveguide-Fed Inductively Coupled Slot Antenna” IEEE Antennas and wireless Propagation Letters, vol. 7, 2008 pp 543-545
- [24] Heba B. El-Shaarawy, Fabio Coccetti, Robert Plana, Mostafa El-Said, and Essam A. Hashish “Novel Reconfigurable Defected Ground Structure Resonator on Coplanar Waveguide” IEEE Trans on Antennas and Propagation, vol. 58, no. 11, November 2010 pp 3622-3628.
- [25] Taehee Jang, Jaehyurk Choi, and Sungjoon Lim “Compact Coplanar Waveguide (CPW)-Fed Zeroth-Order Resonant Antennas With Extended Bandwidth and High Efficiency on Vialess Single Layer” IEEE Trans on Antennas and Propagation, VOL. 59, NO. 2, February 2011 pp363-372
- [26] G. A. Deschamps, “Microstrip Microwave Antennas,” 3rd USAF Symposium on Antennas, 1953
- [27] L. Lewin, “Radiation from Discontinuities in Stripline, Proceedings of Institution of Electronic Engineers, vol. 107, pp. 163-170, 1960

- [28] G. Derneryd, “ Linear Polarized Microstrip Antennas,” IEEE Trans. On Antennas and Propagat., vol. 30, pp. 846-850, 1976 .
- [29] Y. T. Lo, D. Solomon and W. F. Richards, “Theory and Experiment on Microstrip Antennas,” IEEE Trans. on Antennas and Propagat., vol. 27, pp. 137-145,1979
- [30] M. D. Deshpande and M. C. Bailey, “Input impedance of Microstrip antennas,” IEEE Trans. on Antennas and Propagat., vol. 30, pp. 645-650, 1982
- [31] M.D. van Wyk and K.D. Palmer, “Bandwidth enhancement of microstrip patch antennas using coupled lines,” Electronics Lett., vol. 37, pp. 806-807, 2001
- [32] Xing Jiang, Simin Li and Guangjie Su, “Broadband planar antenna with parasitic radiator,” Electronics Lett., vol. 39, no. 23, 2003
- [33] H.K. Kan, R.B. Waterhouse and D. Pavlickovski, “Compact dual concentric ring printed antennas,” IEE Proc.-Microw. Antennas Propag., Vol. 151, pp. 37-42,2004
- [34] G. Ruvio and M.J. Ammann,“From L-shaped planar monopoles to a novel folded antenna with wide bandwidth” IEE Proc.-Microw. Antennas Propag., Vol.153, pp. 456-460, 2006
- [35] M.D. Deshpande and M.C. Bailey, Input impedance of microstrip antennas, IEEE transactions on Antennas and Propagation, vol-AP-30, pp.645-660,1982
- [36] J.T. Aberle and D.M. Pozar, Analysis of infinite arrays of One and two probe fed circular patches, IEEE transactions on Antennas and Propagation, vol-AP-38, pp. 421-432,1990
- [37] M.C. Bailey and M.D. Deshpande, “Analysis of Elliptical and circular Microstrip Antennas Using Moment Method” IEEE transactions on Antennas and Propagation, vol-AP-33, pp. 954-959,1985

- [38] M. Haneshi and S. Yoshida, A Design Method of circularly Polarized Rectangular Microstrip Antenna by one point feed, in K.C. Gupta and A. Benalla, Artech House, pp.313-323,1988.
- [39] Jashwant S. Dahele, Kai-fong Lee and D.P. wong, Dual-frequency stacked annular-Ring microstrip Antenna, IEEE transactions on Antennas and Propagation, Vol. AP-35, No.11, pp. 1281-1285, 1987
- [40] Y. J. Sung, M. Kim, and Y.-S. Kim, "Harmonics Reduction With Defected Ground Structure for a Microstrip Patch Antenna," IEEE Trans. on Antennas and Propagat., vol. 2, pp. 111-113, 2003
- [41] S. Honda, M. Ito and Y.Jinbo, " A Disk Monopole antenna with 1:18 Impedance Bandwidth and Omnidirectional Radiation pattern," Int. Symp. Antennas Propagat. Pp. 1145-1148, 1992
- [42] M. Hammound, P. Poey and F. Colombel, " Matching the Input Impedance of a Broadband Disc Monopole," Electronics Lett., vol. 29, pp. 406-407, 1993
- [43] Narayan Prasad Agrawall, Girish Kumar, and K. P. Ray, "Wide Band Planar Monopole Antennas," IEEE Trans. on Antennas and Propagat., vol. 46, pp. 292-295, 1998
- [44] Z. N. Chen, "Broadband planar monopole antenna," IEE Proc.-Microw. Antennas Propag., Vol. 147pp. 526-528, 2000
- [45] Z. N. Chen and M. Y. W. Chia, "Impedance characteristics of triangular EMC planar monopole," Electronics Lett., vol. 37, pp. 1271-1272, 2001
- [46] Z.N. Chen, M.J. Ammann, M.Y.W. Chia and T.S.P. See, "Annular planar monopole antennas," IEE Proc.-Microw. Antennas Propag., Vol. 149, pp. 200-203, 2002

- [47] Kin-Lu Wong, Gwo-Yun Lee, and Tzung-Wern Chiou, "A Low-Profile Planar Monopole Antenna for Multiband Operation of Mobile Handsets," *IEEE Trans. on Antennas and Propagat.*, vol. 51, pp. 121-125, 2003
- [48] M. J. Ammann and Zhi Ning Chen, "A Wide-Band Shorted Planar Monopole With Bevel," *IEEE Trans. on Antennas and Propagat.*, vol. 51, pp. 901-903, 2003
- [49] Ching-Yuan Chiu, Pey-Ling Teng and Kin-Lu Wong, "Shorted, folded planar monopole antenna for dual-band mobile phone," *Electronics Lett.*, vol. 39, pp. 1301 - 1302, 2003
- [50] E. Antonino-Daviu, M. Cabedo-Fabres, M. Ferrando-Bataller and A. Valero- Nogueira, "Wideband double-fed planar monopole antennas," *Electronics Lett.*, vol.39, pp. 1635-1636, 2003
- [51] Jen-Yea Jan and Liang-Chih Tseng, "Small Planar Monopole Antenna With a Shorted Parasitic Inverted-L Wire for Wireless Communications in the 2.4-5.2, and 5.8-GHz Bands," *IEEE Trans. on Antennas and Propagat.*, vol. 52, pp. 1903-1905, 2004
- [52] Aaron J. Kerkhoff, Member, Robert L. Rogers and Hao Ling, "Design and Analysis of Planar Monopole Antennas Using a Genetic Algorithm Approach," *IEEE Trans. on Antennas and Propagat.*, vol. 52, pp. 2709-2718, 2004
- [53] Shun-Yun Lin, "Multiband Folded Planar Monopole Antenna for Mobile Handset," *IEEE Trans. on Antennas and Propagat.*, vol. 52, pp. 1790-1794, 2004
- [54] Kin-Lu Wong, Chih-Hsien Wu, and Saou-Wen Su, "Ultrawide-Band Square Planar Metal-Plate Monopole Antenna With a Trident-Shaped Feeding Strip," *IEEE Trans. on Antennas and Propagat.*, vol. 53, pp. 1262-1269, 2005

- [55] Wang-Sang Lee, Won-Gyu Lim, and Jong-Won Yu, "Multiple Band-Notched Planar Monopole Antenna for Multiband Wireless Systems," *IEEE Microwave and Wireless Comp. Lett.*, vol.15, pp. 576-578, 2005.
- [56] Wang-Sang Lee, Dong-Zo Kim, Ki-Jin Kim, and Jong-Won Yu, "Wideband Planar Monopole Antennas With Dual Band-Notched Characteristics," *IEEE Trans. on Antennas and Propagat.*, vol. 54, pp. 2800-2806, 2006
- [57] Sheng-Bing Chen, Yong-Chang Jiao, Wei Wang, and Fu-Shun Zhang, "Modified T-Shaped Planar Monopole Antennas for Multiband Operation," *IEEE Trans. On Antennas and Propagat.*, vol. 54, pp. 3267-3270, 2006
- [58] E. Antonino-Daviu, M. Cabedo-Fabre's, M. Ferrando-Bataller and A. Vila-Jimenez, "Active UWB antenna with tunable band-notched behavior," *Electronics Lett.*, vol. 43, pp. 959 - 960, 2007
- [59] Horng-Dean Chen and Hong-Twu Chen, "A CPW-Fed Dual-Frequency Monopole antenna," *IEEE Trans. Antennas Propagat.*, vol. 52, pp. 978-982, 2004
- [60] K. Chung, T. Yun and J. Choi, "Wideband CPW-fed monopole antenna with parasitic elements and slots," *Electron. Lett*, vol. 40, pp, 2008
- [61] W.C.Liu and C.-M. Wu, "Broadband dual-frequency CPW-fed planar monopole antenna with rectangular notch," *Electron. Lett*, vol.40, 2004.
- [62] W.C. Liu, "Broadband dual-frequency meandered CPW-fed monopole antenna," *Electron. Lett*, vol. 40, 2004
- [63] W.-C. Liu, "Wideband dual-frequency double inverted-L CPW-fed monopole antenna for WLAN application," *IEE Proc.-Microw. Antennas Propag.*, vol.152, pp.505-510, 2005
- [64] J. Liang, L.Guo, C.C.Chiau, X.Chen and C.G.Parini, "Study of CPW-fed circular disc monopole antenna for ultra wideband applications," *IEE Proc.-Microw. Antennas Propag.*, vol. 6, pp. 520-526 , 2005

- [65] Yi-Fang Lin, Chia-Ho Lin, Hua-Ming Chen and P. S. Hall, "A Miniature Dielectric Loaded Monopole Antenna for 2.4/5 GHz WLAN Applications," IEEE Microwave and Wireless Comp. Lett., vol.16 , pp. 591-593, 2006.
- [66] V. Zachou, C. G. Christodoulou, M. T. Chryssomallis, D. Anagnostou, and S.Barbin, "Planar Monopole Antenna with attached sleeves," IEEE Antennas and Wireless Pro. Lett., vol. 5, pp. 286-289, 2006
- [67] Yi-Cheng Lin and Kuan-Jung Hung, "Compact Ultrawideband Rectangular Aperture Antenna and Band-Notched Designs," IEEE Trans. Antennas Propagat., vol. 54, pp. 3075-3081, 2006
- [68] M.-T.Zhang,Y.-C.Jiao and F.-S.Zhang,"Dual-band CPW-fed folded-slot monopole antenna for RFID application," Electron. Lett,vol. 42, 2006.
- [69] W.C.Liu and H.J. Liu," Compact CPW-fed monopole antenna for 5 GHz wireless application," Electron. Lett, vol. 42, 2006
- [70] Joon Kim and Yong Jee, "Design of Ultrawideband Coplanar Waveguide-Fed LI-Shape Planar Monopole Antennas," IEEE Antennas and Wireless Pro. Lett., vol. 6, pp. 383-387, 2007
- [71] C.M.Wu,"Dual-band CPW-fed cross-slot monopole antenna for WLAN operation," IET Microw. Antennas Propag., vol.1 , pp. 542-546, 2007
- [72] Djaiz, T. A. Denidni and M. Nedil, "A new CPW-feed miniaturized antenna with Bandwidth Enhancement for Biomedical Localization applications," vol. , pp.539-542, 2007
- [73] Xian-Chang Lin and Cheng-Chieh Yu, "A Dual-Band CPW-Fed Inductive Slot-Monopole Hybrid Antenna," IEEE Trans. Antennas Propagat., vol. 56, pp. 282-285, 2006
- [74] Guorui Han, Wenwen Wang, Tingting An and Wenmei Zhang, "Compact Dual-Band CPW-Fed Antenna," 2008

- [75] Q. Wu, R. Jin, and J. Geng “Pulse preserving capabilities of printed circular disk monopole antennas with different substrates” *Progress In Electromagnetics Research*, PIER 78, 349–360, pp340-360, 2008
- [76] Y.B. Yang, F.S. Zhang, F. Zhang, L. Zhang and Y.-C. Jiao “A novel compact CPW fed planar monopole antenna with modified stair style ground for ultra wide band applications” *Microwave and optical technology letters* Vol. 52, No. 9, pp 2100-2104, September 2010
- [77] Peng Fei, Yong-Chang Jiao, Yang Zhu, and Fu-Shun Zhang” Compact CPW-FED monopole antenna and miniaturized ACS-fed Half monopole antenna for UWB applications” *Microwave and optical technology letters* Vol. 54, No. 7, pp 1605-1609, July 2012
- [78] Andi Hakim Kusuma, Abdel-Fattah Sheta, Ibrahim Elshafiey, Majeed Alkanhal, Saeed Aldosari, Zeeshan Siddiqui, and Saleh A. Alshebeili “A Novel Low SAR PIFA for Mobile Terminal” 2010 IEEE 21st International Symposium on Personal Indoor and Mobile Radio Communications pp 1-5
- [79] R. Augustine, T. Alves, T. Sarrebourg, B. Poussot, K.T. Mathew and J.M. Laheurte “Polymeric ferrite sheets for SAR reduction of wearable antennas” *Electronics Letters*, Vol. 46 No. 3, pp3-4, February 2010
- [80] Mohammad Tariqul Islam, Norbahiah Misran, Tan Sue Ling, Mohammad Rashed Iqbal Faruque,” Reduction of Specific Absorption Rate (SAR) in the Human Head with Materials and Metamaterial” 2009 International Conference on Electrical Engineering and Informatics 5-7 Selangor, Malaysia pp 707-710, August 2009
- [81] K H Chan, S W Leung, W K Lam and Y M Siu “Study of Using Fractional Spherical Phantom on SAR Evaluation” 2007 IEEE International Symposium on Electromagnetic Compatibility pp1-4

- [82] L.K.Ragha, M.S.Bhatia “Evaluation of SAR Reduction in Implanted Spherical Head Model Using RF Shield” pp9-12, 2009
- [83] K. H. Chan, K. M. Chow, L. C. Fung, and S. W. Leung “Effects of using conductive materials for SAR reduction in mobile phones” Microwave and optical technology letters Vol. 44, No. 2,pp140-144, January 2005
- [84] M.A.Mangoud, R.A. Abd-Alhameed, N.J. McEwan, P.S. Excell and E.A. Abdulmula “SAR reduction for handset with two element phased array antenna computed using hybrid MoM/FDTD technique” Electronics Letters, Vol. 35 No. 20 pp1693- 1694, 30th September 1999
- [85] Denise L. Hamblin, Vitas Anderson, Robert L. McIntosh, Ray J. McKenzie, Andrew W.Wood, Steve Iskra, and Rodney J. Croft “EEG Electrode Caps Can Reduce SAR Induced in the Head by GSM900 Mobile Phones” IEEE Transactions on Biomedical Engineering, Vol. 54, No. 5,pp914-920, May 2007
- [86] Cheng-Tse Lee and Kin-Lu Wong “Internal WWAN Clamshell Mobile Phone Antenna Using a Current Trap for Reduced Ground Plane Effects” IEEE Transactions on Antennas and Propagation, Vol.57, No. 10, pp3303-3308, October 2009
- [87] H.O. Ruoss and F.M. Landstorfer “Slot antenna for hand held mobile telephones showing significantly reduced interaction with the human body” Electronics Letters, Vol. 32 No. 6 pp513-514, 14th March 1996
- [88] Jiunn-Nan Hwang and Fu-Chiarng Chen “Reduction of the Peak SAR in the Human Head With Metamaterials” IEEE Transactions on Antennas on Antennas and Propagation, Vol. 54, No. 12,pp3763-3770, December 2006

- [89] Andi Hakim Kusuma, Abdel-Fattah Sheta, Ibrahim Elshafiey, Majeed Alkanhal, Saeed Aldosari, Zeeshan Siddiqui, and Saleh A. Alshebeili “A Novel Low SAR PIFA for Mobile Terminal” 2010 IEEE 21st International Symposium on Personal Indoor and Mobile Radio Communications, pp1117-1121
- [90] R. Augustine, T. Alves, T. Sarrebourg, B. Poussot, K.T. Mathew and J.M. Laheurte “Polymeric ferrite sheets for SAR reduction of wearable antennas” *Electronics Letters*, Vol. 46 No. 3 pp3-4, 4th February 2010
- [91] K. H. Chan, K. M. Chow, L. C. Fung, and S. W. Leung “Effects of using conductive materials for SAR reduction in Mobilephones” *Microwave and optical technology letters* Vol. 44, No. 2, pp140-144, January 2005
- [92] L.K.Ragha and M.S.Bhatia “Evaluation of SAR Reduction for Mobile phones Using RF Shields “ *International Journal of Computer Applications*, Vol.1, No. 13, pp 81-87,2010.
- [93] S.I. Kwak, D.U. Sim, J.H. Kwon and H.D. Choi “Experimental tests of SAR reduction on mobile phone using EBG structures” *Electronics Letters*, Vol. 44 No. 9, pp 2008-2009, 24th April 2008
- [94] M. B. Manapati and R. S. Kshetrimayum “ SAR Reduction in human head from Mobile phone radiation using single Negative Meta materials” *J. of Electromagn. Waves and Appl.*, Vol. 23, pp 1385-1385, 2009.
- [95] Marai M. Abousetta, Member, IEE, Ziad K. Alhamdani, Sal& I. Al-Mously, Mohammed E. Al-Daghistani and Khadija F. Omran “Triple-Frequency Operation for a Hand-Set Mobile Telephone with Reduced EMW Hazard” 10 Meditemean Electrotechnical Conference, MEleCon 2000, Vol. I, pp374-377
- [96] Weiping Dou “Chassis Optimisation of Monopole Antennas for SAR reduction” pp.124-127, 2002

- [97] S V Amos, M S Smith, D Kitchener” Modeling of Handset antenna interaction with the user and SAR reduction Techniques” National Conference on Antennas and Propagation: 30 March - 1 April 1999, Conference Publication No. 461, 12-19, 1999
- [98] Qinjiang Rao, Tayeb A. Denidni, Senior Member and Ronald H. Johnston “Dielectric Reflector Backed Aperture-Coupled Antennas for Reduced Back Radiation” IEEE Transactions on Electromagnetic Compatibility, Vol. 48, No. 2, pp 287-297, MAY 2006
- [99] Sang il Kwak, Dong-Uk Sim, Jong Hwa Kwon and Je Hoon Yun “Design of Multilayer PIFA based on an EBG structure for SAR reduction in mobile Applications” pp645-648, 2009
- [100] Jung-han Kim, Hong-min Lee “Efficient Electrically Small Wide Band Planar Antenna for SAR Reduction” Proceedings, 20th Int. Zurich Symposium on EMC, Zurich 2009, pp-269-272,2009
- [101] Filippo Costa, Agostino Monorchio, and Giuliano Manara “Analysis and Design of Ultra Thin Electromagnetic Absorbers Comprising Resistively Loaded High Impedance Surfaces” IEEE Transactions on Antennas and Propagation, Vol. 58, No. 5, pp1551-1558, May 2010
- [102] Luukkonen, C Simovski, G Granet, George Goussetis, D Lioubtchenko, A V. Raisanen, and Sergei A. Tretyakov “Simple and Accurate Analytical Model of Planar Grids and High-Impedance Surfaces Comprising Metal Strips or Patches” IEEE Transactions on Antennas and Propagation, Vol. 56, No.6, pp 1624-1632, , June 2008
- [103] D Sievenpiper, L Zhang, R F. Jimenez Broas, Nicholas G. Alex and Eli Yablonovitch, “High-Impedance Electromagnetic Surfaces with a Forbidden Frequency Band” IEEE Transactions on Microwave Theory and Techniques, Vol. 47, No. 11, pp 2059-2074, November 1999

- [104] M-Shing Lin , C-Hao Huang , and Chung G. Hsu “Techniques of Evaluating High Impedance Surfaces Used for SAR Reduction”, 2010 Asia-Pacific International Symposium on Electromagnetic Compatibility, April 12 - 16, Beijing, China pp210-213, 2010
- [105] Alireza Foroozesh, and Lotfollah Shafai “Investigation Into the Application of Artificial Magnetic Conductors to Bandwidth Broadening, Gain Enhancement and Beam Shaping of Low Profile and Conventional Monopole Antennas” IEEE Transactions on Antennas and Propagation, Vol.59, No.1,pp 4-20,January2011
- [106] Gallego-Gallego, O. Quevedo-Teruel, L. Inclan-Sanchez , E. Rajo-Iglesias, F. J. Garcia-Vidal “On the Use of Soft Surfaces to Reduce Back Radiation in Textile Microstrip Patch Antennas” Proceedings of the 5th European Conference on Antennas and Propagation (EUCAP),pp534-537
- [107] D.Sevenpiper, R.Broas and E.Yablonovitch “Antennas on High-Impedance Ground Planes” pp1245-1248, 1999.
- [108] J-Shiun Sun, Guan-Yu Chen, Cheng-Hung Lin, Kwong-Kau Tiong and Y. D. Chen “ Reflector Antenna with Artificial Magnetic Conductor Structure” Progress In Electromagnetics Research Symposium, Hangzhou, China, pp1379-1380, March 2008
- [109] J McVay, Ahmad Hoorfar and Nader Engheta, Villan “Thin absorbers using space filling curve Artificial Magnetic Conductors” “Microwave and optical Technology Letters , Vol. 51, No. 3, pp785-790, March 2009
- [110] R Gomez-Villanueva, H Jardon-Aguilar, R Linares y Miranda” State of the Art Methods for Low SAR Antenna Implementation” IEEE Transactions on Antennas and Propagation,pp1-4,2003

- [111] Chen, Z N, Kumar, G Ray “Artificial Magnetic conductor using Split ring resonators and its applications to antennas” Microwave and optical Technology Letters, Vol. 48, No. 2, pp 329-334, February 2006.
- [112] Sang il Kwak, Dong-Uk Sim, and Jong Hwa Kwon “Design of Optimized Multilayer PIFA With the EBG Structure for SAR Reduction in Mobile Applications” IEEE Transactions on Electromagnetic compatibility, Vol.53, No. 2, pp 325-331, May 2011
- [113] Shun-Yun Lin, Yuan-Chih Lin, Yong-Ren Cheng, and Jian- Rong Wu “Folded Wire Antenna with Low SAR” Asia-Pacific Microwave Conference 2011,pp,638-641

.....✂.....

DEVELOPMENT AND ANALYSIS OF MODIFIED MONOPOLE ANTENNA SUITABLE FOR MOBILE HANDSET

<i>Contents</i>	<i>3.1 Introduction</i>
	<i>3.2 Requirements for Antennas used in mobile handsets</i>
	<i>3.3 Coplanar wave guide feed: an overview</i>
	<i>3.4 CPW fed printed monopole antenna</i>
	<i>3.5 Modified CPW fed antenna with radiation characteristic suitable for mobile handset</i>
	<i>3.6 Chapter conclusion</i>

The experimental and simulated investigations towards the development of modified monopole antenna which have radiation characteristics highly suitable for mobile handset are presented in this chapter. The omni directional radiation characteristic of the monopole antenna is modified with single null along one direction and considerable radiation along all other directions. Investigations on the radiation characteristic of the monopole antenna with resonating structures like split ring resonator, single metal strip and vertical stripes are conducted and discussed in this chapter.

3.1 Introduction

In the last two decades, the use of the cellular phones has become the most popular mode of communication across the globe and it is the most common media used for making connections with different people. Moreover, these devices are highly portable and low cost. At the same time, the concerns about the cellular phone radiation effects have increased in the general public. A major controversy exists about the possible adverse, chronic health effects due to human exposure to Electro Magnetic Radiation (EMR). Some researchers hold that exposure to even the low EMR fields for relatively short period of time will positively result in significant increases in cancers, genetic defects and abnormal behavioral patterns [1]. Other experts hold that these findings are failure, so more objective research is required before an accurate risk assessment can be made.

But a working group of 31 scientists from 14 countries after a meeting at the WHO's International Agency for Research on Cancer (IARC), after reviewing all the available scientific evidence suggested that cell phone use should be classified as "possibly carcinogenic". And they admit that mobile phones may increase the risk for brain tumors. In all these aspects, it is necessary to decrease the interaction of electromagnetic energy towards human head when mobile handset is in operation.

3.2 Requirements for Antennas used in mobile handsets

The antenna is the gateway of wireless communication systems. And it interfaces the free-space medium and the RF transceiver systems. In the modern mobile communication systems, due to the technology development, multidisciplinary functional mobile phone antennas are required. Even though a variety of antenna structures have been used in cellular handsets, they are expected to have certain characteristics:

- a) Occupy minimum volume
- b) Light weight
- c) Multi-band operation for different communication standards
- d) Adequate bandwidth
- e) Omnidirectional radiation characteristics
- f) Negligible impact on the biological tissue of the user, to avoid health risks
- g) Low fabrication cost
- h) Conformability with mounting hosts etc.....

It is clear that some of the requirements are mutually exclusive so a compromise has to be worked out in the designing process. The amount of electromagnetic radiation in the environment has increased day by day and at the same time the people are more concerned about the possible health risks of these wireless devices. However, to minimize the amount of energy absorbed by the user is a challenging task from the technical point of view.

To have negligible impact on the biological tissue of the user, two methods can be adopted

- a) Reduce the radiated power towards the user.
- b) Limiting the time of exposure.

The time factor mainly relates to the time duration and the frequency of mobile phone usage. So the only possibility is to find different methods to reduce the radiation towards user. The reduction of power absorbed by the user can tremendously avoid any possible health hazards. The energy absorbed by the

human tissue should fulfill the radiation limitations. Various techniques are adopted by researchers for reducing the antenna radiation effect towards human head.

Adding an external shield to mobile phones is the most common method adopted for reducing the unnecessary radiations [2]. Here, shielding structure has to be integrated with the antenna to provide better shielding effectiveness. The material selection and position of the external shield is also very important. A ferrite sheet attached to the front side, close to head can also reduce radiation [3]. However, the parameters such as attaching location, size and material properties of ferrite sheet played an important role in the reduction effectiveness. Highly directive antennas [4,5] can also reduce radiation towards human head significantly. But the adoption of highly directive antennas certainly causes degradation in signal reception from other directions. Researchers have explored PIFA (Planar Inverted F Antenna) with EBG (Electromagnetic Band Gap) surface [6] on the ground plane to reduce radiation towards human head. All these techniques adopt separate external shielding elements for reducing the radiation. But this deteriorates the structure simplicity and compactness.

In this chapter, the main concern is to develop a mobile antenna which gives reduced RF interference to the user. The investigations are to develop an antenna with an aim to improve the radiation characteristics of monopole antenna with good radiation characteristics in all directions except in one direction. The modification of the radiation pattern of a monopole antenna is implemented by using different resonating structures. It also provides a detailed discussion about the development of different antennas having this radiation characteristic. The simulation results are experimentally verified and an exhaustive parametric analysis is performed to study the effect of various antenna parameters.

The first section briefly describes planar printed CPW (CoPlanar Waveguide) fed monopole antenna, which is used as the basic antenna for developing proposed mobile antennas with less RF interaction towards the user.

3.3 Coplanar Wave Guide feeds: an over view

The coplanar waveguide (CPW) transmission line concept was proposed by Cheng P Wen in 1969. A conventional CPW fed transmission line on a dielectric substrate consists of a centre metallic strip conductor with semi-infinite ground planes parallel and adjacent to the conducting strip on the same side as shown in figure. 3.1.

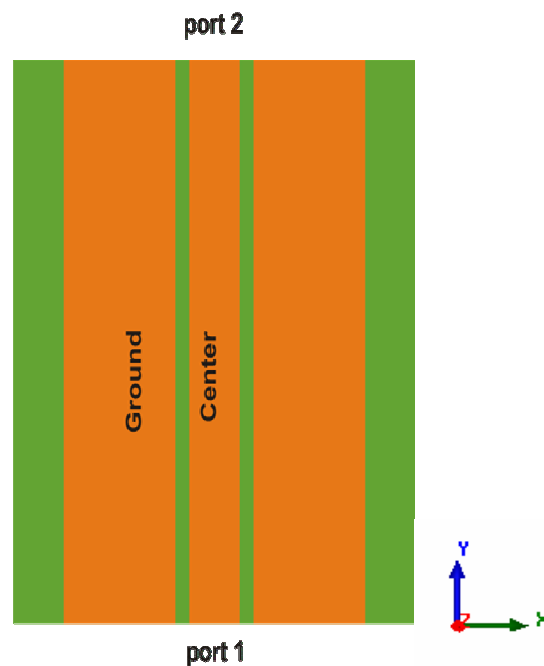


Fig. 3.1. CPW fed transmission line

This structure supports a quasi-TEM mode of propagation. The CPW offers several advantages like, low cost, light weight, ease of fabrication, facilitates easy shunt as well as series surface mounting of active and passive devices, eliminates the need for wraparound and via holes, reduces radiation

loss. In addition a ground plane exists between any two adjacent lines, hence cross talk effects between adjacent lines are very weak. As a result, CPW circuits are ideally suited for MIC as well as MMIC applications.

3.3.1 Field distribution in CPW

Usually the CPW system is excited by connecting center conductor of a coaxial connector to the signal strip and outer ground conductor to the two outer strips. The electric and magnetic field distribution of CPW transmission line is depicted in figure. 3.2. In this case the electric field distributions in the slots are out of phase, and it cancels at the far field with the encircled magnetic field on each strips. This forcefully excites the odd mode like field distribution in CPW. This field distribution is maintained in this structure due to the feed symmetry.

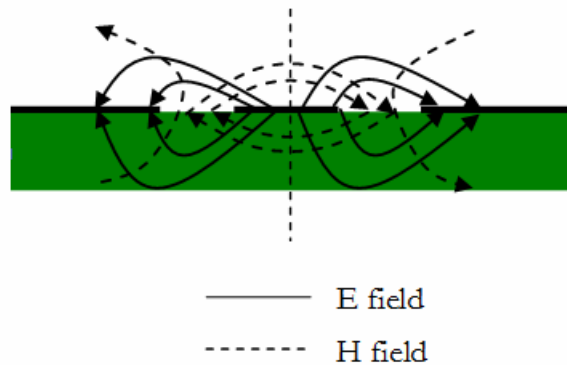
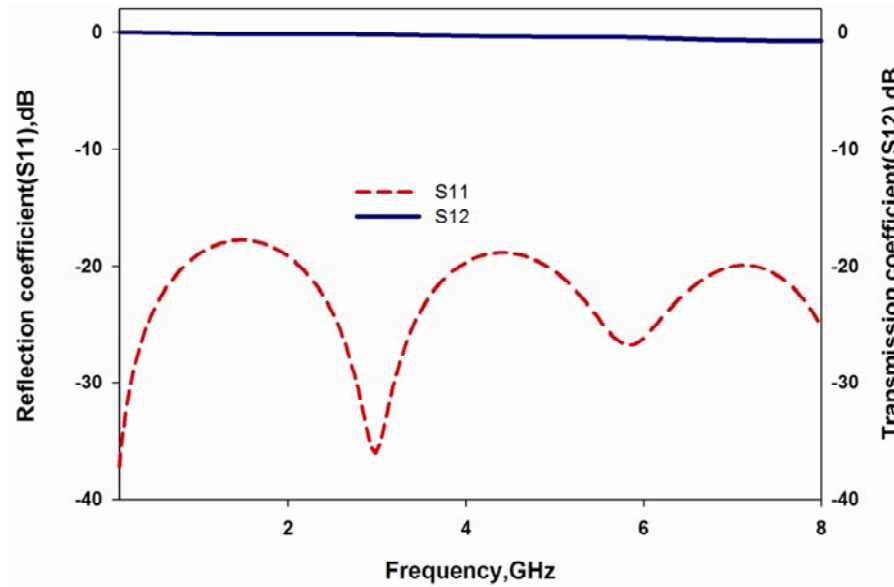


Fig. 3.2. E field and H field distribution in a CPW fed transmission line

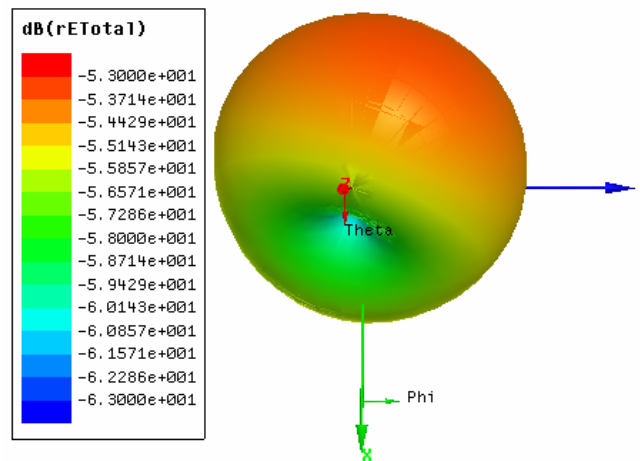
3.3.2 Transmission and reflection characteristics of the conventional CPW transmission line

A 50Ω CPW fed transmission line is designed [7] on a substrate of relative permittivity ϵ_r (4.4) and thickness h (1.6mm). For this transmission line the width is found to be 3mm. The magnitude of transmission and reflection characteristics of a 50Ω matched CPW transmission line is shown in figure 3.3(a). It is found from the figure that the system is acting as a perfect transmission line. The line is perfectly

matched and the return loss is better than -18dB in the band of interest. The insertion loss of the system is also very low. This confirms it is acting as a transmission line. The radiation pattern of the line is shown in figure 3.3(b).



(a)



(b)

Fig.3.3. (a) Transmission and reflection characteristics (b) Radiation characteristic of a CPW transmission line (width=3mm, $\epsilon_r=4.4$,h =1.6mm)

The maximum power radiated along the bore sight direction is -55 dB. This shows the radiation from the system is very feeble. From the above figures it is observed that, this device behaves as a pure transmission line with negligible radiation.

3.4 CPW fed printed monopole antenna

An open ended CPW transmission line can be converted into an efficient radiator by creating discontinuity on the structure. A basic coplanar wave guide (CPW) fed printed monopole antenna is developed by extending the signal strip length of a normal open ended CPW planar transmission line.

The geometry of a CPW fed monopole antenna printed on a substrate of relative permittivity ϵ_r and thickness h (top and side view) is shown in figure .3.4.

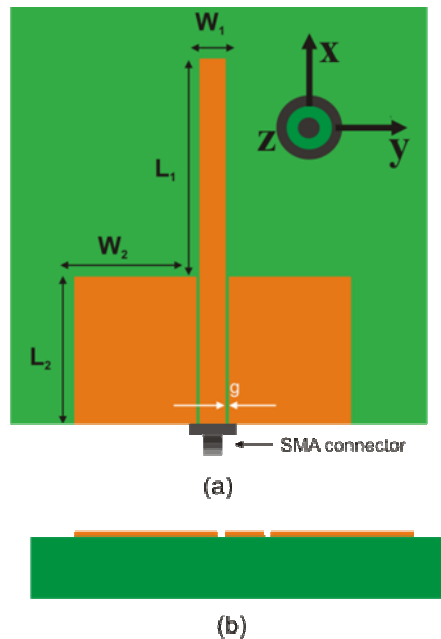


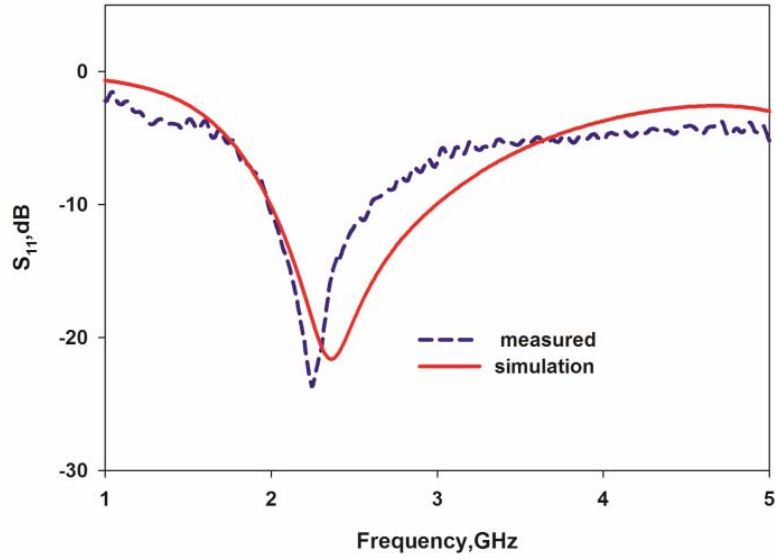
Fig.3.4. Geometry of the Coplanar Waveguide Fed Monopole Antenna.(a) top view (b) side view ($L_1 = 25\text{mm}$, $W_1 = 3\text{mm}$, $g = 0.35\text{mm}$, $L_2 = 17\text{mm}$, $W_2 = 14\text{mm}$, $h=1.6\text{mm}$ and $\epsilon_r=4.4$).

The signal strip width W_1 and signal to ground gap (g) is selected for 50Ω impedance using standard design equations. The main radiating element is a vertical strip of length $L_1 = 25\text{mm}$ and width $W_1 = 3\text{ mm}$. This is acting as a $\lambda_g/4$ monopole, where λ_g is the wavelength in the substrate. The ground plane dimension are $L_2 = 17\text{mm}$ and $W_2 = 14\text{ mm}$. The antenna is excited with a SMA (Sub Miniature Amphenol) connector. The antenna is fabricated using photolithographic technique and the simulation results are experimentally verified using HP8510C Vector Network Analyzer.

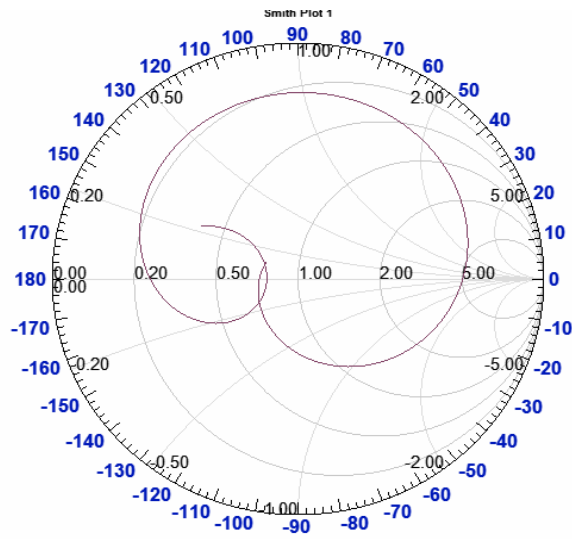
3.4.1 Reflection Characteristics

The measured reflection characteristic of the strip monopole antenna with design parameters $L_1 = 0.25\lambda_g$, $W_1 = 0.03\lambda_g$, $L_2 = 0.17\lambda_g$, $W_2 = 0.14\lambda_g$, $h = 1.6\text{mm}$ and $\epsilon_r = 4.4$ is shown in figure. 3.5(a). From the graph it is clear that the strip monopole provides a resonance at 2.3 GHz from 1.98 GHz to 2.58 GHz with a bandwidth of 0.6 GHz, 26%. The simulated return loss characteristic of the strip monopole antenna is also shown in the same graph for comparison. It is observed that the results are in good agreement.

Figure 3.5(b) shows the input impedance characteristics of the antenna and can be inferred that the input impedance is purely resistive at resonance and both the sides of the resonant frequency the impedance becomes either inductive or capacitive. For the monopole the resonance occurs around 2.3GHz where the input impedance is nearly 50Ω .



(a)



(b)

Fig.3.5. (a) Reflection characteristics (b) input impedance characteristics of the CPW fed monopole antenna at 2.3 GHz ($L_1 = 25\text{mm}$, $W_1 = 3\text{mm}$, $g = 0.35\text{mm}$, $L_2 = 17\text{mm}$, $W_2 = 14\text{mm}$, $h=1.6\text{mm}$ and $\epsilon_r=4.4$).

3.4.2 Resonance phenomenon

The resonance phenomenon of the coplanar wave guide (CPW) fed monopole antenna is similar to a quarter wavelength conventional wire monopole antenna. The resonance of the CPW fed monopole antenna can be explained on the basis of sinusoidal current variation along the strip monopole above finite ground plane.

The simulated surface current distribution of a typical monopole antenna above a finite ground plane is shown in figure. 3.6. The length of the strip monopole is $\lambda_g / 4$ (where $\lambda_g = \frac{\lambda_0}{\sqrt{\epsilon_{eff}}}$ and $\epsilon_{eff} = \frac{\epsilon_r + 1}{2}$) and width W_1 is 3mm.

From the figure it is very clear that there is quarter wavelength variation of field along the strip. From the surface current distribution it can be inferred that the surface current at the tip of the monopole is minimum. Maximum surface current is observed near the ground. The simulated current distributions confirm that antenna is resonant with quarter wavelength current variation along the strip.

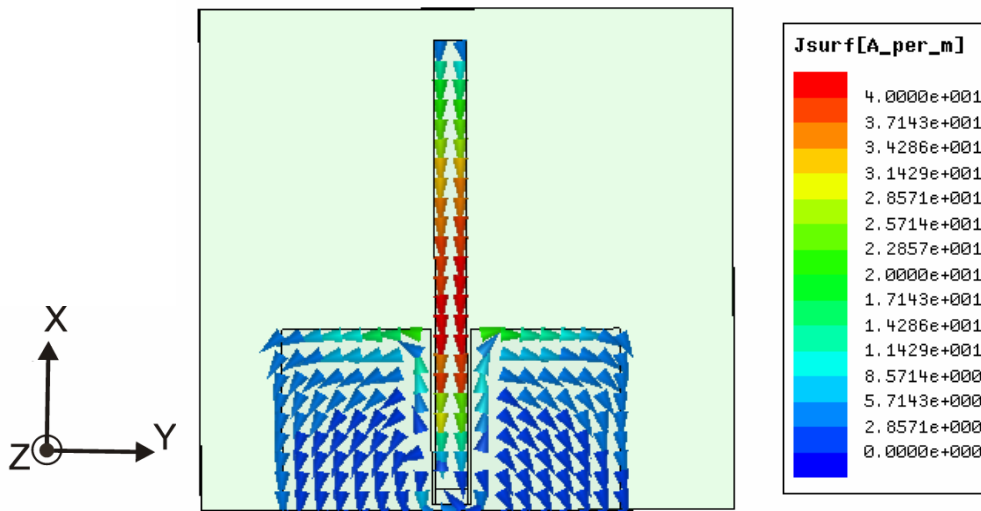


Fig.3.6. Computed surface current density ($L_1 = 25\text{mm}$, $W_1 = 3\text{mm}$, $g = 0.35\text{mm}$, $L_2 = 17\text{mm}$, $W_2 = 14\text{mm}$, $h=1.6\text{mm}$ and $\epsilon_r=4.4$).

As predicted from the current density plot it is clear that the radiated electromagnetic signal is linearly polarized along X direction.

3.4.3 Parametric analysis

The parametric analysis of the proposed CPW fed monopole antenna is conducted and effects of various antenna parameters on the antenna characteristics are studied. The results and discussion on various parametric studies are provided in this session. The parametric analysis is carried out using Ansoft HFSS.

3.4.3.1 Effect of signal strip length (L_1) on reflection coefficient

The influence of the length (L_1) of the signal strip on the resonant frequency of the antenna is shown in figure 3.7. The resonant frequency of the antenna highly depends on the length of the strip. The resonant frequency decrease with increase in length as expected. The length of the monopole L_1 is taken to be equal to a quarter of the dielectric wavelength corresponding to operating frequency in the substrate.

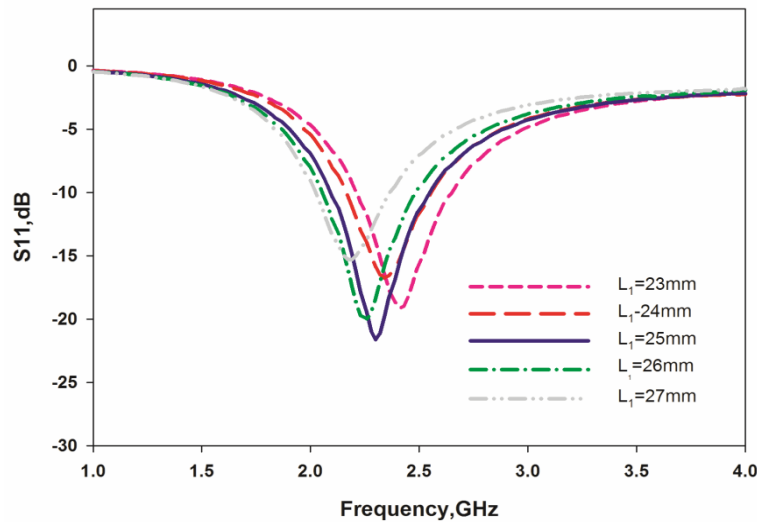


Fig 3.7. Effect of signal strip length L_1 on the input reflection of the monopole antenna
 ($W_1 = 3$ mm, $g = 0.35$ mm, $L_2 = 17$ mm, $W_2 = 14$ mm, $h=1.6$ mm and $\epsilon_r=4.4$).

3.4.3.2 Effect of ground plane width (W_2) on the reflection coefficient

The ground plane dimension is an important factor for the design of compact antenna. The variation of return loss with the ground plane width is shown in figure 3.8. It can be noted that the ground plane width (W_2) significantly affects the band width and matching conditions of the antenna. From the variation studies it is found that better matching is achieved when the ground plane width is $0.14\lambda_g$.

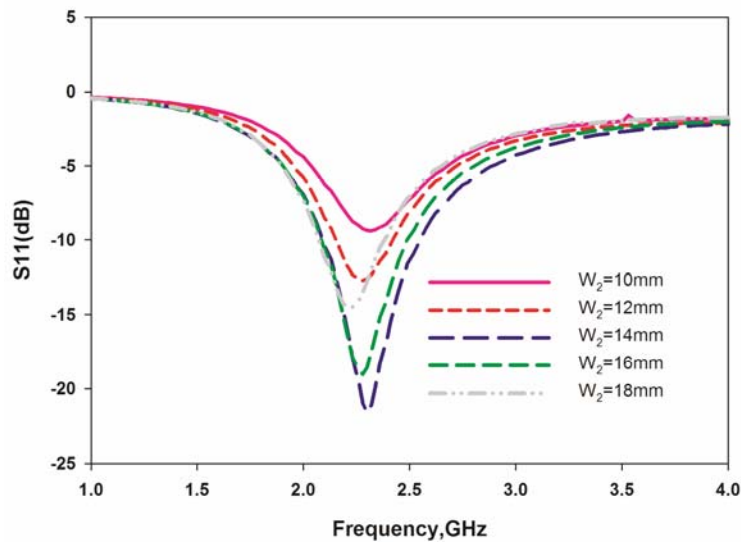


Fig 3.8. Effect of ground plane width (W_2) of the monopole antenna on the reflection coefficient ($L_1 = 25\text{mm}$, $W_1 = 3\text{mm}$, $g = 0.35\text{mm}$, $L_2 = 17\text{mm}$, $h=1.6\text{mm}$ and $\epsilon_r=4.4$).

3.4.3.3 Effect of ground plane length (L_2) on reflection coefficient

The length of the ground plane L_2 is varied by keeping the length of the strip above the ground plane equal to quarter of the dielectric wavelength corresponding to the resonant frequency 2.3GHz. It is not affecting the resonant frequency of the antenna. But it can be noted from figure 3.9 that the ground plane length significantly affects the matching conditions of the antenna. In this case, the ground plane length (L_2) of $0.17\lambda_g$ is taken as optimum as far as the

matching is concerned. It is also noted that the resonance frequency is virtually independent of L_2 .

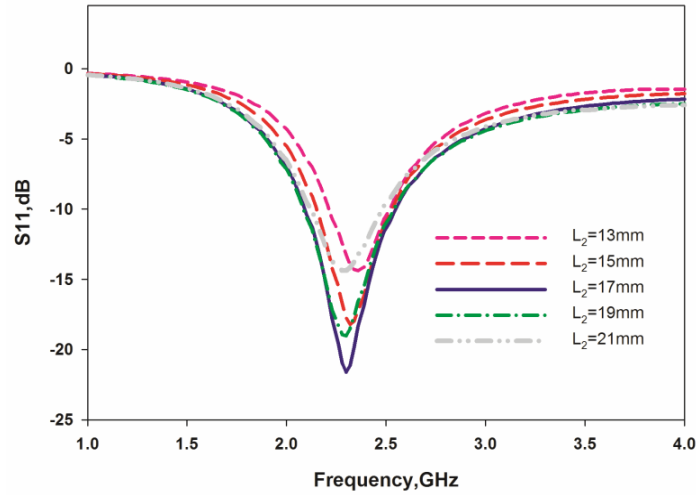


Fig 3.9. Variation of reflection coefficient of the antenna with Ground plane length of the monopole antenna ($L_1 = 25\text{mm}$, $W_1 = 3\text{mm}$, $g = 0.35\text{mm}$, $W_2 = 14\text{mm}$, $h=1.6\text{mm}$ and $\epsilon_r=4.4$).

3.4.4 Gain

The measured gain of the antenna along the bore sight direction is depicted in figure.3.10.

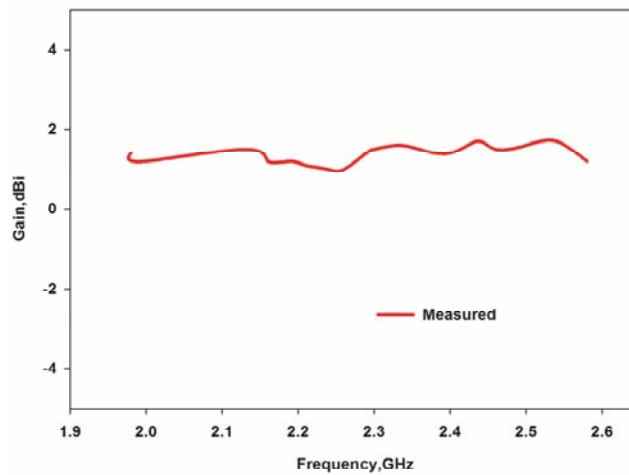


Fig.3.10. Measured gain of the Coplanar Waveguide Fed printed Monopole Antenna ($L_1 = 25\text{mm}$, $W_1 = 3\text{mm}$, $g = 0.35\text{mm}$, $L_2 = 17\text{mm}$, $W_2 = 14\text{mm}$, $h=1.6\text{mm}$ and $\epsilon_r=4.4$).

The antenna provides a moderate gain greater than 1dBi throughout the operating band. The maximum gain in the band is 1.7dBi at 2.43GHz with an average gain of 1.4 dBi.

3.4.5 Radiation characteristics

The radiation characteristics of the CPW fed printed monopole antenna is presented in this section. The three dimensional pattern is shown in figure 3.11. It is clear from the simulated 3D radiation pattern that the pattern is omnidirectional in nature with two deep nulls along positive and negative X direction. The nulls are along the axis of the dipole and cannot be conveniently used for reducing radiation towards the user due to mounting problem in the mobile handset. So for better coverage a pattern with single null is desirable.

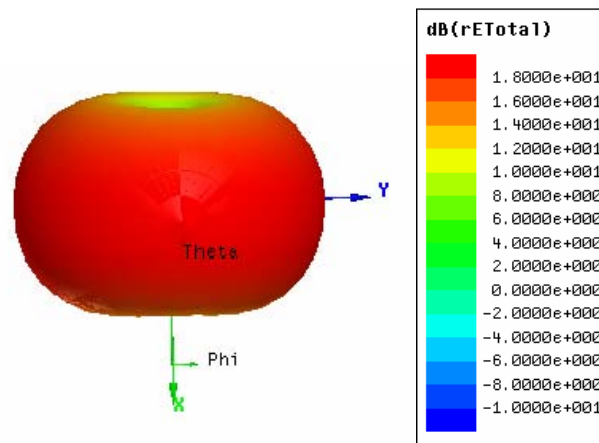


Fig.3.11. Simulated 3D radiation pattern
($L_1 = 25\text{mm}$, $W_1 = 3\text{mm}$, $g = 0.35\text{mm}$, $L_2 = 17\text{mm}$,
 $W_2 = 14\text{mm}$, $h=1.6\text{mm}$ and $\epsilon_r=4.4$).

The 2 D Co-polar and Cross polar radiation patterns of the antenna along E plane and H plane are depicted in figure 3.12(a) and (b) respectively. From the figure it can be seen that the CPW fed monopole antenna exhibits a figure of eight pattern in the E plane and a non-directional pattern in the H plane.

Moreover, the antenna exhibits more than 30dB cross polarization isolation on both E and H plane along the boresight direction.

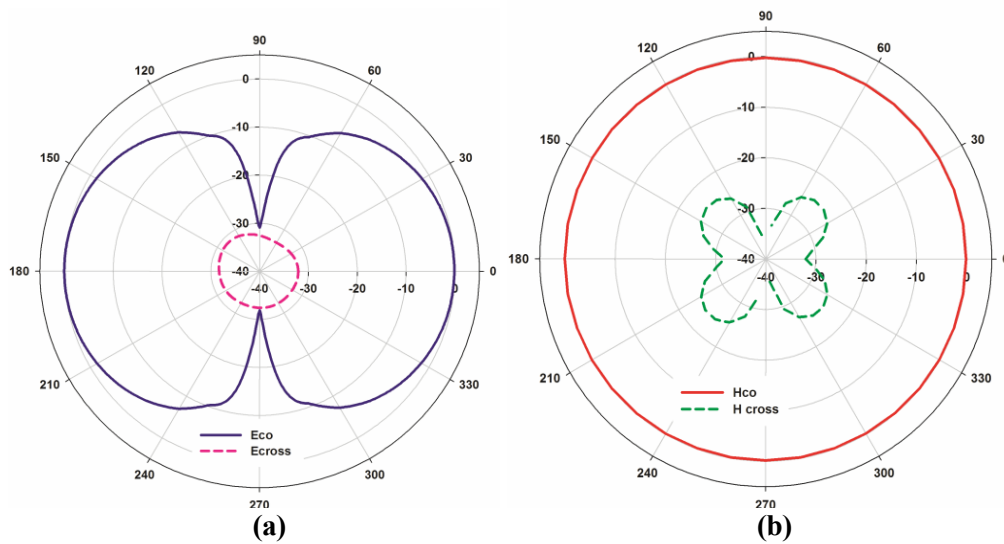


Fig 3.12. 2D radiation pattern of the antenna(a) E plane (b) H plane ($L_1 = 25\text{mm}$, $W_1 = 3\text{mm}$, $g = 0.35\text{mm}$, $L_2 = 17\text{mm}$, $W_2 = 14\text{mm}$, $h=1.6\text{mm}$ and $\epsilon_r=4.4$).

3.4.6 Inferences

Table 3.1 summarizes the characteristics of the CPW fed monopole antenna which is considered as basic antenna for the further studies in the next section of this chapter

Table 3.1. Characteristics of the CPW fed monopole antenna

Characteristics	CPW fed monopole
Resonant frequency and Return loss	2.3 GHz, 23dB
Band width	± 300 MHz
Radiation pattern	E plane-Figure of Eight H plane-Non directional (circular)
Area	42mm X31.7mm $\epsilon_r = 4.4, h=1.6\text{mm}$
Ground dimension	14mmX17mm
Gain	1.4dBi

The omnidirectional radiation pattern of the above antenna has to be modified to reduce the RF exposure to human head.

3.5 Modified CPW fed antenna with radiation characteristic suitable for mobile handset

The finite ground coplanar waveguide fed monopole antenna is an efficient radiator and can be utilized for modern wireless communication gadgets. The major disadvantage of the printed monopole antenna when it is used in mobile handset is that, the RF interaction with the user is extremely high due to its radiation characteristics.

The electromagnetic interaction between the antenna and the human head can be reduced by modifying the radiation pattern of the monopole antenna. This can be achieved by using different resonating elements like

- 1) **Split Ring Resonators (SRR)**
- 2) **Single metallic strip**
- 3) **Parallel vertical strips**

These elements are printed at the back side of a normal CPW fed monopole antenna.

3.5.1 Development of Mobile antenna with Split Ring Resonator (SRR)

The split ring resonators (SRRs) have been used in planar circuit technology for the design of novel compact printed microwave components. SRRs are planar structures with two concentric conducting rings with slits etched on opposite sides.

The schematic diagram of the SRR unit cell is shown in the figure 3.13. It consists of two concentric rings with width 'w' and split gap 't'. These rings with inner radii of r_1 and r_2 are separated by a distance 'd'.

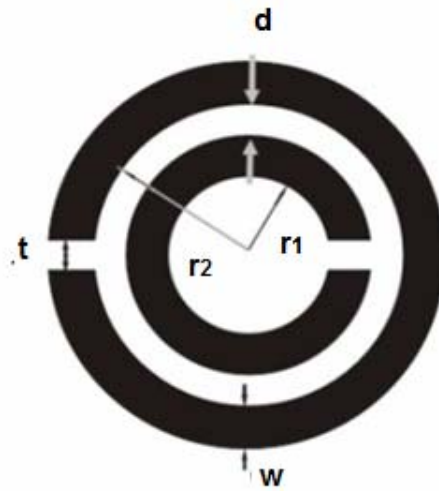


Fig.3.13. Schematic drawing of an SRR unit cell

SRR can be considered as a parallel LC circuit with a resonant frequency, which can be tuned by varying the dimensions. SRRs would be excited by a time varying magnetic field with significant component parallel to the ring axis. A time varying magnetic field applied parallel to the axis of SRR induces rotating currents in the rings, which produces its own magnetic flux to enhance or oppose the incident field. Due to splits in the rings, the SRR unit can be made to resonate at wavelengths much larger than the diameter of the rings [8]. The second split ring inside and the slit opposite to the first will generate large capacitance in the small gap region between the rings, which enables current flow by means of new displacement current. The dimension of the structure is smaller than the free space wavelength resulting in low radiative losses and so very high quality factor.

The resonance frequency of SRR unit cell is calculated by placing the cell on a microstrip transmission line. SRR is coupled to the conventional microstrip line as shown in figure.3.14(a) [9]. To penetrate the maximum H-field lines through the axis of the resonator, the SRR unit cell is shifted laterally with

respect to the transmission line centre along the x-axis [10]. The S_{21} plot for SRR cell placed above the microstrip line is shown in figure 3.14(b). The SRR unit cell is found to resonate at 2.1 GHz.

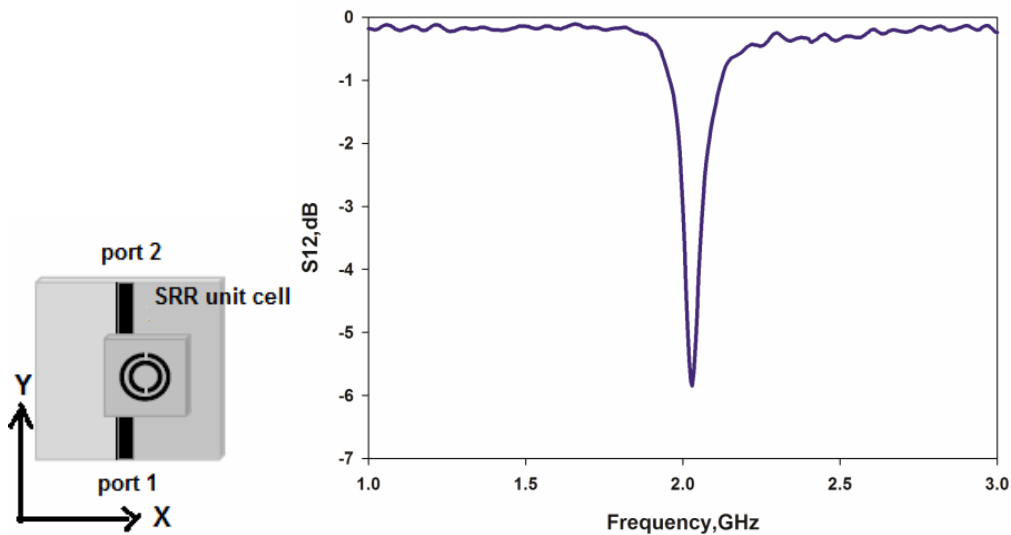


Fig 3.14. (a) SRR unit cell above the microstrip line (b) S_{21} plot of SRR superstrate

In this section the radiation characteristics of a CPW fed monopole antenna loaded with single SRR unit cell is investigated [11]. The presence of SRR at the back of the monopole antenna leads to modify the non directional radiation pattern in the azimuth plane, along with a small shift in the resonant frequency towards the lower side. The impedance matching and radiation pattern at the resonance frequency depends on the height of the superstrate as well as its relative position with respect to the planar monopole antenna.

3.5.1.1 Antenna geometry

The geometry of the SRR based monopole antenna is shown in figure.3.15

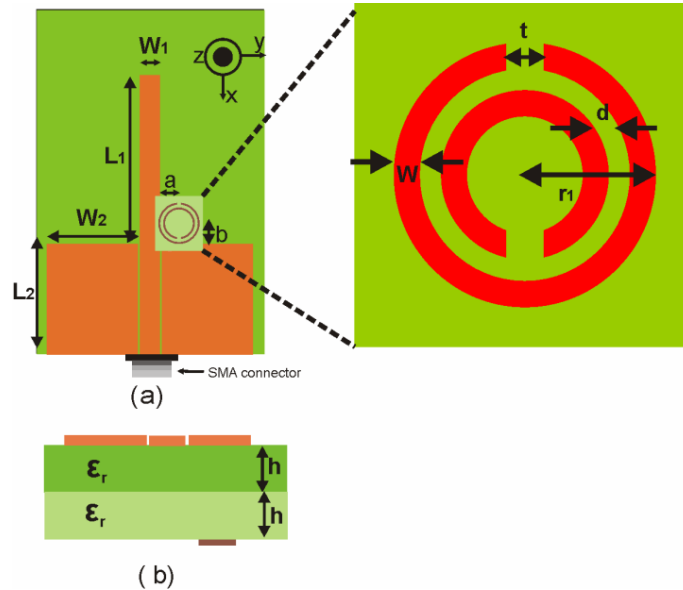


Fig 3.15. Geometry of the CPW fed monopole antenna with SRR as substrate
(a) Top view (b) side view ($L_1 = 25\text{mm}$, $W_1 = 3\text{mm}$, $g = 0.35\text{mm}$, $L_2 = 17\text{mm}$, $W_2 = 14\text{mm}$, $h=1.6\text{mm}$ and $\epsilon_r=4.4$, $r_1 = 6.3\text{mm}$, $W = 0.9\text{mm}$, $d = 0.6\text{mm}$, $t = 0.5\text{mm}$).

The geometry consists of a strip monopole of length, L_1 with lateral ground plane of dimension $L_2 \times W_2$ on dielectric Layer 1. The strip monopole is loaded with a SRR patch on dielectric Layer 2 with outer ring radius of $r_1 = 6.3\text{mm}$, ring width $w = 0.9\text{mm}$, separation between the two rings $d = 0.6\text{mm}$ and split gap $t = 0.5\text{mm}$. Both the strip monopole and the SRR unit cell were fabricated on a substrate of relative permittivity, $\epsilon_r = 4.4$ and thickness, $h = 1.6\text{mm}$. The SRR is placed at the optimum position and electromagnetically excited with the monopole. The center of SRR unit cell is placed with an offset of 1.7mm 'a' from the right edge of the feed and 1.3mm 'b' from the top edge of the right ground (figure 3.15(a)).

3.5.1.2 Reflection and Impedance Characteristics

The reflection characteristics of the SRR loaded monopole antenna along with the real part of impedance are shown in figure 3.16(a) and (b) respectively.

By loading the SRR unit cell at the optimum position, it is observed that a new resonance appears at the lower frequency centered at 1.74 GHz. But the antenna is found to be poorly matched at this resonant frequency. This is due to the inefficient coupling between the monopole and SRR. The real part of impedance at this frequency is found to be 18.68Ω only.

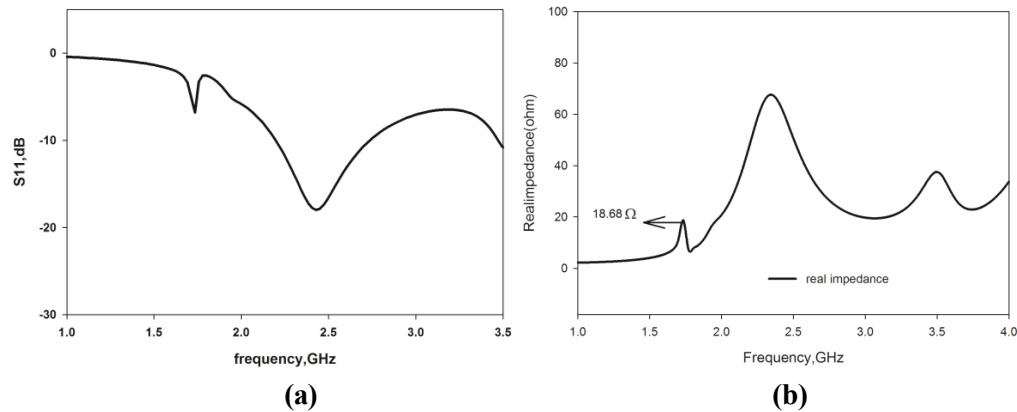


Fig 3.16(a) Reflection characteristics (b) Impedance plot of CPW fed monopole antenna loaded with SRR ($L_1 = 25\text{mm}$, $W_1 = 3\text{mm}$, $g = 0.35\text{mm}$, $L_2 = 17\text{mm}$, $W_2 = 14\text{mm}$, $h=1.6\text{mm}$ and $\epsilon_r=4.4$, $r_1 =6.3\text{mm}$, $W = 0.9\text{mm}$, $d = 0.6\text{mm}$, $t = 0.5\text{mm}$).

3.5.1.3 Simulated 3D radiation characteristics

The simulated 3D radiation pattern of the antenna at the first resonant frequency (1.74GHz) is shown in figure 3.17. It is observed that this antenna provides less radiation towards positive Y direction. Without SRR loading the pattern was omni-directional (figure 3.11). With SRR loading a null is observed along positive Y direction. The creation of null in the radiation pattern with

SRR loading is utilized for reducing the radiation towards the user. The antenna radiation in XZ plane is almost unidirectional.

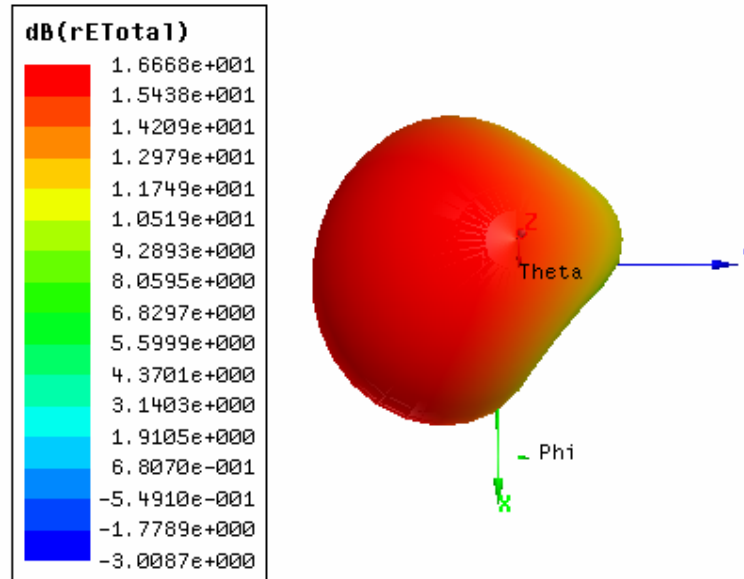


Fig 3.17. Simulated 3D radiation pattern of CPW fed monopole antenna with SRR as substrate

($L_1 = 25\text{mm}$, $W_1 = 3\text{mm}$, $g = 0.35\text{mm}$, $L_2 = 17\text{mm}$, $W_2 = 14\text{mm}$, $h=1.6\text{mm}$ and $\epsilon_r=4.4$, $r_1 = 6.3\text{mm}$, $W = 0.9\text{mm}$, $d = 0.6\text{mm}$, $t = 0.5\text{mm}$)

3.5.1.4 Modified monopole with SRR printed on the same substrate.

From the previous studies, it is clear that the SRR structure can provide a resonance at lower side with radiation characteristics suitable for a mobile handset. Even though the antenna is offering a resonance at lower frequency the impedance matching is poor. Moreover, the structure is bulky and mechanically not robust due to the multilayered structure. In this section, the development of an antenna with improved impedance matching on a single layer substrate is discussed. The antenna radiation characteristics and parametric analysis are also discussed.

The geometry of the proposed SRR printed monopole antenna is shown in figure.3.18. The SRR unit cell structure is directly printed at the back side of the conventional monopole to modify the radiation pattern.

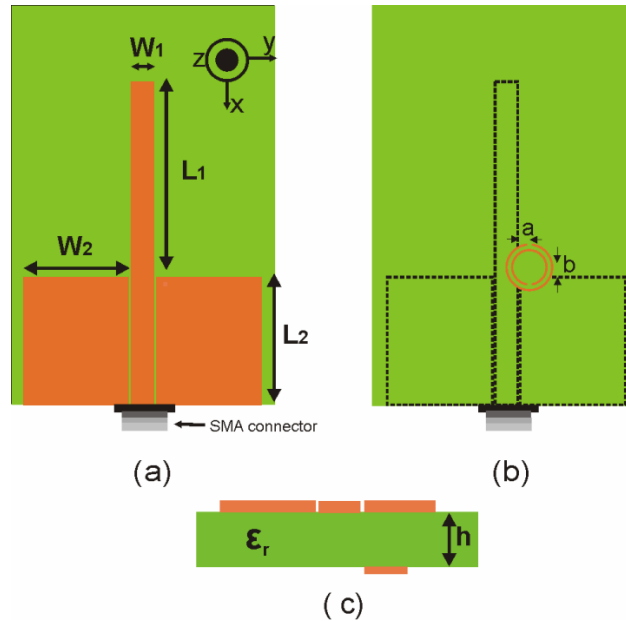


Fig 3.18. Geometry of the CPW fed monopole antenna with printed SRR
 ($L_1 = 25\text{mm}$, $W_1 = 3\text{mm}$, $g = 0.35\text{mm}$, $L_2 = 17\text{mm}$, $W_2 = 14\text{mm}$,
 $h=1.6\text{mm}$ and $\epsilon_r=4.4$, $r_1 = 6.3\text{mm}$, $W = 0.9\text{mm}$, $d = 0.6\text{mm}$,
 $t = 0.5\text{mm}$, $a=1.7\text{mm}$, $b=1.3\text{mm}$).

The monopole is excited with a 50Ω CPW feed line. The antenna is etched on a substrate of thickness 1.6mm and relative permittivity (ϵ_r) 4.4. The parameters of the monopole antenna and SRR are same as the previous design ($L_1=25\text{mm}$, $W_1 = 3\text{mm}$, $L_2=17\text{mm}$ and $W_2 = 14\text{mm}$, $g=0.35\text{mm}$, $r_1=6.3\text{mm}$, $d=0.6\text{mm}$, $w=0.9\text{mm}$, $t=0.5\text{mm}$, $a=1.7\text{mm}$ and $b=1.3\text{mm}$) but are printed on either side of a single layer substrate.

3.5.1.5 Reflection characteristics

The experimental and simulated reflection coefficients of the SRR loaded monopole antenna are shown in figure.3.19. The simulation result is in good agreement with the measured values. It is seen from the reflection characteristics that the antenna operates from 1.75GHz to 1.91GHz with a fractional bandwidth of 8.7% centered at 1.8GHz. Thus by loading the SRR structure at the optimum position, it is observed that the monopole resonance shifts to a lower resonance of 1.8GHz. The single layer structure of this prototype provides better coupling between the SRR and monopole, resulting in improved impedance matching. Due to the high quality factor of SRR structures the bandwidth of the antenna is only 160MHz.

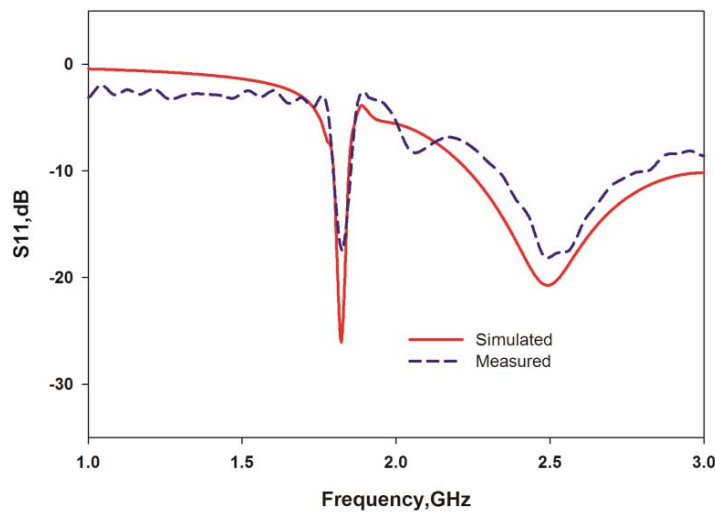


Fig 3.19. Reflection coefficient of the CPW fed monopole antenna with printed SRR
 $(L_1 = 25\text{mm}, W_1 = 3\text{mm}, g = 0.35\text{mm}, L_2 = 17\text{mm}, W_2 = 14\text{mm}, h=1.6\text{mm}$ and $\epsilon_r=4.4, r_1=6.3\text{mm}, W = 0.9\text{mm}, d = 0.6\text{mm}, t = 0.5\text{mm})$

3.5.1.6 Radiation pattern

The simulated 2D radiation patterns along the principle planes at resonance are shown in figure.3.20. It is observed that the antenna provides

nearly constant radiation patterns along XZ plane. The antenna radiation in YZ plane is almost non-directional with single null along the positive Y-direction. This pattern is suitable for mobile handset devices. Compared to the radiated power along the boresight direction it is seen that the radiated power is reduced by nearly 18 dB along the null direction. The antenna is providing very good coverage in the three quadrants with less coverage in one quadrant. This less coverage area can be directed towards the user to reduce the strong illumination. This is an ideal pattern required for a mobile phone with reduced illumination towards the user.

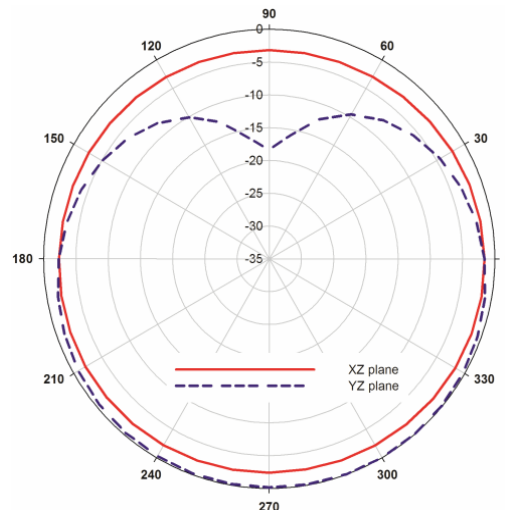


Fig 3.20 Simulated 2D radiation pattern in XZ and YZ plane of the monopole antenna with printed SRR
($L_1 = 25\text{mm}$, $W_1 = 3\text{mm}$, $g = 0.35\text{mm}$, $L_2 = 17\text{mm}$, $W_2 = 14\text{mm}$, $h=1.6\text{mm}$ and $\epsilon_r=4.4$, $r_1=6.3\text{mm}$, $W = 0.9\text{mm}$, $d = 0.6\text{mm}$, $t = 0.5\text{mm}$)

The measured 2D radiation patterns of the antenna in XY and YZ planes are shown in figure 3.21 (a) and (b) respectively. From the patterns it is clear that there is a reduction in radiated power along the positive y direction ($\phi = 90^\circ$ degree). It is very interesting to note that the radiated power along the Y direction is reduced considerably and better than -20 dB.

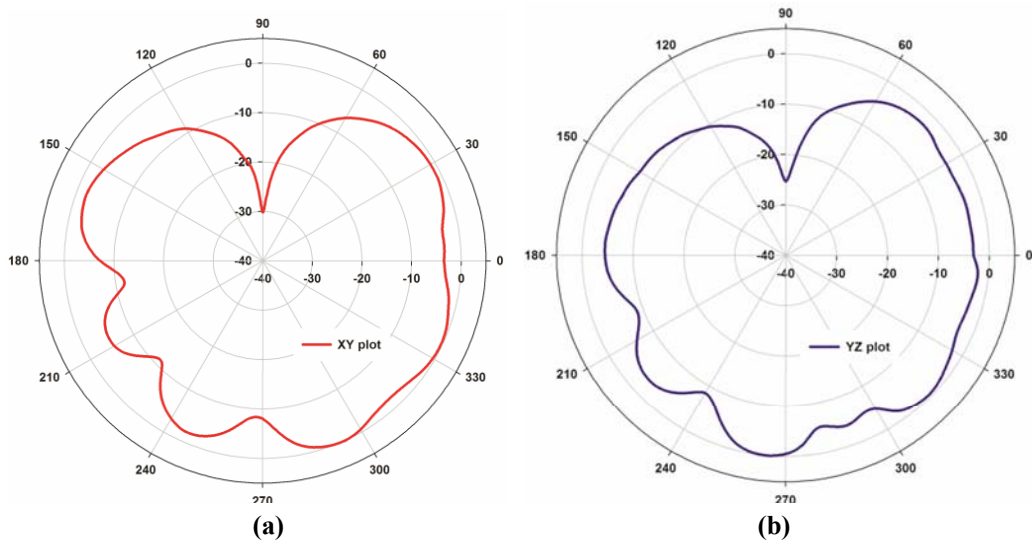


Fig 3.21 Measured 2D radiation pattern of the monopole antenna with printed SRR (a)XY plane (b)YZ plane
 $(L_1 = 25\text{mm}, W_1 = 3\text{mm}, g = 0.35\text{mm}, L_2 = 17\text{mm}, W_2 = 14\text{mm}, h=1.6\text{mm}$
 and $\epsilon_r=4.4, r_1=6.3\text{mm}, W = 0.9\text{mm}, d = 0.6\text{mm}, t = 0.5\text{mm})$

3.5.1.7. 3D radiation pattern

The simulated 3D far field radiation pattern at 1800MHz of the proposed antenna is shown in figure 3.22.

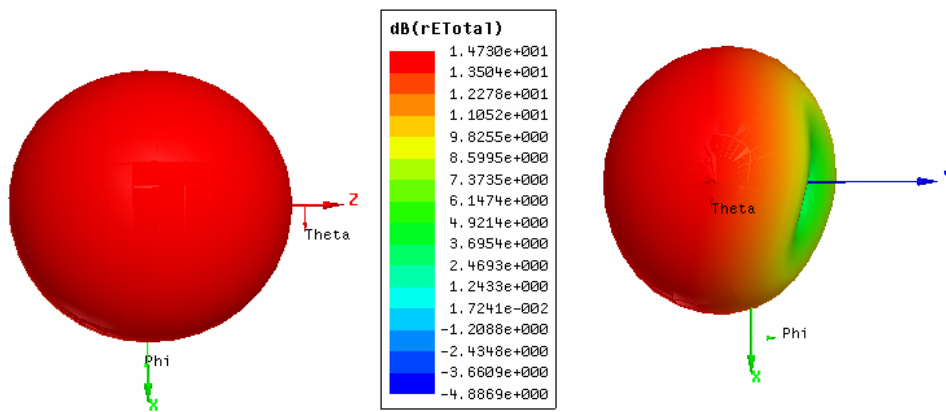


Fig 3.22. Simulated 3D radiation pattern of the monopole antenna with printed SRR
 $(L_1 = 25\text{mm}, W_1 = 3\text{mm}, g = 0.35\text{mm}, L_2 = 17\text{mm}, W_2 = 14\text{mm},$
 $h=1.6\text{mm}$ and $\epsilon_r=4.4, r_1=6.3\text{mm}, W = 0.9\text{mm}, d = 0.6\text{mm}, t = 0.5\text{mm})$

The directional pattern of the monopole antenna in the elevation plane is modified to a pattern suitable for mobile handset. The figure shows that the proposed antenna is radiating in the negative Y direction and offers a null along the positive Y direction. Moreover, there is only one null appeared in the pattern. The reduction in the field intensity is nearly -18dB.

3.5.1.8 Effect of SRR parameters on antenna performance

The parametric analysis of the proposed antenna is conducted and effects of SRR parameters over the antenna characteristics are studied. The results and discussion on various parametric studies are provided in this section.

3.5.1.8.1. SRR location

The effect of 'a' (the position from the right edge of the monopole strip to the center of SRR) on the reflection characteristics of the antenna is shown in figure.3.23. It is found that this affect the impedance match of the antenna.

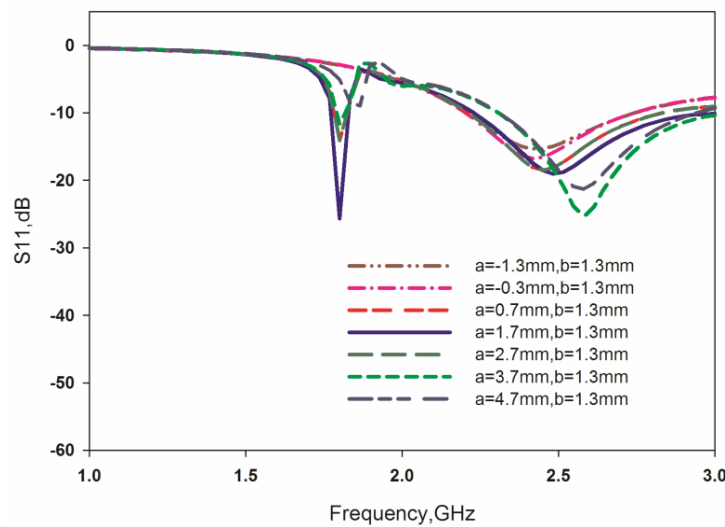


Fig 3.23. The variation of reflection characteristic with the effect of position 'a' of the printed SRR
($L_1 = 25\text{mm}$, $W_1 = 3\text{mm}$, $g = 0.35\text{mm}$, $L_2 = 17\text{mm}$, $W_2 = 14\text{mm}$, $h=1.6\text{mm}$ and $\epsilon_r=4.4$, $r1 =6.3\text{mm}$, $W = 0.9\text{mm}$, $d = 0.6\text{mm}$, $t = 0.5\text{mm}$, $b=1.3\text{mm}$)

The effect of 'b' over the reflection characteristics is depicted in figure 3.24. It is found from the plot that as the position of the SRR varies vertically from 0.5mm to 2.1mm the impedance matching varies drastically. The optimum position is found to be $a = 1.7\text{mm}$ and $b = 1.3\text{mm}$ for maximum impedance matching.

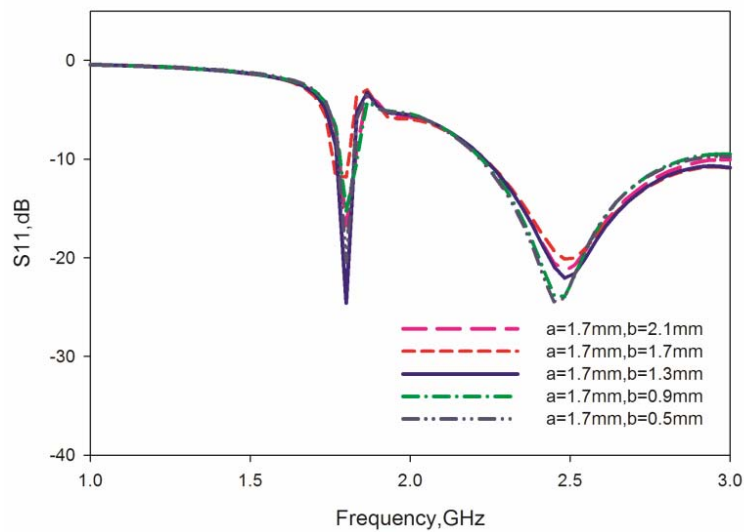


Fig 3.24. The variation of reflection characteristic with the effect of position 'b' of the printed SRR

($L_1 = 25\text{mm}$, $W_1 = 3\text{mm}$, $g = 0.35\text{mm}$, $L_2 = 17\text{mm}$, $W_2 = 14\text{mm}$, $h = 1.6\text{mm}$ and $\epsilon_r = 4.4$, $r_1 = 6.3\text{mm}$, $W = 0.9\text{mm}$, $d = 0.6\text{mm}$, $t = 0.5\text{mm}$, $a = 1.7\text{mm}$)

The SRR is placed at an offset position determined by the parameters 'a' (the position from the right edge of the monopole strip to the center of SRR along Y direction) and 'b' (distance from the right top edge to SRR center position along negative X direction). Figure 3.25 shows 3D radiation pattern of the antenna at two different positions of SRR ($[a = 8\text{mm}, b = 1.3\text{mm}]$ and $[a = 10\text{mm}, b = 1.3\text{mm}]$), printed above the ground of monopole antenna. In both cases SRR unit cell is positioned without overlapping with the ground plane. This resonating structure like SRR is not showing a radiation pattern suitable for mobile handset when it is

placed with an offset from the ground plane. Thus a ground coupling is essential for the structure to modify the pattern suitable for handheld mobile devices. The patterns shown in figure 3.25 (a) and (b) have two nulls along X axis. As far as the coverage is concerned this is not desirable one.

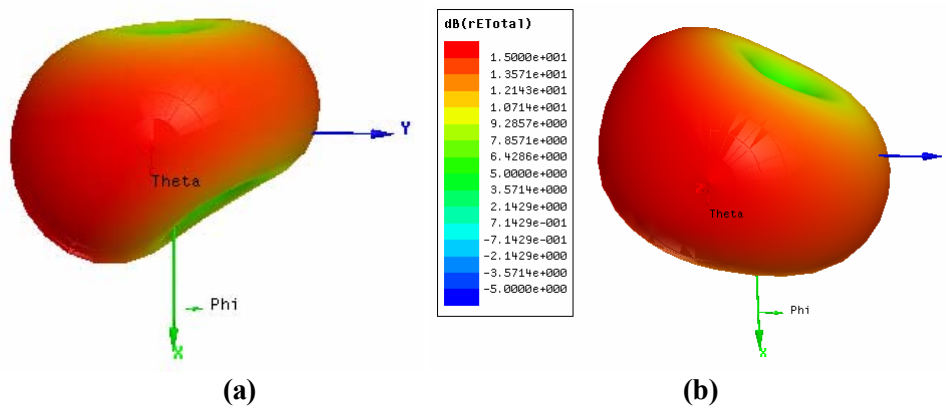


Fig. 3.25. Simulated 3D radiation pattern at different position of SRR
(a) a=8mm,b=1.3mm (b) a=10mm,b=1.3mm ($L_1 = 25\text{mm}$,
 $W_1 = 3\text{mm}$, $g = 0.35\text{mm}$, $L_2 = 17\text{mm}$, $W_2 = 14\text{mm}$, $h=1.6\text{mm}$ and
 $\epsilon_r=4.4$, $r_1 = 6.3\text{mm}$, $W = 0.9\text{mm}$, $d = 0.6\text{mm}$, $t = 0.5\text{mm}$)

It is found that the location of the SRR and its dimension plays an important role in the antenna characteristics. The impedance of the antenna at the lower resonance is highly depending on the offset location of the SRR structure. The SRR structure should have a direct coupling below the ground plane of monopole antenna to modify the radiation pattern. Impedance matching at the resonance changes with the position of SRR.

3.5.1.9 Inferences

The radiation characteristics of CPW fed monopole antenna loaded with SRR unit cell as superstrate and printed SRR on the ground plane are presented. The proposed antenna operates at GSM 1800 MHz operating band. Modification of the radiation characteristics of monopole antenna depends on

relative position of SRR with respect to the ground plane. Investigation shows that SRR structure at the back side of a CPW fed monopole antenna can modify the radiation characteristics with less RF exposure.

3.5.2 Development of Mobile antenna with single metal strip

The CPW fed printed monopole antenna with metamaterial structure (SRR) gives a distinct resonance as discussed in the previous section. But the main drawback for that design is the lower bandwidth (8.7%) due to the high quality factor of SRR. In this section the design, development and analysis of a single metal strip printed antenna suitable for mobile handset is presented and discussed.

3.5.2.1 Antenna Geometry

The geometry of the proposed antenna with front, back and side view is shown in figure 3.26. The main radiating element is a vertical strip of length $L_1=25\text{mm}$ and width $W_1=3\text{mm}$ which is acting as a $\lambda_g/4$ monopole. The ground plane dimension are $L_2=17\text{mm}$ and $W_2=14\text{mm}$. The gap between monopole strip and ground plane ($g=0.35\text{mm}$) is designed for 50Ω impedance matching. A single metal strip with length $L_3=26\text{mm}$, width $W_3=9.9\text{mm}$ is printed on the back side of same substrate with a separation (S) of 2mm with an offset (P) of 4.5mm from the top of the monopole. By properly optimising the metal strip position, the radiation pattern can be modified. The prototype of the antenna is fabricated on a substrate of dielectric constant (ϵ_r) 4.4 and $h=1.6\text{mm}$ with an overall dimension of $42\times 28\text{mm}^2$.

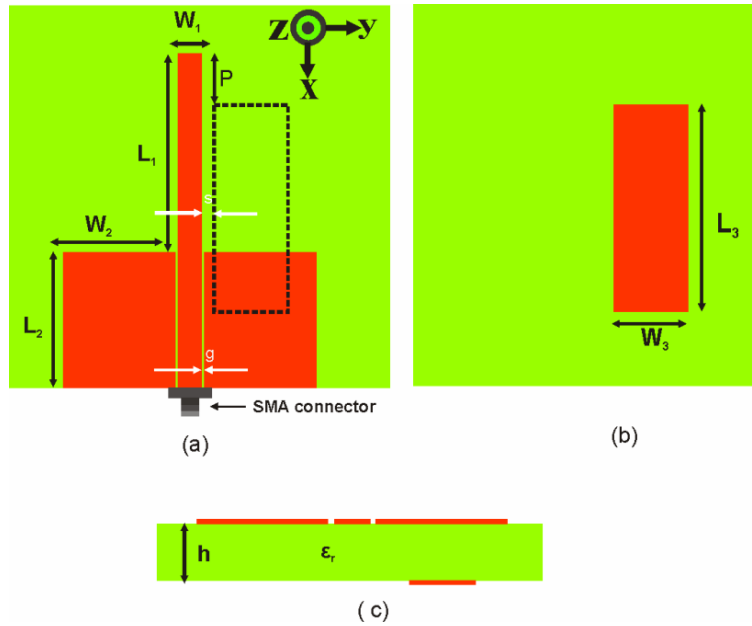


Fig3.26. Geometry of the monopole antenna with single strip (a)3D schematic diagram (b)bottom view (c) Side view ($L_1=25\text{mm}$, $W_1=3\text{mm}$, $L_2=17\text{mm}$, $W_2=14\text{mm}$, $g=0.35\text{mm}$, $L_3=26\text{mm}$, $W_3=9.9\text{mm}$, $h=1.6\text{mm}$, $\epsilon_r=4.4$, $P=4.5\text{mm}$ and $S=2\text{mm}$.)

3.5.2.2 Reflection characteristics

The simulated and experimental reflection characteristic of the single strip loaded monopole antenna is shown in figure. 3.27(a). The antenna is found to resonate at 1.81GHz with a 2:1 VSWR bandwidth of 230MHz (1.76 GHz to 1.99 GHz), which is wide enough to cover the 1.8GHz application band.

The reflection coefficient with and without the metallic strip for this prototype is shown in figure. 3.27(b). It is seen from the plot that by introducing the metallic strip the resonant frequency shift to a lower frequency region. Thus the metallic strip can improve the compactness of the antenna at a particular frequency of operation when compared to a normal CPW fed monopole antenna.

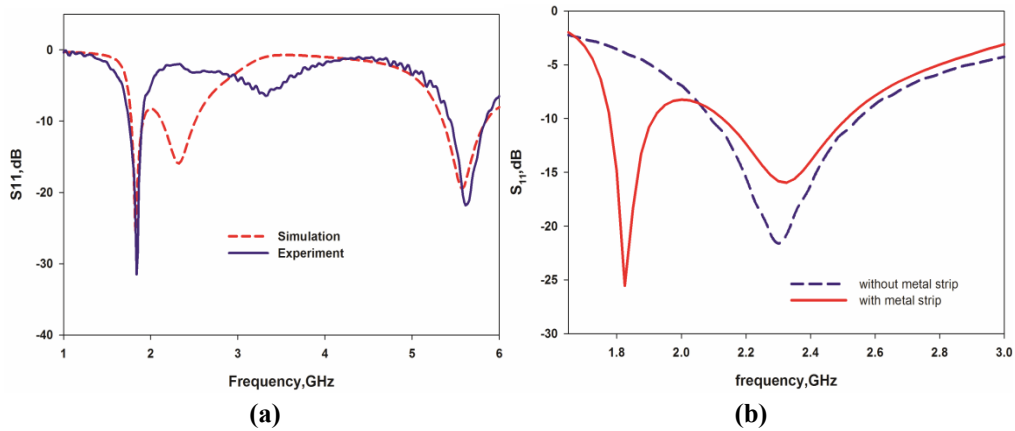


Fig.3.27. The reflection characteristic of the antenna (a) Experiment and simulation (b) with and without metal strip ($L_1=25\text{mm}, W_1=3\text{mm}, L_2=17\text{mm}, W_2=14\text{mm}, g=0.35\text{mm}, L_3=26\text{mm}, W_3=9.9\text{mm}, h=1.6\text{mm}, \epsilon_r=4.4, P=4.5\text{mm}$ and $S=2\text{mm}$.)

3.5.2.3 Radiation pattern

The simulated 3D far field radiation pattern of the proposed antenna at 1810MHz is shown in figure.3.28. It is interesting to note that the antenna provides a considerable reduction in total radiated power along the positive Y direction. There is only one null in the pattern and the antenna is radiating on all the other three quadrants with almost equal power which is highly suitable for a mobile handset.

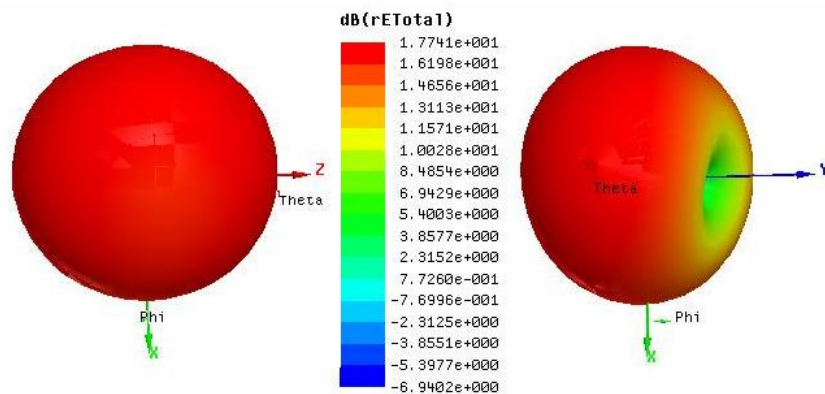


Fig 3.28. Simulated 3D pattern of the monopole antenna with printed single strip ($L_1=25\text{mm}, W_1=3\text{mm}, L_2=17\text{mm}, W_2=14\text{mm}, g=0.35\text{mm}, L_3=26\text{mm}, W_3=9.9\text{mm}, h=1.6\text{mm}, \epsilon_r=4.4, P=4.5\text{mm}$ and $S=2\text{mm}$)

Thus by placing a metallic strip at the optimum position, the harmful effect of electromagnetic radiation can be avoided. This reduction is approximately 20dB as seen from the figure.

Measured 2D radiation patterns of the antenna in YZ and XY plane at the resonance frequency are shown in figure 3.29(a) and (b) respectively. The measured pattern is very suitable for mobile handset with good radiation in three space quadrants with reduced radiation in one quadrant. This property can be conveniently employed to reduce the EM interaction towards the head of a mobile phone user.

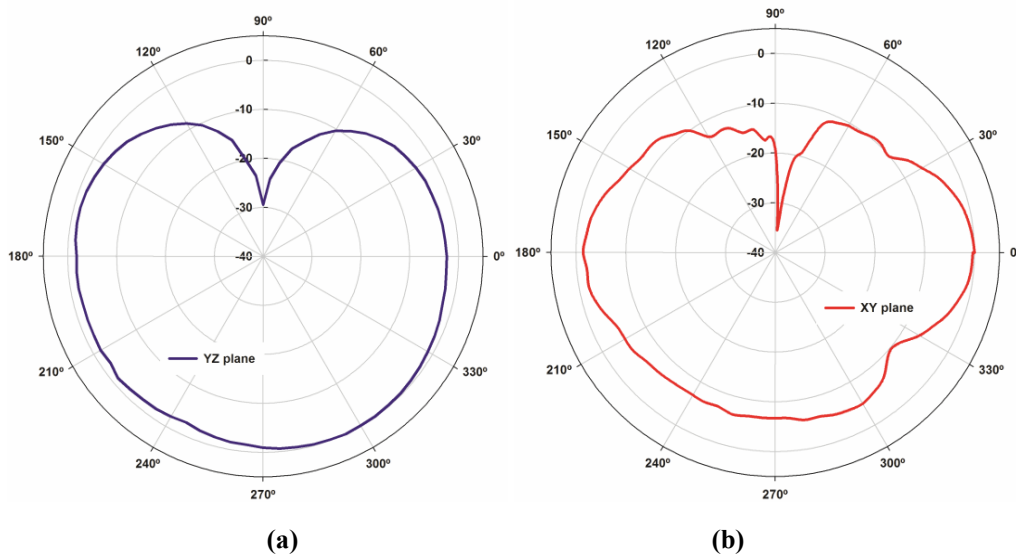


Fig. 3.29. Measured radiation pattern (a) YZ plane (b) XY plane
($L_1=25\text{mm}$, $W_1=3\text{mm}$, $L_2=17\text{mm}$, $W_2=14\text{mm}$, $g=0.35\text{mm}$, $L_3=26\text{mm}$, $W_3=9.9\text{mm}$, $h=1.6\text{mm}$, $\epsilon_r=4.4$, $P=4.5\text{mm}$ and $S=2\text{mm}$)

The antenna patterns in YZ plane with and without metal strip at the backside are shown in figure.3.30. From the figure it is observed that the figure of eight pattern of the monopole antenna gets modified with a pattern having a single null along positive Y direction. Thus omnidirectional characteristic of the monopole antenna is modified to that suitable for specific mobile applications.

The radiated power is reduced to more than 25dB along the positive Y-direction. Moreover the power remains same in the negative Y-direction. Thus the radiated power was rearranged to that suitable for mobile gadgets.

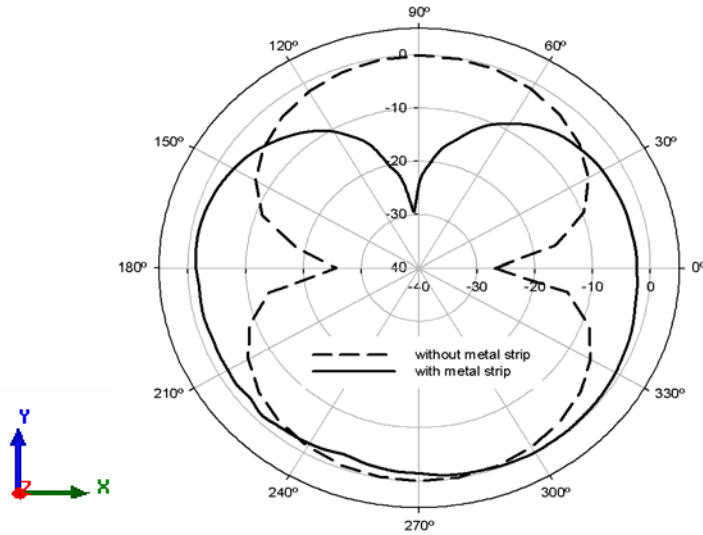


Fig. 3.30. Radiation pattern of the antenna with and without printed strip ($L_1=25\text{mm}, W_1=3\text{mm}, L_2=17\text{mm}, W_2=14\text{mm}, g=0.35\text{mm}, L_3=26\text{mm}, W_3=9.9\text{mm}, h=1.6\text{mm}, \epsilon_r=4.4, P=4.5\text{mm}$ and $S=2\text{mm}$)

3.5.2.4 Parametric Analysis

In this section the parametric analysis of metal strip on the antenna characteristics, are narrated.

3.5.2.4.1 Effect of strip width (W_3) on reflection characteristics of the antenna

The strip width, W_3 is varied from 9.5 to 10.3mm and its influence on the reflection characteristics are shown in figure.3.31. From the figure it is seen that the first resonance frequency is virtually independent of strip width. But the strip width has considerable effect on the second frequency. The strip width of 9.9mm is taken as optimum width, which gives the maximum impedance matching.

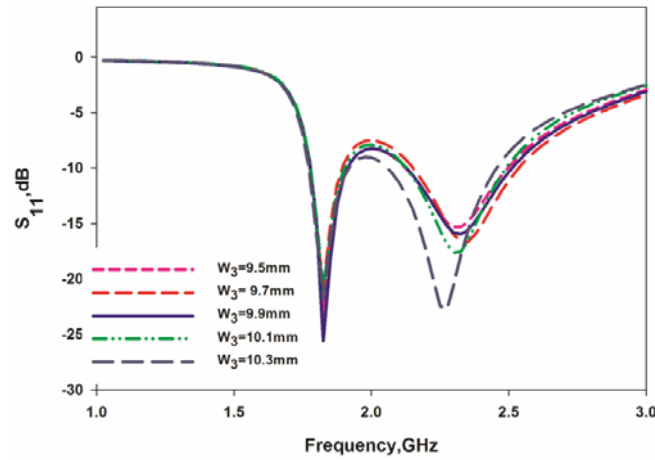


Fig. 3.31. Effect of W_3 on reflection characteristics
 ($L_1=25\text{mm}$, $W_1=3\text{mm}$, $L_2=17\text{mm}$, $W_2=14\text{mm}$, $g=0.35\text{mm}$,
 $L_3=26\text{mm}$, $h=1.6\text{mm}$, $\epsilon_r=4.4$, $P=4.5\text{mm}$ and $S=2\text{mm}$)

3.5.2.4.2 Effect of strip length (L_3) on reflection characteristics:

The variation of reflection coefficient with L_3 is shown in figure.3.32. Strip length L_3 is varied from 24mm to 28mm and hence the resonance frequency shifts by 0.055GHz. By increasing L_3 the resonant length increases which lowers the resonant frequency. Length of the strip is taken as 26mm by considering the application band.

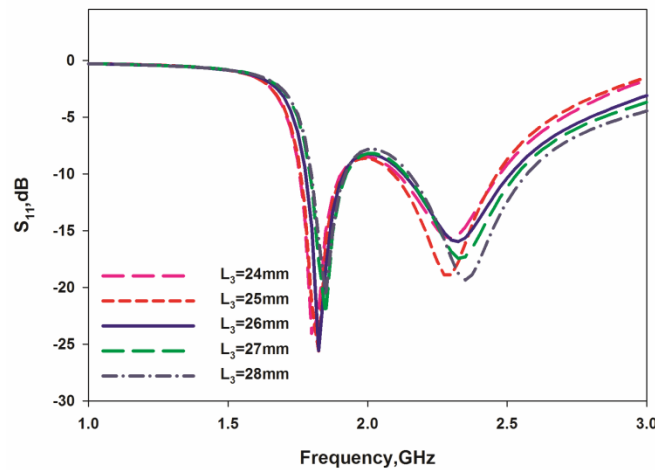


Fig. 3.32. Effect of L_3 on reflection characteristics
 ($L_1=25\text{mm}$, $W_1=3\text{mm}$, $L_2=17\text{mm}$, $W_2=14\text{mm}$, $g=0.35\text{mm}$, $W_3=9.9\text{mm}$,
 $h=1.6\text{mm}$, $\epsilon_r=4.4$, $P=4.5\text{mm}$ and $S=2\text{mm}$)

3.5.2.5 Gain

The gain of the CPW fed monopole antenna with metal strip is depicted in figure. 3.33. The proposed antenna shows an average gain of 1.12dBi. It is also worth to note that, the addition of metallic strip is not adversely affecting the gain of the antenna.

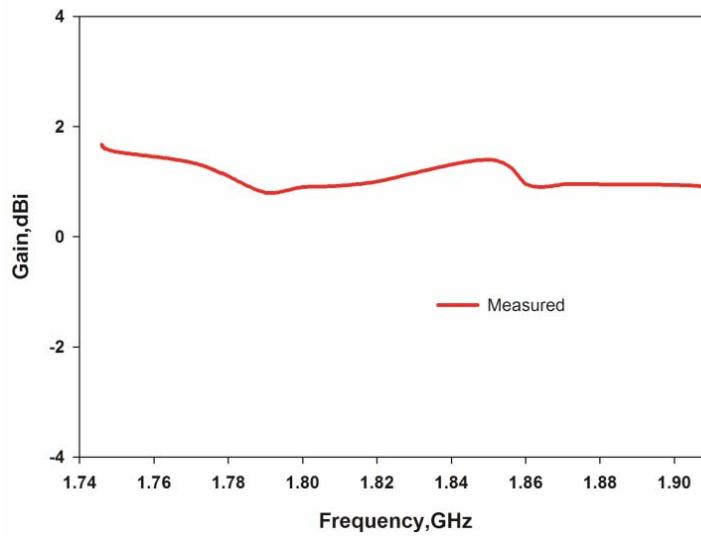


Fig 3.33. Measured gain of the antenna with printed strip
 ($L_1=25\text{mm}$, $W_1=3\text{mm}$, $L_2=17\text{mm}$, $W_2=14\text{mm}$, $g=0.35\text{mm}$, $L_3=26\text{mm}$, $W_3=9.9\text{mm}$, $h=1.6\text{mm}$, $\epsilon_r=4.4$, $P=4.5\text{mm}$ and $S=2\text{mm}$)

3.5.2.6 Resonance phenomenon

A better understanding about the resonance and radiation behavior of the proposed antenna can be obtained by analyzing the computed current density plots at three different frequencies. The 3D radiation characteristics at the resonant frequency, at frequencies below and above the resonant frequency are studied.

Radiation characteristics studies revealed that the metal plate affects the nulls of the E plane pattern of a monopole. Without printed metal strip at the back side, antenna is a monopole. The monopole will resonate at a particular

frequency corresponding to $\lambda_g/4$ length. When a metal strip of length 26mm is introduced, the system is resonating at 1.81GHz.

The radiation patterns along with the current plots are shown at three different frequencies in figure 3.34 (a), (b) and (c).

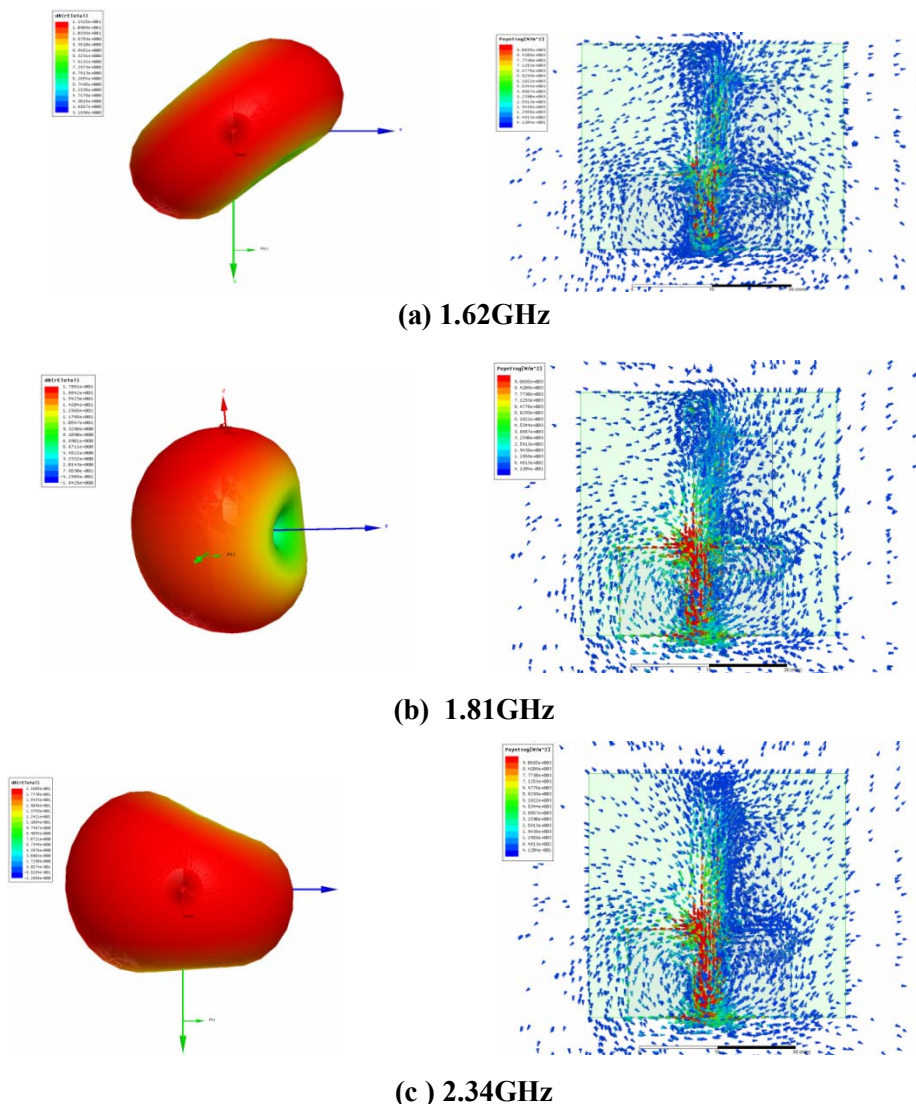


Fig. 3.34. 3D radiation characteristic and current density plots at (a) 1.62GHz (b)1.82GHz(c)2.34GHz
($L_1=25\text{mm}$, $W_1=3\text{mm}$, $L_2=17\text{mm}$, $W_2=14\text{mm}$, $g=0.35\text{mm}$, $L_3=26\text{mm}$, $W_3=9.9\text{mm}$, $h=1.6\text{mm}$, $\epsilon_r=4.4$, $P=4.5\text{mm}$ and $S=2\text{mm}$)

From patterns it is observed that at resonance (1.82 GHz) the pattern is highly suitable for mobile gadgets with single null along positive y direction. But the patterns outside the band are similar to that of monopole. From the studies it is found that a single null pattern is obtained for a band 1.76 GHz to 1.99GHz.

It is found that the pattern is tilted and irregular outside the resonating band from the conventional monopole pattern due to the corresponding coupling with metal plate.

From the above exhaustive parametric studies design parameters for various antenna dimensions are given in the following equations, (3.1)-(3.7)

$$L_1 = 0.247\lambda_g \text{ -----(3.1)}$$

$$L_2 = 0.168 \lambda_g \text{ -----(3.2)}$$

$$W_2 = 0.139 \lambda_g \text{ -----(3.3)}$$

$$L_3 = 0.26 \lambda_g \text{ -----(3.4)}$$

$$W_3 = 0.098 \lambda_g \text{ -----(3.5)}$$

$$S = 0.019 \lambda_g \text{ -----(3.6)}$$

$$P = 0.045 \lambda_g \text{ -----(3.7)}$$

3.5.2.7 Validation at different substrates

The parameters of the antenna resonating at 1.8GHz were calculated from the design equation for different dielectric substrates. The results are summarized in Table 3.2. Reflection characteristics of the antenna with different dielectric substrates are shown in figure 3.35.

Table 3.2. Parameters of the antenna for different dielectric substrates at 1.8GHz

Dielectric Material	Relative dielectric constant (ϵ_r)	L_1 mm	W_1 mm	g mm	h mm	L_2 mm	W_2 mm	L_3 mm	W_3 mm
RT Duroid 5880	2.2	31	5	0.2	1.575	21.08	17.36	32.2	12.276
Rogers RO 4003	3.38	26.25	3	0.24	1.524	17.85	14.7	27.3	10.395
FR4 epoxy	4.4	25	3	0.35	1.6	17	14	30	9.9
Rogers RO 3006	6.15	22.5	3	0.5	1.28	15.3	12.6	23.4	8.91

All the antennas are resonating at 1.8GHz with good impedance matching. This validates the design criteria.

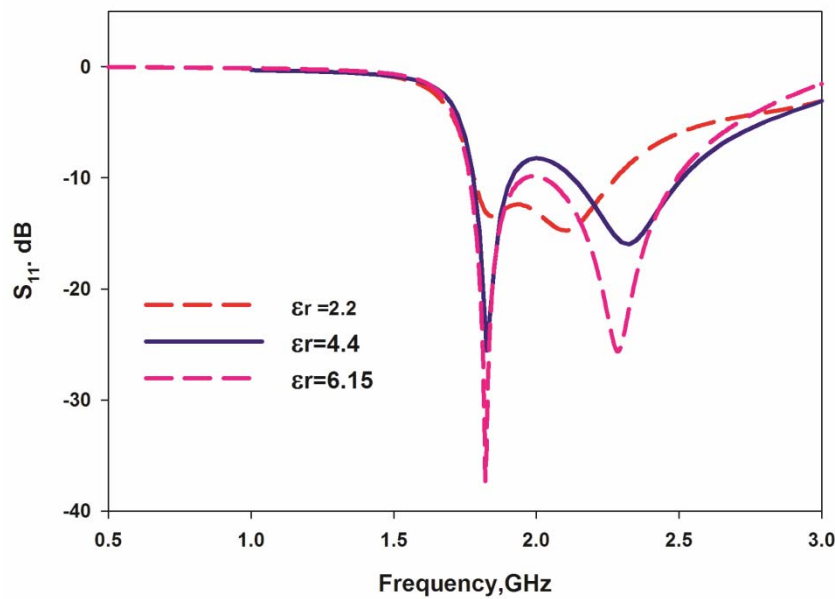


Fig 3.35. Reflection characteristics of the antenna with different substrate materials

($L_1=25\text{mm}, W_1=3\text{mm}, L_2=17\text{mm}, W_2=14\text{mm}, g=0.35\text{mm}, L_3=26\text{mm}, W_3=9.9\text{mm}, h=1.6\text{mm}, \epsilon_r=4.4, P=4.5\text{mm}$ and $S=2\text{mm}$)

These developed design equations are validated for different application frequencies on an FR4 substrate and the antenna parameters are shown on Table.3.3.

Table 3.3. Parameters of the antenna for different frequencies

Frequency	L1 (mm)	L2 (mm)	W2 (mm)	L3 (mm)	W3 (mm)	S (mm)	P (mm)
900 MHz	50.2	34.15	28.15	52.85	19.9	4.03	9.04
1.8GHz	25	17	14	26	9.9	2	4.5
2.4GHz	18.82	12.8	10.55	19.81	7.47	1.51	3.39

The simulated reflection characteristics of the antenna developed for these different frequencies are shown in figure.3.36. The antennas are showing good impedance characteristics in their corresponding application bands. The simulated 3-Dimensional radiation patterns at the above frequencies are shown in figure.3.37. The pattern shows the antenna is highly suitable for mobile handset with reduced radiation along one direction and wide coverage on all other directions.

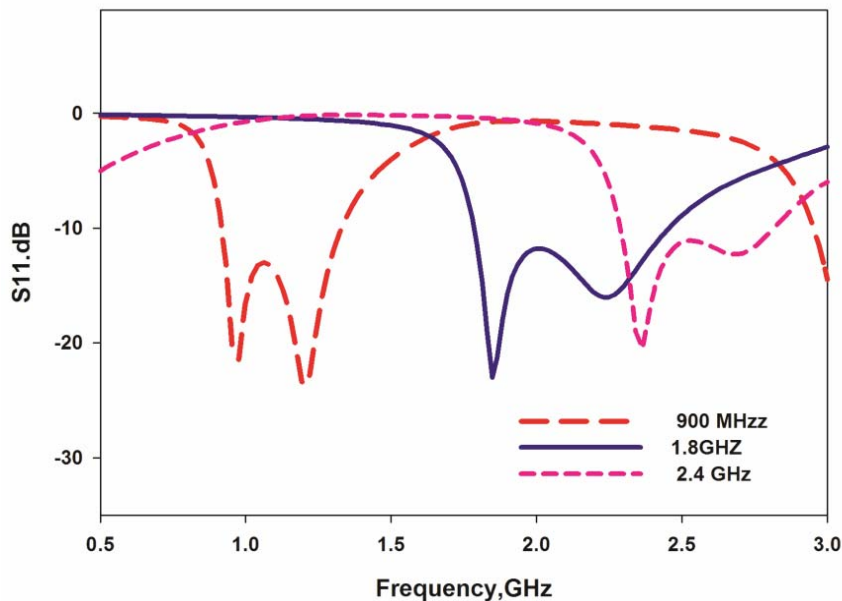


Fig.3.36. Reflection characteristics of the monopole antenna with strip at different frequencies
 $(L_1=0.247\lambda_g, L_2=0.168\lambda_g, W_2=0.139\lambda_g, L_3=0.26\lambda_g, W_3=0.098\lambda_g, h=1.6\text{mm}, \epsilon_r=4.4, S=0.019\lambda_g, P=0.045\lambda_g)$

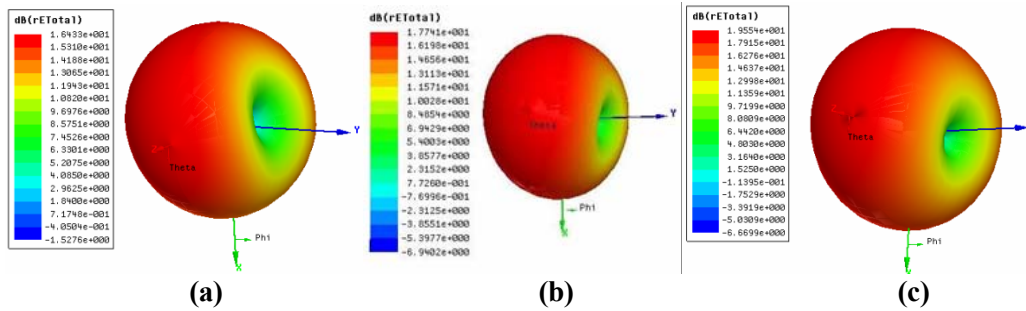


Fig.3.37. 3-Dimensional radiation pattern of the antenna with printed strip at (a) 900MHz (b) 1.8GHz (c) 2.4GHz ($L_1=25\text{mm}, W_1=3\text{mm}, L_2=17\text{mm}, W_2=14\text{mm}, g=0.35\text{mm}, L_3=26\text{mm}, W_3=9.9\text{mm}, h=1.6\text{mm}, \epsilon_r=4.4, P=4.5\text{mm}$ and $S=2\text{mm}$)

3.5.2.8 Inferences

Antenna with reduced radiation hazard and operating at GSM 1810 band is developed from the finite ground coplanar waveguide fed strip monopole by integrating a single metal strip at the backside. The antenna offers a bandwidth of 230MHz which is wide enough to cover the band. This antenna structure is very simple with an average gain of 1.12dBi in the application band. Antenna offers 20 dB reduction of radiated power in one quadrant with an enhancement in radiation at other quadrants.

3.5.3 Development of Mobile antenna with vertical metal stripes

Printed vertical metal stripes at the back side of the monopole are used to modify the far field radiation pattern in this study[12]. Experimental and simulation studies of the antenna radiation characteristics are presented and discussed. The power towards the users head can be reduced by 23dB (3dB more than the single strip structure) by using printed vertical metal stripes.

3.5.3.1 Antenna Geometry

The monopole antenna with printed vertical stripes is shown in figure 3.38. Thirteen metal stripes with length(L_3)=30mm and width(W_3)=0.3mm and

a separation of (d) 0.5mm is printed on the back side of CPW fed monopole antenna. These stripes are placed by an offset (P) 4.5mm from the top of the monopole and ground overlapping distance (Q) of 8.5mm. By properly placing the metal stripes position the radiation pattern can be modified. The prototype was fabricated on a substrate of dielectric constant (ϵ_r) 4.4 and thickness (h) 1.6mm with an overall dimension of 42X31.7mm².

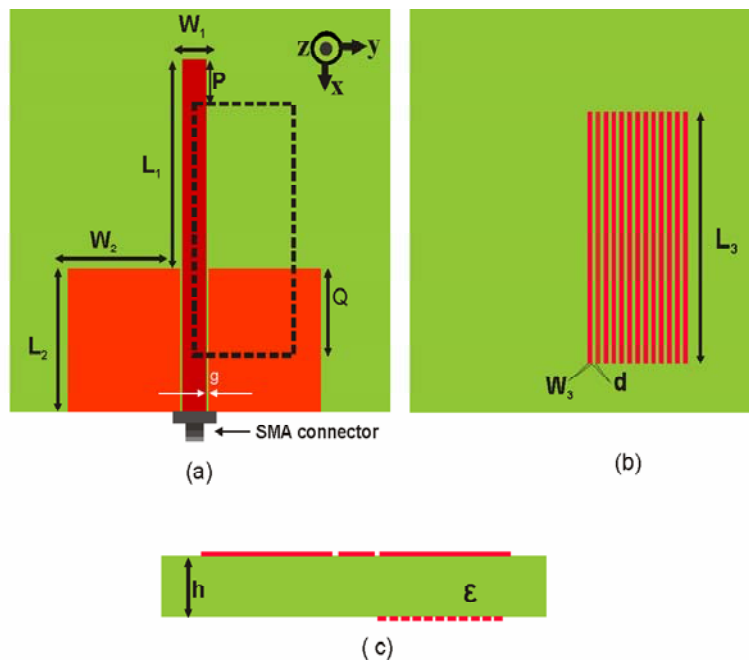


Fig. 3.38. Geometry of the antenna (a) 3D schematic diagram (b) bottom view (c) side view
($L_1=25\text{mm}$, $W_1=3\text{mm}$, $L_2=17\text{mm}$, $W_2=14\text{mm}$, $g=0.35\text{mm}$, $L_3=30\text{mm}$, $W_3=0.3\text{mm}$, $d=0.5\text{mm}$, $h=1.6\text{mm}$, $\epsilon_r=4.4$.)

3.5.3.2 Reflection characteristics

Measured and simulated reflection characteristics of the antenna with and without vertical stripes are shown in Fig.3.39. It is seen from the plot that the antenna loaded with stripes exhibits 2:1 VSWR bandwidth of 200MHz (1.76GHz -1.96GHz) centered at 1.8GHz. By placing the metal stripes the

antenna resonance is shifted from 2.3GHz to 1.8GHz. The measurement result reveals that metallic stripes loading can reduce the overall size of the antenna.

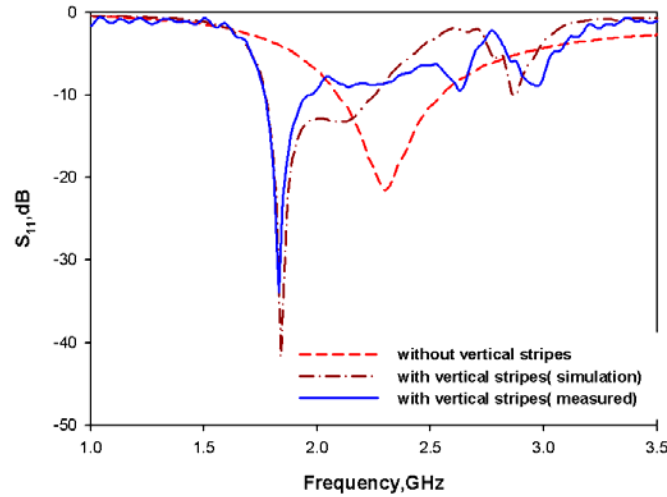


Fig. 3.39. Reflection characteristics of the monopole antenna with vertical stripes ($L_1=25\text{mm}$, $W_1=3\text{mm}$, $L_2=17\text{mm}$, $W_2=14\text{mm}$, $g=0.35\text{mm}$, $L_3=30\text{mm}$, $W_3=0.3\text{mm}$, $d=0.5\text{mm}$, $h=1.6\text{mm}$, $\epsilon_r=4.4$.)

3.5.3.3 Input impedance characteristics

The real and imaginary parts of the impedance of the antenna with varying the number of metal stripes (n) are shown in figures. 3.40 /8(a) and (b) respectively. The smith chart showing the impedance characteristics is also shown in figure.3.40(c). Addition of parasitic stripes increases the inductive reactance which shifts resonant frequency to lower side. It also increases the coupling between the stripes and ground plane to achieve good impedance match. An optimized strip number of $n=13$ is chosen by considering the application band and impedance matching.

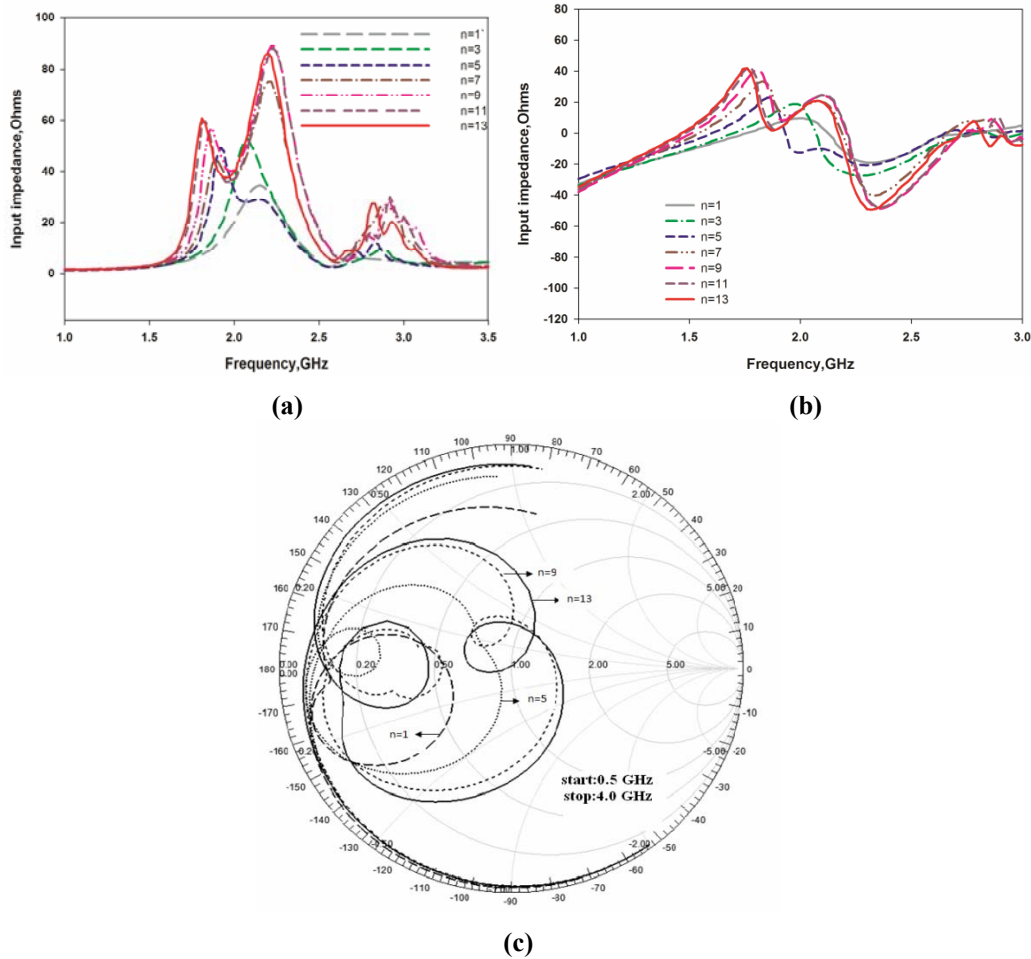


Fig. 3.40. Variation of (a) real part (b) imaginary part of the input impedance (c) Smith chart with different number of stripes
 $L_1=25\text{mm}, W_1=3\text{mm}, L_2=17\text{mm}, W_2=14\text{mm}, g=0.35\text{mm}, L_3=30\text{mm}, W_3=0.3\text{mm}, d=0.5\text{mm}, h=1.6\text{mm}, \epsilon_r= 4.4.)$

3.5.3.4 Far field radiation characteristics

Measured 2D radiation patterns of the antenna in YZ and XY plane at the resonance frequency are shown in figure 3.41 (a) and (b) respectively. It is observed that the radiation pattern of the conventional monopole gets modified by the addition of the metallic stripes. The printed vertical stripes affect the fringing field between the monopole and any of the lateral ground plane. As a

result the electric field gets redistributed giving a null along positive Y direction and filling the original two nulls of the conventional monopole.

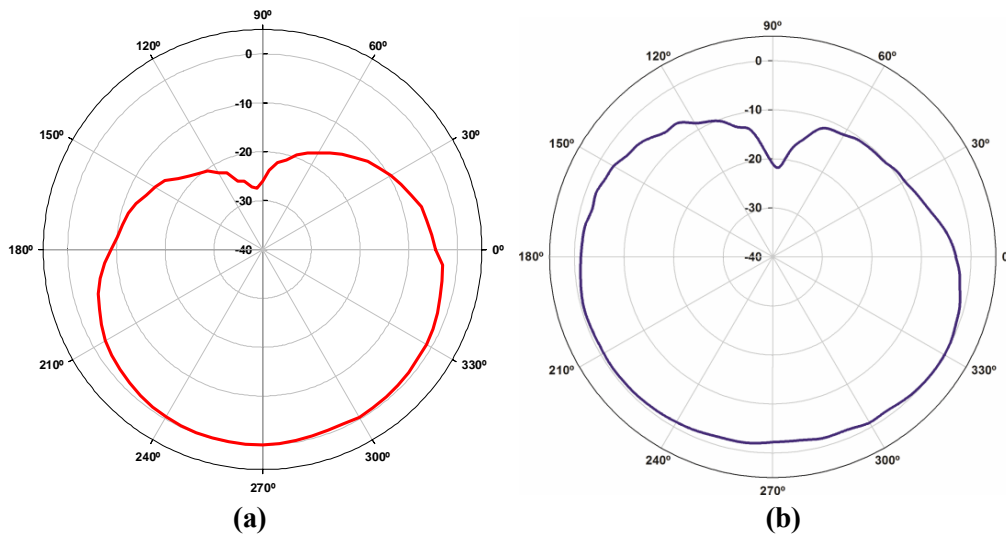


Fig. 3.41. Measured radiation pattern of the proposed antenna in (a) YZ (b) XY plane.
($L_1=25\text{mm}$, $W_1=3\text{mm}$, $L_2=17\text{mm}$, $W_2=14\text{mm}$, $g=0.35\text{mm}$, $L_3=30\text{mm}$, $W_3=0.3\text{mm}$, $d=0.5\text{mm}$, $h=1.6\text{mm}$, $\epsilon_r=4.4$.)

The measured 2D radiation patterns in YZ plane with and without vertical stripes are also shown in figure 3.42. From the observed results it is clear that the figure of eight pattern in YZ plane is modified to a pattern with single null along positive Y-axis. A measured 27dB reduction in radiated power is observed along the positive Y-direction, with appreciable power in all other directions.

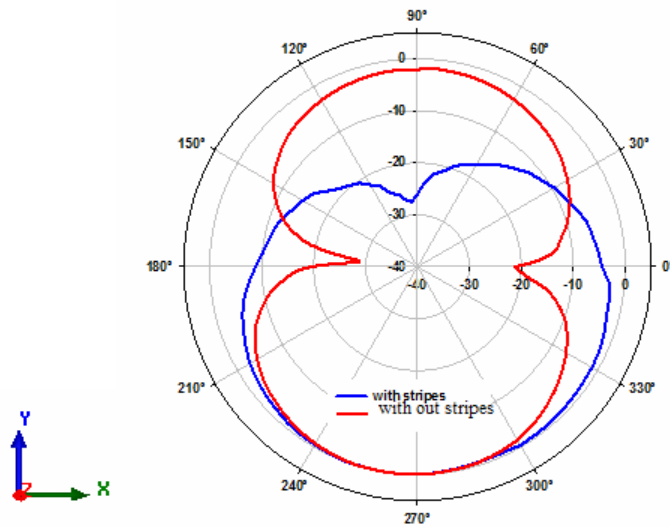


Fig.3.42. The 2D radiation patterns of the antenna with and without stripes in YZ plane

($L_1=25\text{mm}, W_1=3\text{mm}, L_2=17\text{mm}, W_2=14\text{mm}, g=0.35\text{mm}, L_3=30\text{mm}, W_3=0.3\text{mm}, d=0.5\text{mm}, h=1.6\text{mm}, \epsilon_r=4.4$.)

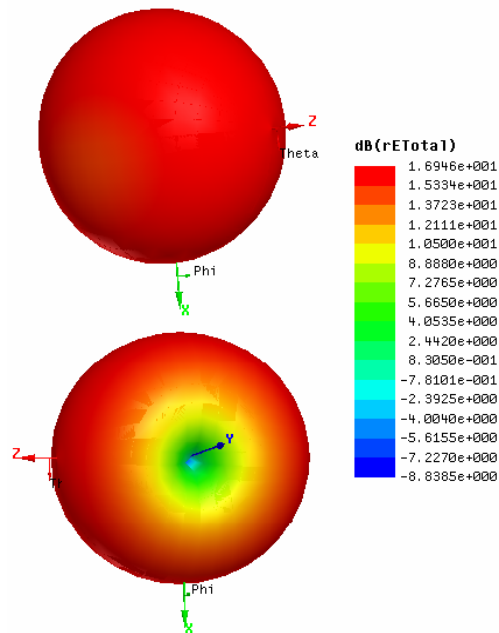


Fig. 3.43. 3D radiation pattern

($L_1=25\text{mm}, W_1=3\text{mm}, L_2=17\text{mm}, W_2=14\text{mm}, g=0.35\text{mm}, L_3=30\text{mm}, W_3=0.3\text{mm}, d=0.5\text{mm}, h=1.6\text{mm}, \epsilon_r=4.4$.)

The simulated 3D radiation pattern of the antenna is shown in figure 3.43. The antenna radiates in all directions with single null along positive Y direction, which again confirms the suitability of the antenna for mobile handset application.

3.5.3.5 Parametric Analysis

A parametric analysis is performed in order to investigate the effect of various antenna parameters over the antenna characteristics.

3.5.3.5.1 The effect of printed metal stripes parameters (W_3 & d) on reflection characteristics

The reflection characteristics of the antenna for different printed metal stripes parameters are shown in figures 3.44(a) and 3.44(b). It is seen from the Fig 3.44(a) that there is no shifts in the resonant frequency with W_3 by keeping the total length W_3+d as a constant (0.8mm). This in turn reveals that a small change in the parameter W_3 does not affect the resonance frequency.

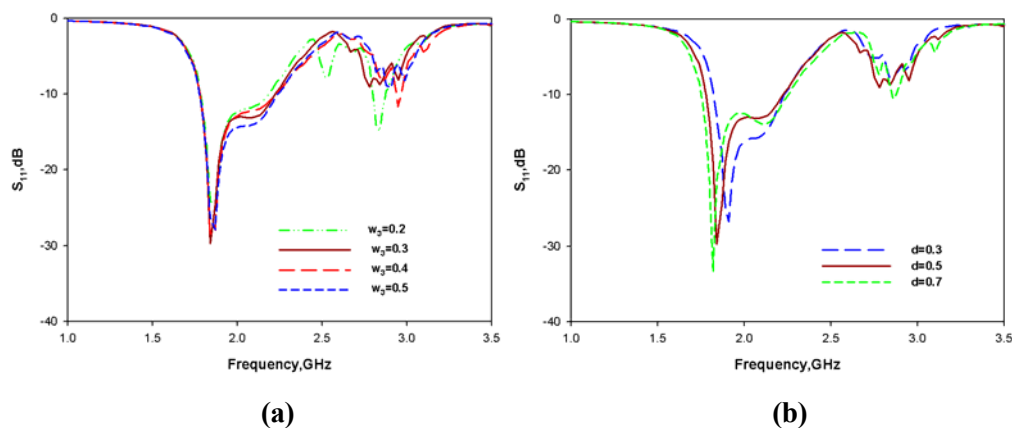


Fig. 3.44. Effect of W_3 (a) & d (b) of metal stripes on reflection characteristics of monopole antenna with vertical stripes ($L_1=25$ mm, $W_1=3$ mm, $L_2=17$ mm, $W_2=14$ mm, $g=0.35$ mm, $L_3=30$ mm, $h=1.6$ mm, $\epsilon_r= 4.4$.)

The influence of the separation between the stripes d on the reflection is presented in Figure 3.44(b). From the Figure it can be seen that as d is increased, the entire band shifts to lower side without changing bandwidth. It is due to increase in the capacitive coupling between stripes and ground plane. Its value is optimized to 0.5mm by considering the resonance in the application band. Therefore it is concluded that by varying d , the resonance frequency can be tuned without much change in the impedance bandwidth.

From the parametric studies, the design parameters of the antenna obtained for the required resonant frequency are given below (equations 3.8-3.14), where λ_g is the dielectric wavelength.

$$L_1 = 0.25 \lambda_g \text{ -----(3.8)}$$

$$L_2 = 0.17 \lambda_g \text{ -----(3.9)}$$

$$W_2 = 0.14\lambda_g \text{ -----(3.10)}$$

$$L_3 = 0.31\lambda_g \text{ -----(3.11)}$$

$$W_3 = 0.0031\lambda_g \text{ -----(3.12)}$$

$$P = 0.044 \lambda_g \text{ -----(3.13)}$$

$$Q = 0.084 \lambda_g \text{ -----(3.14)}$$

3.5.3.5.2 Effects of substrate parameters on reflection characteristics

The studies are conducted on substrates with different relative dielectric constants. The structural parameters of the antenna operating in the 1.8GHz operating band for different dielectric constants are shown in table 3.4.

Table 3.4. The simulated parameters for different dielectric substrate.

Dielectric Material	Relative dielectric constant(ϵ_r)	L_1 mm	g mm	h mm	L_2 mm	W_2 mm	L_3 mm	W_3 mm
RT Duroid 5880	2.2	31	0.15	1.575	21.08	17.36	37.2	0.37
Rogers RO 4003	3.38	28.5	0.25	1.524	19.38	15.96	34.2	0.34
FR4 epoxy	4.4	25	0.35	1.6	17	14	30	0.3
Rogers RO 3006	6.15	22.5	0.15	1.28	16.15	12.5	27	0.27
RT Duroid 6010 LM	10.2	19.25	0.13	1.27	13.49	12.29	23.05	0.23

The relative permittivity (ϵ_r) of the substrate material is varied from 2.2 to 10.2. It is found from the plot (Fig 3.45) that the band width of the antenna decreases rapidly as ϵ_r increases.

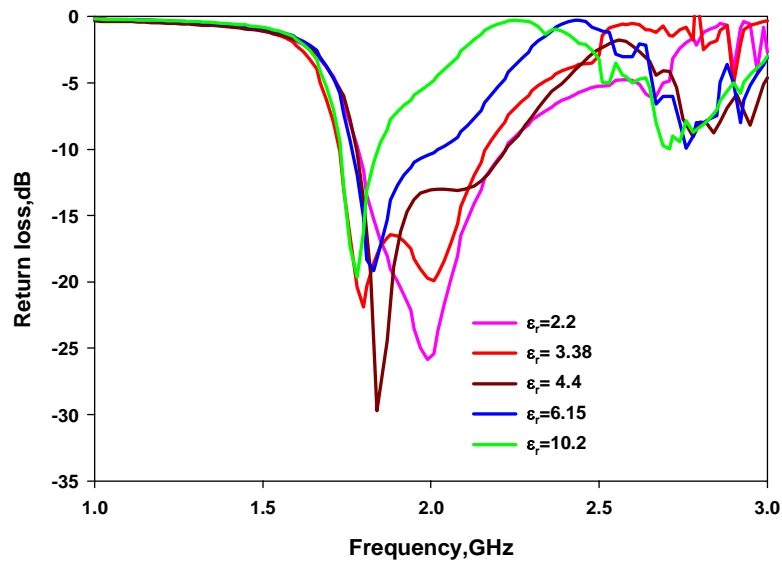


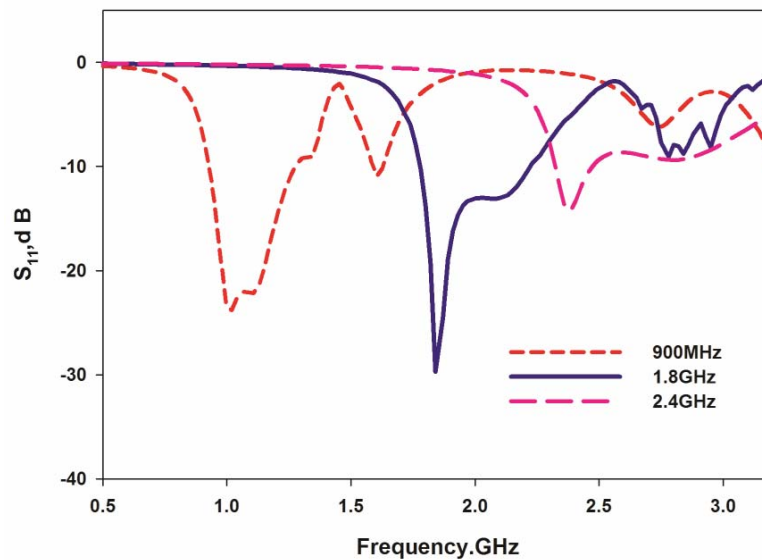
Fig. 3.45. Variation of Reflection characteristics with different substrate materials (ϵ_r)
 ($L_1=25\text{mm}, W_1=3\text{mm}, L_2=17\text{mm}, W_2=14\text{mm}, g=0.35\text{mm}, L_3=30\text{mm}, W_3=0.3\text{mm}, d=0.5\text{mm}, h=1.6\text{mm}, \epsilon_r= 4.4.$)

The developed design equations are validated on FR4 substrate for three different application frequencies. The antenna parameters used are shown on table 3.5.

Table 3.5. Parameters of the antenna with vertical stripes for different frequencies

Frequency	L_1 (mm)	L_2 (mm)	W_2 (mm)	L_3 (mm)	W_3 (mm)	P(mm)	Q(mm)
900 MHz	50.2	34.15	28.15	63	0.63	8.94	17.07
1.8GHz	25	17	14	31.32	0.313	4.45	8.49
2.4GHZ	18.82	12.8	10.55	23.62	0.24	3.35	6.40

The simulated reflection characteristics of the antenna developed for these different application frequencies are shown in Figure 3.46. The antennas are showing good impedance characteristics in their corresponding application bands. The simulated 3-Dimensional radiation patterns at the above frequencies are shown in figure .3.47. The antenna pattern shows, it is highly suitable for mobile handset with reduced radiation on one direction and wide coverage on all other directions.

**Fig 3.46 Reflection characteristics of the antenna at different frequencies**

($L_1=0.25 \lambda_g$, $L_2=0.17 \lambda_g$, $W_2=0.14 \lambda_g$, $L_3=0.31 \lambda_g$, $W_3=0.0031 \lambda_g$,
 $P=0.044 \lambda_g$, $Q=0.084 \lambda_g$)

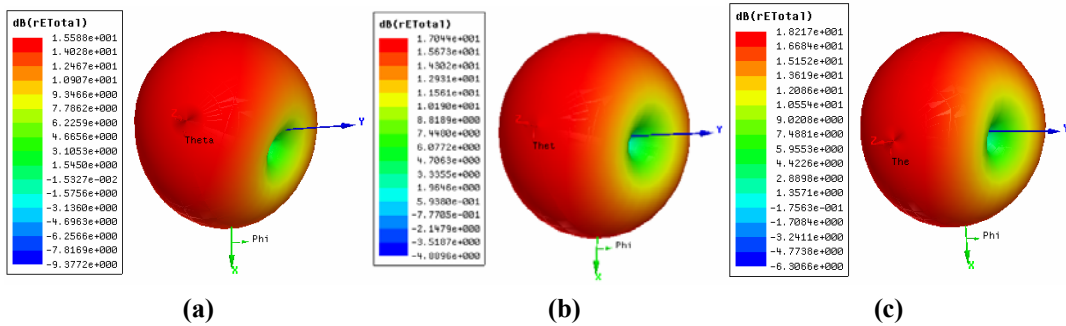


Fig 3.47. 3D radiation pattern of the antenna at different frequencies
 (a)900MHz (b) 1.8GHz (c) 2.4GHz ($L_1=0.25 \lambda_g$, $L_2=0.17 \lambda_g$, $W_2=0.14\lambda_g$,
 $L_3=0.31\lambda_g$, $W_3=0.0031\lambda_g$, $P=0.044 \lambda_g$, $Q=0.084 \lambda_g$)

3.5.3.5.3 Effect on radiation pattern with number of stripes (n)

Simulated 2D radiation patterns in YZ plane with different number of stripes (n) at the corresponding resonant frequency are shown in Figure .3.48.

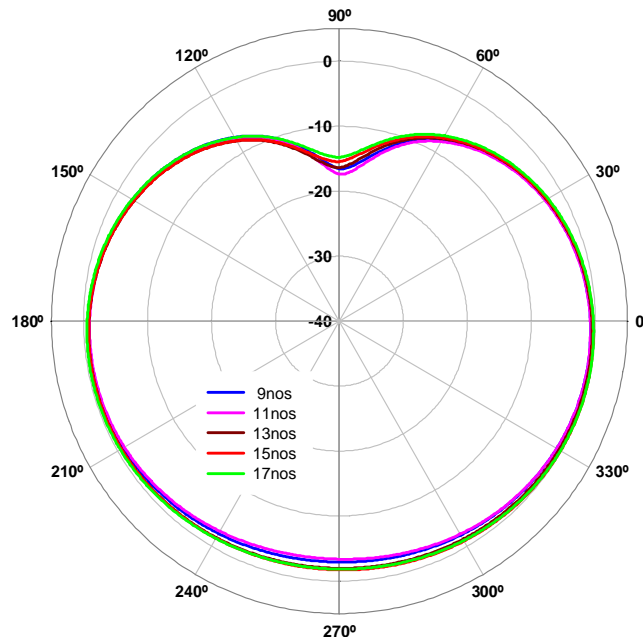


Fig. 3.48. 2D radiation pattern with different number of stripes.
 ($L_1=25\text{mm}$, $W_1=3\text{mm}$, $L_2=17\text{mm}$, $W_2=14\text{mm}$, $g=0.35\text{mm}$, $L_3=30\text{mm}$,
 $W_3=0.3\text{mm}$, $d=0.5\text{mm}$, $h=1.6\text{mm}$, $\epsilon_r=4.4$.)

It is observed that for different number of stripes, the patterns are almost ideal for our specific application. Moreover, the pattern is not varying much with small changes in number of stripes. The strip number is chosen as 13 for using the antenna at GSM 1.8GHz application band.

3.5.3.6 Gain

The measured gain of the antenna by gain comparison method is shown in Fig 3.49. The antenna offers peak gain of 1.9dBi at 1.81GHz with an average gain of 1.14dBi in the frequency band.

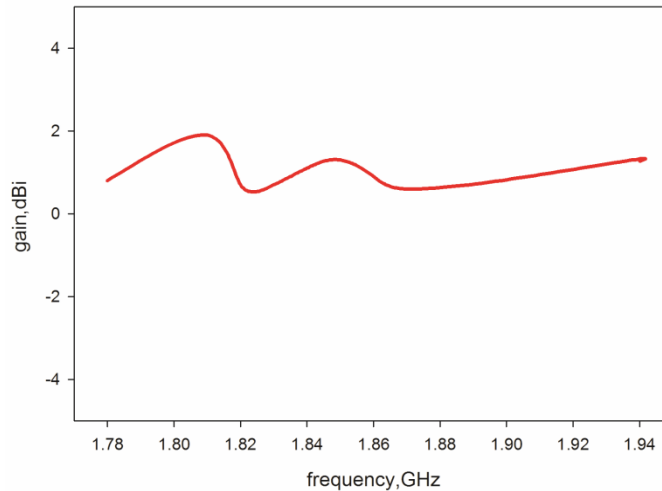


Fig. 3.49. Measured gain of the monopole antenna with vertical stripes antenna. ($L_1=25\text{mm}$, $W_1=3\text{mm}$, $L_2=17\text{mm}$, $W_2=14\text{mm}$, $g=0.35\text{mm}$, $L_3=30\text{mm}$, $W_3=0.3\text{mm}$, $d=0.5\text{mm}$, $h=1.6\text{mm}$, $\epsilon_r=4.4$.)

3.5.4 Inferences

A CPW fed monopole antenna with printed vertical stripes at the back side, produces radiation characteristics suitable for a wireless handset. The proposed antenna operates at GSM 1800 band. A good agreement between measurement and simulation is obtained. The antenna offers a bandwidth of 200MHz when printed on a substrate of dielectric constant (ϵ_r) 4.4 and

thickness 1.6mm with an overall dimension of $42 \times 31.7 \text{mm}^2$. It offers an average gain of 1.14dBi. A 27dB reduction in radiated power is observed at the beam minima, which is more than the previously mentioned structures.

3.5.5 Surface Impedance Plot for Proposed Antennas

From the above studies the radiation pattern is modified to use it for mobile handset with reduced radiation along one direction at resonance frequency. The total radiated power is not found to vary, but redistributed as evident from the radiation patterns. The change in radiation pattern is analysed from the surface impedance plot.

The simulated surface impedance of the proposed antenna, at resonance as well as lower and upper frequencies is shown in figure.3.50, figure.3.51 and figure.3.52. It is clearly evident from the figure that the surface impedance at the resonant frequency is higher than at other frequencies outside the band. This high impedance restricts the propagation of electromagnetic waves towards that direction.

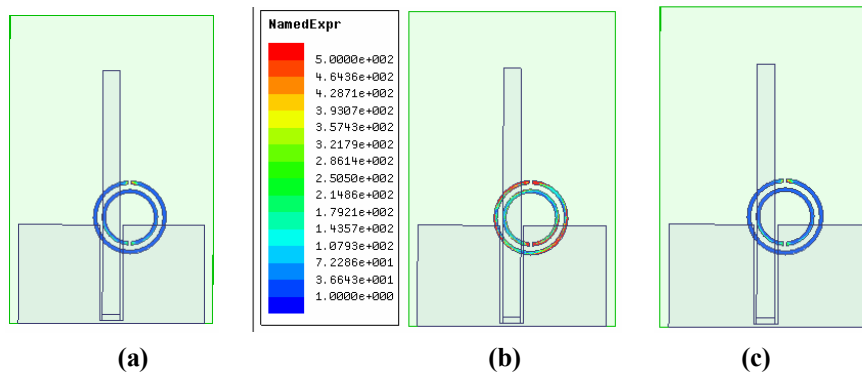


Fig. 3.50. Simulated surface impedance at different frequencies of monopole antenna with printed SRR (a)1.6GHz (b)1.81GHz (c)2.2GHz ($L_1 = 25\text{mm}$, $W_1 = 3\text{mm}$, $g = 0.35\text{mm}$, $L_2 = 17\text{mm}$, $W_2 = 14\text{mm}$, $h=1.6\text{mm}$ and $\epsilon_r=4.4$, $r_1=6.3\text{mm}$, $W = 0.9\text{mm}$, $d = 0.6\text{mm}$, $t = 0.5\text{mm}$)

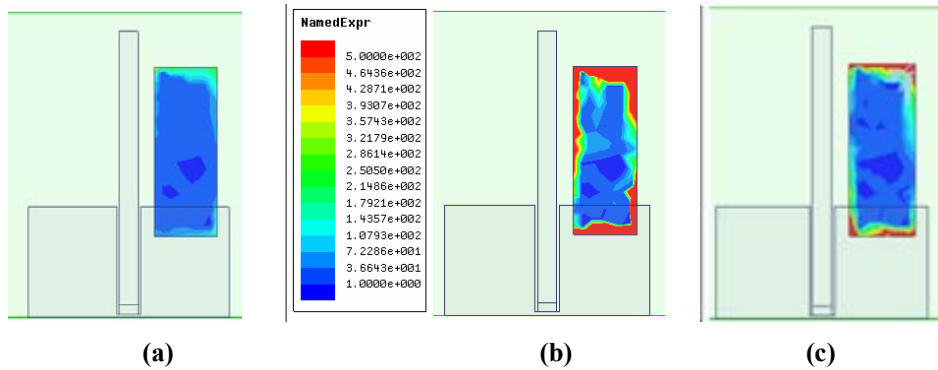


Fig. 3.51. Simulated surface impedance at different frequencies of the monopole antenna with single (a)1.6GHz (b)1.81GHz (c)2.2GHz strip
 $(L_1=25\text{mm}, W_1=3\text{mm}, L_2=17\text{mm}, W_2=14\text{mm}, g=0.35\text{mm}, L_3=26\text{mm}, W_3=9.9\text{mm}, h=1.6\text{mm}, \epsilon_r=4.4, =4.5\text{mm and } S=2\text{mm})$

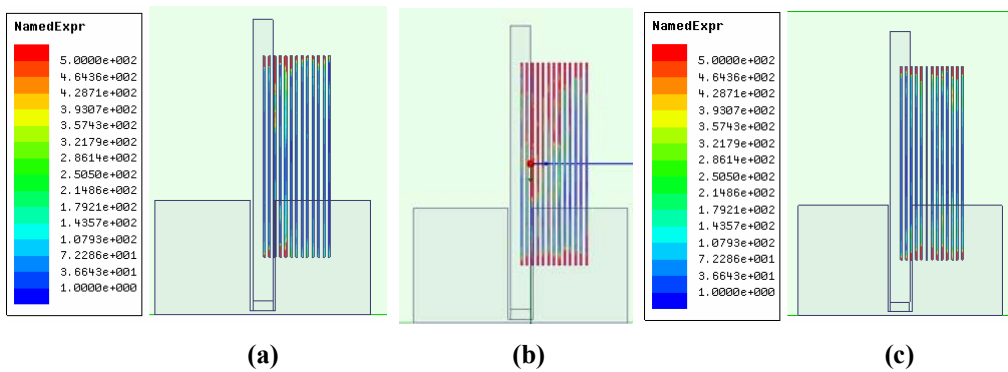


Fig.3.52. Simulated surface impedance at different frequencies of the monopole antenna with vertical stripes (a)1.6GHz (b)1.81GHz (c)2.2GHz
 $(L_1=25\text{mm}, W_1=3\text{mm}, L_2=17\text{mm}, W_2=14\text{mm}, g=0.35\text{mm}, L_3=26\text{mm}, W_3=9.9\text{mm}, h=1.6\text{mm}, \epsilon_r=4.4, =4.5\text{mm and } S=2\text{mm})$

3.6 Chapter conclusion

The following conclusions can be made from the analysis of different structures from this chapter,

- A mobile antenna operating at GSM 1800 band is developed from the finite ground coplanar waveguide fed strip monopole antenna by integrating a parasitic element at the backside with reduced radiation hazards

- The measurement results reveal that, the integration of the add-on element has an influence over the resonance and radiation behavior of the antenna.
- The parasitic element can modify antenna characteristics which is suitable for a mobile handset
- It is found from the measured antenna characteristics that the antenna modifies the omni-directional radiation pattern to radiation pattern with single null.
- This antenna structure is very simple.
- Reduction of radiated power in one quadrant of the radiation pattern offers, a reduction of radiation towards the users head.

Table 3.6 show the results of the antennas discussed in this chapter.

Table 3.6. Summarised result

Antenna	Resonant Frequency	Frequency band (GHz) Bandwidth(MHz) % BW	Average gain	Reduced power in null direction (simulation)
Printed monopole	2.3	1.98-2.58 600 26%	1.4dBi	-----
Printed monopole with SRR	1.82	1.75-1.91 160 8.7%	1.2dBi	18dB
Printed monopole with single strip	1.81	1.76-1.99 230 12.26%	1.12 dBi	20dB
Printed monopole with vertical stripes	1.8	1.76-1.96 200 10.75%	1.14 dBi	23dB

The non directional radiation characteristic in the azimuth plane of the planar CPW fed monopole antenna is modified with different structures printed at the backside. These microwave frequency selective devices, designed as parasitic resonators offer high surface impedance. Radiation pattern of the monopole antenna is modified with these different parasitic resonators. Out of this SRR added structure has the lowest operating band and all other antennas have almost same bandwidth. Antenna with vertical stripes provides maximum power reduction along the user. These antennas can be used for mobile applications with less RF interference towards the user.

References

- [1] James c Lin “Advances in Electromagnetic field in living systems” volume 5
- [2] Fung, L. C., S. W. Leung, and K. H. Chan, “Experimental study of SAR reduction on commercial products and shielding materials on mobile phone applications," *Microwave and Optical Technology Letters*, Vol. 36, 419-422, 2003.
- [3] Wang, J. and O. Fujiwara, “Reduction of electromagnetic absorption in the human head for portable telephones by a ferrite sheet attachment," *IEICE Transation Communications*, Vol. 80, 1810-1815, 1997.
- [4] Rowley, J. T. and R. B. Waterhouse, “Performance of shorted microstrip patch antennas for mobile communication handset at 1800 MHz," *IEEE Transaction in Antennas Propagation*, Vol. 47, No. 815-822, 1999.
- [5] Wunk, M., W. Kolosowski, and M. Amamowicz, “Microstrip antennas on multilayer dielectric for mobile system communication” *Proceeding 14th International Wroclaw Symposium on Electro-magnet Compact*, 346-350, Poland, 1998.
- [6] Kwak, S. I., D.-U. Sim, and J. H. Kwon, “SAR reduction on mobile phone antenna using the EBG structures," *Proceeding 38th European Microwave Conference*, 1308-1311, The Netherlands, 2008.
- [7] Cheng P Wen “Coplanar Waveguide: “A Surface Strip Transmission Line Suitable for Nonreciprocal Gyromagnetic Device Applications”*IEEE Trans on microwave theory and techniques*,vol-MTT17,No 12,pp1087-1090, December 1969
- [8] L.J.Rogla, J. Carbonell and V.E. Boria “Study of equivalent circuits for open-ring and split-ring resonators in coplanar waveguide technology” *IET Microwave. Antennas Propag.*, Vol. 1, No. 1,pp170-176, February 2007

- [9] F Martin , F Falcone, J Bonache, T Lopetegi, R Marque's, and M Sorolla "Miniaturized CPW stop band filters based on multiple tuned split ring resonators", IEEE Microw. Wirel. Compon. Lett., No 13, pp. 511–513, 2003.
- [10] B Jitha "Development of compact microwave filters using microstrip loop resonators" P.hD thesis, cochin university of science and technology-2010
- [11] Jiunn-Nan Hwang and Fu-Chiarng Chen "Reduction of the Peak SAR in the Human Head with Metamaterials" IEEE Trans. Antennas Propag ,vol. 54, No. 12, pp 3763-3770, December 2006
- [12] O. Luukkonen, C. Simovski, G Granet, George Goussetis, "Simple and Accurate analytical Model of Planar Grids and High-Impedance Surfaces Comprising Metal Strips or Patches" IEEE Trans. Antennas Propag vol. 56, No. 6, pp 1624-1632, June 2008.

.....✂.....

DEVELOPMENT AND ANALYSIS OF A GROUND FOLDED PLANAR ANTENNA (GFPA)

C o n t e n t s	4.1 <i>Introduction</i>
	4.2 <i>Folded antenna-review</i>
	4.3 <i>Characteristics of the conventional CPW transmission line</i>
	4.4 <i>Introduction to ground folded transmission line</i>
	4.5 <i>Compact Ground Folded Monopole Antenna</i>
	4.6 <i>Modified ground folded antenna for mobile handset</i>
	4.6 <i>Chapter conclusion</i>

This chapter highlights the development and analysis of a Ground Folded Planar Antenna (GFPA) with radiation characteristics suitable for a mobile handset. The proposed antenna offers a null towards the user and reduces the Specific Absorption Rate (SAR). The antenna may find application for mobile handset with reduced radiation hazards. A printed monopole antenna is suitably folded to a low profile antenna. The proposed 3D structure of ground folded monopole antenna has non directional radiation characteristic in azimuth plane. Investigations were carried out to modify the radiation characteristics of the folded monopole antenna by judiciously placing a single vertical strip at the back side of the ground plane. Thus a novel compact folded antenna is derived with single null in radiation pattern suitable for low radiation hazard mobile applications. Experimental and simulation analysis of ground folded monopole antenna and folded monopole antenna with additional strip is elaborately presented.

4.1 Introduction

A major trend in mobile communication technology is the dramatic reduction in the size and weight of the mobile handset with reduced human RF interference. Antenna designers are therefore encountered with the difficulties of designing compact, highly efficient antennas with less radiation hazards to the user. Among all the components, the antenna is one of the most challenging devices to be scaled down in size. And the size of the conventional antennas depends on the operation frequency, which is usually in the MHz or low GHz range. Compact antennas with folding techniques are reviewed in the following section.

4.2 Folded antenna-review

Due to the size constraints on the mobile devices and the need to reduce the physical antenna space in a mobile device, novel ways of antenna designs are required. The topic of small antennas has been a subject of interest for more than half a century. The following section describes different antenna folding miniaturization techniques reported in the open literature.

J. Leonhard, [1] reported folded unipole antenna less than a quarter wavelength long. This is used to transform the input resistance of short vertical antennas to a more acceptable value, by a transformation within the antenna itself.

The theory of linear arrays consisting of two or more closely spaced elements interconnected by lumped reactances is presented by C W Harrison [2].

M. C. Elias developed [3] the integral equation (MoM) for the current on a folded dipole to predict the input impedance with frequency.

Ross w Lampee [4] developed the design formulae for a planar folded dipole and calculated the impedance of the transmission line mode, the impedance of the dipole mode and the impedance step up ratio.

E. Lee proposed [5] an antenna structure based on the geometry of a bent folded monopole antenna capable of dual resonance covering the GSM/DCS1800 communication system bands.

Shun-Yun Lin [6] introduced a folded planar monopole antenna, which has a very low profile of about one twentieth of the wavelength of the lowest operating frequency. The proposed antenna can be used for multiband operation, with omni directional radiation patterns.

Yu-Seng Liu et al. [7] presented two different geometries of triple band antennas to operate for WLAN/HIPERLAN/ISM applications. The meander line antenna with one or two inverted planar L shaped structure is used to excite three distinct resonant modes.

Chia-Hao Ku [8] proposed a folded dual-loop antenna using a pair of symmetric meander strips to form two loops suitable for GSM/DCS/PCS/UMTS applications. The resonant characteristics of the antenna can be tuned by various strip lengths and space between the radiator and the ground plane.

A low-profile and small Circularly Polarized (CP) antenna proposed is Xi Yang [9] consisting of two modified Linearly Polarized (LP) Inverted-L Antenna (ILA) elements with double-folded arms to improve impedance matching and radiation characteristics

Xiaoyu Cheng [10] introduced a self-packaged folded patch antenna in a rectangular waveguide with greatly reduced size by loading a Complimentary

Split Ring Resonator (CSRR) on the edge of its ground plane. The antenna has 72% volume reduction compared to one without CSRR loading at the same radiation frequency.

The impact of a magneto dielectric resonator on a DVB-H antenna is investigated by F Ferrero [11]. A frequency reconfigurable antenna using a folded monopole antenna structure and varactor diodes with measured 6-dB bandwidth wider than 8 MHz is obtained between 470 and 862 MHz.

A.Vallecchi proposed [12] fully planar antenna design, incorporating a High Impedance Surface (HIS) by a periodic array of subwavelength dogbone-shaped conductors printed on top of a thin dielectric substrate and backed by a metallic ground plane.

Nguyen Tuan Hung proposed [13] the characteristics of V-shaped Folded Dipole Antenna (VFDA) upon a ground plane which cover frequency bands of WiMAX (2.3-2.7 GHz and 3.4-3.8GHz) with a large relative bandwidth of 51.5%.

A dual-wideband circularly-polarised slot antenna with a modified tuning stub by adding an L-shaped strip and slit to the conventional L-shaped stub is proposed by R. Zaker [14]. The reported antenna bandwidth (BW) is 69%.

4.3 Characteristics of the conventional CPW transmission line

A conventional CPW fed transmission line on a dielectric substrate is excited by connecting center conductor of a coaxial connector to the signal strip. The outer ground conductor of the connector is connected to the two parallel semi-infinite ground plane. The transmission line with width 3mm is designed on a substrate of relative permittivity ϵ_r (4.4) and thickness h (1.6mm). The magnitude of transmission and reflection characteristics of a 50 Ω matched CPW transmission

line is shown in figure 4.1. It is found from the figure that the system is acting as a perfect transmission line. The line is perfectly matched and the return loss is better than -18dB in the band of interest. The insertion loss of the system is also very low.

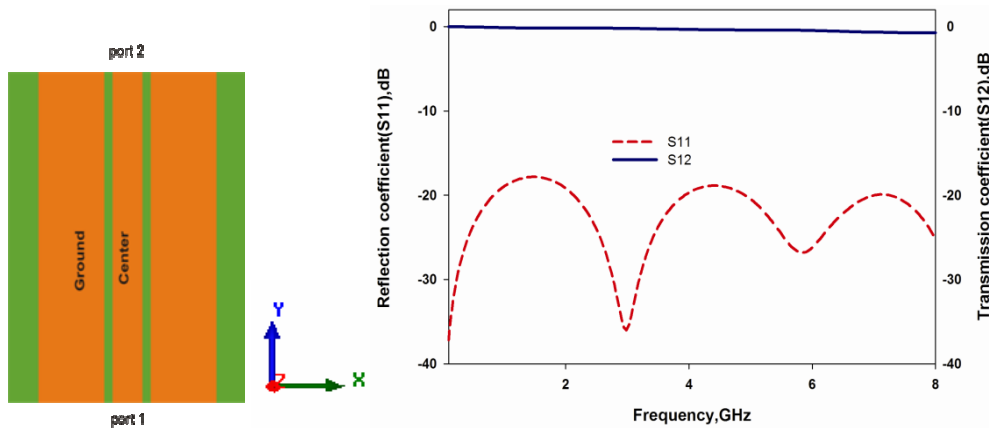


Fig.4.1. Transmission and reflection characteristics of a CPW transmission line (width=3mm, $\epsilon_r=4.4$,h =1.6mm)

4.4 Introduction to Ground Folded transmission line

To reduce the overall width of the structure, the ground plane of the conventional CPW fed transmission line is folded as in Fig 4.2(a). This makes the structure compact and can be conveniently applied to the mobile handset as the chassis. The coming section of the chapter deals with the design and development of a Ground Folded Transmission line.

4.4.1 Geometry of the Ground Folded Transmission line

The 3D Folded transmission line geometry is derived from a CPW fed planar transmission line by folding the finite ground plane perpendicular to the conducting strip arm as shown in figure 4.2(a). The photograph of the proposed geometry is shown in figure 4.2(b). The folded 50Ω transmission line with

signal strip width $W= 3\text{mm}$ and the gap $g = 1.7\text{ mm}$ is printed on a substrate of dielectric constant (ϵ_r) 4.4 and thickness (h) 1.6mm. Two ground lines are attached to it in the YZ plane.

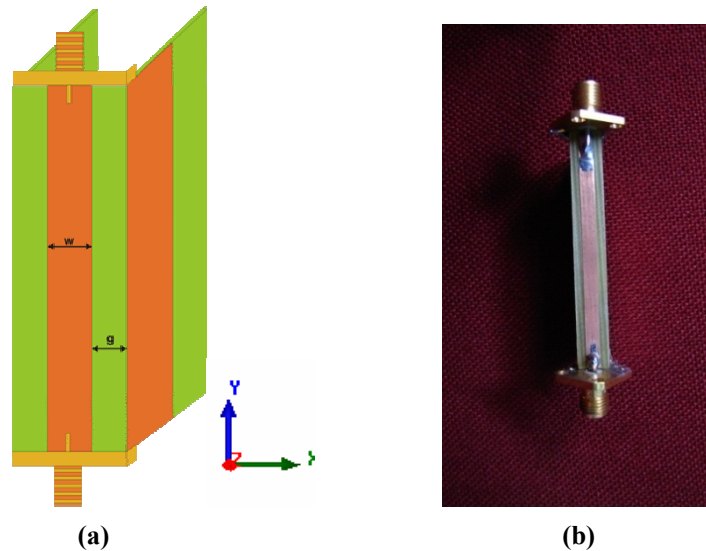


Fig.4.2. (a) Ground folded transmission line (b) photograph of the folded transmission line
($w=3\text{mm},g=1.7\text{mm}, \epsilon_r =4.4$ and $h =1.6\text{mm}$)

4.4.2 Transmission and reflection characteristics of the folded transmission line

The folded transmission line under matched load condition will produce a travelling wave with no reflections. The structure is not radiating electromagnetic energy and this can be observed from the simulated transmission and reflection characteristics of the proposed transmission line depicted in figure 4.3. The good transmission and reflection characteristics as that of an ordinary CPW fed planar transmission line, confirms that it is behaving as a transmission line.

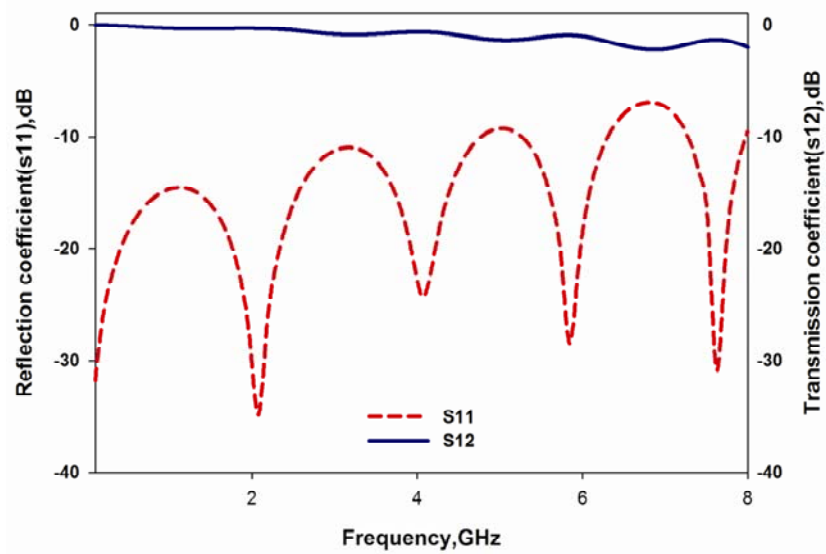


Fig. 4.3. Transmission and reflection characteristics of ground folded transmission line ($w=3\text{mm}, g=1.7\text{mm}, \epsilon_r =4.4, h =1.6\text{mm}$)

Figure.4.4 shows the impedance characteristics of the open ended folded structure. From the figure it is found that the reflection coefficient is very high in the band and is behaving as an open ended transmission line with low radiation.

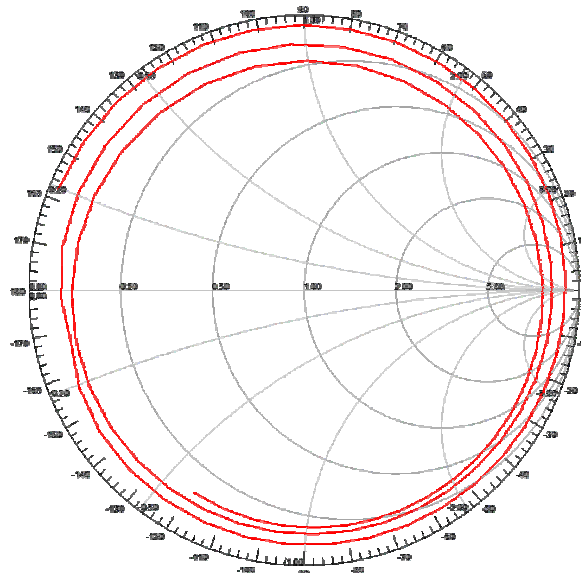


Fig.4.4. Impedance diagram of open ended ground folded transmission line ($w=3\text{mm}, g=1.7\text{mm}, \epsilon_r =4.4, h =1.6\text{mm}$)

The smith chart gives a clear picture on the impedance characteristics of this structure from 1GHz to 6 GHz. From the figure it is evident that for all frequencies the locus of impedance curve is on the outer region of the smith chart. Thus the open ended structure is unmatched in this frequency band.

Figure.4.5 shows the radiation characteristics of the open ended CPW structure. It is clear that the maximum radiation intensity is very low. So it is acting as a low efficient antenna.

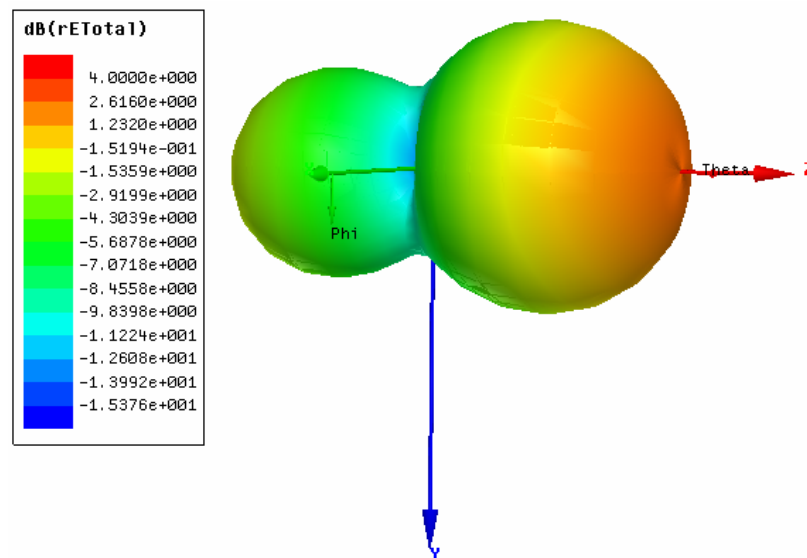


Fig. 4.5. 3D radiation pattern of open ended structure

A transmission line can be transformed to radiate electromagnetic energy by creating discontinuity on the structure [15,16]. An open ended transmission line can be converted into an efficient radiator by improving the matching at the desired frequency by properly optimizing the structural parameters. This property is utilized to convert a transmission line to operate as a radiating antenna.

In a normal CPW, discontinuity can be created in three different ways.

- a) Modifying the signal strip.
- b) Modifying the ground plane.
- c) Modifying the signal strip and ground plane simultaneously so that both will contribute to impedance match and effective radiation.

4.4.3 Parametric analysis

Parametric analysis of the transmission line is conducted to understand effects of various parameters over the transmission line characteristics and discussed in this section.

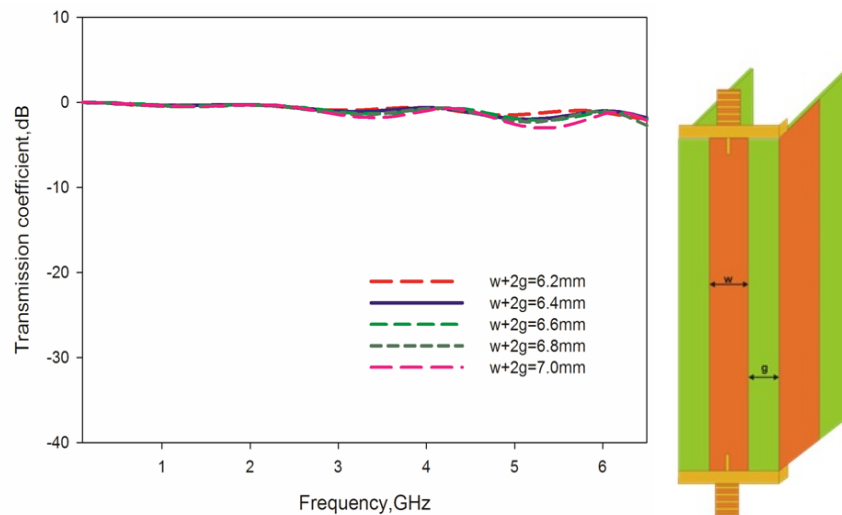


Fig.4.6. Variation of transmission coefficient for different $w+2g$ of ground folded transmission line ($w=3\text{mm}$, $\epsilon_r=4.4$, $h=1.6\text{mm}$)

Figure 4.6 shows the simulated transmission coefficient (S_{21}) for different ($w+2g$) from 0.01 GHz to 7 GHz band, by keeping $w=3\text{mm}$ constant. The results demonstrate very smooth transmission line performance with very less amount of transmission losses. Moreover, no resonance occurs in the

transmission coefficient curves. It is found that when the spacing ($w+2g$) is varied from 6.2mm to 7mm the transmission loss is less than 1.6dB. Even though for the spacing of 6.2mm the loss is slightly less than this value. For a substrate thickness of 1.6mm, $w+2g$ length is optimized as 6.4mm. This is nearly the normal thickness of a slim mobile phone and considered for the design of antennas developed in this thesis.

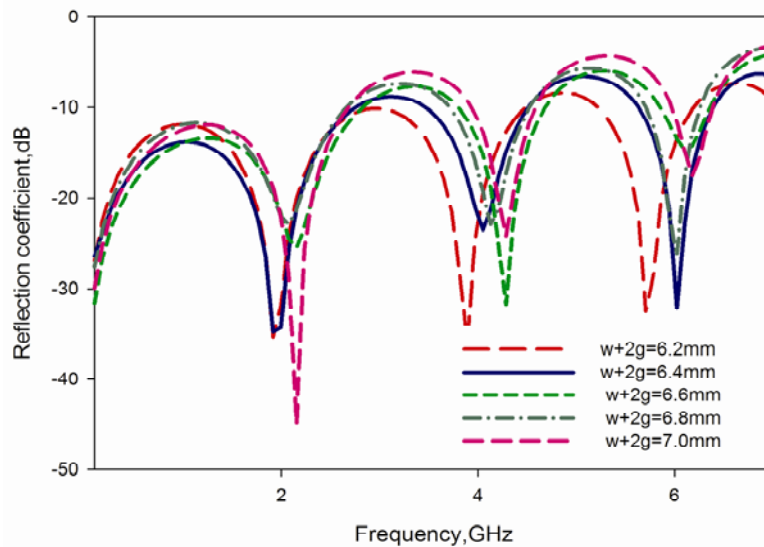


Fig.4.7. Variation of reflection coefficient for different $w+2g$ of ground folded transmission line ($w=3\text{mm}, g=1.7\text{mm}, \epsilon_r=4.4, h=1.6\text{mm}$)

Figure 4.7 shows the reflection characteristics (S_{11}) of the ground folded transmission line. Reflection coefficient is less than 10 dB for a spacing of $w+2g=6.4\text{mm}$, up to 6GHz. The loss increases with frequency as $2g$ increases for $w=3\text{mm}$, transmission line.

A finite length open ended transmission line can radiate electromagnetic energy at the desired frequency, if the structural parameters are properly optimized. This property is utilized to convert the structure folded structure to operate as a monopole antenna.

4.5 Compact ground folded monopole antenna

This section highlights the experimental and simulation outcome of a ground folded monopole antenna for mobile application. The ground plane dimension of the folded transmission line is modified to get the fundamental quarter wavelength monopole [17]. This folding technique is adopted to make this antenna suitable for a mobile handset. The direction of less radiation can be changed by modifying the radiation characteristics of this ground folded monopole antenna structure. This modified structure is suitable for modern wireless handheld devices with less user RF interference.

4.5.1 Antenna Geometry

Antenna geometry is derived from a CPW fed planar monopole antenna by folding the ground plane perpendicular to the monopole main arm as shown in Figure.4.8 (a) and (b). The photograph of the proposed antenna is shown in Figure.4.8(c). The antenna parameters selected for the prototype are same as that of a planar monopole antenna, as mentioned in the previous chapter $L_1=25\text{mm}$ and $W_1=3\text{mm}$, with a folded ground plane dimension of $L_2=17\text{mm}$, $W_2=14\text{mm}$ and the gap between strip monopole & folded ground edge $g=1.7\text{mm}$. The antenna is fabricated on a substrate of thickness (h) 1.6mm and relative permittivity (ϵ_r)=4.4.

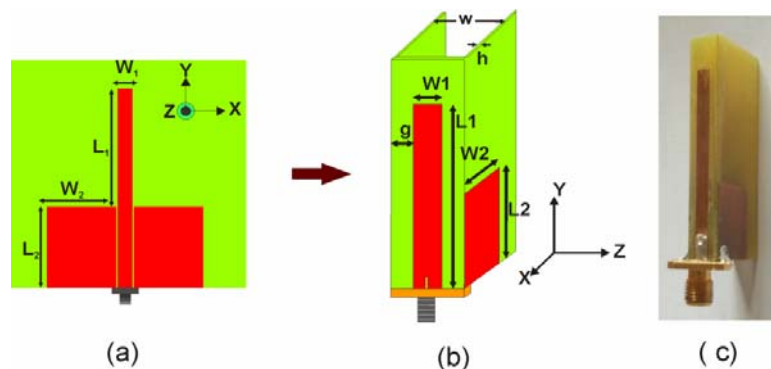


Fig.4.8. Geometry of (a) planar (b) folded antenna (c) photograph of the antenna ($L_1=25\text{mm}$, $W_1=3\text{mm}$, $L_2=17\text{mm}$, $W_2=14\text{mm}$, $g=1.7\text{mm}$, $h=1.6\text{mm}$, $\epsilon_r=4.4$.)

The antenna occupies a volume of $14 \times 42 \times 6.4 \text{ mm}^3$. To achieve compactness the overall spacing W of the system is selected as 6.4 mm , which is the lowest possible value by considering the thickness of the substrate used. Hence the design reduces the antenna size significantly and suitable for hand held devices.

4.5.2 Return loss Characteristics

Measured (HP 8510C Vector Network Analyzer) and simulated (Ansoft HFSS) reflection characteristics of the ground folded monopole are shown in figure.4.9. It is noted that the antenna resonates at 2.34 GHz , as same as the resonating frequency of the planar monopole antenna. The results show an excellent agreement between the measurement and simulation. The folded monopole shows a measured 2:1 VSWR bandwidth of 44 % from 1.99 GHz to 2.92 GHz .

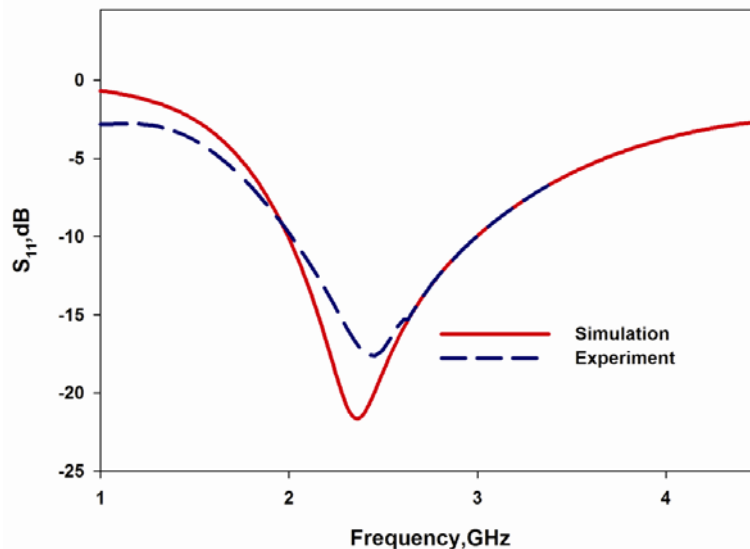


Fig. 4.9. Reflection coefficient of the ground folded antenna
($L_1=25 \text{ mm}$, $W_1=3 \text{ mm}$, $L_2=17 \text{ mm}$, $W_2=14 \text{ mm}$, $g=1.7 \text{ mm}$, $h=1.6 \text{ mm}$, $\epsilon_r=4.4$.)

4.5.3 Effect of strip length L_1 on the resonant frequency

The effect of signal strip length (L_1) on the resonant frequency of the folded monopole antenna is shown in figure.4.10. The signal strip length is

arbitrarily varied from 21mm to 29mm for this study. It is evident from the reflection characteristics that the resonance frequency is proportional to the length. It is found that the resonance occurs when L_1 is approximately equal to quarter wavelength in the substrate.

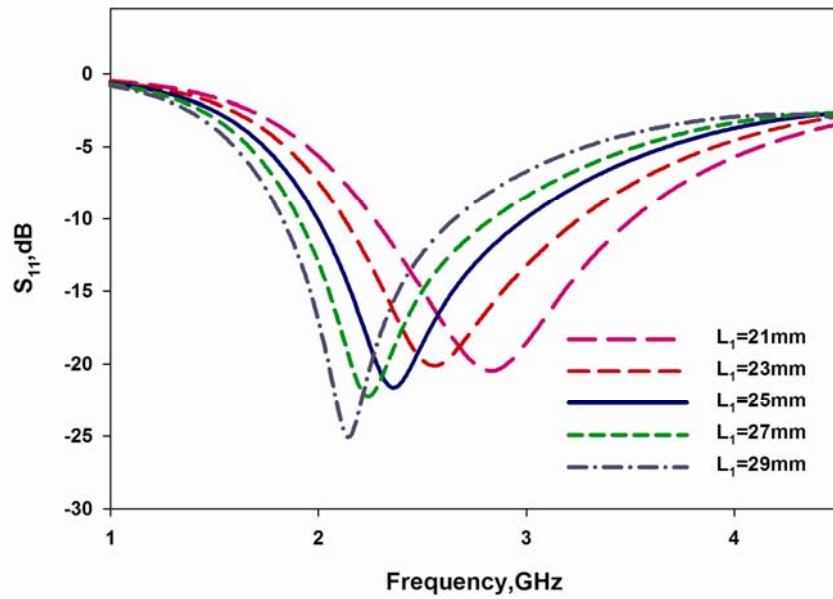


Fig. 4.10. Effect of L_1 on reflection coefficient of the ground folded antenna ($W_1=3\text{mm}, L_2=17\text{mm}, W_2=14\text{mm}, g=1.7\text{mm}, h=1.6\text{mm}, \epsilon_r=4.4.$)

The current variation at the surface of the folded ground strip monopole is plotted in figure. 4.11, at the resonant frequency. It can be found from the surface current density plot of folded monopole antenna that, the current is maximum at the bottom end and a minimum at the other end (open end) of the monopole. That is nearly a quarter wave variation along the length of the strip monopole. A strong interaction between the ground plane and strip monopole is observed at the interface. It is also observed that the current variation along the ground plane is feeble.

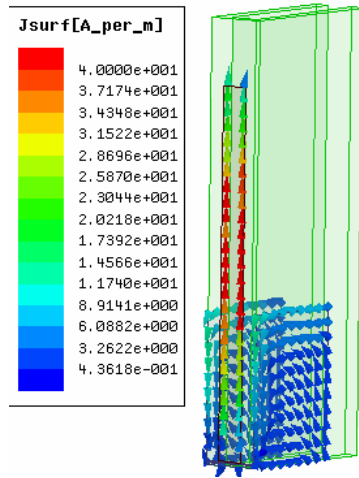


Fig. 4.11. Surface Current distribution of the ground folded antenna
 ($L_1=25\text{mm}, W_1=3\text{mm}, L_2=17\text{mm}, W_2=14\text{mm}, g=1.7\text{mm}, h=1.6\text{mm}, \epsilon_r=4.4$.)

4.5.4 Radiation patterns

Measured 2D radiation patterns in the XZ and YZ plane of the folded antenna are shown in figure.4.12 (a) and (b) respectively.

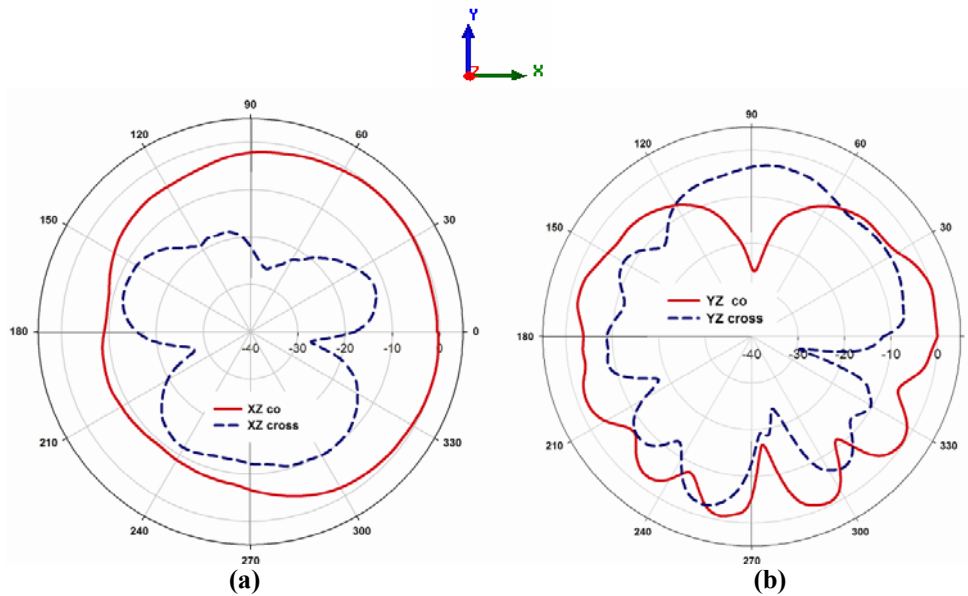


Fig.4.12. Measured radiation pattern of the ground folded antenna at resonant frequency (a) XZ plane (b) YZ plane
 ($L_1=25\text{mm}, W_1=3\text{mm}, L_2=17\text{mm}, W_2=14\text{mm}, g=1.7\text{mm}, h=1.6\text{mm}, \epsilon_r=4.4$.)

It is noted that the folded antenna exhibits a non-directional pattern along the azimuth plane. The polarization is linear as that of ordinary monopole, throughout the band. The antenna radiation in XZ plane is non-directional, while in the orthogonal plane is directional.

The simulated 3D radiation pattern at 2.34 GHz using Ansoft HFSS is shown in the figure.4.13. It can be seen from the plot that the folded antenna exhibits a non-directional pattern along the azimuth plane and directional pattern along the elevation plane as that of a planar monopole. The peak radiation from this antenna is 18 dB. This nearly omni-directional radiation coverage can be used for applications in mobile communication field.

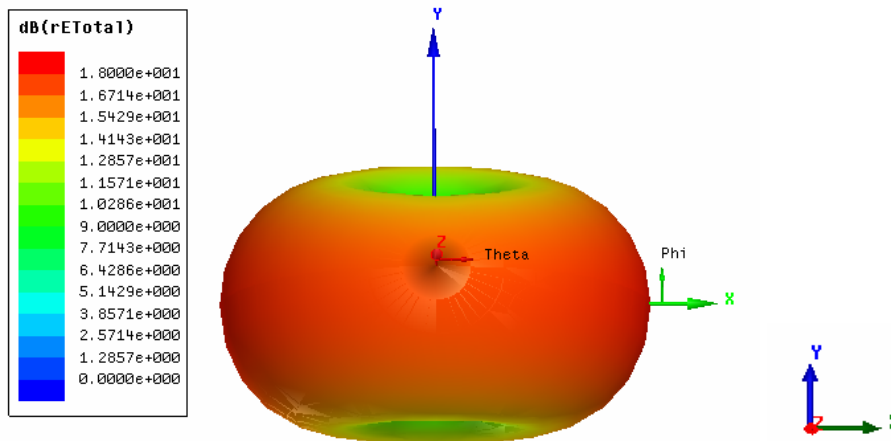


Fig.4.13. 3D radiation pattern of the ground folded antenna at resonant frequency ($L_1=25\text{mm}, W_1=3\text{mm}, L_2=17\text{mm}, W_2=14\text{mm}, g=1.7\text{mm}, g=1.7\text{mm}, h=1.6\text{mm}, \epsilon_r=4.4.$)

4.5.5 Antenna Gain

The gain of the antenna is measured using gain comparison method. The measured gain of the folded antenna is depicted in figure 4.14. It is noted that the folded antenna has a peak gain of 5.2dBi at 2.74 GHz due to additive field along XZ plane. The average gain of the antenna is 3.75dBi.

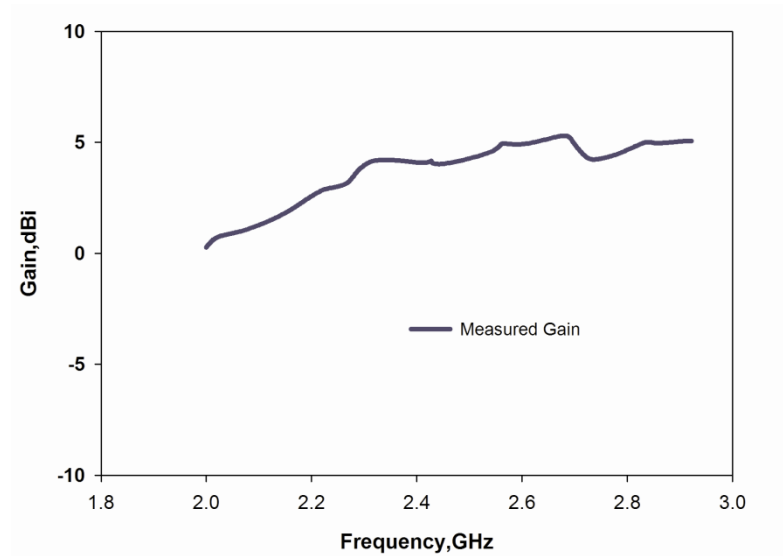


Fig.4.14. Measured gain of the ground folded antenna
 ($L_1=25\text{mm}, W_1=3\text{mm}, L_2=17\text{mm}, W_2=14\text{mm}, g=1.7\text{mm}, h=1.6\text{mm}, \epsilon_r=4.4.$)

4.5.6 Electric field distribution at resonance frequency

The enhancement in gain can be best understood by comparing the fringing electric field patterns of the ordinary monopole and the folded monopole as shown in figure.4.15 (a) and (b).

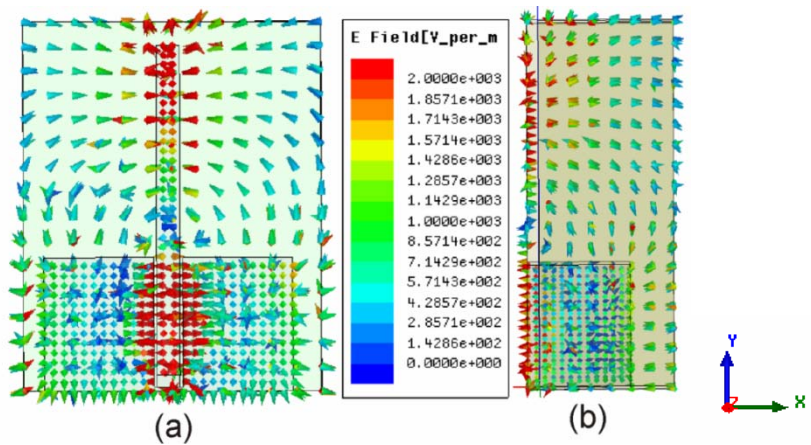


Fig.4.15. Simulated Electric field distribution at resonant frequency of
 (a) monopole (b) folded monopole
 ($L_1=25\text{mm}, W_1=3\text{mm}, L_2=17\text{mm}, W_2=14\text{mm}, g=1.7\text{mm}, h=1.6\text{mm}, \epsilon_r=4.4.$)

It is observed that the fringing electric field between the ground planes and the monopole arm are out of phase in the case of ordinary printed monopole antenna and it cancels the field at the far field giving reduced gain. But the folding technique, effectively adds the fringing fields at the bore sight giving an enhanced gain.

4.5.7 Inferences

The antenna has an average gain of 3.75dBi with a 2:1 VSWR band width of 44 % from 1.99GHz to 2.92GHz. High gain performance is achieved by folding the ground plane of a CPW fed printed monopole perpendicular to the plane of the monopole main arm. The antenna exhibits good radiation and impedance matching characteristics as that of a CPW fed ordinary printed monopole. The antenna has a dimension of 14 X 42 X 6.4 mm³ and highly suitable for slim mobile handsets.

4.6 Modified ground folded antenna for mobile handset

The ground folded strip monopole antenna discussed in the previous section has similar far field radiation characteristics as that of a vertical strip monopole antenna. It has nearly omni-directional characteristics in azimuth plane and nearly non directional pattern in orthogonal plane. Investigations are carried to modify the radiation pattern of the ground folded monopole antenna by judiciously placing another vertical strip at the back side of the ground plane. By incorporating an additional strip at the opposite side, the resonance of the folded strip monopole is shifted to lower frequency. Thus a novel compact antenna with excellent radiation characteristics suitable for mobile handset is derived. This section of the thesis provides a detailed discussion about the development of a novel antenna with reduced radiation hazard towards the human head. The simulation results are experimentally verified and an

exhaustive parametric analysis is performed to study the effect of various antenna parameters.

4.6.1 Antenna Geometry

The geometry of the folded mobile antenna is illustrated in Figure.4.16.

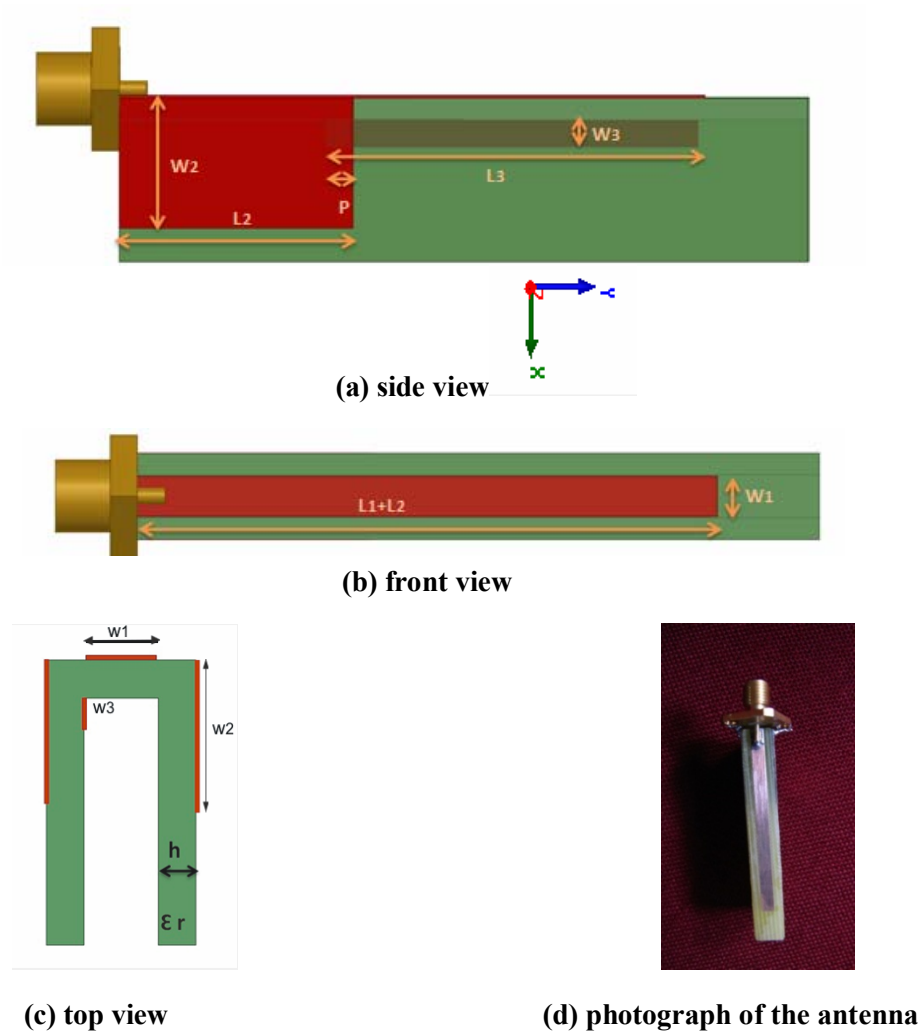


Fig.4.16. Geometry of the ground folded monopole antenna with printed metal strip (a)side view (b) front side(c)top view(d) photograph of the antenna ($L_1=25\text{mm}, W_1=3\text{mm}, L_2=17\text{mm}, W_2=9.5\text{mm}, L_3=27\text{mm}, W_3=2\text{mm}, P=2\text{mm}, g=1.7\text{mm}, h=1.6\text{mm}, \epsilon_r=4.4$.)

The geometry consists of a strip monopole of length, L_1 and width W_1 on YZ plane. The truncated ground plane dimension is $L_2 \times W_2$. A single metal strip of dimension $L_3 \times W_3$ is printed at the optimum position (off sited P mm below from the top edge of the ground plane) in the inner wall of the ground plane to modify the radiation pattern. Both the strip monopole and the ground plane are fabricated on a substrate of relative permittivity, $\epsilon_r = 4.4$ and thickness, $h = 1.6$ mm.

4.6.2 Reflection characteristics

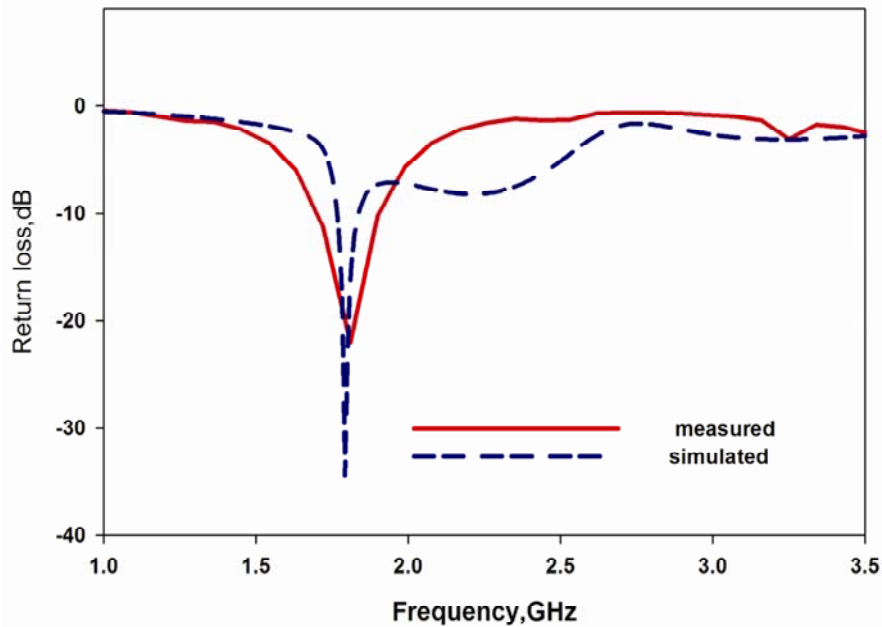


Fig.4.17. Reflection characteristics of the GFPA with printed metal strip ($L_1=25$ mm, $W_1=3$ mm, $L_2=17$ mm, $W_2=9.5$ mm, $L_3 =27$ mm, $W_3=2$ mm, $g=1.7$ mm, $h=1.6$ mm, $\epsilon_r=4.4$.)

A metal strip of width (W_3) = 2mm and length (L_3) = 27 mm is placed 2mm (P) below the ground plane edge. At this position, the antenna offers a measured 2:1 VSWR band from 1.68 GHz to 1.92 GHz with 15% bandwidth centered at 1.81 GHz as shown in Figure. 4.17. The simulated return loss characteristic of the antenna is also shown in the same graph for comparison.

4.6.3 Radiation pattern

The simulated 3D far field radiation patterns at 1810MHz of the proposed antenna in different views are shown in Figure.4.18. There is a considerable reduction of radiated energy along the positive X direction for the antenna. Moreover, there is only one null appeared in the pattern. This reduction is nearly 11dB as evident from the figure. The radiation pattern is modified with good radiation in three space quadrants and reduced radiation in one quadrant as suitable for a mobile handset.

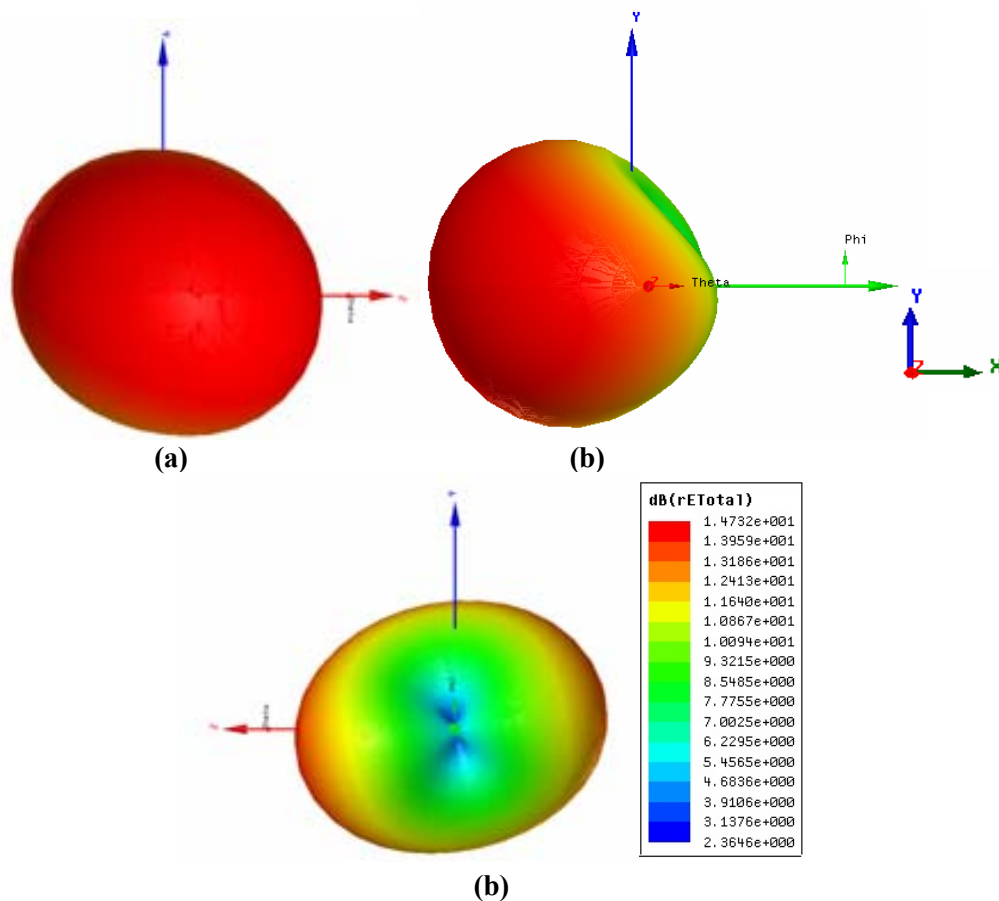


Fig.4.18. 3D Radiation pattern of the GFPA with printed metal strip for different viewing angle
 (a) $\phi = -180^\circ$ (b) $\phi = 0^\circ$ (c) $\phi = 180^\circ$ ($L_1 = 25\text{mm}$, $W_1 = 3\text{mm}$, $L_2 = 17\text{mm}$, $W_2 = 14\text{mm}$, $L_3 = 27\text{mm}$, $W_3 = 2\text{mm}$, $g = 1.7\text{mm}$, $h = 1.6\text{mm}$, $\epsilon_r = 4.4$.)

It is found that the radiation from the radiating element and the induced radiation from the strip cancelled each other along the positive X direction. This is more clear from the field distribution of the antenna.

Measured radiation patterns of the antenna at 1.81GHz are shown in figure. 4.19(a) and (b). The radiation pattern is modified with single null along positive X direction. It is also interesting to note that the radiation in the XZ plane is almost constant for most of the angles. The half power beam width in the XZ plane is 300° . The pattern in the YZ plane is somewhat directional.

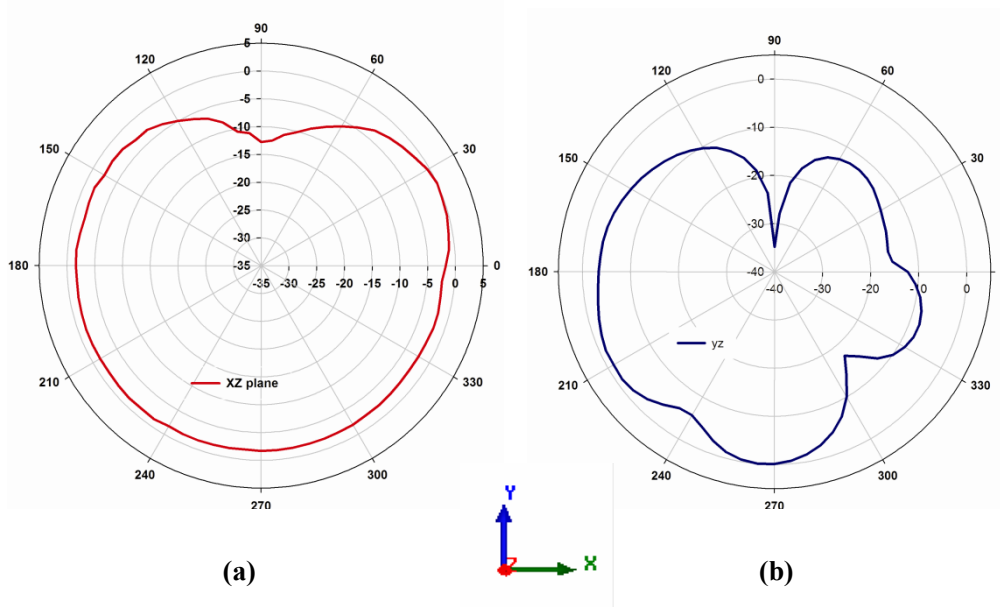


Fig.4.19. Measured Radiation characteristics of the GFPA with printed metal strip (a)xz plane(b)yz plane ($L_1=25\text{mm}, W_1=3\text{mm}, L_2=17\text{mm}, W_2=9.5\text{mm}, L_3=27\text{mm}, W_3=2\text{mm}, g=1.7\text{mm}, p=2\text{mm}, h=1.6\text{mm}, \epsilon_r=4.4$.)

4.6.4 Parametric Analysis

A parametric analysis is performed to study the effect of the strip element on the antenna characteristics. Various antenna parameters of the add-on element including its length, width and position are studied and the results are discussed in the following sections.

4.6.4.1 Effect of strip position (P)

The effect of overlapping length between signal strip and ground plane (P) on the reflection characteristics of the antenna is shown in figure. 4.20. The lower end of the printed strip is at the top edge of the ground plane ie, the overlapping length is zero (P=0) or when the lower strip end is shifted 4mm along positive Y direction from the top ground edge (P=-4) the resonance frequency is independent of addon strip length. It is also observed that when the lower edge of the strip has an overlap area with ground plane ie, for different overlapping lengths (P= 2, 4, and 8mm below the top edge of the ground plane) the resonant frequency of the antenna remains unaltered as in the figure.

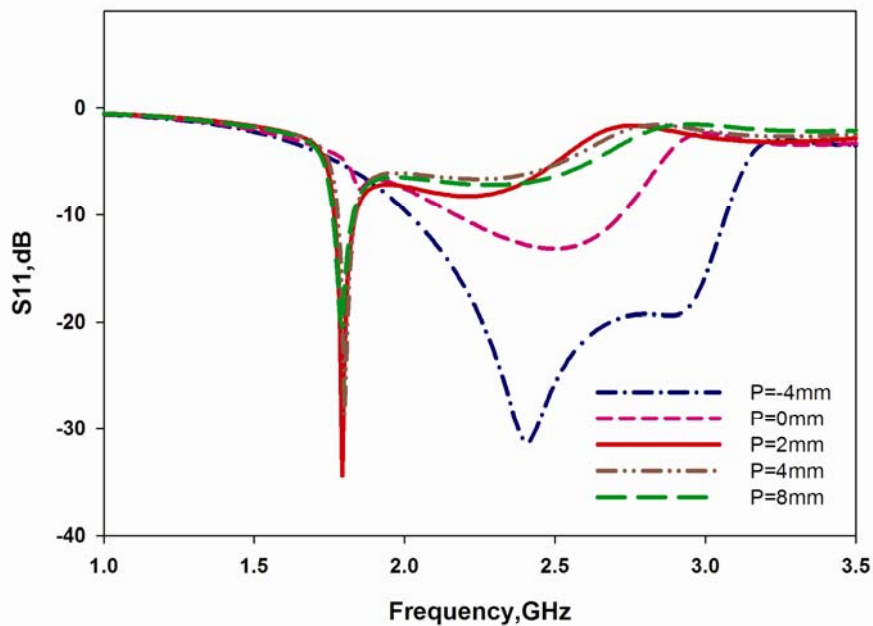


Fig.4.20. Effect of strip position on reflection characteristics of the GFPA with printed metal strip
 ($L_1=25\text{mm}$, $W_1=3\text{mm}$, $L_2=17\text{mm}$, $W_2=9.5\text{mm}$, $L_3=27\text{mm}$, $W_3=2\text{mm}$, $g=1.7\text{mm}$, $h=1.6\text{mm}$, $\epsilon_r=4.4$.)

The 3D radiation patterns with different offset distances along positive Y directions (P values) are plotted in figure. 4.21. It is clear that the position of the strip has a significant effect on the reflection characteristics of the antenna. The antenna shows nearly omni-directional pattern when there is no overlapping distance (P=0 and 4 mm above the ground plane). The pattern is suitable for a typical mobile gadget only when the strip has an overlapping distance along negative Y direction ie, for P=2mm, 4mm and 8mm etc. So it can be concluded that proper ground coupling is required for modifying the radiation pattern.

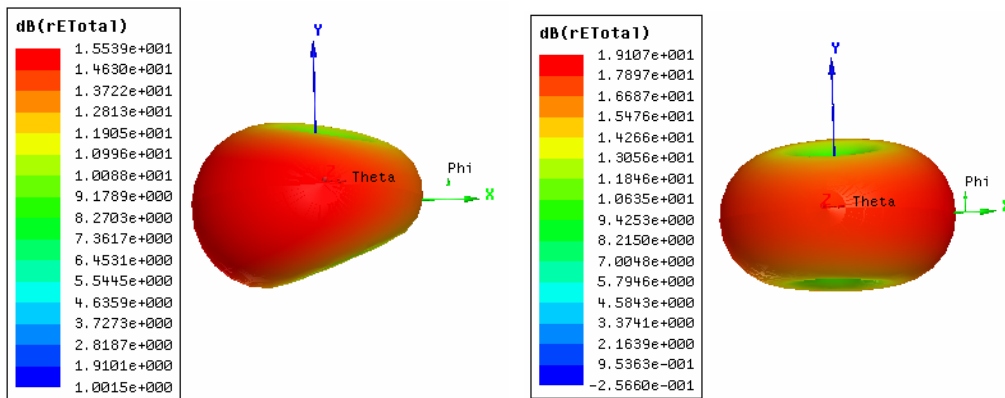


Fig.4.21. 3 D radiation pattern of the GFPA with printed metal strip at (a) P=0mm, (b) P=(-4)mm, ($L_1=25\text{mm}, W_1=3\text{mm}, L_2=17\text{mm}, W_2=9.5\text{mm}, L_3=27\text{mm}, W_3=2\text{mm}, g=1.7\text{mm}, h=1.6\text{mm}, \epsilon_r=4.4$.)

4.6.4.2 Effect of ground width (W_2)

The effect of ground plane width, W_2 , on the reflection characteristics is illustrated in figure. 4.22. It is observed from the results that the resonant frequency changes with the ground plane width due to coupling effect and the resonant frequency shifts towards the low frequency region as W_2 increases. Maximum impedance matching at the required resonance occurs for $W_2=9.5\text{mm}$. This is due to the increased capacitance of the upper and lower strips. The increased capacitance will lower the resonant frequency.

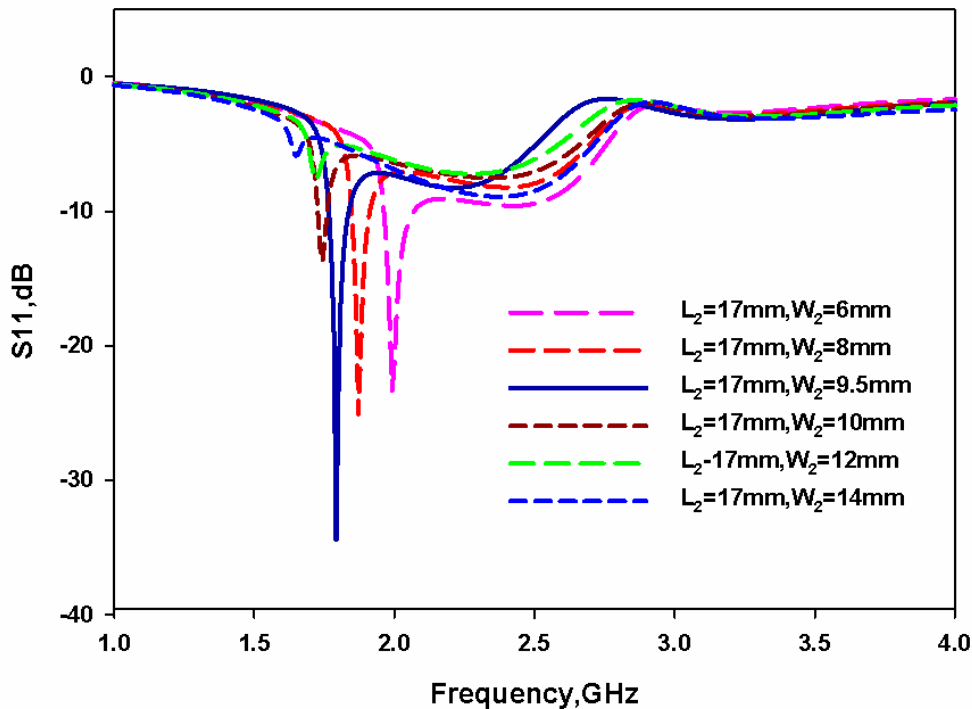


Fig.4.22. Effect of ground width (W_2) on reflection characteristics of the GFPA with printed metal strip
 ($L_1=25\text{mm}$, $W_1=3\text{mm}$, $L_2=17\text{mm}$, $L_3=27\text{mm}$, $W_3=2\text{mm}$, $g=1.7\text{mm}$, $P=2\text{mm}$, $h=1.6\text{mm}$, $\epsilon_r=4.4$.)

4.6.4.3 Effect of strip width (W_3)

The effect of W_3 over the resonant frequency is illustrated in the figure.4.23. The width of the strip-element is varied from 2mm to 5mm and found that the resonant frequency remains unaltered. However, the matching is affected with the width of the strip. It is also seen from the analysis that the impedance matching around the center frequency of the first resonance becomes maximum for strip width W_3 is equal to 2mm.

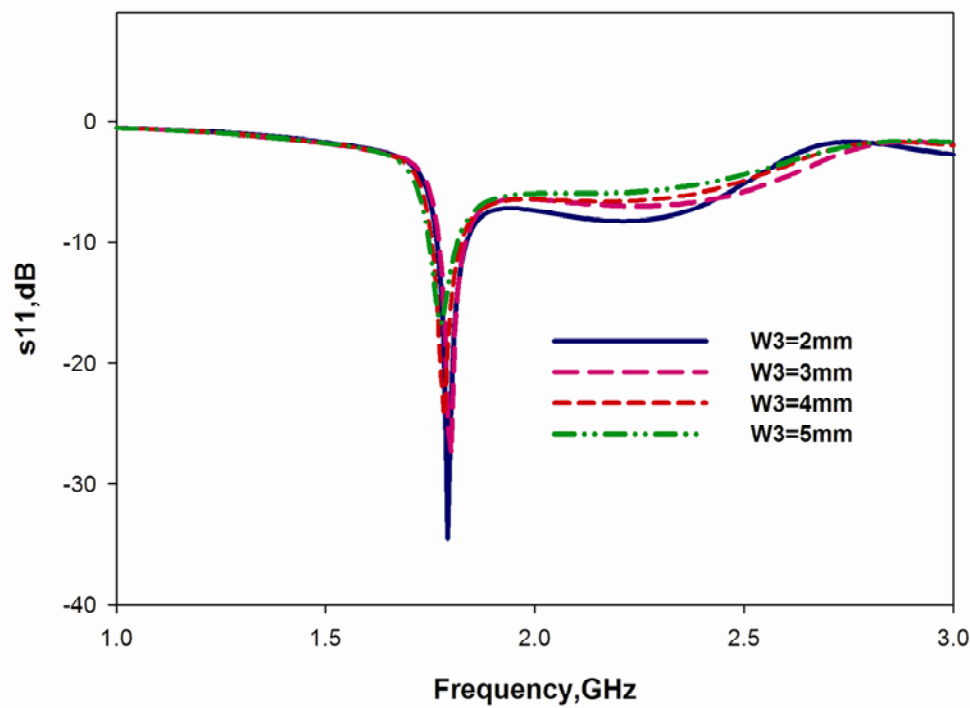


Fig.4.23. Effect of strip width (W_3) on reflection characteristics of the GFPA with printed metal strip

($L_1=25\text{mm}$, $W_1=3\text{mm}$, $L_2=17\text{mm}$, $W_2=9.5\text{mm}$, $L_3=27\text{mm}$, $W_3=2\text{mm}$, $g=1.7\text{mm}$, $P=2\text{mm}$, $h=1.6\text{mm}$, $\epsilon_r=4.4$.)

4.6.4.4 Effect of strip length (L_3)

The length of the add-on element is also varied from 8.5mm to 10.5mm and the effect over the return loss characteristics is depicted in Figure. 4.24. It is seen that the resonant band remains almost unaltered with the L_3 . From the graph it is found that $L_3=27\text{mm}$ is optimum for this antenna as far as the impedance match is concerned.

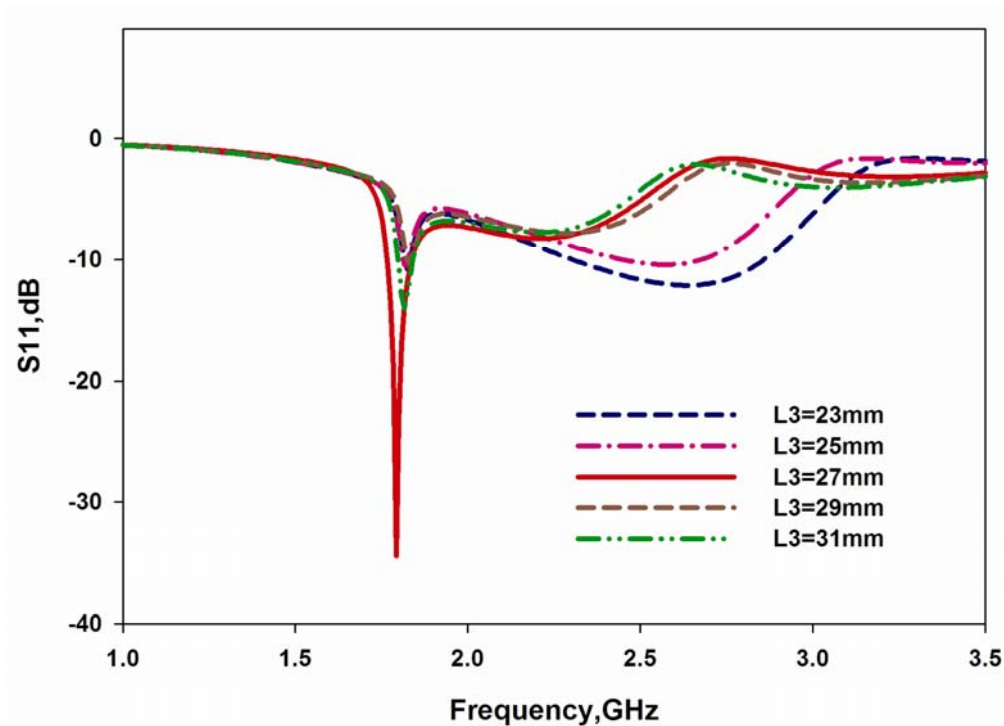


Fig.4.24. Effect of strip strip length (L_3) on reflection characteristics of the GFP antenna with printed metal strip ($L_1=25\text{mm}, W_1=3\text{mm}, L_2=17\text{mm}, W_2=9.5\text{mm}, W_3=2\text{mm}, g=1.7\text{mm}, h=1.6\text{mm}, \epsilon_r=4.4$.)

4.6.4.5 Effect of dielectric constant (ϵ_r) of Substrate Material

The effect of dielectric constant on antenna performance has been studied by simulating the antenna on different substrate materials. ϵ_r has been varied from 2.2 to 10.2. The reflection characteristics are shown in figure 4.25 and as expected resonant frequency decreases with increase in dielectric constant. The 3D radiation patterns at the resonance frequencies are shown in Table 4.1. It exhibits the pattern as required for a mobile handset.

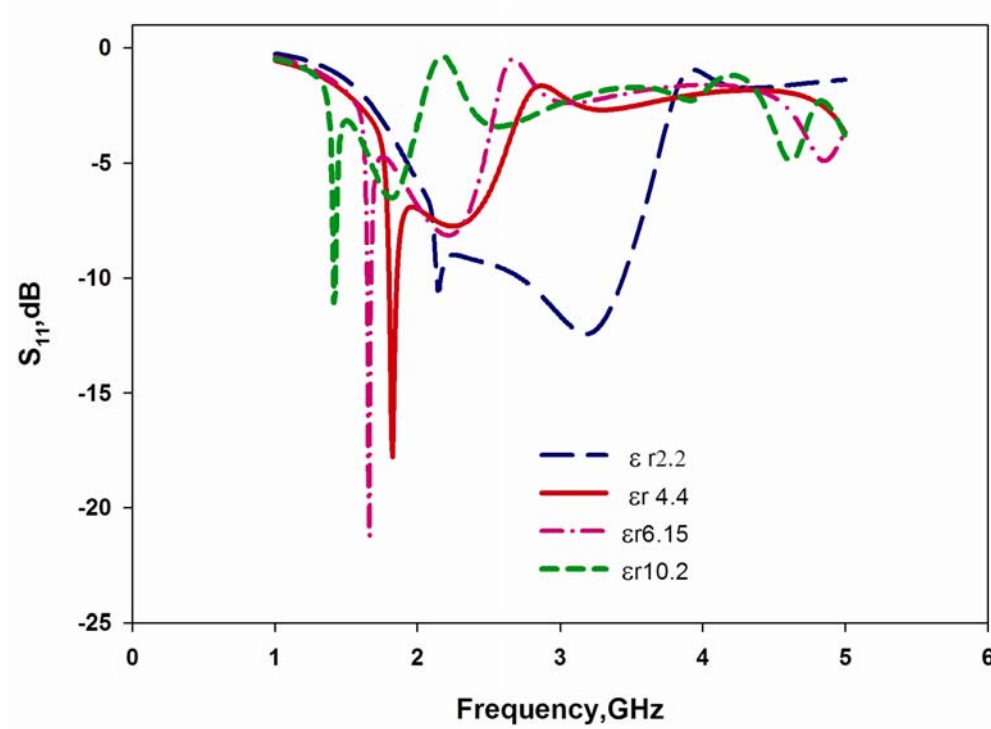


Fig.4.25. Effect of dielectric constant on reflection characteristic of the GFPA with printed metal strip
($L_1=25\text{mm}$, $W_1=3\text{mm}$, $L_2=17\text{mm}$, $W_2=9.5\text{mm}$, $L_3=27\text{mm}$, $W_3=2\text{mm}$, $g=1.7\text{mm}$, $h=1.6\text{mm}$.)

Table 4.1. Radiation pattern of the Ground Folded antenna with metallic strip on different substrates

Dielectric material	Dielectric constant	Resonance frequency(GHz)	3D Radiation pattern
RT Duroid 6010LM	10.2	1.42	
RT Duroid 6006	6.16	1.66	
FR4 Epoxy	4.4	1.82	
RT Duroid 5880	2.2	2.14	

From the table it is found that for all the cases the radiation pattern is with reduced radiation in the positive X direction.

4.6.5 Polarization

Antenna is linearly polarized along x direction with a cross polar level better than -23dB along the bore sight direction. H-plane pattern measured along XZ plane is given in the figure. 4.26. The radiation pattern is minimum

towards the strip side and maximum in the opposite side. Half power beam width along the H-plane is nearly 180° .

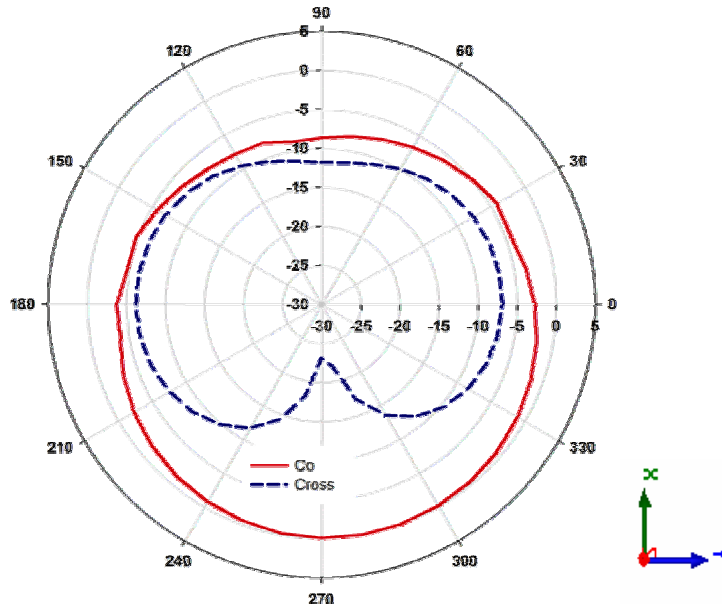


Fig.4.26. Co and Cross polarization along H plane of the GFPA with printed metal strip
 ($L_1=25\text{mm}, W_1=3\text{mm}, L_2=17\text{mm}, W_2=9.5\text{mm}, L_3=27\text{mm}, W_3=2\text{mm}, g=1.7\text{mm}, h=1.6\text{mm}, \epsilon_r=4.4.$)

4.6.6 Gain

Figure.4.27 depicts the measured gain of the antenna. The gain of the antenna remains almost constant throughout the operating band with an average gain of 1.43dBi. The maximum gain is 1.8dBi at 1.79GHz. It is also found that gain of antenna with strip is less compared to antenna without strip. At the resonance frequency the effective ground area of the proposed antenna is reduced from $17 \times 14 \text{ mm}^2$ (without strip) to $17 \times 9.5 \text{ mm}^2$ (with strip).

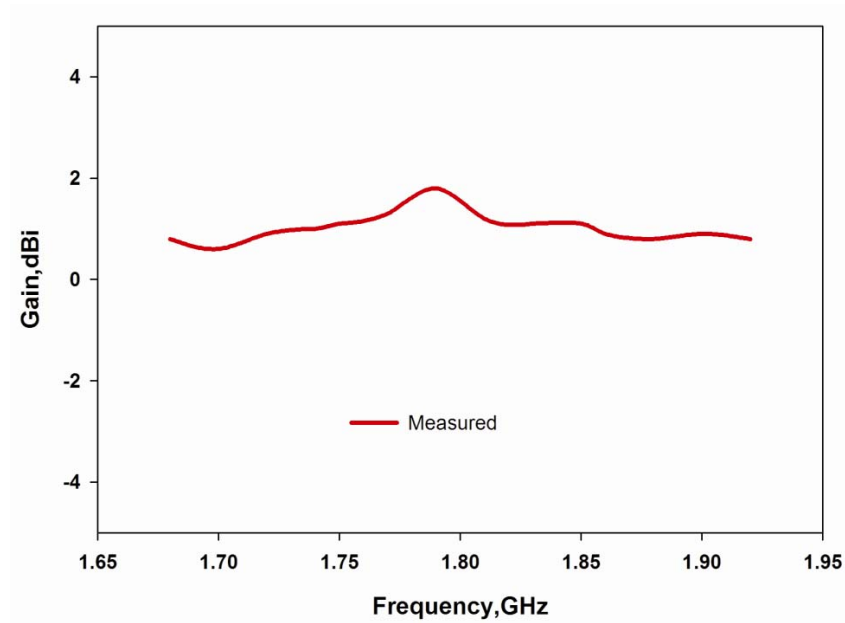


Fig.4.27. Measured gain of the GFPA with printed metal strip
**($L_1=25\text{mm}$, $W_1=3\text{mm}$, $L_2=17\text{mm}$, $W_2=9.5\text{mm}$, $L_3=27\text{mm}$,
 $W_3=2\text{mm}$, $g=1.7\text{mm}$, $P=2\text{mm}$, $h=1.6\text{mm}$, $\epsilon_r=4.4$.)**

Table 4.2 summarizes the measured radiation characteristics of the ground folded antenna with printed metal strip which is considered as mobile antenna for slim and compact handset.

Table 4.2. Characteristics of the ground folded antenna

Characteristics	CPW fed monopole
Resonance frequency and Return loss	1.81 GHz, (-35dB)
Band width	240MHz, 1.68GHz-1.92 GHz
Radiation pattern	E plane omni directional H plane-Non directional with single null
Area	9.5mmX42mm X 6.4mm
Ground dimension	9.5mmX17mm
Gain	1.43dBi

The following conclusions can be made from the analysis of different structures from this thesis.

- Mobile antennas operating at GSM 1800 band is developed
- The influence of add on structures on the resonance and radiation characteristics of the antennas are studied and it is found that the radiation pattern can be tailored effectively suitable for the necessities of mobile antennas.
- The non directional radiation characteristic of the monopole antenna in azimuth plane is modified with a radiation characteristics having single null in that plane.
- It is observed that SAR value decreases with distances for the proposed antennas.

The above conclusions are summarized in table 4.2.1

Table 4.2.1. Summarized result

Antenna	Ground dimension (mm)	Average gain	Radiation pattern	Volume(mm ³) Substrate height h=1.6mm	Simulated SAR Value(1gm) (W/kg)	Reduced power in null direction (simulation)
Printed monopole with SRR	31.7X14	1.2dBi	E plane omni directional H plane-Non directional with single null	42X31.7	1.54	18dB
Printed monopole with single strip	31.7X14	1.12 dBi	„	42X31.7	1.32	20dB
Printed monopole with vertical stripes	31.7X14	1.14 dBi	„	42X31.7	0.647	23dB
Folded monopole antenna with vertical strip	9.5X17m m	1.43dBi	„	42X9.5X6 .4	1.86	12dB

The comparison study is also done with similar works related to this field and is illustrated below.

When metamaterials are used for SAR reduction, periodical arrangement of SRRs are placed between dipole and head model to reduce SAR by 44%. Different positions, sizes, and negative medium parameters of metamaterials are the critical factors for designing such antenna.

Multilayer planar inverted-F antenna (PIFA) is located on an electromagnetic bandgap structure (EBG), is also used to reduce SAR value by 31%. The EBG cell numbers, height, and location of the antenna has to be optimized to get the reduced SAR value.

4.7 Chapter conclusion

The important conclusions from the present investigations on different antennas from this chapter are summarized below.

- A CPW fed transmission line can be folded into a low profile 3D structure with good transmission and reflection characteristics.
- The ground folded strip monopole antenna has similar far field radiation characteristics as that of conventional strip monopole antenna.
- The non directional radiation characteristic of the folded monopole antenna in azimuth plane is modified with a radiation characteristics having single null in that plane by adding a single strip.
- The addon metal strip reduces the resonant frequency to 1.8GHz.
- The ground folded antenna with added strip has an average gain of 1.43dBi

References

- [1] J. Leonhard, R D Mattuck, and A. J. Pote “Folded Unipole Antennas” IRE Transactions-Antennas and propagation pp111-116, July 1955
- [2] W Harrison and R W P King” Folded Dipoles and Loops” IRE Transactions-Antennas and propagation pp181-187, July 1961
- [3] M. c. ELIAS AND C. T. CARSON “Direct Analysis of Folded Dipole by Method of Moments” Electronics Letters Vol.9 No.22, PP 520-521, 1st November 1973
- [4] Ross w Lampee “Design Formulas for an Asymmetric Coplanar Strip Folded Dipole” IEEE Trans on Antennas and Propagation,, vol. AP-33, no. 9, pp1028-1031, September 1985
- [5] E. Lee, P.S. Hall and P. Gardnei “Dual band folded monopole/loop antenna for terrestrial communication system” Electronics Letters Vol. 36 No. 24, pp 1990-1991, 23rd November 2000
- [6] Shun-Yun Lin, “Multiband folded planar monopole antenna for mobile handset”, IEEE Transactions on Antennas and Propagation Vol. 52, No7, pp.1790 – 1794, July 2004
- [7] Yu-Seng Liu 1, Jwo-Shiun Sun, Rui-Han Lu, Yi-Jay Lee “New multiband printed meander antenna for wireless applications” Microwave and optical technology letters, Vol. 47, Issue 6 , pp. 539 – 543, Oct 2005
- [8] Chia-Hao Ku, Hsien-Wen Liu, and Sheng-Yu Lin” Folded Dual-Loop Antenna for GSM/DCS/PCS/UMTSMobile Handset Applications” IEEE Antennas and wireless propagation Letters ,Vol. 9, pp 998-1001, 2010
- [9] Xi Yang, , Ying Zeng Yin, Wei Hu, and Shao Li “ Low-Profile, Small Circularly Polarized Inverted-L Antenna With Double-Folded Arms” IEEE Antennas and wireless propagation Letters ,vol. 9, p.p767-770, 2010

- [10] Xiaoyu Cheng*, Jun Shi, Cheolbok Kim, David Senior and Yong-Kyu Yoon” A Compact Self-packaged Patch Antenna with Non- Planar Complimentary Split Ring Resonator Loading” IEEE 1036, pp 1036-1039, AP-S/URSI 2011
- [11] F. Ferrero, A. Chevalier, J. M. Ribero, R. Staraj, J. L. Mattei, and Y. Queffelec “New Magneto-Dielectric Material Loaded, Tunable UHF Antenna for Handheld Devices” IEEE Antennas and wireless propagation Letters, vol. 10, PP951-955,2011.
- [12] Vallecchi, J. R. De Luis, F. Capolino, F. De Flaviis,” Low Profile Fully Planar Folded Dipole Antenna on a High Impedance Surface” IEEE Trans. Antennas and Propagat.,2011.
- [13] Nguyen Tuan Hung', Sohei Watanabe', Hisashi Morishita” Fundamental study on U-shape folded dipole antenna for WiMAX” Proceedings of the 5th European Conference on Antennas and Propagation (EUCAP), pp1318-1321, 2011
- [14] R. Zaker and A. Abdipour” Dual-wideband circularly-polarised slot antenna using folded L-shaped stub” Electronics Letters Vol. 47, No. 6, 17th March 2011
- [15] Mikio Tsuji, Hiroshi Shigesawa and Arthur A. Oliner, “New interesting leakage behaviour on coplanar waveguides of finite and infinite widths,” IEEE Trans. Microwave Theory and Techniques, vol. 39, no. 12, Dec.1991.
- [16] Suma M.N, Investigations on broadband planar monopole antennas with truncated ground plane, Ph.D Thesis, Cochin University of Science and Technology, January 2008
- [17] P. A. J. Duuis and C. K. Campbell “ Characteristic impedance of surface strip coplanar waveguides” Electronics Letters Vol.9, No. 1, pp 354-355, August 1973.

.....✂.....

SIMULATION AND EXPERIMENTAL ANALYSIS OF NEAR-FIELD PERFORMANCE OF THE ANTENNAS

C o n t e n t s	5.1 <i>Introduction</i>
	5.2 <i>SAR Definition</i>
	5.3 <i>RF Exposure Limits</i>
	5.4 <i>Tissue equivalent liquid parameters</i>
	5.5 <i>Near field characteristic study of antennas</i>
	5.6 <i>Experimental result in the Near Field Phantom</i>
	5.7 <i>Chapter Conclusion</i>

With the explosive growth of the wireless communication technology, there has been more concern about the safety aspects and the potential hazardous effects associated with EM radiation on human body. Therefore, the near field interaction between the human head with antennas has to be taken into account in determining the characteristics of antenna. Simulation and experimental analysis of antennas are performed to determine the near field effects and Specific Absorption Rate (SAR) in the phantom head model.

5.1 Introduction

The antenna is optimized in terms of return loss and radiation characteristics in the previous chapters. This chapter mainly deals with near field measurements and analysis of the above optimized antenna.

The rapidly expanding use of mobile phones utilizing radiofrequency (RF), has raised public concern on health effects. To protect people from any possible adverse effects of RF radiation, the International Commission on Non-Ionizing Radiation Protection (ICNIRP) has formulated guidelines on exposure levels (ICNIRP 1998) [1]. This exposure limits are set as Specific Absorption Rates (SARs). The Specific Absorption Rate (SAR) is used to denote the transfer of energy from the EM fields to biological materials when exposed to radio frequency (RF). The propagation and radiation of microwaves in biological tissues depends on the frequency of the energy source, the amount of power delivered, time of exposure, the antenna radiation pattern characteristics, the tissue composition and dielectric permittivity. As microwave fields propagate in the tissue medium, microwave energy is absorbed by the medium. This absorption results in a progressive reduction of the microwave power intensity as it advances through the tissue [2][3]. The portion of energy absorbed from the propagating microwave field is converted into heat. This heat leads to the damage of human tissue. Thus by reducing the radiated microwave power towards the human tissue, the tissue damage can be reduced.

5.2 SAR Definition

SAR is an indication of the amount of radiation that is absorbed into a human tissue ie, the higher the SAR rating the more will be radiation that is absorbed into the human tissue. The SAR at a point is defined as the rate of change of energy absorbed by the tissue particles within an infinitesimal

volume at that point, averaged by the mass of that small volume (in either 1g or 10g) and expressed in units of Watts per Kilogram[4].

$$SAR = \frac{\partial W / \partial t}{\rho_m} \quad (\text{W/kg}) \text{ -----(5.1)}$$

where ρ_m is the mass density

However, the rate of change of energy $\partial W / \partial t$ is equivalent to power density (P). Hence, the above equation (5.1) can be rewritten as:

$$SAR = \frac{P}{\rho_m} \quad (\text{W/kg}) \text{ -----(5.2)}$$

Since $J = \sigma E$, the equation (5.2) is modified as

$$SAR = \frac{\sigma |E|^2}{\rho_m} \quad (\text{W/kg}) \text{ -----(5.3)}$$

where σ represents the conductivity of the material, and in general $|E|$ is the Root Mean Square (RMS), magnitude of the electric field (V/m), is given by

$|E|^2 = |E_x|^2 + |E_y|^2 + |E_z|^2$ where E_x , E_y and E_z are the RMS values of the x, y, and z components of the electric field and ρ_m is the mass density.

In the IEEE standard C95.3 [5], the SAR is also defined as the time derivative of the incremental energy (∂W) absorbed or dissipated in an incremental mass (∂m) contained in a volume element (∂V) of a given density (ρ_m). Equation (5.1) is equivalent to (5.4) as presented below.

$$SAR = \frac{\partial \partial W}{\partial t \partial m} = \frac{\partial W}{\rho_m \partial V} \quad (\text{W/kg}) \text{ -----(5.4)}$$

SAR is usually averaged either over the whole body, or over a small sample volume containing typically 1 g or 10 g of tissue. It is nothing but the electromagnetic power density deposited per unit mass of biological tissues.

The SAR in a tissue media can also be related to the rise in temperature due to the RF energy absorption as equation 5.5.

$$\text{SAR} = C (dT/dt) \text{-----(5.5)}$$

where C is the specific heat of tissue, dT is the temperature rise and dt is the exposure duration.

However, in order to use temperature techniques, relatively high power is required to expose the tissue over a very short duration to avoid thermal diffusion errors. Therefore, temperature methods are not preferred for evaluating SAR value of low power transmitters.

5.3 RF Exposure Limits

Cellular and PCS telephones are portable devices, whose radiating part is designed to use in direct contact with the user's body or very near to the body under normal operating conditions. And these portable devices are evaluated with respect to SAR limits for RF exposure. The field distributions near the device are highly dependent on the location, orientation and electromagnetic characteristics of the antenna and adjacent objects. The user of a mobile handset is normally in the reactive near field region of the antenna where the most of the electromagnetic field is non-propagating. The energy absorbed by the user is mainly due to the electric fields induced by magnetic fields generated from current flowing along the antenna and other radiating structures of the device. The RF energy is scattered and attenuated as it propagates through the body

tissues[6]. Maximum energy absorption is usually expected in the more absorptive high water content tissues mainly near the surface of the head or body.

Most of the countries have developed regulations with exposure limit to an acceptable RF safety value via SAR levels to protect the public and workers from exposure to RF EM radiations. The International Commission on Non-Ionizing Radiation Protection (ICNIRP) was launched as an independent commission in May 1992. This group publishes guidelines and recommendations related to human RF exposure [1]. In August, 1996, the Federal Communications Commission (FCC) adopted a *Report and Order* in ET Docket 93-62 amending its rules for evaluating the environmental effects of Radio Frequency (RF) electromagnetic fields [7]. The FCC guidelines differentiate between portable and mobile devices according to their proximity to exposed persons. For portable devices (47 CFR §2.1093), [8] RF evaluation must be based on specific absorption rate (SAR) limits. Human exposure to RF emissions from mobile devices (47 CFR §2.1091)[8] can be evaluated with respect to Maximum Permissible Exposure (MPE) limits for field strength or power density or with respect to SAR limits, whichever is most appropriate. SAR evaluation must be performed using the guidelines and procedures prescribed by the applicable standard and regulation. The RF safety sections of the American National Standards Institute (ANSI), operates as part of the Institute of Electrical and Electronic Engineers (IEEE) has wrote the standard safety levels [9]. The European standard EN 50360 specifies the SAR limits [10] for exposure of the whole body, partial body (e.g., head and trunk), hands, feet, wrists, and ankles. SAR limits are based on whole-body exposure levels of 0.08 W/kg. Limits are less stringent for exposure to hands, wrists, feet, and ankles. For Europe, the SAR limit is 2 W/kg in 10g of tissue. For the United

States and a number of other countries, the limit is 1.6 W/kg for 1g volume, defined for a tissue volume in the shape of a cube. Canada, South Korea and Bolivia have adopted the U.S. limits of 1.6 W/kg for 1g volume averaged SAR. Australia, Japan and New Zealand have adopted 2 W/kg for 10g volume averaged SAR, as used in Europe[11]. Recently the Department of Telecommunication (DoT) of India put in place more stringent radiation norms from September 1, 2012 onwards. According to the new rules, SAR value of mobile handset has to follow the American SAR limits (1.6W/Kg over 1 gram of human tissue) rather than the current European norm that allows for a more lenient 2W/Kg over 10 grams of human tissue.

INCIRP (International Commission on Non-Ionizing Radiation Protection) guidelines [1] apply the same spatial peak SAR limits. For example, the SAR limit specified by IEEE C95.1:1999 is 1.6 W/kg in 1g averaging mass, while that specified in the ICNIRP guidelines is 2 W/kg in 10g averaging mass. Table 5.1 shows the recommended SAR limits for a non-occupational /uncontrolled environment set in different countries and regions.

Table 5.1. Recommended SAR limits for a non-occupational /uncontrolled environment set in different countries and regions.

	USA	Europe	Australia	Japan
Organization/Body	IEEE/ANSI/FCC	ICNIRP	ASA	TTC/MPTC
Measurement method	C95.1	EN50360	ARPANSA	ARIB
Whole body averaged SAR	0.08 W/kg	0.08 W/kg	0.08 W/kg	0.04 W/kg
Spatial-peak SAR in head	1.6 W/kg	2 W/kg	2 W/kg	2 W/kg
Averaging mass	1g	10g	10g	10g
Spatial-peak SAR in limbs	4 W/kg	4 W/kg	4 W/kg	4 W/kg
Averaging mass	10 g	10g	10 g	10 g
Averaging time	30 min	6 min	6 min	6 min

In Europe the ICNIRP recommendations are the most widely followed, while the slightly stricter standards set by IEEE are applied in the United States.

5.4 Tissue equivalent liquid parameters

Tissue equivalent liquids are used to simulate human tissues in phantom filled SAR measurement experiments. The RF energy absorption characteristic of body tissues is related to the tissue water content. High water-content tissues such as muscle and skin can absorb more RF energy than low water-content tissues such as fat, bone or skull. At RF and microwave frequencies, tissue properties are characterized by their permittivity and conductivity at normal body temperatures, about 37⁰C. There are several formulations for making high water content simulated tissues. An opaque gel consisting of water, salt, polyethylene powder and a gelling agent called TX-151 has been used for high power applications using thermographic or temperature methods to measure SAR [12]. A liquid mixture of water, sugar, salt and a compound called HEC (hydroxyethyl cellulose) is commonly used for measuring the SAR at low power transmitters [13]. The liquid is contained in a shell representing the head or body, typically molded from fiberglass or other plastic materials with very low RF absorption.

The tissue recipe reported in [14] is shown in Table 5.2 and used to simulate phantom fluid for the present study.

Table 5.2. Ingredients (% by weight) Head/Brain Body/Muscle

Ingredients (% by weight)	Head/Brain	Body/Muscle
Water	40.4	52.5
Salt (NaCl)	2.5	1.4
Sugar	56.0	45.0
HEC	1.0	1.0
Bactericide	0.1	0.1

The gel, specially developed for this work, is prepared by mixing 56% sugar, 40.1%water, 2.5%NaCl and 1% HEC (Hydroxyethyl cellulose, a gelling agent) to achieve the desired properties. The resulting product is very firm and transparent. The addition of bactericide (0.1%) to the gel allows for the preservation of it for weeks at room temperature. Tissue conductivity is directly associated to the EM wave energy dissipation in tissue. Tissue's dielectric properties change with microwave frequency. Permittivity and conductivity of body tissue depends on functional frequencies. Table 5.3 shows the permittivity and conductivity of tissue equivalent liquids as a function of frequency.

Table 5.3. Dielectric values for tissue equivalent liquids at specific frequencies

Frequency (MHz)	Conductivity(S/m)	Relative Permittivity
300	0.87	45.3
450	0.87	45.3
835	0.90	41.5
900	0.97	41.5
1450	1.20	40.5
1800	1.40	40.0
1900	1.40	40.0
2000	1.40	40.0
2450	1.80	39.2
3000	2.40	38.5

Required value of dielectric constant and conductivity at 1800MHz are given below.

Dielectric constant at 1800 MHz - 40.0

Conductivity at 1800 MHz - 1.4(S/m)

The dielectric constant of the above fluid was measured and found to be 39.4 with $\tan\delta$ 0.298 [15] at 1.8GHz. The experimental error was found to be less than 2% in case of permittivity.

5.5 Near field characteristic study of antennas

Since the antenna modeled is a mobile handset antenna, the near field characteristics are also studied. Near field radiation characteristics of different antennas and also with head model is investigated in this section. Simulations together with the experimental results are discussed.

5.5.1 Simulated near field radiation pattern of the proposed antenna

Simulation of the antennas on the near field have been carried out and their three dimensional patterns are discussed below. These simulated near field radiation pattern for different fabricated antennas are plotted for different distances at 1800MHz.

5.5.1.1 Simulated 3D near field radiation pattern of planar monopole antenna

Initially the normal planar monopole antenna is analysed and radiation patterns are shown in figure 5.1. The far field pattern (fig 5.1.(a)) and the near field patterns for different distances from the centre of the antenna (fig 5.1(b,c,d and e)) are shown for better understanding. In the far field the radiation pattern of normal monopole antenna is non-directional along H-plane and figure of eight pattern along the E-Plane. As the distance is reduced the angular field distribution is dependent upon the distance from the antenna and disturbed as in the figure 5.1. It is observed that, the near field radiation patterns of monopole antenna illuminate the nearby objects strongly along positive Y direction.

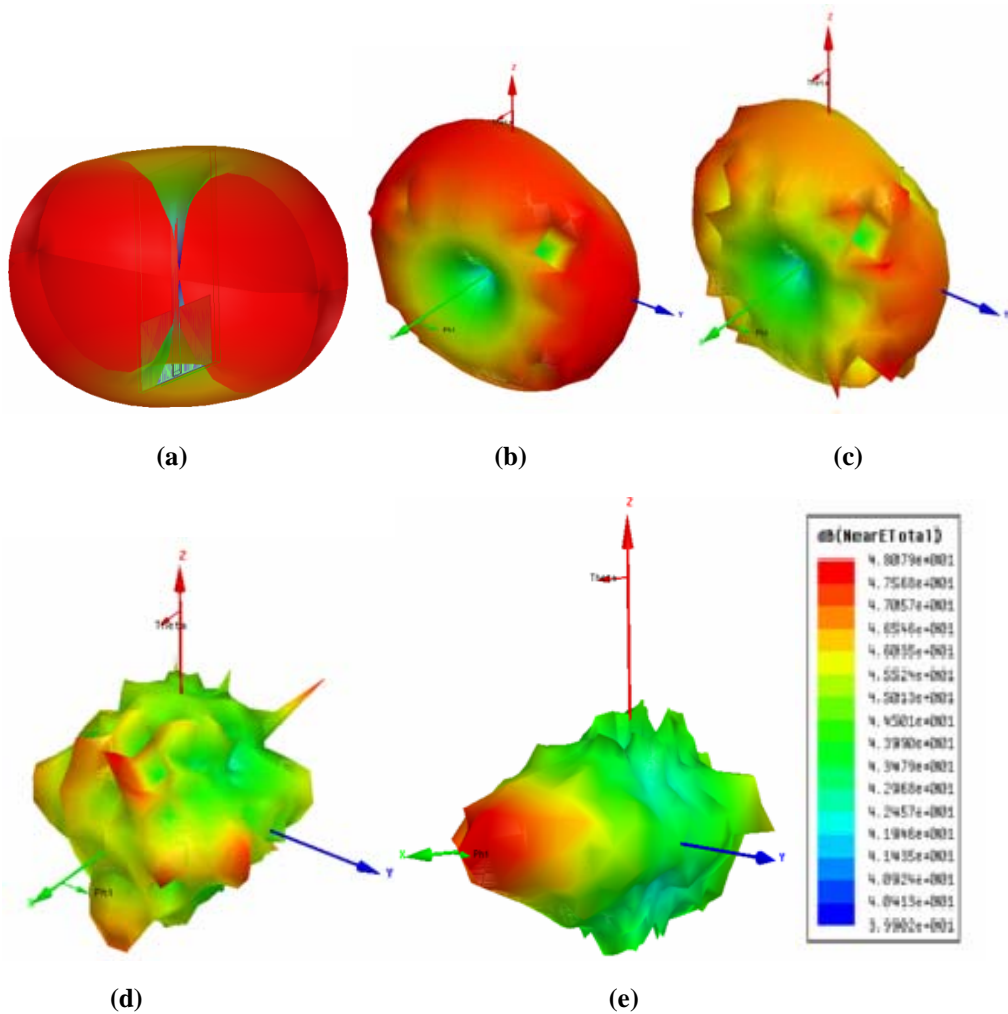


Fig 5.1. Simulated 3D radiation patterns of Monopole antenna (a) in far field region (b)50mm (c)40mm(d)30mm(e)20mm from center of the antenna

5.5.1.2 Simulated 3D near field radiation pattern of the SRR embedded antenna

The far field pattern and the near filed pattern with different reduced distance from the centre of the SRR loaded antenna are carried out and shown in figure 5.2 (b,c,d and e). This is used to study field distribution in the near field region of the antenna. Figure 5.2(a) shows the far field pattern of the SRR loaded antenna. It is observed that the pattern is still disturbed with reduced field strength along positive

Y direction, where the SRR structure is printed at the back side of the monopole antenna. It is also observed that the SRR repel the electromagnetic field and hence a null is observed in that direction. Almost the same characteristic is retained in the near field patterns also. This again confirms that the SRR can be conveniently used to reduce the strength of radiation. This reduction is nearly 7.76dBi. So the SRR backed antenna is providing less radiation along positive Y direction in the far field and near fields. This can reduce the overall SAR considerably.

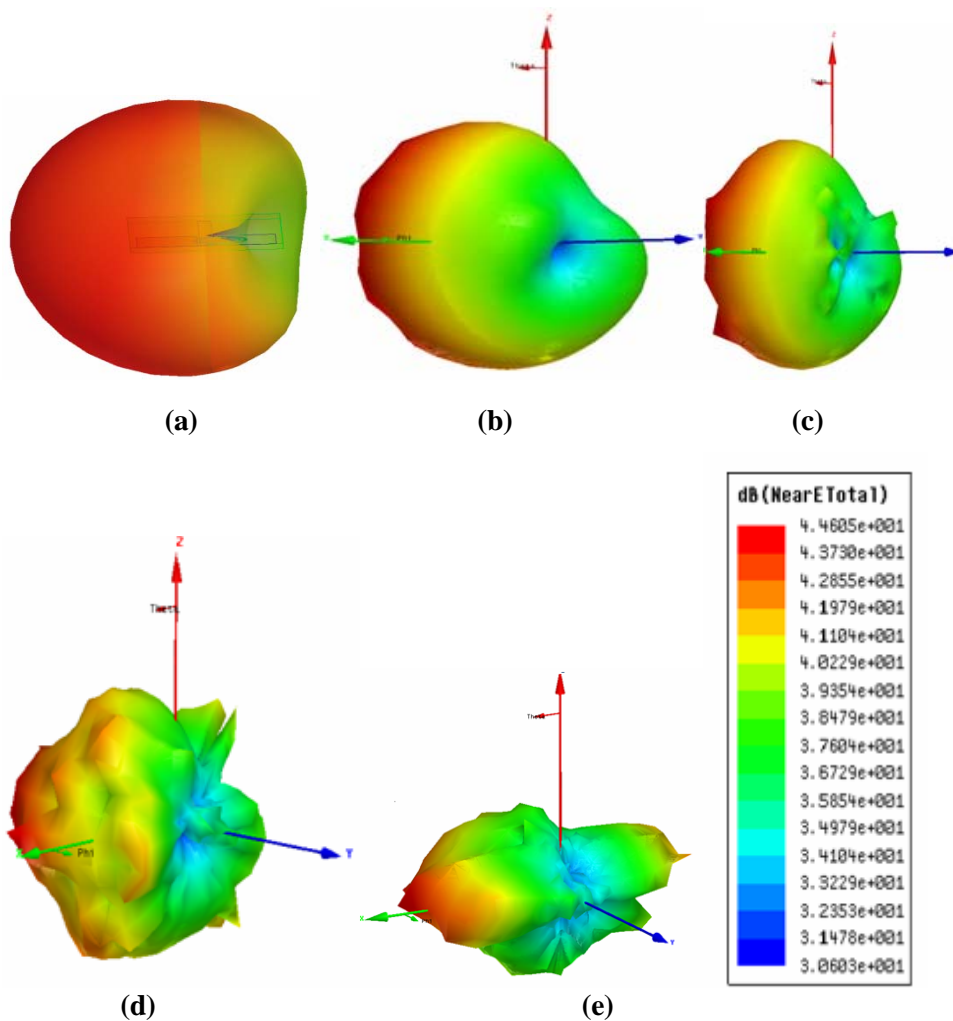


Fig 5.2. 3D radiation patterns of Monopole antenna with SRR (a) in far field (b)50mm (c) 40mm (d)30mm (e)20mm from center of the antenna

5.5.1.3 Simulated 3D near field radiation pattern of the Single strip embedded monopole antenna

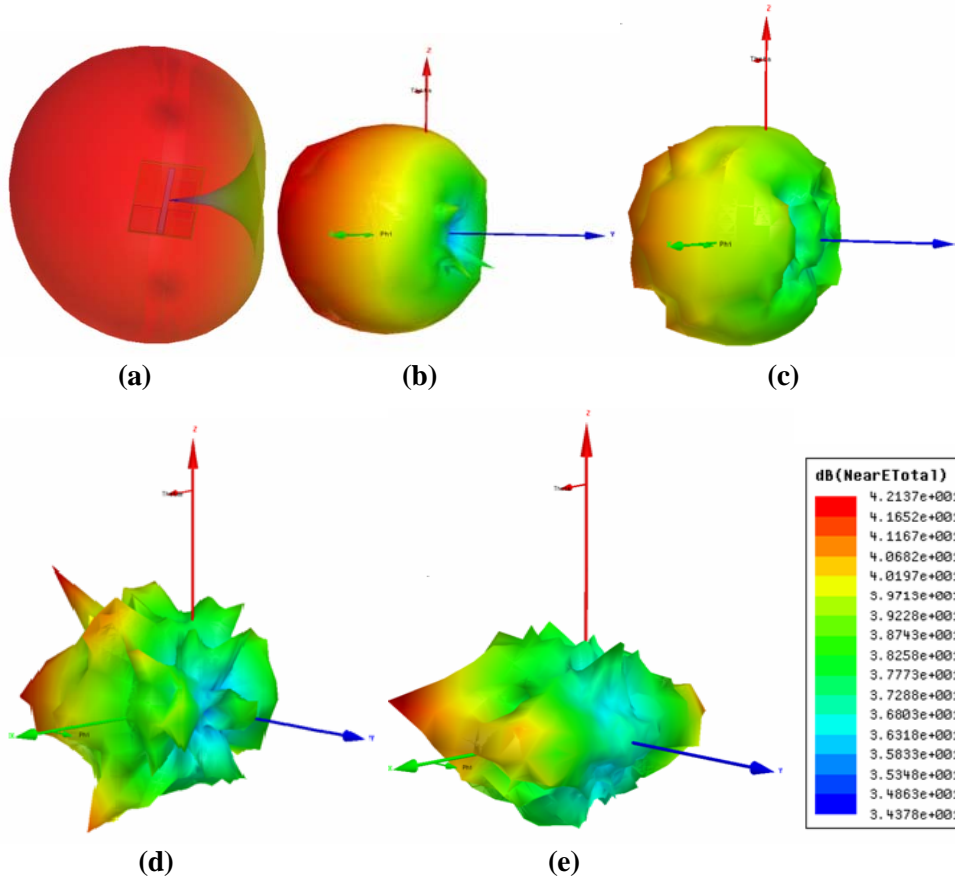


Fig. 5.3. 3D radiation patterns Monopole antenna with singlestrip (a)farfield (b)50mm (c)40mm (d) 30mm(e) 20mm from center of the antenna

The above observation of single strip antenna (figure 5.3) in the near field region, for decreasing distance reveals that the reduced radiation property along positive Y direction of the antenna in the far field is also valid in the near field region. A mobile handset with this type of antenna can reduce microwave radiation towards the user. Antenna with single strip at the back side reduces field strength of 7.759dBi towards the user.

5.5.1.4 Simulated 3D near field radiation pattern of the antenna with printed vertical stripes

Figure 5.4(a) shows the far field distribution of the monopole antenna with printed vertical stripes at the backside. Figure 5.4 (b,c,d, and e) shows the field distribution close to antenna for different distances, from the center. It is observed that field strength along the positive Y direction is very much less than other two cases. The field strength is reduced by 9.8dBi. Normally mobile handset operates with in this region.

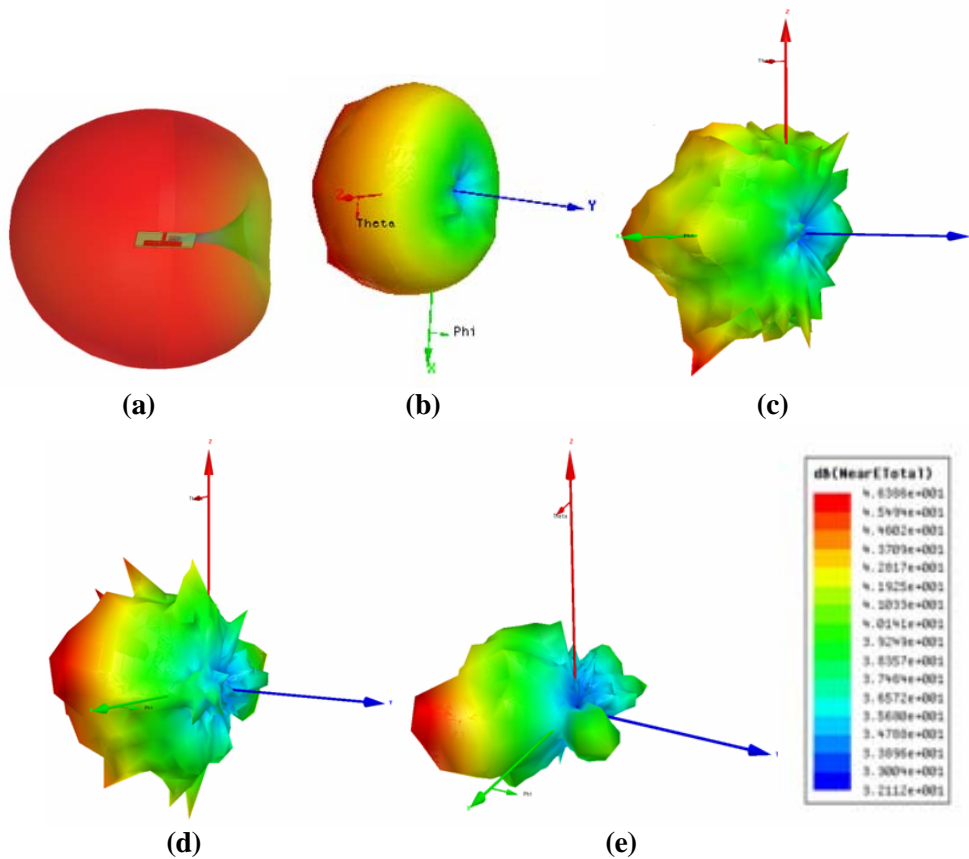


Fig. 5.4. 3D simulated radiation patterns of Monopole antenna with vertical stripes (a) in far field(b)50mm(c)40mm(d)30mm(e)20mm from center of the antenna

From the results shown in figures 5.2, 5.3 and 5.4 it can be concluded that the parasitic element has significant effect in the near field region of the

antenna. There will be reduced variation of field strength along positive Y direction due to this parasitic element.

5.5.1.5 Simulated 3D near field radiation pattern of the Ground Folded Monopole antenna

A ground folded monopole antenna resonate at 2340MHz have non-directional radiation pattern in H plane and directional pattern in E plane as shown in figure 5.5(a). The field patterns at different distances from the center of the antenna are shown in figure 5.5 (b) to (e).

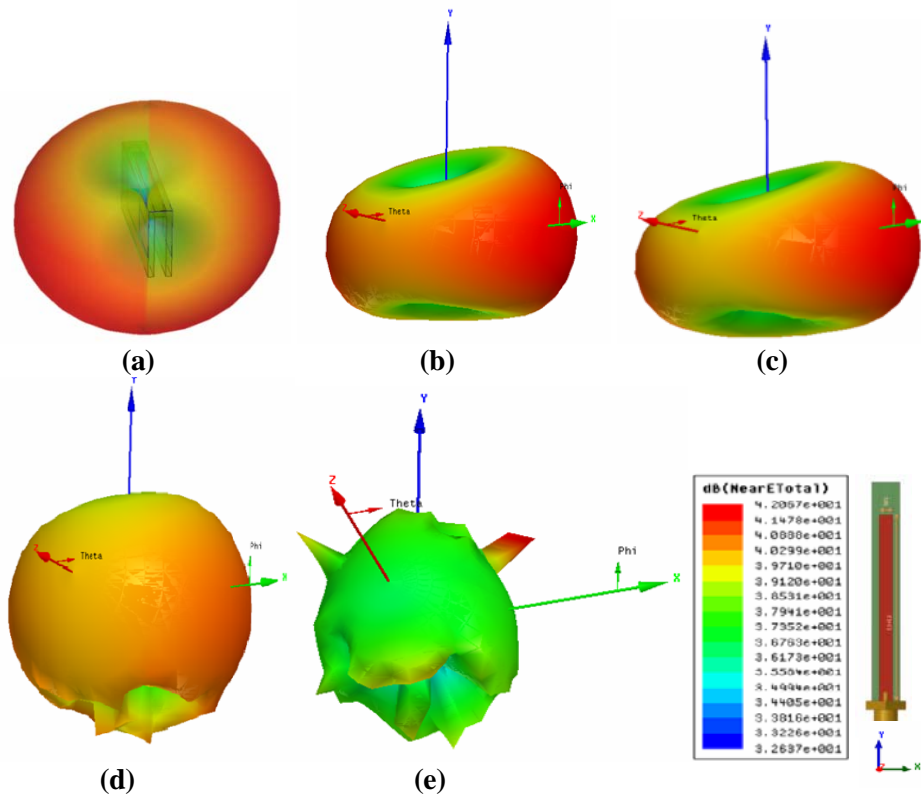


Fig. 5.5. Simulated 3D radiation patterns of Ground folded monopole antenna (a) farfield (b) 50mm (c) 40mm (d) 30mm (e) 20mm from center of the antenna

From the simulated results, it can be concluded that radiation properties in the near field region is similar to the far field properties of the antenna along positive and negative X axis. The maximum radiated electric field in the azimuth plane is nearly

42dBi. From the radiation patterns it is found that ground folded monopole can strongly illuminate the tissues.

5.5.1.6 Simulated 3D near field radiation pattern of the Ground Folded monopole with printed strip

The direction of reduced radiation in the far field is changed as shown in figure 5.6(a) along positive X axis, when the strip is internally printed. The resulting antenna resonates at 1810MHz and its near-field radiation patterns for distances from 50mm to 20mm from the center of the antenna are demonstrated in figures 5.6(b) to (e). It is observed that in the close region of the antenna the field is reduced along positive X direction by 6.434dBi.

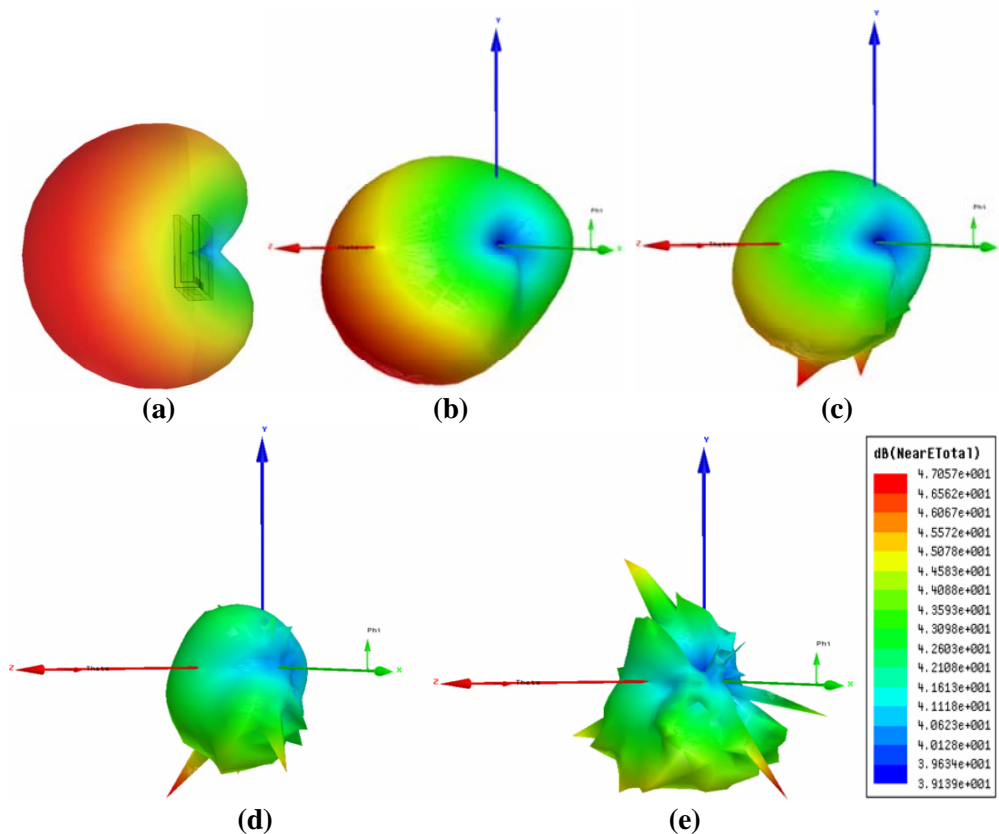


Fig. 5.6. 3D simulation of Ground folded Monopole antenna with single strip (a)farfield(b)50mm(c)40mm(d)30mm(e)20mm from center of the antenna

5.5.2 Simulated SAR value of proposed antennas with head model

The simplified physical model (phantom) of the human head specified in IEEE-Std. 1528 and IEC 62209-1 is the SAM (Specific Anthropomorphic Mannequin) phantom [16]. SAM has also been adopted by the European Committee for Electrotechnical Standardization (CENELEC), the Association of Radio Industries and Businesses in Japan, and the Federal Communications Commission (FCC) in USA. The SAM head model provided by CST microwave studio is used for the simulation in this thesis. The head model together with antenna is shown in figure 5.7. This SAM model offers clear reference lines such as the back–mouth and neck–front lines, that can be conveniently used for accurately positioning antenna device for simulation. Thus by keeping the head model as such and by changing the antenna we can compare the SAR values of different prototypes.

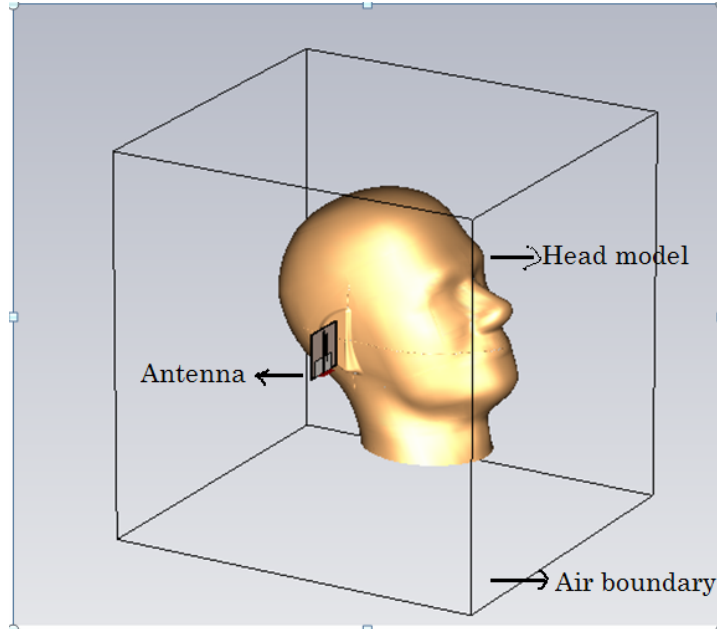


Fig. 5.7. SAM head model provided by CST microwave studio

The simulated SAR value of planar monopole antenna, antenna with single strip, antenna with vertical stripes, ground folded monopole and ground folded antenna with strip with head model are presented in the following sections.

5.5.2.1 Simulated SAR of planar monopole antenna, (Antenna1)

The fundamental quarter wavelength monopole antenna with omnidirectional radiation characteristics (uniform pattern along H-plane and figure of eight along E-Plane) is studied. The simulated electric field distribution of the monopole antenna with head model is shown in figure 5.8. But it is found that there is high radiation towards the head side. The omnidirectional pattern of the antenna is changed to a directional pattern with the introduction of head model.

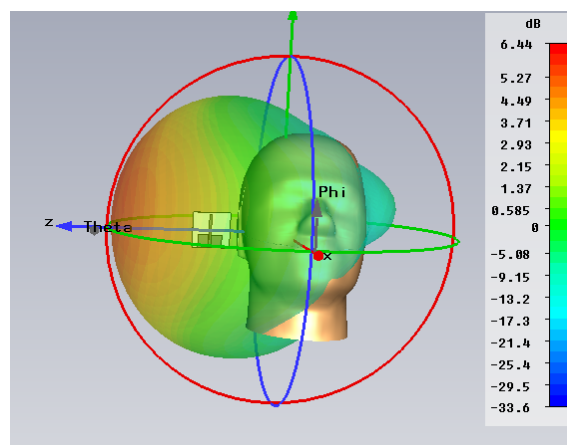


Fig 5.8 Simulated electric field distribution of the antenna with head model

The Specific Absorption Rate (SAR) due to this monopole antenna should be analysed with varying the distance between the antenna and head model. The variations of SAR with distance between head model and antenna are shown in figure 5.9 (a,b,c,d).

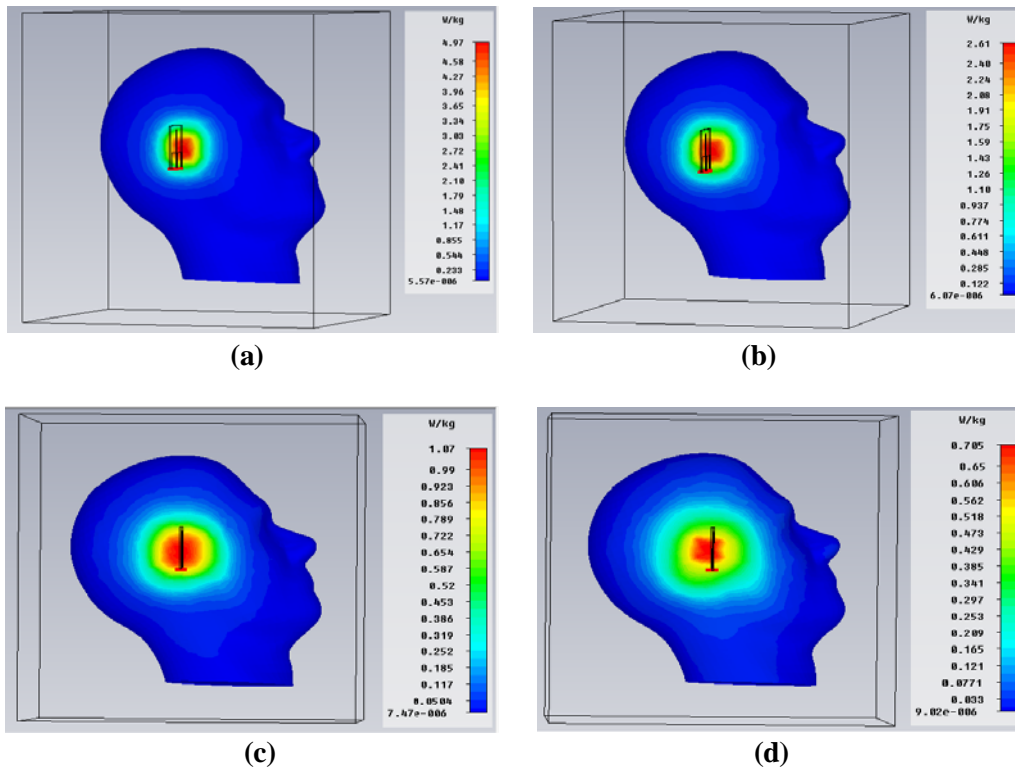


Fig.5.9. Simulated SAR with planar monopole structure for different distances (a)10mm(b)20mm(c)30mm(d)40mm

The simulated SAR on a phantom head model by keeping the planar monopole antenna (Antenna 1) at a distance of 10mm from the head model is shown in fig 5.9 (a). It is found from the SAR scale that the maximum SAR value observed is 4.97 W/kg for 1 gram of tissue. As the antenna is nearer to the head model the radiation covers a smaller area of human tissue. But when the distance is 40mm from the head, the SAR value is reduced to 0.705 W/kg. The SAR affecting area on the human tissue is more because antenna illumination area increases as distance increases. So there is an inverse relationship between the SAR value and radiation illuminating area.

5.5.2.2 Simulated SAR of antenna with SRR (Antenna 2)

The simulated electric field distribution of the antenna 2, when kept near the head model is analysed and is shown in figure 5.10. From the figure it is clear that the pattern is more directive on the side opposite to the head for the same input power. The electric field distribution is concentrated more in opposite direction of the head model for the same input power. Thus antenna 2 is radiating less towards the user head (negative Z-direction).

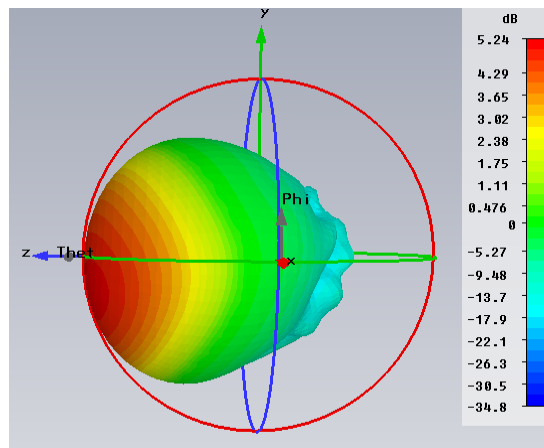


Fig. 5.10. Simulated electric field distribution of the SRR printed antenna with head model

The SAR value of antenna 2 is simulated with the head model by varying the distance from the head model. The distance is varied from 10mm to 40mm from the head model and is shown in fig 5.11(a) to (d). When the antenna is nearer to the head model (10mm from the head model) the simulated SAR value is 1.54 W/kg for 1gram of tissue and when the distance is 40mm from the head, the SAR value is reduced to 0.509 W/kg. The SAR value is decreased from 1.54 w/kg for 10mm to 0.509 W/kg for 40mm. Values are calculated for 1 gram of tissue.

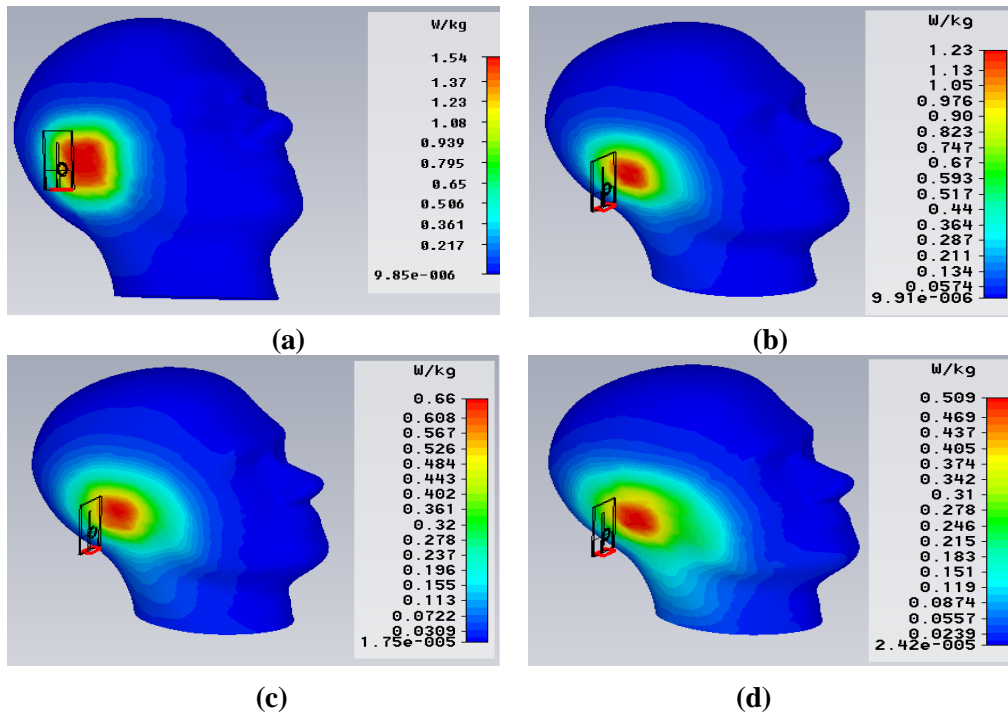


Fig 5.11. Simulated SAR with SRR structure for different distances (a) 10mm (b) 20mm(c)30mm(d)40mm

5.5.2.3 Simulated SAR value of antenna with Single strip (Antenna3)

Antenna 3 is simulated with head model to get the electric field distribution and is shown in figure 5.12.

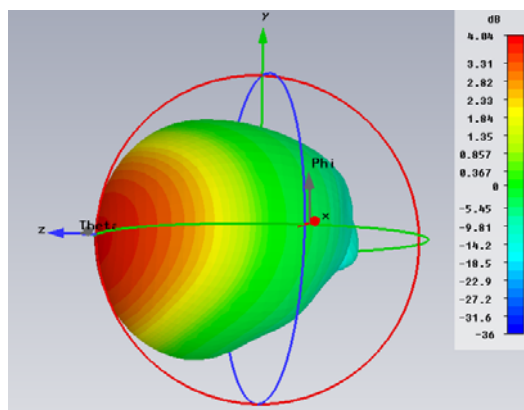


Fig. 5.12. Simulated electric field distribution of the antenna with single strip and head model

The pattern is more directive on the opposite side of the head model. The maximum electric distribution is found to be 4.04 dB, which is a smaller value compared with the other planar antennas.

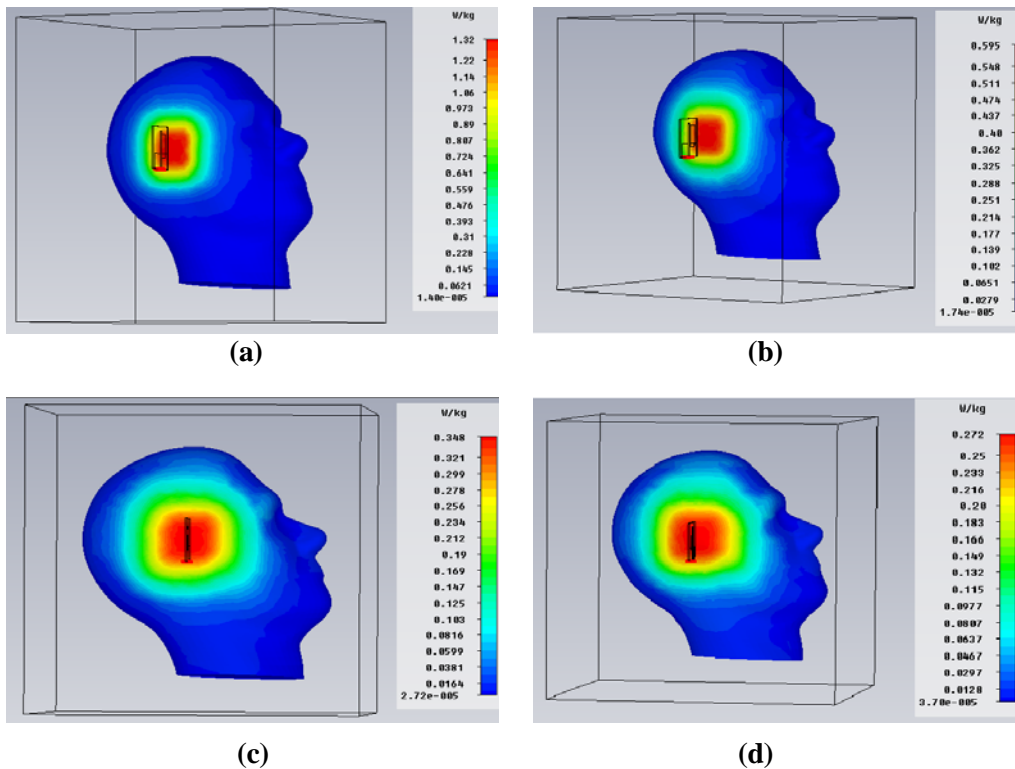


Fig. 5.13. Simulated SAR with single strip structure for different distances (b)10mm(c)20mm(d)30mm(e)40mm

The simulated SAR value of the antenna 3, when the antenna is 10mm from the head model is 1.32 W/kg for 1 gram of tissue. Simulated SAR of the antenna with increasing distance from the phantom head model are 0.595 W/kg, 0.348 W/kg, 0.272 W/kg for 20mm, 30mm and 40mm respectively are shown in figure 5.13(a) to(d).

5.5.2.4 Simulated SAR of antenna with vertical stripes (Antenna 4)

Simulated electric field distribution of the monopole antenna having modified radiation characteristics with printed stripes at the back side is shown in figure 5.14. From the figure it is observed that the field distribution is maximum in the Z direction than the opposite side where the head model is placed. The maximum electric field distribution is 5.4dB.

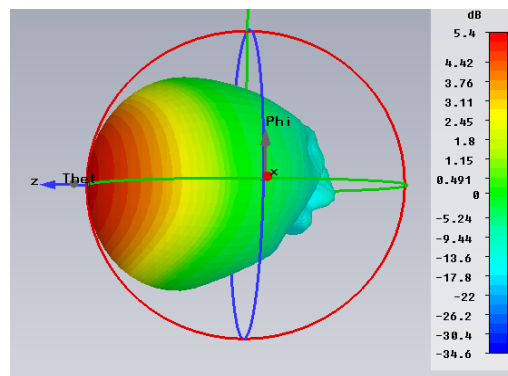


Fig. 5.14. Simulated electric field distribution of the vertical stripes printed antenna with head model

This antenna is also simulated with headmodel to calculate SAR value. The simulated SAR value with head model as shown in figure 5.15(a). This is the smallest SAR value among the different planar antennas mentioned. Its value is found to be 0.65 W/kg for a separation of 10mm distance. And this value decreases to 0.401W/kg,0.29W/kg and 0.235W/kg respectively for a separation of 20mm,30mm and 40mm as shown in figure 5.15(b),(c) and (d). The SAR is calculated for 1 gram of tissue.

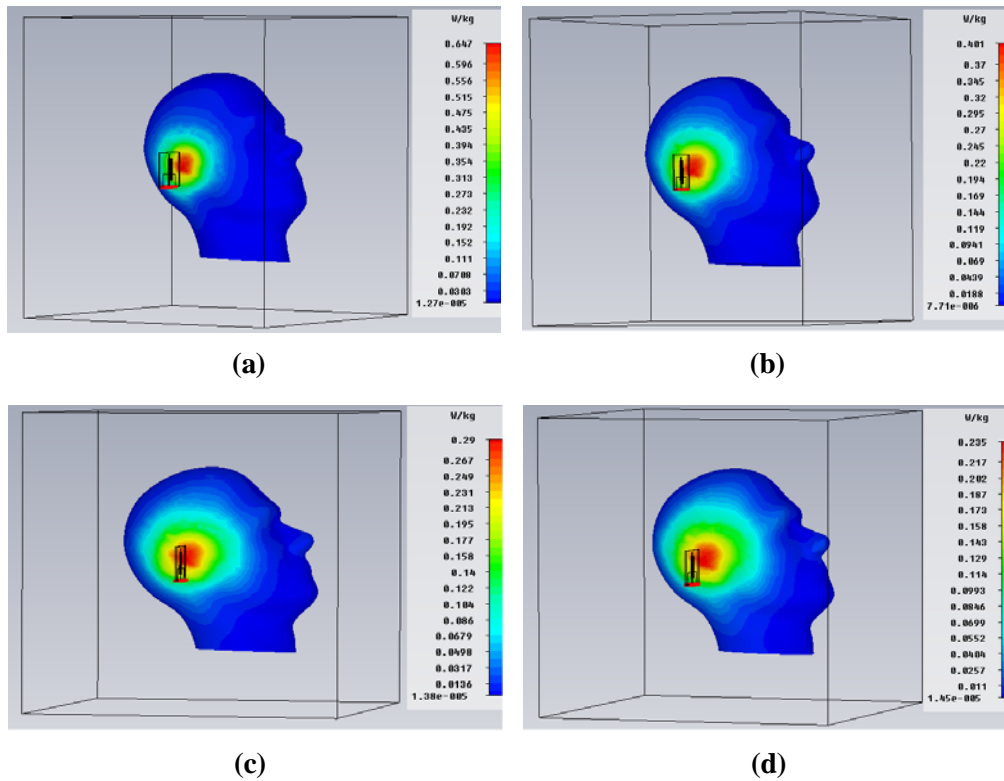


Fig.5.15. Simulated SAR with vertical stripes structure for different distances (a)10mm (b)20mm (c)30mm(d)40mm

5.5.2.5 Simulated SAR of Ground Folded Monopole antenna (Antenna 5)

Ground Folded monopole antenna with non-directional radiation characteristic in azimuth plane is considered in this section for SAR measurement. For a distance of 10mm from the antenna SAR value is found to be high (10.7W/kg). As the separating distances increases, the SAR value decreases from 10.7W/kg to 1.03 W/kg for 40mm separation is shown in figure 5.16(a) to (d).

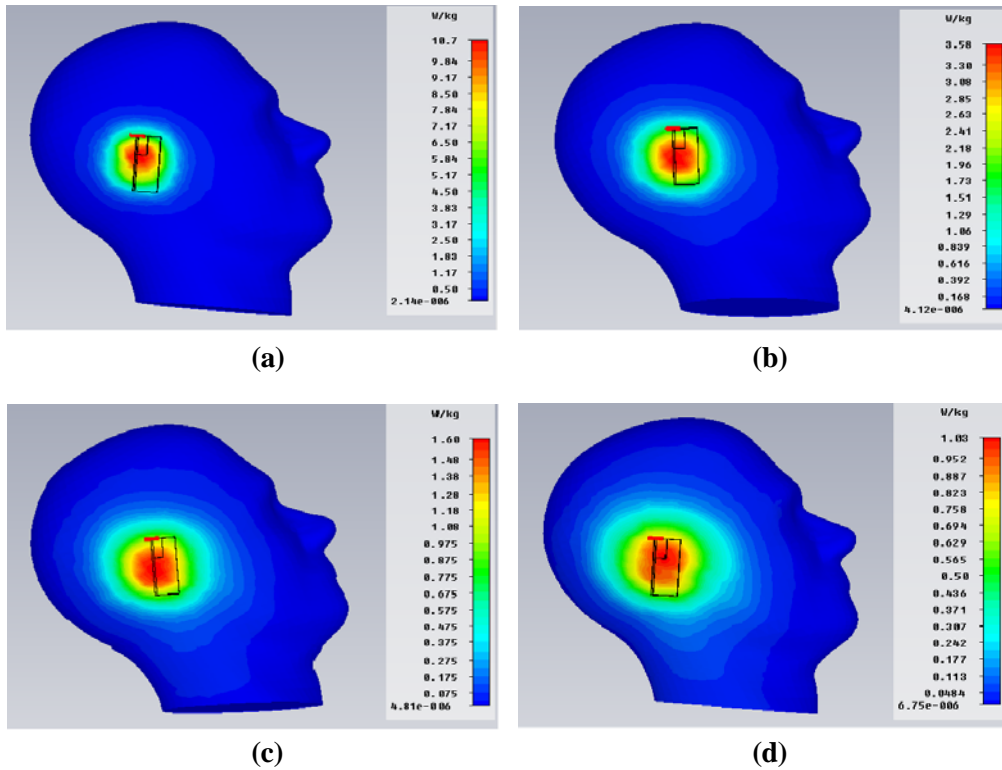


Fig 5.16. Simulated SAR with Ground Folded monopole structure for different distances (a)10mm (b) 20mm(c)30mm(d)40mm

5.5.2.6 Simulated SAR of Ground Folded Monopole antenna with vertical strip (Antenna 6)

The simulated electric field distribution of the folded antenna with reduced radiation towards the user is kept near the head model and is shown in figure 5.17. The electric field distribution is concentrated more in opposite direction of the head model for the same input power. Thus antenna 6 is more directive towards positive Z-direction.

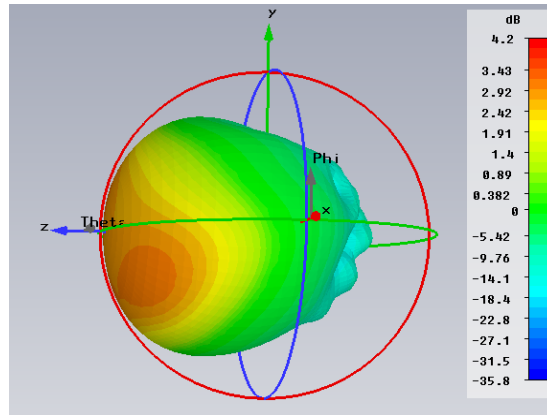


Fig. 5.17. simulated electric field distribution of ground folded monopole antenna with single strip and head model

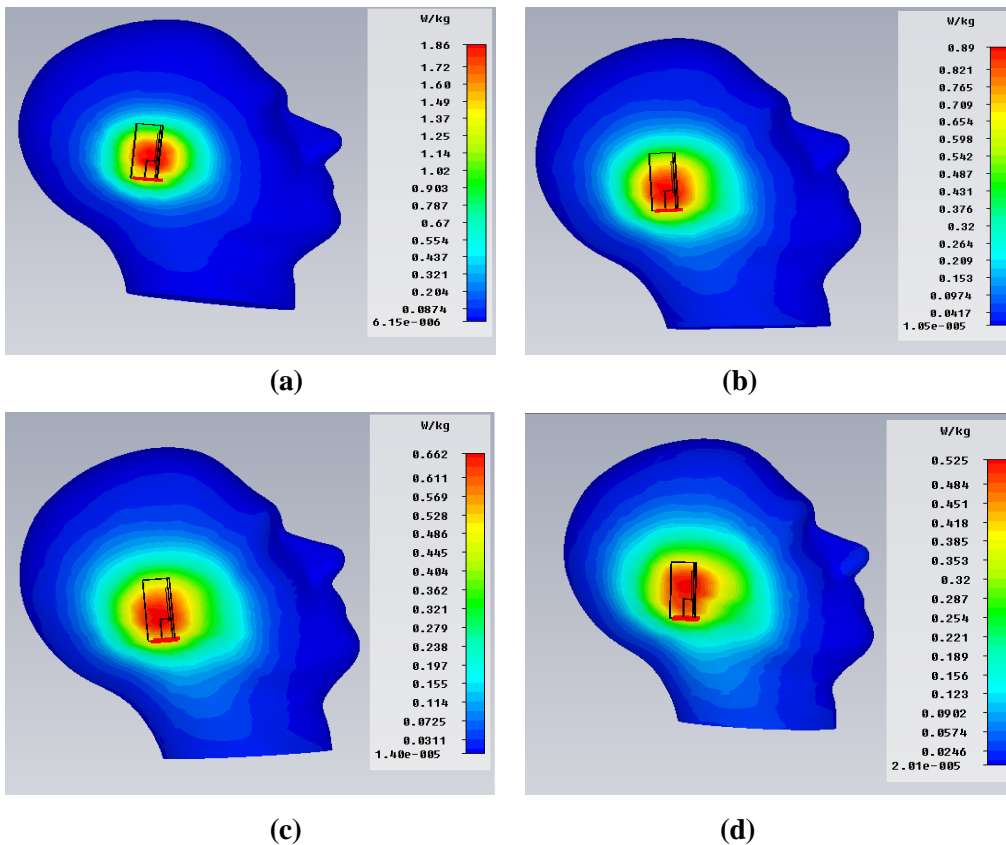


Fig. 5.18. simulated SAR with Ground Folded monopole structure with vertical strip for different distances(a)10mm (b) 20mm(c)30mm(d)40mm

Antenna 6 which is designed for mobile handset with less radiation interference towards the user side is simulated with head model to measure SAR value. The power absorbed by the head model by this antenna is studied by varying the separation between the antenna and the head model. For the shortest distance of 10mm separation the simulated SAR value is 1.86W/kg and it reduces drastically to 0.89W/kg for a distance of 20mm etc. For a distance of 30mm and 40mm it reduces to 0.66W/kg and 0.53W/kg respectively as shown in figure 5.18 (a) to (d).

Simulated SAR values of the proposed antennas are compared with monopole antenna of same dimension is shown in Table 5.4.

Table 5.4. Simulated SAR value of the antenna with various distances from the head model.

Distance from phantom side to antenna	SAR W/kg (1 gm) Planar monopole with SRR (Antenna2)	SAR W/kg (1 gm) Planar monopole (Antenna1)	SAR W/kg (1 gm) Planar monopole with single strip (Antenna3)	SAR W/kg(1 gm) Planar monopole with parallel stripes(Antenna4)	SAR W/kg(1 gm) GroundFolded monopole (Antenna5)	SAR W/kg(1 gm) GroundFolded monopole with metal strip(Antenna6)
10mm	1.54	4.97	1.32	0.647	10.7	1.86
20mm	1.23	2.616	0.595	0.401	3.58	0.89
30mm	0.66	1.074	0.348	0.29	1.68	0.662
40mm	0.509	0.705	0.272	0.235	1.03	0.525

It is observed that SAR [17] value decreases with distances for the proposed antennas. SAR value is very less than recommended value for antenna

2, 3 and 4, even for a distance of 10mm. Antenna 4 has SAR value reduction of 47.38% for a distance of 40mm and for antenna 6 it is 53.8% for the same distance.

5.6 Experimental result in the Near Field Phantom

The principle of the near field SAR measurement technique is to measure the electric field on a planar surface in XY plane inside the phantom, and to reconstruct the electric field in the phantom. An inherent and unavoidable limitation of this procedure is that the probe antenna must be very small for high resolution measurements. Field readings in the measurements are relative rather than absolute. The probe antenna consists of a coaxial cable with 3 mm of the center conductor extended beyond the outer conductor. The probe can only measure the phase and amplitude of a single polarization of the electric field. The squared magnitudes of all electric field polarizations are summed to determine the relative power pattern in the phantom.

Initially a minimum distance of 10mm between the probe and the phantom model wall has been maintained. After it scans in the XY plane, the Z location is increased by 1cm and the scan process is repeated in the next XY plane. The figures below plotted show the variation in the E field distribution within the phantom with increased distance in Z axis. Experimental results for a planar antenna with and without vertical stripes and ground folded antenna with and without vertical strip are shown in the figures 5.19 and 5.20 respectively

Figure 5.19(a) show the radial E field variation of planar monopole antenna for increasing distance from phantom head model edge. The E field plot of planar monopole antenna with 10mm, 20mm, 30mm, 40mm, 50mm

distances from phantom shell edge indicates that the field strength value decreases as the scanning plane moves from the radiating antenna.

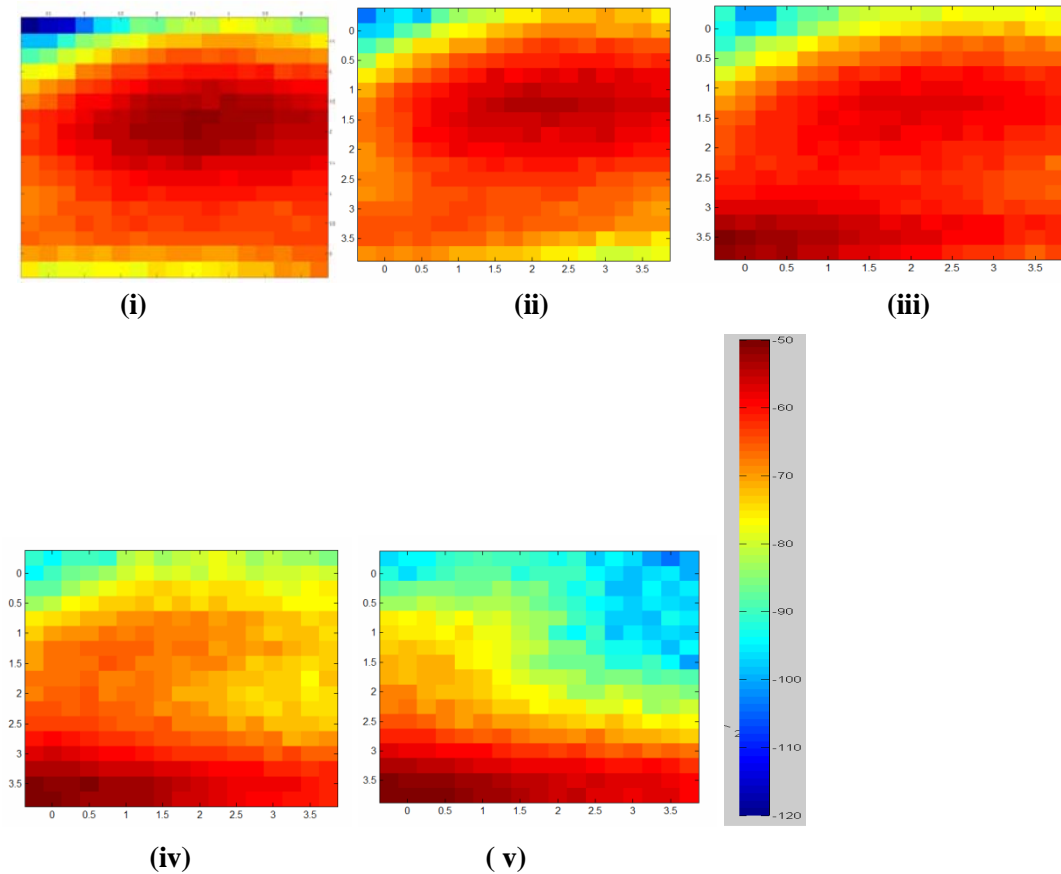


Fig. 5.19.(a) Radial variation in E field distribution of planar monopole antenna for different distances from phantom head model edge (i)10mm (ii)20mm (iii)30mm(iv)40mm(v)50mm

E field distribution of planar monopole antenna with vertical stripes from the phantom head model edge is shown in figure 5.19(b).

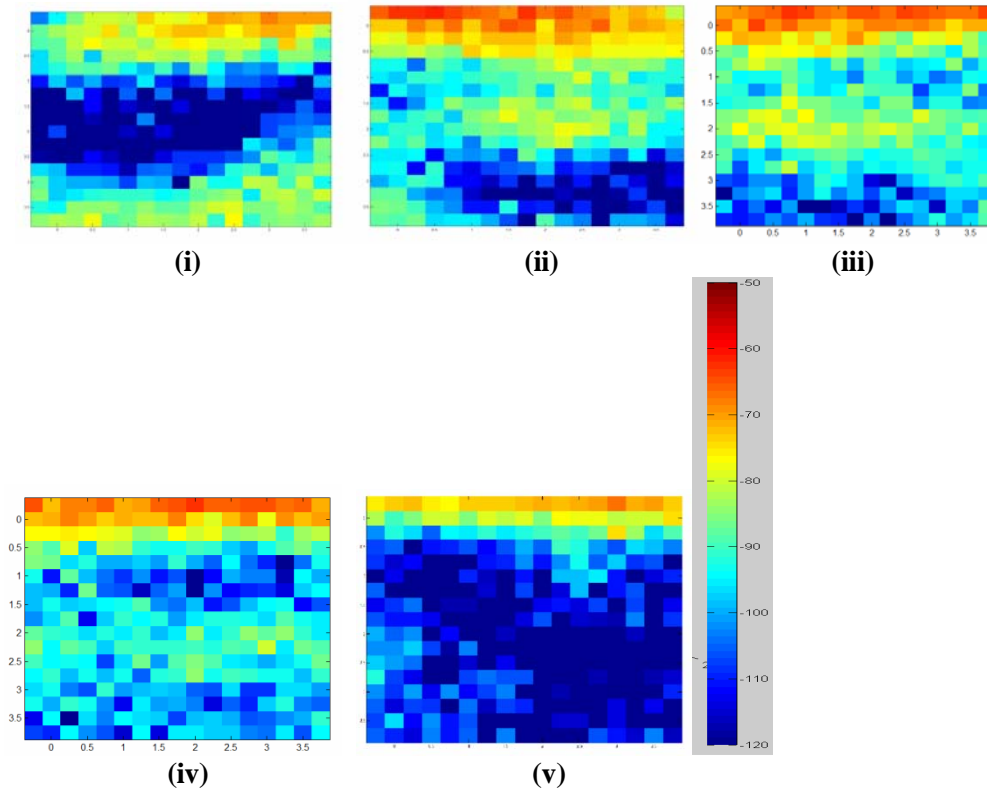


Fig. 5.19.(b) Radial variation in E field distribution of planar monopole antenna with vertical stripes for different distances from phantom head model edge (i)10mm(ii)20mm(iii)30mm(iv)40mm(v)50mm

Fig 5.20(a) represents variation in E field distribution of Ground Folded monopole antenna from the head model edge. E field plot in XY plane for increasing distance of 10mm, 20mm, 30mm, 40mm and 50mm from the head model edge indicates that field decreases with increasing distance.

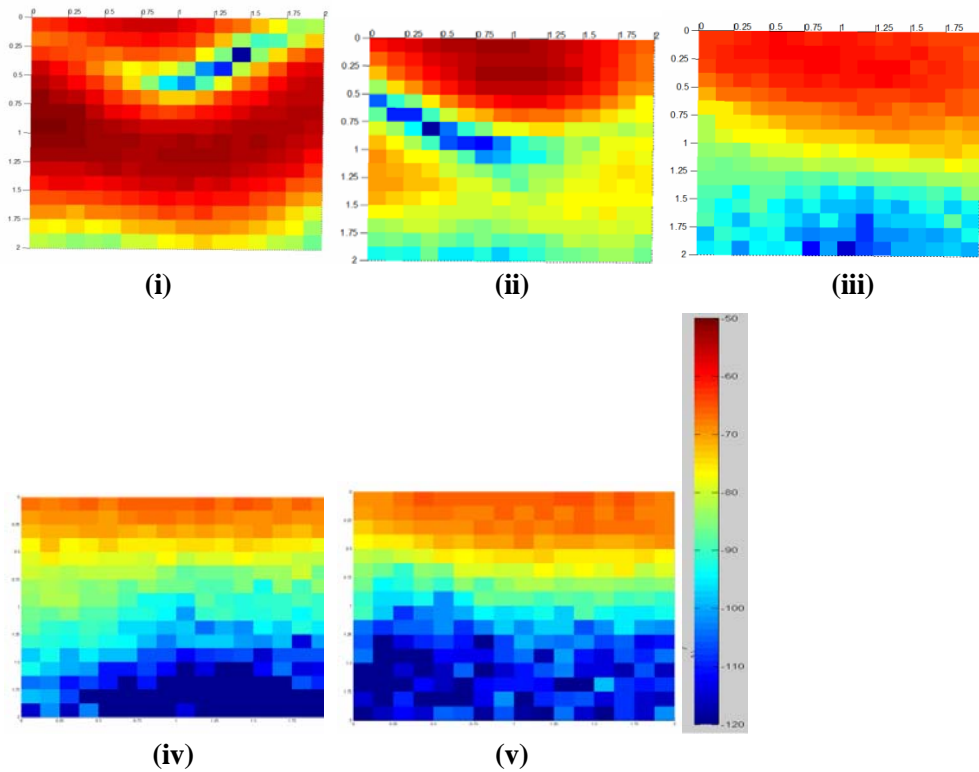


Fig. 5.20. (a) Radial variation in E field distribution of Ground folded monopole antenna for different distances from phantom head model edge (i)10mm (ii)20mm(iii)30mm(iv)40mm(v)50mm

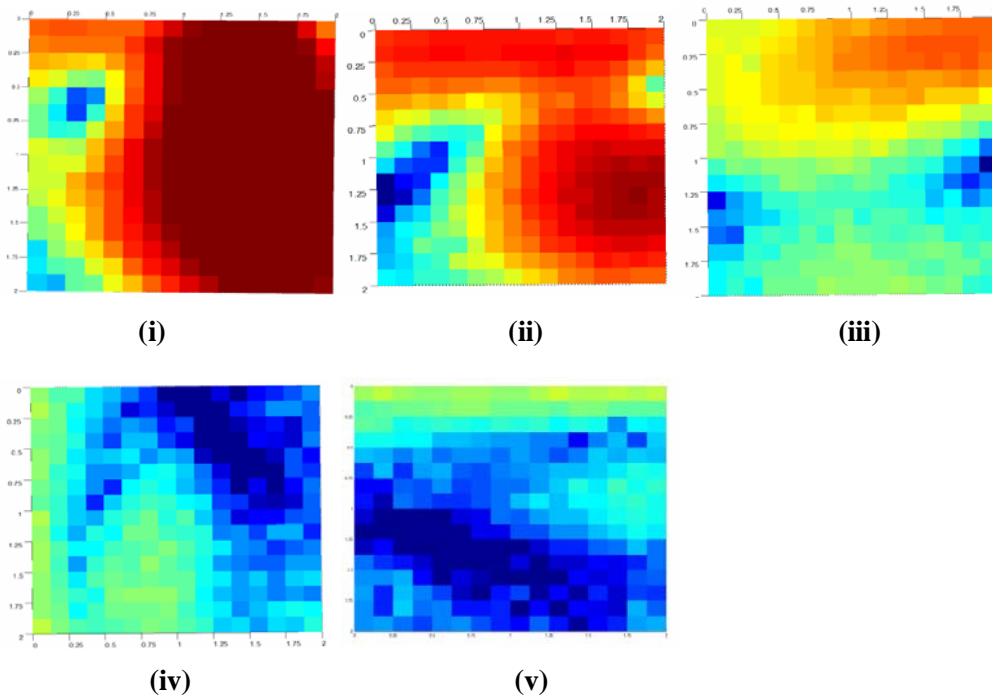


Fig.5.20. (b) Radial variation in E field distribution of Ground folded monopole antenna with strip for different distances from phantom head model edge (i)10mm(ii)20mm(iii)30mm(iv)40mm(v)50mm

E field distribution of ground folded monopole antenna with vertical strip from the phantom head model edge is shown in figure 5.20(b).

SAR measurements based on the effects of the E-field are not absolutely accurate because input power given through network analyser (HP8510c) is in the order of 1mw. So the normalized SAR plot is shown in figure 5.21 (a) and (b) respectively for planar monopole and Ground folded monopole antenna for comparison with stripes. It is clear from the figure that for both the cases the SAR is very much reduced with strip backed antenna. It is very interesting to note that in the case of folded dipole the SAR is very much reduced compared to a planar monopole with strip.

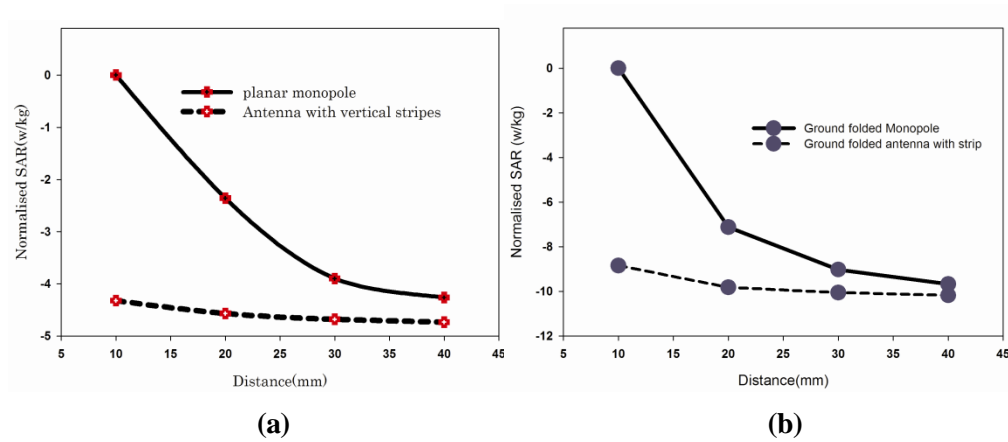


Fig 5.21. (a)Radial variation in normalized SAR value of planar monopole antenna with and without vertical stripes (b)) Radial variation in normalized SAR value of Ground folded monopole antenna with and without strip

5.7 Chapter conclusion

This chapter presented an overview for the standards, exposure limits, and testing procedures for the calculation of SAR and the experimental and simulated methods for the evaluation of SAR. It is concluded that a strip backed ground folded monopole can reduce the SAR considerably.

References

- [1] International Commission on Non-Ionizing Radiation Protection (ICNIRP), “Guidelines for limiting exposure to time-varying electric, magnetic, and electromagnetic fields (up to 300 GHz)”, *Health Physics*, Vol. 74, No. 4, pp. 494-522, April 1998.
- [2] Cleary,S.F., "Microwave Radiation Effects on Humans," *Bio Science*, 33(4): 269 (1983).
- [3] J. D. Hardy, “The nature of pain,” *J. Chronic Dis.*, vol. 4, no. 22, 1956.
- [4] Zhao Wang “Electromagnetic Field Interaction with Biological Tissues and Cells”Ph.D Thesis School of Electronic Engineering and Computer Science,Queen Mary, University of London April, 2009
- [5] C95.3-1991-IEEE Recommended Practice for the Measurement of Potentially Hazardous Electromagnetic Fields□RF and Microwave 1992
- [6] Biological effects of radio frequency radiation united states environmental protection agency September 1984 report.
- [7] Federal Communications Commission Office of Engineering &Technology” Evaluating Compliance with FCC Guidelines for Human Exposure to Radiofrequency Electromagnetic Fields”
- [8] Title 47-telecommunication “Radiofrequency radiation exposure evaluation: mobile devices and portable devices.” volume 1, 2008
- [9] IEEE standard for safety levels with respect to human exposure to radio frequency electromagnetic fields 3KHz to 300GHz,1999 edition
- [10] EN 50360, “Product Standard to Demonstrate the Compliance of Mobile Phones with the Basic Restrictions Related to Human Exposure to Electromagnetic Fields (300 MHz3GHz),” CENELEC, 2001.

- [11] EN 50361, “Basic Standard for the Measurement of Specific Absorption Rate Related to Exposure to Electromagnetic Fields from Mobile Phones (300 MHz-3 GHz),” European Committee for Electrical Standardization (CENELEC), Brussels, 2001.
- [12] IEEE Standard C95.3, Guidelines for Limiting Exposure to Time-Varying Electric, Magnetic, and Electromagnetic Fields (up to 300 GHz), 2002.
- [13] K. Fukunaga, S. Watanabe, and Y. Yamanaka “Dielectric Properties of Tissue-Equivalent Liquids and their Effects on Specific Absorption Rate” IEEE Transactions on Electromagnetic Compatibility, vol.46, no1, pp. 126-129, February 2004.
- [14] Hartsgrove “Simulated Biological Materials for Electromagnetic Radiation absorption Studies,” Bioelectromagnetics 8:29-36,1987.
- [15] G. T. Fallenstein, V. D. Hulce and J. W. Melvin “Dynamic Mechanical Properties of human brain tissue” J. Biomechanics. Vol. 2, Pergamon Press, pp. 217-226, 1969
- [16] B. B. Beard, W. Kainz, T. Onishi, et al., “Comparisons of computed mobile phone induced SAR in the SAM phantom to that in anatomically correct models of the human head,” IEEE International Journal of Antennas and Propagation Transaction on Electromagnetic Compatibility, vol. 48, no. 2, pp. 397–407, 2006
- [17] J.C. Lin, Specific Absorption Rates (SARs) Induced in Head Tissue by Microwave Radiation from Cell Phones, IEEE Ant. Propagat. Mag., vol. 42, No. 5, pp. 138, Oct. 2000

.....✂.....

CONCLUSION AND FUTURE PERSPECTIVE

<i>C</i> <i>o</i> <i>n</i> <i>t</i> <i>e</i> <i>n</i> <i>t</i> <i>s</i>	6.1	<i>Thesis Highlights</i>
	6.2	<i>Inferences from the analysis of planar CPW fed monopole antenna and CPW fed monopole antenna with a parasitic element for reduced RF interference towards user</i>
	6.3	<i>Inferences from the Ground Folded monopole antenna</i>
	6.4	<i>Inferences from the near field study of antenna with modified radiation pattern</i>
	6.5	<i>Comparison of Different antennas presented in this thesis.</i>
	6.6	<i>Suggestions for future work</i>

This Chapter gives the highlights of the thesis along with major conclusions derived from the simulation and experimental analysis carried out in the previous chapters. Mobile antennas with reduced RF interference towards the user have been developed. This is achieved by modifying the radiation characteristics of a planar CPW fed monopole antenna and ground folded monopole antenna. Suggestions for the future work in this field are also included in this chapter.

6.1 Thesis Highlights

This chapter brings the thesis to a close by summarizing the results obtained from simulation and experimental investigations conducted on a modified planar and ground folded monopole antenna that can be used for mobile applications. The main objective of the thesis is to develop an antenna for mobile handset with reduced RF interference towards the user. This is achieved by altering the radiation characteristics of the antenna by modifying its geometry.

Overviews of Electromagnetic spectrum, the different energy radiations in the spectrum, introduction to mobile antenna research, different antenna analysis techniques and the motivation of the present work are summarised in chapter 1. Chapter 2 provides the details of antenna fabrication and measurement techniques and thorough review of CoPlanar Waveguide fed monopole antenna which is used as the basic antenna for further studies followed with review of mobile antenna with reduced SAR.

Chapter 3 starts with the study of the characteristics features of the CoPlanar Waveguide fed monopole antenna. Antenna with modified radiation characteristics using printed parasitic element for mobile application is introduced in that chapter. Chapter 4 describes the radiation characteristics of a ground folded monopole antenna. This single band antenna operates with a suitable radiation pattern for mobile hand set. It is found that this antenna is radiating all the three quadrants effectively with a null in the fourth quadrant. The near field radiation characteristics of these antennas are described in chapter 5. Appendix A of the thesis presents a Compact Asymmetric Coplanar Strip (ACS) fed antenna for wideband applications and Appendix B describes

Compact Complementary Split Ring Resonator (CSRR) based patch antenna for wireless applications.

6.2 Inferences from the analysis of planar CPW fed monopole antenna and CPW fed monopole antenna with a parasitic element for reduced RF interference towards user

The omni directional radiation characteristic of the CPW fed monopole antenna is modified with single null by a parasitic element printed at back side with indirect coupling. Studies are conducted to change the radiation characteristic of the monopole antenna with high impedance resonating structures like split ring resonator, single metal strip and with vertical stripes. All the antennas can be operated at 1800MHz GSM band with reduced RF interference towards the user.

The inferences after analysing the planar CPW fed printed monopole antenna are as follows

- The finite ground CPW fed planar monopole antenna provides a resonance at 2.3 GHz with an impedance bandwidth from 1.98 GHz to 2.58 GHz.
- The CPW fed monopole antenna exhibits a figure of eight pattern in the E plane and a non-directional pattern in the H plane.
- The antenna provides a moderate gain greater than 1dBi throughout the operating band. The maximum gain observed is 1.7dBi at 2.43GHz with an average gain of 1.4dBi.

The major inferences from the studies of CPW fed monopole antennas with resonating element printed at the back are as follows.

- The radiation characteristics of CPW fed monopole antenna can be modified by a pattern suitable for mobile handset with SRR unit structure, single strip and parallel vertical stripes.
- The proposed single band antenna operates at GSM 1800 MHz band.
- Modification of the radiation characteristics of monopole antenna depends on relative position of SRR or vertical stripes with respect to the ground plane of the monopole antenna.
- The fringing field between the monopole and any of the lateral ground plane is affected by adding these structures, as a result the electric field gets redistributed giving a null along positive Y direction and filling the original two nulls of the conventional monopole.

6.3 Inferences from the Ground Folded monopole antenna

A printed monopole antenna is suitably folded to make a low profile, small size folded antenna. The proposed 3D structure of ground folded monopole antenna has non directional radiation characteristic in azimuth plane. To modify the radiation characteristics of the folded monopole antenna a single vertical strip is printed at the back side of the ground plane. Thus a novel compact folded antenna is derived with single null in radiation pattern suitable for mobile applications. To develop and to study the characteristics of that antenna, studies were conducted from the open ended coplanar waveguide transmission line and the inferences from the study are:

- Open ended ground plane folded modified CPW transmission line will also provide similar characteristics.

- A ground folded monopole antenna resonating at the same frequency of planar monopole antenna mentioned in the third chapter is developed using this concept.
- Modification in the direction of the ground plane of the antenna can change the direction of reduced radiation pattern.
- Folding technique effectively makes the antenna more compact and highly suitable for slim mobile handset with reduced RF interaction.
- The introduction of printed strip will generate a lower resonance at GSM band with modified radiation patterns.

6.4 Inferences from the near field study of antenna with modified radiation pattern

Antennas are simulated in the near field region to study the field distribution near the antenna. Experimental setup using CREMA software to measure normalized SAR are discussed in this chapter.

- Antennas are simulated with SAM phantom model to estimate specific absorption rate (SAR).
- The SAR value is found to be drastically reduced by printing SRR structure, single or vertical stripes at the back of the monopole antenna at the optimum position below the ground plane.

6.5 Comparison of Different antennas presented in this thesis

The radiation characteristics of CPW fed printed monopole antenna has been modified by adding a printed parasitic element which has a coupling to the ground plane. The resultant single band antenna has been analyzed. For further compactness and to change the null direction of radiation, folding study has

been conducted. Performance comparisons of different antennas are summarized in Table 6.1.

Table 6.1. Performance comparisons of different antennas

Antenna	Resonant Frequency	Frequency band(GHz) Bandwidth(MHz) % BW	Average gain	Reduced power in azimuth plane(simulation)	Volume(mm ³) Substrate height h=1.6mm	Simulated SAR Value(1gm) (W/kg)
Printed monopole	2.3	1.98-2.58 600 26%	1.4dBi	Non directional	42X31.7	4.97
Printed monopole with SRR	1.82	1.75-1.91 160 8.7%	1.2dBi	18dB	42X31.7	1.54
Printed monopole with single strip	1.81	1.76-1.99 230 12.26%	1.12 dBi	20dB	42X31.7	1.32
Printed monopole with vertical stripes	1.8	1.76-1.96 200 10.75%	1.14 dBi	23dB	42X31.7	0.647
Folded monopole antenna	2.34	1.99-2.92 930 44%	3.75dBi	Non directional	42X14X6.4	10.706
Folded monopole antenna with vertical strip	1.81	1.68-1.92 240 13%	1.43dBi	12dB	42X9.5X6.4	1.86

From the above study it is found that folded monopole antenna with vertical strip on the ground plane will provide all the desirable radiation characteristics suitable for a mobile handset.

6.6 Suggestions for future work

In the present work single resonance antenna working in the GSM band with a radiation characteristic suitable for a mobile handset has been explained. The radiation characteristic of a CPW fed monopole antenna in the azimuth plane has been modified to a pattern with single null towards the user. It is also observed that the printed parasitic element on the other side shifts the frequency to the lower side.

In this work, antenna operating in a single band is discussed. Future studies can be carried out to achieve dual band or multiband antenna with similar radiation characteristics, by properly modifying the basic antenna and the parasitic structure. Studies can be extended to reduce the dimension of the antenna to make it more compact. This can be tried out by using micro wave passive elements. The antenna size can be further reduced by using zeroth order antennas. It may be very useful to use extremely compact zeroth order antenna with reduced radiation towards the head. Multiband zeroth order antenna can also be explored. The possibility of achieving reduced radiation towards the user using coplanar structure using other high impedance surface can also result interesting results.

The reconfigurability is a demanding antenna quality. Modification in the design can be done to achieve radiation and frequency reconfigurable antenna.

The antenna can be designed on Low Temperature Low Loss Cofired Ceramic (LTCC) substrates in future, which have the advantage of direct integration with monolithic micro wave circuits.

Active antenna can be implemented using coplanar antenna concept. Transistors, diodes, MOSFETs etc. can be integrated on the antenna element for amplification, oscillation etc.



APPENDICES

Appendix -1

COMPACT ASYMMETRIC COPLANAR STRIP FED ANTENNA FOR WIDE BAND APPLICATIONS

1. Introduction

The demand for wideband antennas has experienced a booming growth in the wireless industry. Several interesting designs of wide band antennas have been demonstrated recently. A resonant aperture with stacked patches of different dielectric constants is employed for bandwidth enhancement in microstrip antenna [1]. The wideband E shape microstrip patch antenna in [2] incorporates two parallel slots in the patch to obtain a wide band. This antenna is excited by a probe feed and is mounted on large ground plane. The microstrip fed planar Quasi-Yagi antenna presented in [3] has a band width of 48%. These methods usually enlarge the volume and complexity of the antenna structure. Unlike the above mentioned microstrip configurations uniplanar antennas are popular due to easy fabrication and integration with MMIC's. Hwang et.al [4] has reported a coplanar wave guide fed T shaped antenna with an overall dimension of 37.5 X 80 mm² having 61.5% band width . The ACS fed monopole antenna in [5] has only a bandwidth of 16 %. In this paper we present a design of a simple and compact ACS fed antenna for wideband applications. A very large bandwidth of 110% is obtained within an overall area of 35 X 44 mm² on a substrate of dielectric constant 4.4 and thickness 1.6 mm.

2. Antenna Geometry

Figure.1 shows the geometry of the proposed ACS fed antenna. The antenna is designed on a substrate of dielectric constant 4.4 and height 1.6 mm.

In a compact Asymmetric Coplanar Strip feed the lateral strip width (in this case W_1), the ground plane length (in this case L_2) and the gap g determine the characteristic impedance [6]. In the present design the strip dimensions are taken as $L_1 = 35\text{mm}$ and the width $W_1 = 5\text{mm}$. The ground plane dimensions are $L_2 = 44\text{mm}$, $W_2 = 15\text{mm}$ consists a gap g of 1mm . The antenna is fed between the points S_1 and S_2 . These dimensions are chosen after exhaustive simulation and experimental studies for obtaining wide band width. The resulting antenna exhibits poor impedance matching. To improve the matching a small triangular cut of dimensions $\Delta x \times \Delta y$ (shown in dotted lines) is inserted in the ground plane.

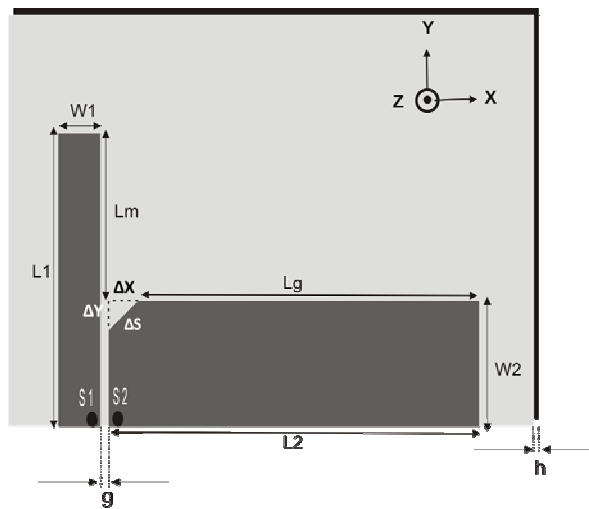


Figure 1 Antenna Geometry ($L_2=44\text{mm}$, $W_2=15\text{mm}$, $L_1=35\text{mm}$, $W_1=5\text{mm}$, $g=1\text{mm}$, $h=-1.6\text{mm}$, $\epsilon_r=4.4$ and $L_v = L_m + \Delta y$, $L_h = L_g + \Delta x$, $\Delta x = \Delta y = 3.5\text{mm}$)

3. Results and Discussion

The Antenna is tested using HP8510C network analyzer. The Experimental and Ansoft HFSS simulated return loss curves of the antenna are shown in Figure.2. The return loss characteristics of the antenna without the triangular cut is also shown in the above figure for comparison. It is found that

this triangular cut is highly influencing the return loss characteristics the antenna. The antenna exhibits a bandwidth of 110 % from 1.58 GHz to 5.48 GHz with good impedance matching. This wide bandwidth is due to the merging of three individual resonances centered at 1.85 GHz, 3.18 GHz and 4.4 GHz. The broad band behavior of the antenna is confirmed by scaling the antenna for different frequencies and substrates.

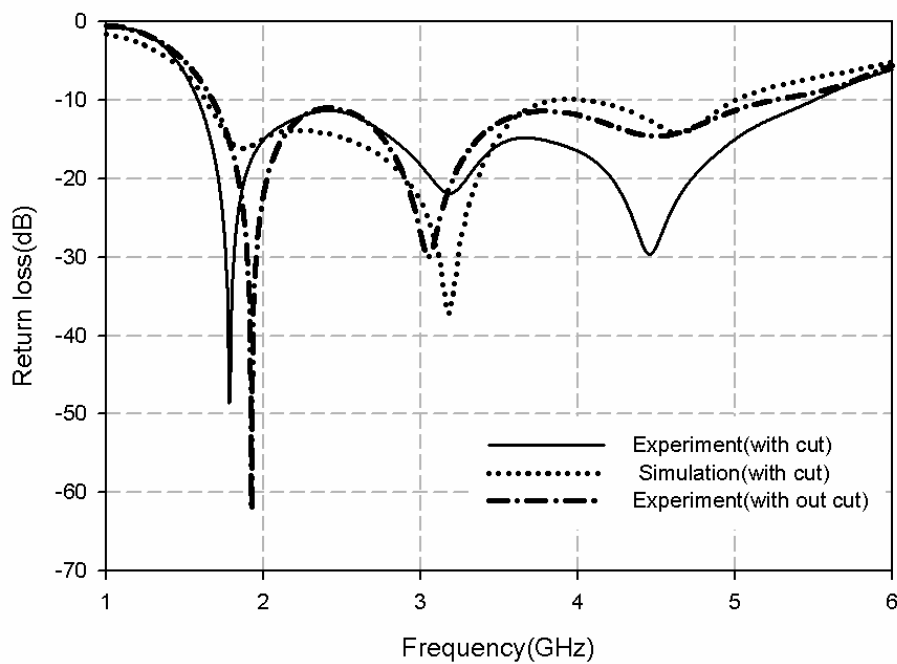


Figure 2 Experimental and simulated Reflection characteristics of the proposed antenna

Design equation:

To design a wide band antenna operating at a center frequency f_c , the dimensions L_v and L_h are taken as

$$L_h + L_v = 0.81 \lambda_c$$

$$L_h = 0.53 \lambda_c$$

$$L_v = 0.27 \lambda_c$$

Where λ_c is the free space wave length corresponding to the center frequency f_c . It is also observed that the relation between vertical and horizontal lengths L_v and L_h as $L_h=2 \times L_v$

To substantiate the veracity of the above equations the dimensions are scaled and various prototypes for different frequencies are constructed and measured (Figure 3). It has to be noted that at higher frequencies the bandwidth is found to be decreasing.

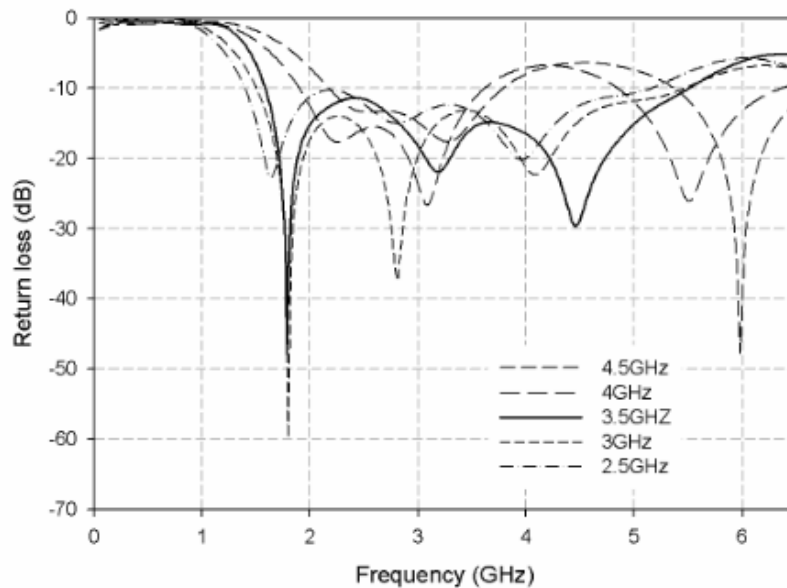


Figure 3 Reflection characteristics of the antennas with different center frequencies

In the proposed antenna the ground plane width W_2 is optimized as 0.33 times the length L_2 for maximum bandwidth. Similarly the width W_1 is optimized as 0.2 times L_v when the gap g is 1mm. From the series of simulation and experimental studies it is found that the first resonance is due to the total length L_v+L_h , the second resonance is mainly due to L_h and the third resonance is mainly due to L_v .

The Principal E and H plane patterns of the antenna for the three resonances are shown in Figure 4(a) (b) and (c) respectively. It has to be noted that the polarization of the antenna is tilted by -45° in the XY plane. This tilt is due to the asymmetry in the feed configuration. The antenna exhibits almost identical patterns with very good coverage.

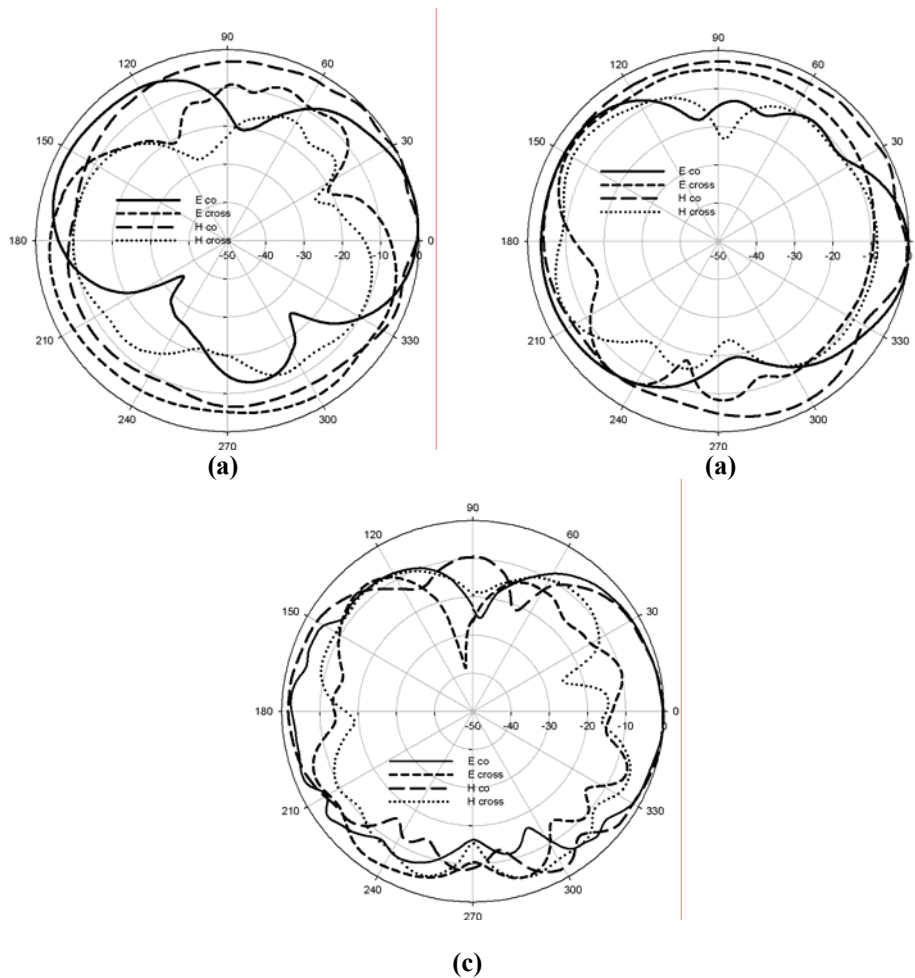


Figure 4 Measured radiation pattern of the proposed wide band antenna (a) at 1.85 GHz ,(b) at 3.18 GHz and (c) at 4.4GHz

The gain of the antenna is measured and depicted in figure 5.

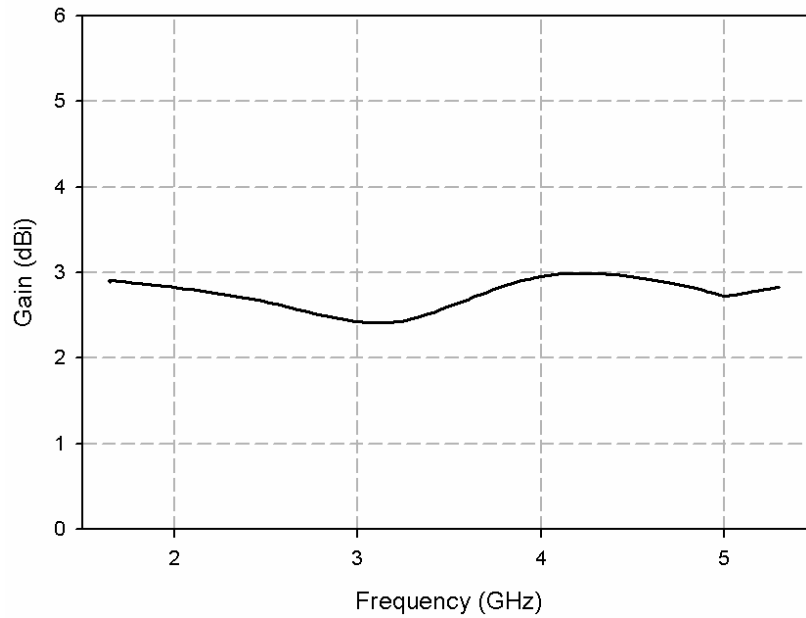


Figure 5 Measured gain of the proposed antenna

The antenna exhibits a gain greater than 2.5 dBi in the entire band.

4. Conclusion

A simple, compact Asymmetric Coplanar Strip fed antenna operating from 1.58 GHz to 5.48 GHz with 110% bandwidth is presented. This wide band antenna is obtained from exhaustive optimization studies on a simple ACS fed strip monopole. The antenna exhibits good radiation characteristics with a gain better than 2.5 dBi in the entire operating band.

References

- [1] S D Targon ski and R B Waterhouse ,Design of wide band Aperture stacked patch microstrip antennas, IEEE Trans.Antennas Propag 46(1998),1245-1251
- [2] Fan Yang, Xue-Xia Zhang,Xiaoning Ye and Yahya Rahmat-samii ,Wideband E shaped patch Antennas for wireless communication, IEEE Trans.Antennas Propag 49 (2001),1094-1100
- [3] Noriaki Kaneda,W.R.Deal,Yongxi Qian,Rod Waterhouse and Tatsuo Itoh, A Broad Band planar Quasi-Yagi Antenna, IEEE Trans.Antennas Propag 50 (2002),1158-1160
- [4] R B Hwang, A broadband CPW-fed T-shaped antenna for wireless communications, IEE Proc Microwaves Antenna Propag 151 (2004), 537-543
- [5] Deepu V, Rohith K Raj, Manoj Joseph, Suma M N and P.Mohanan, Compact Asymmetric Coplanar strip fed Monopole antenna for multiband applications, IEEE Trans.Antennas Propag 55(2007),2351-2357.
- [6] R.Garg.P.hartia and I.Bahl Microstrip Antenna Design Hand book,Is ted.Boston,M.A:Artech House(2001),794-795.

CSRR BASED MICROSTRIP ANTENNA FOR COMPACT WIRELESS APPLICATIONS

1. Introduction

Recently, there has been a growing interest in applying artificial materials (metamaterials)[1] on antennas to drastically reduce their size[2]. One of the most commonly used element of metamaterials is the split ring resonator which was designed by Pendry [3]. The characteristics of the split ring resonator (SRR) have already been studied by many researchers [3]-[4]. In its complementary structure, the CSRRs behave as an electric dipole excited by an axial electric field to create an effective negative ϵ medium and inhibit signal propagation at resonance [5]-[6]. A technique of multiple ring complementary split ring resonator (multiple ring CSRR)[7] in the ground plane is employed here to realize a compact antenna. Experimental and simulation study of the proposed antenna is presented and discussed.

2. Antenna Design

The geometry of the proposed antenna is shown in figure 1. In the proposed antenna, the solid metal ground plane is replaced with CSRR etched ground plane. A circular patch of radius $R_1 = 5.6\text{mm}$ is etched on one side of the substrate as in figure 1(a). A multiple ring CSRR is etched on the ground as shown in figure 1(b). The geometrical dimensions of the CSRR structure are as follows. The radius of the ground plane is $R_2(10)\text{mm}$. The CSRR ring radii are $r_1 = 4.5\text{mm}$, $r_2 = 3.9\text{mm}$, r_3 is 3.3mm and r_4 is 2.7mm , where r_1, r_2, r_3 and r_4 are the outermost, second, third and fourth innermost radius of the CSRR respectively. Width of the rings w is 0.3mm and separation between the adjacent rings t is

0.3mm the split gap g is 0.3mm. The center of the multiple ring CSRR ring is offseted by 5mm from the center of the ground circle along Y direction. The antenna is fabricated on a substrate of relative permittivity $\epsilon_r = 4.4$ and the thickness (h) of 1.6mm. The antenna is excited by a coaxial feed. The feed point is offset by 4mm from the ground circle center in positive Y direction. figure 1(c) is side view of the antenna.

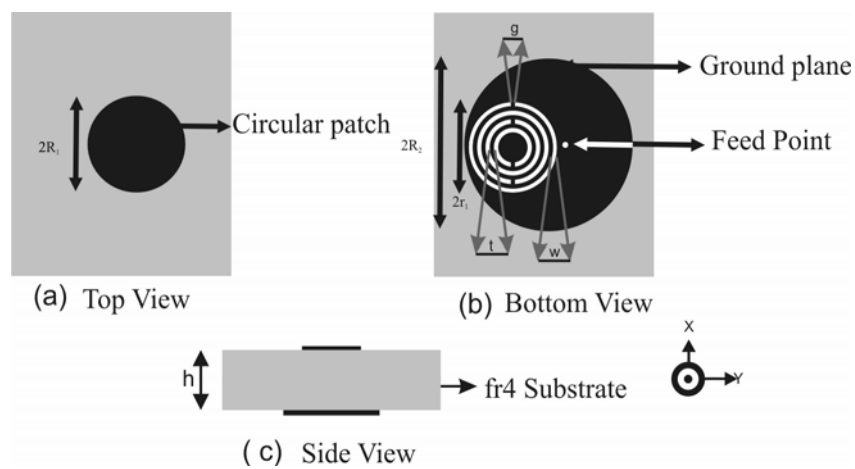


Figure 1 Geometry of the proposed antenna. 1(A)circular patch antenna $R_1=5.6\text{mm}$, figure 2(B) $R_2=10\text{mm}$, $r_1=4.5\text{mm}$, $r_2=3.9\text{mm}$, $r_3=3.3\text{mm}$, $r_4=2.7\text{mm}$, $w = 0.3\text{mm}$, $t=0.3\text{mm}$, $g=0.3\text{mm}$, $h=1.6\text{mm}$, $\epsilon_r=4.4$ figure 3(C)side view

The photograph of the proposed antenna (top and bottom view) is shown in figure 2.

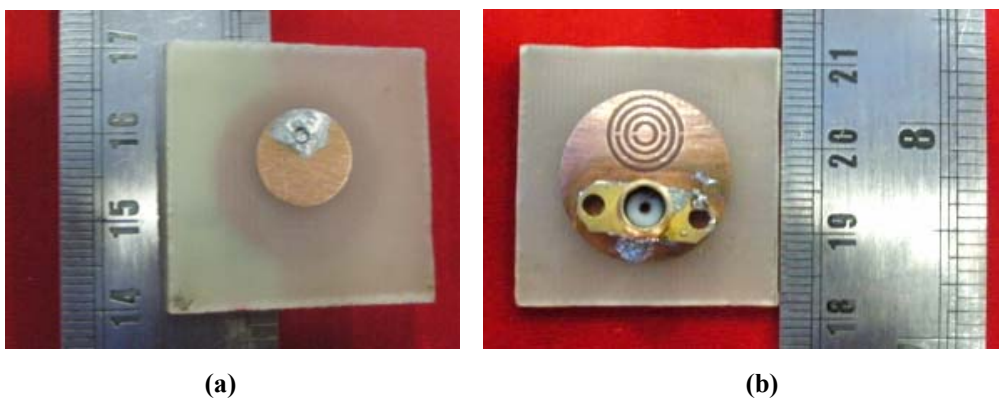


Figure 2. The photograph of the proposed antenna (a) top view (b) bottom view

3. Results and Discussion

The proposed antenna operates at 2.48 GHz as the center frequency with 2:1 VSWR bandwidth from 2.44GHz to 2.50GHz. . Figure 3 shows the simulated and experimental result of the reflection coefficient S_{11} of the CSRR loaded antenna. A good agreement is shown between simulated (Ansoft HFSS) and measured (HP8510C Network analyzer) reflection characteristics of the antenna.

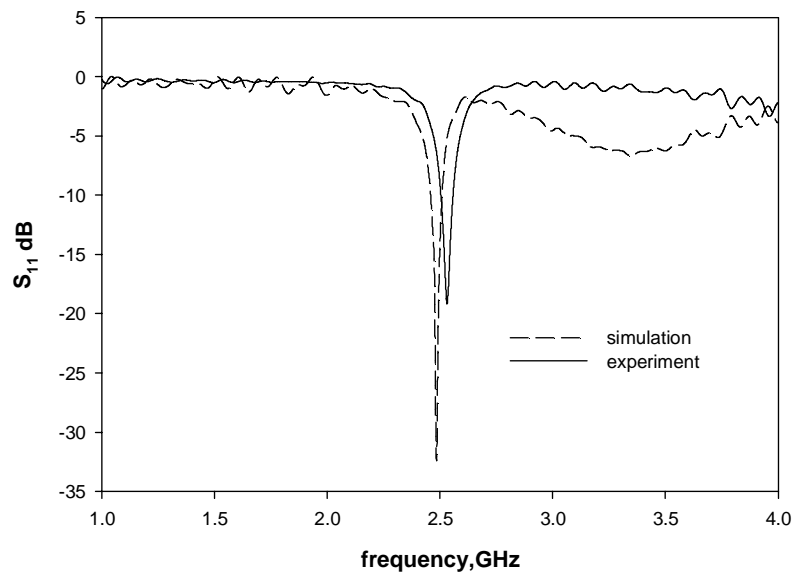


Figure 3. Reflection characteristics of the proposed antenna

Reflection coefficient S_{11} of the antenna with different number of CSRR loaded rings are shown in figure 4. It is noticed that the circular patch antenna of the same dimension without CSRR in the ground plane operates at 6.7GHz. The operating resonance of the antenna is shifted to 2.48 GHz when CSRR structure is loaded. Thus structure gives an area reduction of 83% as compared to conventional circular patch antenna.

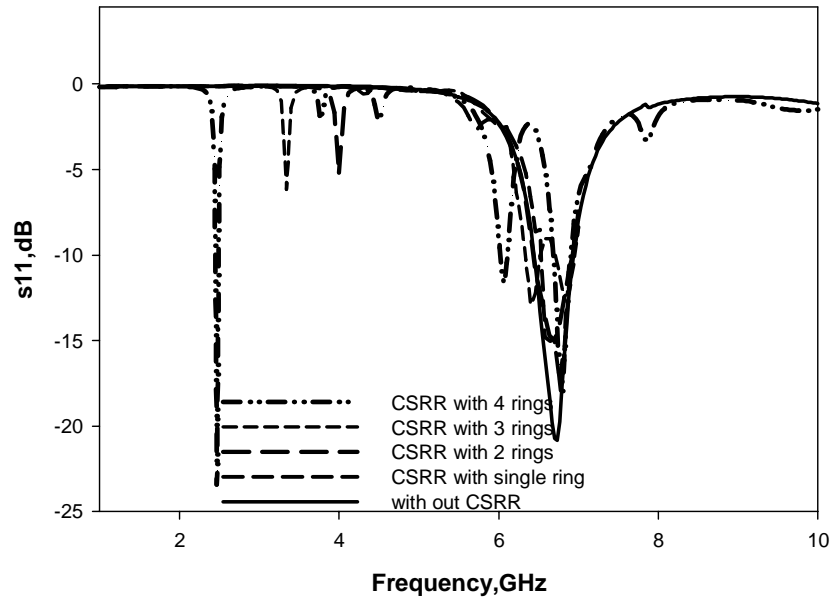


Figure 4. Reflection coefficient of the antenna with different number of rings

Figure 5(a) and (b) shows the surface current distributions simulated by Ansoft HFSS. From the figure it is clear that the CSRR structure is responsible for the antenna resonance. The advantage of the four ring CSRR patch antenna, compared to simple patch antenna resonator is that electric resonance of the CSRR patch antenna occurs at a relatively lower frequency.

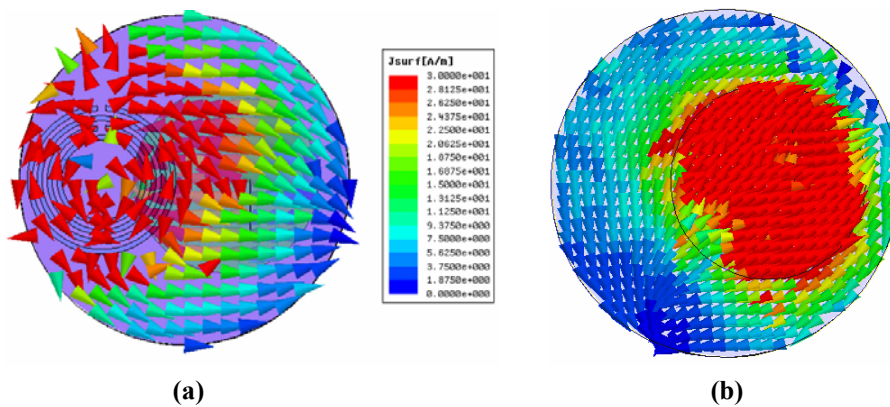


Figure 5 Surface current distribution of the antenna (a) With CSRR resonating at 2.48GHz (b)without CSRR resonating at 6.7GHz

To confirm the effect of metamaterial property of CSRR the simulated E and H field magnitude plot of the proposed antenna is shown in Figure 6. From the figure it is clear that antenna is electrically excited. Since CSRRs are complementary image of SRRs, these particles are electrically excited [8].

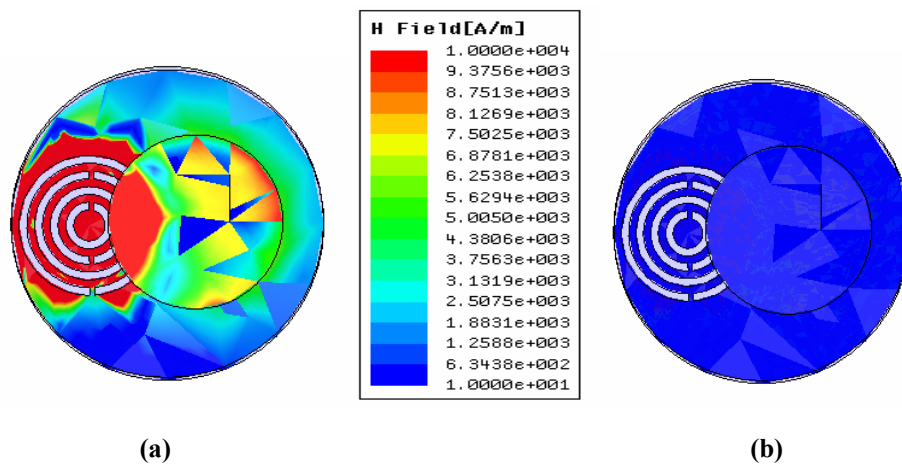


Figure 6 Magnitude plot of E and H fields at resonance frequency (a)E field (b)H field

The E plane and H plane radiation patterns of the proposed antenna at the resonant frequency are shown in figure 7 and 8 respectively.

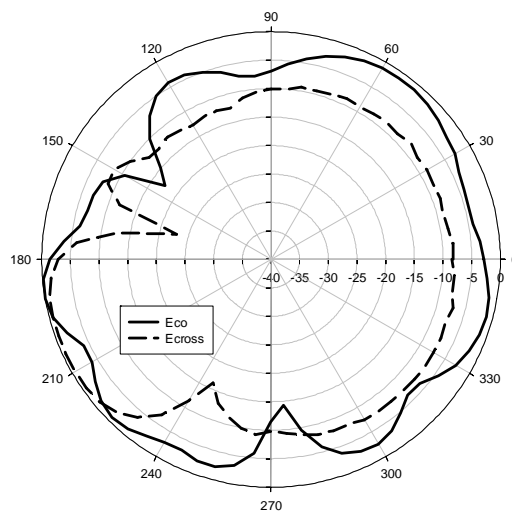


Figure 7. Measured E plane radiation pattern

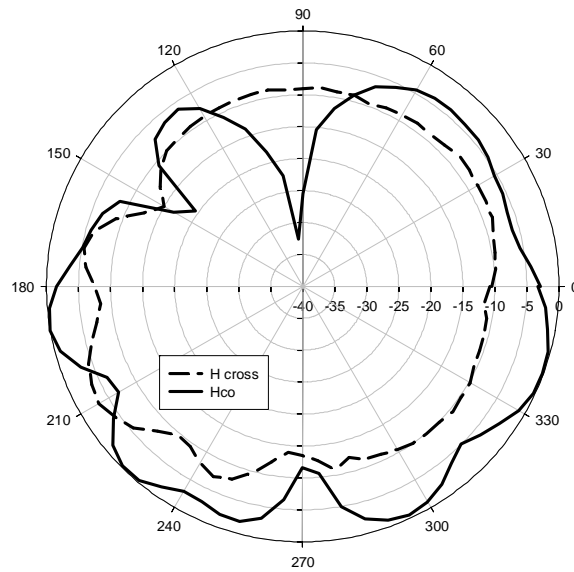


Figure 8. Measured H plane radiation pattern

The gain of the antenna is measured and depicted in figure 9. The average gain of the antenna is 1.22dBi.

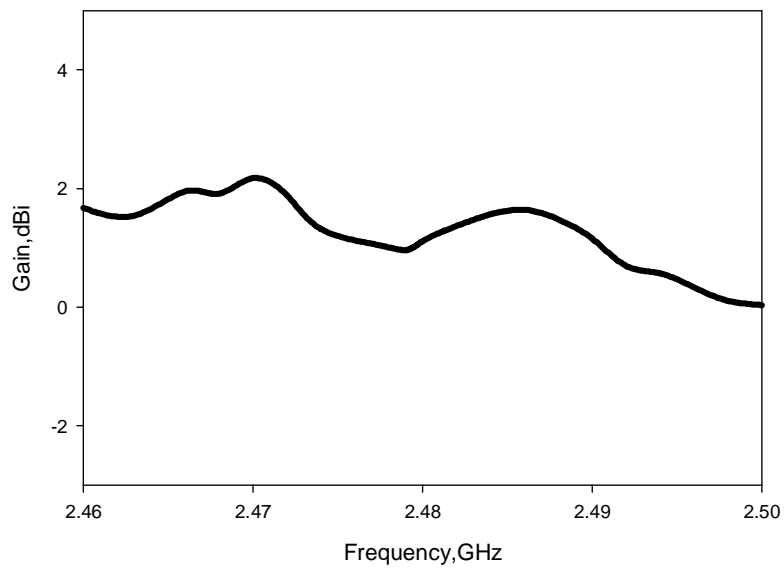


Figure 9. The gain plot of the proposed antenna

4. Conclusion

A compact circular patch antenna using multiple ring complimentary split ring resonator(multiple ring CSRR) in the ground plane is presented. The proposed antenna has an area reduction of 83% as compared to a standard circular patch antenna of the same size. The prototype exhibits a 2:1 VSWR bandwidth from 2.44GHz to 2.50GHz. The antenna exhibits moderate gain and good radiation characteristics in the entire band.

References

- [1] V.G.Veselago "The electrodynamics of substances with simultaneously negative values of ϵ and μ "Sov.Phys.-Usp., ,pp509-514, vol.10, no.4,January-februart 1968.
- [2] Kamil Boatay and Ekmel Ozbay"Electrically small split ring resonator antennas" Journal of applied phy.101,083104(2007)
- [3] D.R.Smith,W.J.Padilla,D.C.Vier,S.CNemat-Nasser and S.Schultz, Negative permeability from split ring resonator arraysPhys.Rev.Lett.vol84,pp 4184,2000
- [4] A.A Houck,J.B.Brock andI.L Chuang.phy.Rev.Lett 94,063901,2005
- [5] Falcone, F., T. Lopetegi, J. D. Baena, R. Marques, F. Martin, and M. Sorolla, "Effective negative-epsilon stop-band microstrip lines based on complementary split ring resonators," *IEEE Microwave Wireless Compon. Lett.*, Vol. 14, 280-282, 2004.
- [6] Gil,I,J.Bonache,M.Gil,J.Garcia-Garcia F.Martin and R.Marques. "Modeling complimentary split ring resonator (CSRR)left handed lines with inter resonator's coupling" ,IEEE MELCON2006 pp. 225-228, May 2006.
- [7] F.Bilotti,A.Toscano,L.Vegni,K.Aydin,K.Boratay and E.Ozbay ",Equivalent circuit models for the design of metamaterials based on artificial magnetic inclusions IEEE Trans.AntennasPropag,pp2865-2873,vol 5.no.12.December 2007.
- [8] J D Baena,J.Bonache,F Martin,R Marquies,F Falcone,T Lopetegi,MAG Laso,J Garcia,I Gil and Sorolla"Equivalent circuit models for split ring resonators and complimentary split rings resonators coupled to planar transmission lines" IEEE Transactions on Microwave Theory and Techniques.vol 53 PP1451-1461 April 2005.

.....✂.....

List of Publications

International Journals

- [1] **Laila D**, Deepu.V, Sujith R, P.Mohanan, C.K.Aanandan, and K.Vasudevan "Compact asymmetric coplanar strip fed antenna for wide band applications" *Microwave and Optical Technology Letters*, May 2009
- [2] **D. Laila**, R. Sujith, M. N. Sreejith, C. K. Aanandan, K Vasudevan and P.Mohanan "Mobile antenna with reduced radiation hazards towards human head" *Progress In Electromagnetics Research Letters*, Vol. 17, 39-46, 2010.
- [3] **Laila.D**, Sujith.R, Shameena V.A,Deepak.U,Nijas.C.M and P.Mohanan"CPW fed antenna for mobile handset with metal wire mesh", *Proceedings published by International Journal of Computer Applications® (IJCA), Number 1 - Article 1, pp 25-28, 2011.*
- [4] **Laila.D**, Sujith R, Nijas C.M, C. K Aanandan, K Vasudevan and P. Mohanan "Modified CPW fed monopole antenna with suitable radiation pattern for mobile handset" *Microwave Review Journal* pp 8-12 September 2011.
- [5] **Laila D**, Sujith R, Nijas C M, Sarin V P and P Mohanan "Compact modified printed monopole antenna for enhanced gain performance" *International Journal of Applied Information Systems*, Volume 1– No.5,pp 1-3 February 2012
- [6] R Sujith, Deepu.V, **Laila D**, C.K.Aanandan,K.Vasudevan and P.Mohanan, "A Compact Dual-Band Modified T-shaped CPW-Fed Monopole Antenna", *Microwave and Optical Technology Letters*, Vol. 51, No. 4, April 2009.
- [7] R. Sujith, S. Mridula, P. Binu, **D. Laila**, R. Dinesh and P. Mohanan, "Compact CPW-fed ground defected H-shaped slot antenna with harmonic suppression and stable radiation characteristics" *Electronics letters* 10th June 2010 Vol. 46 No. 12.
- [8] R. Sujith, V. Deepu, S. Mridula, Binu Paul, **D. Laila**, P. Mohanan " Compact CPW-fed uniplanar antenna for multiband wireless applications" *AEU - International Journal of Electronics and Communications*, In Press, Corrected Proof, Available online 10 October 2010.
- [9] R.Sujith, Mridula S, **Laila D**, C K Aanandan, K Vasudevan and P Mohanan, " Compact CPW-Fed Slot Antenna with harmonic suppression", *International journal of RF and Microwave computer-Aided Engineering*, Volume 21, Issue 5, pages 543–550, September 2011

Conferences

- [1] **Laila, D.;** Deepu, V.; Sujith, R.; Mohanan, P.; Anandan, C.K.; Vasudevan, K. “Asymmetric Coplanar Strip fed wide band antenna “IEEE international conference on Recent advances in microwave theory and applications, 21-24 November 2008, Jaipur, India
- [2] **Laila D,** Sujith R, Deepu V, K. vasudevan, C.K Aanandan and P.Mohanan “Compact uniplannar antenna for wide band applications” Antennas and propagation Symposium (APSYM) 2008
- [3] **Laila D,** Sujith.R, Deepu.V, C.K. aanandan, K.Vasudevan,”Compact CSRR based patch antenna for wireless application” Applied Electromagnetic conference-2009 (AEMC-09),Kolkatta, India.
- [4] **Laila D,** Sujith Raman, Sreejith M Nair, Aanandan C.K, Vasudevan K. and Mohanan P “Modified CPW fed monopole antenna with a radiation pattern suitable for mobile handset”, 2011 International Conference on Communications and Signal Processing(ICCSP2011), Calicut, India.
- [5] **Laila.D,** Sujith.R, Shameena V.A, Deepak.U, Nijas.C.M and P.Mohanan”CPW fed antenna for mobile handset with metal wire mesh” ICVCI-2011,St.Gits,Kottayam.
- [6] Sujith.R, Deepu. V, **Laila.D,** S. Mridula and P.Mohanan, ”CPW-fed Quad Band antenna for Compact wireless application” IEEE Applied Electromagnetic conference-2009 (AEMC-09), Kolkatta, India.
- [7] Sujith, Mridula S, Binu Paul, **D. Laila,** C.K. Aanandan, K. Vasudevan and P. Mohanan “Compact CPW-FED Defected Ground Antenna”, EUCAP2010, Barcelona,Spain 2010
- [8] **Laila D ,** Mohanan P “Modified CPW fed monopole antenna with reduced SAR value for mobile application, Applied Electromagnetic conference-2011 (AEMC-11), Kolkatta, India
- [9] **Laila D,** Sujith R, Nijas,C M, Shameena V.A, Dinesh R, P Mohanan “A Metamaterial antenna with reduced radiation hazards towards human head”PIERS 2012 Kuala Lumpur

List of Publications

- [10] Shameena V A, **Laila D** ,Sujith R ,Dinesh R ,Deepak U “Band notched UWB notch antenna ” PIERS 2012 Kuala Lumpur
- [11] Dinesh.R, **Laila D**, V P Sarin, Nijas,C M, Shameena V A, P Mohanan “Asymmetric coplanar strip semielliptical dual band antenna” PIERS 2012 Kuala Lumpur
- [12] Sujith.R, **Laila.D**, Nijas.C.M Deepak.U ,R.Dineshand P.Mohanan”CPW ” Feeding techniques to excite slot on an Open Ended coplanar waveguide transmission line” PIERS 2012 Kuala Lumpur
- [13] Sujith R, **Laila D** and P Mohanan “CPW fed mobile antenna with reduced RF interference towards human head” 24th kerala science congress,kottayam 2012 (Best poster award 2012)
- [14] Vineetha,Vishnu K ,**Laila D**, Pradeep C,V P N Nampoori”Effect of mobile phone radiation on DNA,its harmful effects and possible solution”24th kerala science congress,kottayam 2012

.....❧.....

2D radiation patterns,
118,127,138,145,146
2G, 8,
3G, 8,9,10

A

Agilent E8362B, 41
Anechoic chamber, 31, 42,46
ANSOFT, 37,106,164
Asymmetric, 59,68,222, 229

B

Bandwidth,
12,17,31,38,97,149,164,171,223,226

C

Calibration, 44,47
Cavity perturbation, 37,53
Cellular,5,96
Characteristic impedance,57,58,
Communication, 1, 2, 4, 5, 6, 7, 8, 9,
10,11,12,13,14,20,26,57,61,63,66,70,71,7
3,75,79,96,97,111,154,167,187,191,202
Coplanar waveguide, 28, 37, 55,57, 58,
59, 64, 65, 66,67,68,80, 99,111,135, 148,
222,224
CPW, 27,56,57,58,59,64,65,66,67,68, 77,
95,99,100,102,105,106,109,110,111,11
3,117,123,124,125,130,136,146,150,15
3,156,157,157,160,161,163,169,183,22
1,223,224,225,227
CREMA SOFT,40,42,43,44,46,47,225
cross polar level, 180

D

DCS, 10,62,155
Deschamps, 59
Dielectric Resonator, 31,156
Dielectric substrate, 14,57,67,78,80,99,
132,133,143,156
Dipole, 10,12,70,71,109,154,155,156,
217,236

E

Electromagnetic, 1,2,3,4,5,6,7,9,10,19,
20,23,25,26,27,37,43,53,55,56,57,62,6
8,69,70,74,75,76,77,78,79,96,97,98,10
6,111,114,127,147,158,160,162,190,19
1,197,222
Experimental19,26,27,28,37,43,48,50,
58,60,71,74,76,95,98,103,118,125,135,
153,163,169,187,195,213,218,221,225,
230,231,232,236,238

F

Far field,
28,37,43,45,46,80,100,120,126,136,13
8,183,195,196,198,199,200,201 1
FDTD, 21 25, 26

G

Gain, 7,12,13,15,25,26,37,43,47,68,77,
79,80,108,109,110,130,135,141,146,14
7,167,169,181,183,197,223,234,241,241
Ground folded planner antena,153
GSM,
7,10,28,62,72,123,135,146,148,155,22
3,225,227

H

HFSS,37,55,106,164,167,230,238,239
HP8510C,40,46,51,103,217,230,238,

M

Metamaterials, 19,70,73,75,80,236
Microstrip,14,15,55,59,60,67,76,79,112,
113,229,236
MMIC, 100, 229
Mobile antenna, 1,12,26,28,37,68,75,80,
98,111,124,135,148,170,182,221,222
Mobile handset, 6,12,28,71,77,95,111,
116,119,122,126,134,144,149,157,169,
172,178,190,192,195,198,212,225,227

Monolithic,64,227

Monopole antenna, 12, 27,60,63,67,77, 98,102,105,109,111,115,117,121,124,127,130,135,146,150,155,163,169,183,195,198,200,204,222,224,229,235

N

Near field, 27,29,37,48,71,80,187,188,190,195,196,197,198,199,200,213,212,222,225

O

Omnidirectional, 27,68,71,97,109,111,127,203 parasitic, 27,28,60,62,63,65,68,137,148,149,150,221,222,223,225,227

P

PBG, 20
Phantom, 37, 48,49,50,51,52,53,54,56,187,193,202,204,207, 213,217,225
PIFA, 17,18,69,73,76,77
PILA, 17
Planar Antennas, 28, 37,56,208,229
Polarization,15, 17, 24,50,63,67,76,79,110,167,180,213,233

Q

Quality factor, 15,54,112,118,124
Quasi-TEM,99

R

Radiation pattern, 37,72,98,113,115, 122,123,124,126,134, 135,138,144,147, 149,150

S

SAR 29,37,50,51,56,153,187,188,189, 190,191,192,193,197,202,203,204,205, 206,207,208,222,225
Smith chart, 137,160
Sub Miniature Amphenol, 103
Surface current, 105,165,239

T

THRU calibration, 47
Transmission line, 56,158

U

Uniplanar, 229

V

VSWR, 44,45,61,125,136,164,169,171

W

Waveguide,20,28,37,53,54,55,99,155,222,224
Wideband, 43,46,61,69,156,222,229
wireless, 1,2,6,7,8,10,11,13,15,63,68, 96,97,163,187,223,229
WLAN, 66,67

.....∞∞∞.....

Curriculum Vitae

LAILA D

Research Scholar
Department of Electronics
Cochin University of Science and Technology
Cochin-22, Kerala, India.

E-mail: lailacusat@gmail.com
Mob: 9847 734728

Objective:

To be a part of an organization to pursue research activities in the field of Electromagnetics and antennas and to do something that is innovative and beneficial to mankind.

Education:

- B.Sc (Physics)- First class(1987)
- BE(Electronics and communication Engineering)- First class (1991)
- M.Tech (Digital systems and communication)- First class (2002)

Awards and Honours received:

- Best poster award of the Kerala State Council for Science, Technology and Environment in the subject area **science and society** in 24th Kerala Science Congress 29-31 January 2012 Kottayam, Kerala, India

EXPERIENCE

Research

- Research scholar with the center for Research in Electro-Magnetics and Antennas (CREMA), Department of Electronics, Cochin University of Science and Technology, Cochin, India from September 2007 to October 2012.

Teaching

- Lecturer in Electronics, Model Polytechnic, Vadakara, Calicut, Unit of Institute of Human Resources and Development (IHRD)Kerala, India (December 1993 – August 1996).
- Assistant Professor, Department of Electronics, Model Engineering College, Ernakulam, Kerala, India. (August 1996 –July 2007).
- Associate Professor, Department of Electronics, Model Engineering College, Ernakulam, Unit of Institute of Human Resources and Development (IHRD), Kerala, India (July 2007 onwards).

Publications:

International Journal	: 09
International Conference	: 11
National Conference	: 03
Citation in international journal	: 09

Citation

1. **Laila D.**, Deepu.V, Sujith R, P.Mohanana, C.K.Aanandan, and K.Vasudevan "Compact asymmetric coplanar strip fed antenna for wide band applications" *Microwave and Optical Technology Letters*, May 2009
 - a. SW Su "Compact coaxial - line - fed printed mobile - unit antenna for SM850/900/1800/1900 /UMTS WWAN operation" *Microwave and Optical Technology Letters*, Vol. 52, Issue 4, pp 961–966, April 2010

2. **D. Laila**, R. Sujith, M. N. Sreejith, C. K. Aanandan, K Vasudevan and P.Mohanana "Mobile antenna with reduced radiation hazards towards human head" *Progress In Electromagnetics Research Letters*, Vol. 17, 39-46, 2010.
 - a. M. T. Islam, H. Z. Abidin, M. R. I. Faruque, and N. Misran, "Analysis of materials effects on radio frequency electromagnetic fields in human head," *Progress In Electromagnetics Research*, Vol. 128, 121-136, 2012
 - b. S. M. Alia & H. Gub "Electrically Controlling the Chassis Via A Notching Approach for Improved Handset Performance" 973-986.
 - c. S. M. Ali , H. Gu " Electrically Controlling the Chassis Via A Notching Approach for Improved Handset Performance" *Journal of Electromagnetic Waves and Applications*, Volume 25, Issue 7, 2011

3. R Sujith, Deepu.V, **Laila D**, C.K.Aanandan,K.Vasudevan and P.Mohanana, "A Compact Dual-Band Modified T-shaped CPW-Fed Monopole Antenna", *Microwave and Optical Technology Letters*, Vol. 51, No. 4, April 2009.
 - a. H.F. AbuTarboush R. Nilavalan K.M. Nasr S.W. Cheung T. Peter , H.S. Al-Raweshidy D. Budimir "Reconfigurable tri-band H-shaped antenna with frequency selectivity feature for compact wireless communication systems" *IET Microw. Antennas Propag.*, Vol. 5, Iss. 14, pp. 1675–1682, 2011

- b. Abutarboush, H.F, Nilavalan, R. ; Cheung, S.W. ; Nasr, K.M.” Compact Printed Multiband Antenna With Independent Setting Suitable for Fixed and Reconfigurable Wireless Communication Systems”, IEEE Transactions on Antennas and Propagation Vol 60 , no 8 ,pp 3867 - 3874
- c. J Chen, G Fu, GD Wu, SX Gong –“ Compact Graded Central Feeder Line CPW-fed Broadband Antenna” Journal of Electromagnetic Waves and Applications Volume 23, Issue 14-15, 2009
- d. J. Chen, G. Fu, G.-D. Wu, S.-X. Gong & X. Chen” Combinational Structure Open Sleeve Antenna for Multiband Applications” Journal of Electromagnetic Waves and Applications Volume 24, Issue 11-12, 2010
- e. Kyunghaeng Lee, Yong Jee “Multiresonance coplanar waveguide-fed monopole antennas with meander strips for GSM/GPS/PCS/DCS/WCDMA applications” Volume 53, Issue 10, pages 2438–2441, October 2011, Microwave and Optical Technology Letters

.....✂.....